Photocapacitance, photoconductivity and AC conductivity of semiconductors containing deep impurities

A thesis

presented by

Parminder Singh Mudhar BSc

to the

University of St Andrews

in application for the

Degree of Doctor of Philosophy

Certificate

I certify that Parminder Singh Mudhar,BSc,has spent nine terms at research work in the Wolfson Institute of Luminescence,within the School of Physical Science in the University of St Andrews under my direction,that he has fulfilled the conditions of the resolution of the University Court,1967,No 1,and that he is qualified to submit the accompanying thesis in application for the Degree of Doctor of Philosophy.

Research Supervisor

Declaration

I hereby certify that this thesis has been composed by me,and is a record of work done by me,and has not been presented previously for a Higher degree

The research was carried out in the Wolfson Institute of Luminescence,within the School of Physical Science in the University of St Andrews,under the supervision of Prof J W Allen.

P S Mudhar

Career

I matriculated in the University of Lancaster in October 1979 to study Physics. In 1982 I obtained the Degree of Bachelor of Science with First Class Honours in Physics.

In October 1982,following the award of a grant from the Science and Engineering Research Council,I was enrolled as a Research Student under the resolution of the University Court,1967,No 1,as a candidate for the Degree of Doctor of Philosophy.

ਮੇਰੇ ਪਾਪਾਜੀ ਤੇ ਬੀਬੀਜੀ - ਮੇਰੇ ਮਾਸਟਰਜੀ
(My father,my mother - my teachers)

Acknowledgements

Firstly I thank the SERC for providing a grant that enabled me to complete this project.Dr Vincent of the Chemistry Department and Mr Armitage of the Physics department are to be thanked for allowing the use of the Solartron frequency response analyser and the General Radio 1615A capacitance bridge respectively.I would also like to thank Dr Cattel,of RSRE,for supplying the thin film electroluminescent devices.

During my stay at St Andrews,a lot of equipement was borrowed from the teaching laboratories in the Department of Physics .I thank Derek Bayne and Les Kirk for use of the equipement.(I hope most of it still works!)

The following people are to be thanked for useful discussions: Ralph "where is that noise coming from" Hall,Steve Ayling (who also cheered up Monday mornings with '2000 AD') and Alistair Kean.Ian "sav-a" Park supplied the weekly 'New Scientist'.Ralph Hall is to be further thanked for proof-reading chapter 2 .I would also like to thank members of the women's basketball club who made Wednesdays and Sundays interesting.

Last,but not least,I would like to thank my supervisor,Prof J W Allen,for his patience (which must have been tested at times) and his invaluable guidance throughout the project.

Abstract

Photocapacitance and photoconductivity are used to characterise deep impurities in wide band gap binary semiconductors.The former method is used to characterise the Ni centre in GaP:Ni.In particular we show that the Ni (d^9) -> $Ni(d^8)$ + e^- has a photoionisation threshold of (0.88 ± 0.01)eV below the conduction band at 0^oC.A new feature observed in the spectrum of the optical cross section for electrons is a dip at a photon energy of 1.24eV.This dip is shown to be consistent with the transition d^8 -> d^9 + h.Photoconductivity is used to characterise a copper related centre in two ZnS:Mn based (dc) thin film electroluminescent devices (TFED) and the M centre in two samples of ZnSe.The copper related centre and the M centre are shown to have photoionisation thresholds of (2.49 ± 0.25)eV and 2.01eV below the conduction band respectively.

AC electrical properties of one of the TFED's and the ZnSe samples were studied when the materials were in the dark and when light was made incident upon them. When the materials are in the dark the dispersion in the measured capacitance and resistance of the materials can be understood in terms of equivalent circuits.When light is continuously left on the materials the dispersion in the measured capacitance and resistance cannot be decomposed into an equivalent circuit.The dispersion is understood in terms of a new form of hopping conduction which is associated with the photoconductive process of capture and thermal emission of photoexcited carriers between a set of traps and one of the free carrier bands.

Index

1 Introduction.The role of impurities in semiconductors.

1.1 Importance of impurities in semiconductors

Pure crystalline semiconductors would have been of little technological importance.The ability to contaminate a semiconductor, in a controlled and systematic way,has yielded semiconductors that can have their conductivity tailored (to some extent) to meet specific requirements . This ability as well as the existence of two types of conductivities in semiconductors has yielded a large variety of devices whose existence is taken for granted.However the effect of impurities in semiconductors is not always beneficial.This is borne out by experiments that reveal that during the doping process of tailoring the conductivity small amounts of unwanted impurities are incorporated into the semiconductor.Such impurities,although occurring in small concentrations (compared with the wanted impurities) may completely ruin the function of the device.

The work to be presented in later chapters is the characterisation of impurities in binary semiconductors and their role in the electrical conductivity. The majority of the work presented in chapters two through to six are self contained and there is little,if any,cross reference.It is the object of the present chapter to present a unification of this work.We begin this unification by noting the types of impurities encountered experimentally and how such impurities are described theoretically.In the former we will consider the

techniques of photoconductivity (PCON) and photocapacitance (PCAP) as methods of characterising impurities in semiconductors.The merits of the two methods will be discussed in terms of the relevant information that can be obtained from these.For the theoretical description,we will define the approaches used and leave the detail to references quoted in the text. Later,an outline of the work is presented.The present work is the characterisation of deep levels and their influence on the electrical properties in wide band gap semiconductors that are used in the optoelectronic industry.

1.2 Role of impurities in semiconductors

As mentioned in the previous section ,impurities are at the heart of semiconductor devices.This section attempts to outline the main forms of impurities in a classification,attempts to describe them theoretically and also describe the relevance of the impurity type to device function.

The impurities can be classified into three types:isoelectronic,deep and shallow.Isoelectronic impurities are those that have the outer electronic configuration the same as the atom it replaces in the host lattice.The ground state of such impurities sometimes lies deep in the valence band.Such impurities can be important (as in the impact excitation of Mn in ZnS:Mn thin film electroluminescent devices).We shall not dwell upon them as they are difficult to observe in experiments such as PCAP and PCON.Technologically the impurities of importance are those that have been labelled deep and shallow.A classification of deep and shallow

impurities could be based on the location of the ground energy level produced by such an impurity relative to the band edge.It has become practice to regard impurities as 'shallow' if the ground level is less than 0.1eV (measured from a band edge).An impurity is labelled deep if the energy level produced by it is more than 0.1eV away from the band edge. The shallow and the deep impurity perform different roles in device physics. For a shallow donor,the outer electron will be loosely bound to the donor and at room temperatures the donor is expected to be ionised and thus able to contribute to the free carrier concentration.Similar reasoning applies to shallow acceptors.Hence the primary reason for introducing shallow impurities is to increase the conductivity of the material and in particular to make it into n-type or p-type.This in turn has led to a large number of devices to be fabricated.In particular,without the advent of the 'electronic switch' (the transistor) modern day wonders that are taken for granted could never have occurred.

Deep impurities play an important role in luminescent and photo-devices (such as the solar cell and the photoconductor).The energy level produced by the deep impurity lies well away from the band edge.If a host with a large band gap is doped with a suitable impurity it is possible to achieve luminesence throughout the visible region.Luminescence is usually achieved through some form of excitation,as for example by passing a current through the sample which has been fabricated into a pn junction diode .Alternatively if a semiconductor with deep impurities is placed in the dark prior to shining monochromatic light,it is found that the conductivity of the sample increases (in some cases) by many orders of magnitude.Photodetectors are based on this principle. The effect of

the deep impurities is not purely beneficial.An example is GaAs:Cr which is used as a substrate in GaAs IC's.It was found that the chromium impurity can diffuse to the active regions of the device and thus completely ruin its function.This is rather unfortunate,but GaAs:Cr is widely used in the manufacture of GaAs IC's.Other impurities that produce deep energy levels can capture free electrons and holes and thus reduce the conductivity of the material (that may have been intentionally doped with shallow impurities to increase the conductivity of the material).

The theoretical understanding of the two types of impurities presented in the discussion above are,to some extent,based on the location of the energy level produced by the impurity in the band gap in relation to a band edge.For shallow donors we mentioned that the outer electron is expected to be loosely bound to the donor and at room temperatures the donor is expected to be ionised. The potential produced by an ionised donor will be Coulombic at large distances The outer electron of the donor will move in a central field;that is , the shallow donor can be described by a modified hydrogen model.The modifications required are to replace the free electron mass by its effective mass in the host crystal and take screening due to the lattice into account. Although this model of the shallow donor is useful,detailed interpretation of the excited donor states observed in experiment may have to use more advanced theories.Alternatively we can say that the wavefunction of the outer electron will extend over a large volume of the lattice so that in $\underline{k}$ space the wavefunction will be localised.The wavefunction of the donor can be constructed from taking a linear combination of the lattice wavefunctions (usually from the band that the impurity level is nearest to) as the basis

functions.The constructed wavefunction will converge rapidly as the number of bases required will be small.Hence,in principle,calculation of transition probabilities in an absorption experiment for example,is straightforward. When the outer electron is closer to the core,the potential that the outer electron experiences is no longer Coulombic and so the modified hydrogenic model is no longer applicable.In such cases it is better to abandon the hydrogen model and construct the wavefunction of the donor from the lattice wavefunctions and hope for convergence.

Deep impurities are characterised by a wavefunction that is highly localised in real space and thus extended in $\underline{k}$ space. To construct the deep impurity wavefunction using the lattice wavefunctions as a basis will require lattice wavefunctions taken from the entire Brillouin zone.Convergence of the wavefunction using this approach may prove to be difficult. In general theoretical study of deep levels is difficult.For transition metal ions (for example Ni) in semiconductors a starting point to collate a large amount of data is the crystal field theory.This is a semi-empirical theory used by experimentalists to interpret,for example,absorption spectra. To use the crystal field theory,the energy levels and the wavefunction of the atomic ionised transition metal ion are found (an excellent source for a procedure to calculate them is in the book by Theissing and Caplan[8]).Once the transition metal ion is placed substitutionally into the lattice,it will be acted upon by a crystal potential.The form of the crystal potential will have the full symmetry of the host crystal.For the free atomic ionised transition metal ion,the d electron will occupy an energy level that is ten fold degenerate.Treating the crystal potential as a perturbation it is

found that the crystal potential will lift this ten fold degenerate level into one that is six fold degenerate (the so-called t_2 orbital) and one that is four fold degenerate (the e orbital).The separation of the two levels is called the crystal field splitting and is usually denoted by Δ or 10Dq.Detailed procedures for calculating the energy levels when more than one electron occupies the d shell can be found in the books by Ballhausen[2],Griffiths[4] and in the article by Allen and Pearson[1].Further refinement to the procedure outlined above can include spin-orbit coupling and the Jahn-Teller effect. A practical version of the crystal field theory that acknowledges the difference of an electron in an e orbital and that in a t_2 orbital has recently been proposed by O'Neill and Allen (see for example reference 9).Difficulties with the crystal field theory arise when the transition metal ion does not occupy a substitutional position.Further difficulties may be encountered when we have complexes. In such cases it would be better to consider other approaches,such as the the scattered wave method and molecular orbital approaches.It is clear from the above brief outline of the theoretical approaches to study shallow and deep impurities that the latter are the more difficult to describe theoretically.

A brief discussion will be made here concerning the energy levels of a multielectron impurities such as the transition metal ions.In photoionisation experiments,as measured for example in PCAP and PCON,we take an electron from the impurity and place it in the conduction band (for the sake of argument) and leave one less electron bound to the impurity.This implies for the transition metal ions with n electrons in the d shell (a d^n configuration) and n-1 electrons after the photoionisation transition,the photoionisation threshold

will correspond to the $d^n - d^{n-1}$ level (for the notation, see the article by Allen and Pearson). A difficulty arises in that the theoretician works with one electron energy while the experimenter measures many-electron energies.

We mentioned that two experiments to characterise impurities were PCON and PCAP. As the names suggest, in one case the change in the electrical conductivity is measured when the sample is exposed to light while in the other the change in the capacitance is measured. PCON is perhaps the easier to carry out experimentally and can be used to characterise both deep and shallow impurities while PCAP is best suited to the study of deep impurities.

PCON involves measuring the change in the resistance of the sample when light is shone on it. The effect will be greatest in semi-insulating materials. When light is shone onto the material, the dark occupancies of the impurities will be changed. It is straightforward to write down the equations describing the various occupancies but much more difficult to find a general solution for the free carrier concentration. Thus most of the text books deal with the steady-state photoconductivity and derive various models in terms of a free carrier time (see for example Rose[6] and Blakemore[3]). However, it will be shown in chapter 5 that under certain approximations it is possible to obtain a general solution that does not rely upon matrix formulation or numerical solutions. It will be further shown in chapter 5 that the time dependence of the photoconductivity gives more information than just studying the steady-state values. Using a monochromatic light source it is possible to study both deep and shallow impurities . The excited states of the shallow impurities can

be analysed in terms of a modified hydrogen model which was discussed earlier in this section.

Study of impurities using PCAP requires that the sample with the required impurity doped into it is fabricated either into a pn junction diode or as the semiconductor in a Schottky diode,the latter being easier to fabricate than the former.We will describe the PCAP as applied to a Schottky diode as the description for a pn junction diode is similar.It is known that there is a region adjacent to the metal contact that is devoid of free carriers (the depletion region) except for a few Debye lengths at the edge of the depletion region.The depletion region contains a space charge and hence it follows that there is a capacitance associated with it.A sensitive capacitance bridge is required for PCAP experiments as the change in the capacitances to be measured may be the order of 0.01pF on a background capacitance of the diode which could be many hundreds of pF.Shining light on the diode (with the depletion region facing the light) will change the capacitance of the diode. Consider the case of exciting electrons from the impurity into the conduction band.The photoexcited electron will be swept out of the depletion region by the high electric field which is present in the depletion region.Thus a net positive charge will be left on the impurity.This implies that the capacitance will change (positively).Similarly when holes are excited from the impurity they will leave behind a net negative charge and thus again the capacitance will change (negatively). The sign of the capacitance change gives the additional information about the band involved in the optical transitions.Furthermore,PCAP can be adapted so that information about capture cross sections for electrons and holes can be found as well as the spectrum of the optical cross section for

electrons and holes.A number of differences exist between PCAP and PCON. PCON cannot tell which band is involved in the optical transitions as the measured electrical current cannot be easily used to distinguish between a hole current and an electron current.The capture of free carriers can to a large extent be neglected in the PCAP experiments while in PCON this cannot be done.The main effect of the free carrier concentration in PCAP is that some capture does occur at the edge of the depletion region and is sometimes responsible for the capacitance not returning to the dark value after illumination of the diode.In our studies of impurities in semiconductors,both methods were used.As mentioned the dynamics of capture/thermal emission of carriers from a shallow impurity and one of the bands was best studied by photoconductivity while the photocapacitance was used to characterise an impurity that has been labelled as a possible killer centre in an optoelectronic material.

1.3 Summary of the work carried out

As mentioned PCAP and PCON are used for different purposes.Chapter 2 is a study of the nickel impurity in n-type GaP.GaP is used to fabricate LED's when a suitable impurity has been doped into it.For example GaP:Zn,O is used in the manufacture of red LED's.In competition with transitions that involve the emission of photons (radiative transitions) there are other centres that promote non-radiative transitions.Nickel is such an impurity that occurs in device grade GaP.The nickel impurity occurs in three charge states in GaP: d^7,d^8 (in predominantly p-type GaP) and d^9 (in n-type GaP).Although the Ni (d^9) impurity had been established in GaP,the

$d^9 - d^8$ energy level had not been measured accurately and thus an investigation was carried out to establish such a level. We present a detailed photocapacitance spectra which is consistent with the Ni in the d^9 charge state. In particular the $d^9 - d^8$ level is found to have a photoionisation threshold of (0.88 ± 0.01)eV below the conduction band at 0^{o}C. A band seen in the photocapacitance spectrum shows structure which has not been previously reported.

During the course of carrying out the PCAP experiments, it was noticed that the PCAP experiment is time consuming (due to the small optical cross section of the deep impurities) and is repetitive. An automated system was required that would be capable of reproducing all the manual operations of a PCAP experiment. Certain equipment that was required for an automated system was not available commercially. An example of this is a (digital) voltmeter that has a band width of 1MHz. A system was developed around a PET$^{(TM)}$ microcomputer that was able to reproduce all the manual operations in a PCAP experiments. The system is presented in chapter 3. Although no experiments were done by the author with the system, R Hall (private communication) has used it to characterise deep impurities in semiconductors.

Chapter 4 is a study of the optical and electrical properties of dc thin film electroluminescent devices (TFED). A TFED consists of thin film of ZnS:Mn phosphor sandwiched between a transparent conducting electrode and a metal electrode. TFED's are thought to be suitable candidates for the display of digital information in a form that can be read as for example in a screen monitor and display units of the types that are used at airports and railway stations. There were a number of new properties of the device found in our study on the

TFED. One of these was that the 'capacitance' measured on a capacitance bridge corresponded to a photoconductive process.This conclusion does not agree with work published by some Japanese workers on the characterisation of a deep centre in a thin film of ZnS:Ag fabricated in a structure similar to a TFED.Two devices were studied:one where the sputtering of the active ZnS:Mn took place in an atmosphere of argon (the 'non-hydrogenated'device) and another where the sputtering of the ZnS:Mn took place in an atmosphere of argon and hydrogen (the 'hydrogenated' device).We showed that both devices have the same deep centre,although the hydrogenated device had other impurities in the band gap.An equivalent circuit for the non-hydrogenated device was found.It was found that when the TFED was in the dark,the dispersion observed in the measured equivalent circuit consisting of a series combination of a resistor and a capacitor could be decomposed to an equivalent circuit that consisted of the resistance of the contacts in series with a parallel combination of a capacitor (C) representing the ZnS:Mn as a dielectric and a resistor (R) representing leakage.When light was shone on the device,the same equivalent circuit is useful except that R and C become frequency dependent.The form of the frequency dependence of R and C is interpreted in terms of hopping conduction. We believe that this is the first time that hopping conduction has been observed in ZnS in a well characterised device.

The type of hopping conduction observed in ZnS:Mn was extended to ZnSe:Mn,a material that is similar to ZnS:Mn.The work on ZnSe:Mn is presented in chapter 5.Two samples were studied which were characterised by photoconductivity.The characterisation process revealed the existence of the so-called M centre in our samples as

well as the existence of shallow impurities that produced energy levels below the conduction band. One rather surprising result from the characterisation process was that if the dark current was subtracted from the photocurrent then the photocurrent decayed approximately as a power law once the light had been blocked off.The capacitance of the samples measured from 20Hz to 100KHz showed dispersion only when light was shone on them.The form of this dispersion was that the capacitance decreased as the frequency increased as a power law (with the exponent positive and less than unity).The dispersion of the capacitance is interpreted in terms of hopping conduction.

There are no general theories that describe the hopping conduction.The situation is further compounded by the fact that hopping conduction is seen in a variety of materials (Jonscher[5]).This in turn has led authors (especially the Chelsea group (Jonscher,Hill and Dissado)) to propose the existence of the so-called universal law connected with hopping conduction,that is $((\chi' - \chi'(\infty))/\chi'' = \tan(s\pi/2))$ where s is positive and less than unity.In chapter 6,some commonly reported models of the ac conductivity($\sigma_{ac}=\omega(\chi' + i\,\chi'')$ are analysed as to which material they apply to other than the ones that they were formulated for.The ac conductivity which is associated with hopping varies with frequency as $\sigma_{ac} = k\,f^{s}$. We show that s has a temperature dependence which is often glossed over in the literature and show that the form of this temperature dependence is a linear decrease of s with increasing temperature;the value of s at 0 K depends on the material. Use of the Kramers-Kronig relationship is usually made to compare the real and the imaginary parts of the ac conductivity.

Finally in chapter 7 some concluding remarks on the work carried out is presented

Since the work is presented in self contained chapters,it is hoped that the present discussion has to some extent unified the work.

References

(1) J W Allen and G L Pearson "Transition metal impurities in semiconductors" Stanford Electronics Laboratories: Technical report no. 5115-1 (1967)

(2) C J Ballhausen "Introduction to ligand field theory" McGraw-Hill, New York, 1962

(3) J S Blakemore "Semiconductor Statistics" , Pergamon, 1962

(4) J S Griffiths "Theory of transition metal ions" CUP, Cambridge, 1964

(5) A K Jonscher Nature 267, 673(1977)

(6) A Rose "Concepts in photoconductivity and related phenomena" Wiley, New York, 1963

(7) R A Stradling in "Recent development in condensed matter Physics" vol 1, p155 (1981)

(8) H H Theissing and P J Caplan "Spectroscopic calculations for a multielectron ion" Interscience New York, 1966

(9) A G O'Neill PhD Thesis St Andrews University 1984 Unpublished

2 GaP:Ni - Optical Measurements

2.1 Introduction

GaP is a material that is used for manufacturing LEDs.The light output from these devices is found to be controlled by the so-called non-radiative centres (sometimes called "killer centres" in LED's).These non radiative centres lose excess energy in the electroluminescence process by multiple phonon emission rather then by emitting a photon.The non radiative centres are caused by the inclusion of unwanted impurities in semiconductors during growth.

Ennen and Kaufmann (1980) have noted that the transition metal impurities,such as nickel,are fast diffusing in GaP.Nickel is a multivalent impurity with three charge states:d^7,d^8 and d^9.The d^9 configuration can act as an efficient recombination centre for holes and thus can limit,for example,the light output on the n side of a p-n junction LED by capturing the injected holes.Ennen and Kaufmann have suggested that this may account for the fact that the observed light output is better on the p side of a pn junction GaP:Zn LED than on the n side.An understanding of the nickel impurity in n-type GaP can have implications on the perfomance of commercial GaP LED's.

In this chapter ,we present a detailed spectrum of the optical electron cross section for Ni d^9 in n-type GaP.This spectrum shows a band which is due to a photothermal process,a photoionisation threshold and a dip at a photon energy of 1.24eV that has not been

seen in previous published work. This spectrum is explained on the basis that the charge state of the nickel is d^9, and the three features of the electron optical cross section spectrum are consistent with this assumption.

The free nickel atom has the configuration $[Ar]3d^8 4s^2$. The outer three electrons will go to bonding with the lattice when the nickel atom is introduced substitutionally on the gallium site in n-type GaP. Thus the neutral charge state of nickel in n-type GaP is expected to be d^7. Nickel d^7 has been detected using ESR by Kaufmann and Schneider(1979) who find the splitting of the ground state to be consistent with a charge centre of spin 4, and by Ueda et al (1983) using ENDOR who conclude the Ni d^7 to be subsititutional on a Ga site and with tetrahedral symmetry. The d^7 configuration can capture one or two electrons to form d^8 or d^9 configurations respectively. Internal transitions corresponding to Ni d^8 were first observed by Baranowski et al (1967) in absorption experiments. Liro and Baranowski (1982) later carried out piezoabsorption and Zeeman studies on the $^3T_1(P)$ state of Ni d^8. The d^9 configuration has been identified by Kaufmann et al(1979). The d^9 configuration occurs mainly in n-type GaP, although it can be created in p type GaP by irradiating light of above band gap energy (Ennen and Kaufmann (1980)). In addition to the three charge states of Ni, when large concentration of nickel occur in n-type GaP, nearest neighbour complexes can form as well as next nearest neighbours(Ennen and Kaufmann (1980)).

In experiments involving photoionisation we are measuring the energy level $d^n - d^{n-1}$ if the photoionisation involves an electron in the conduction band. In figure 2.1, the transitions of this type for nickel in n-type GaP are summarised. This figure uses the notation first put forward by Allen and Pearson (1967).

Section 2.2 describes the principle of the photocapacitance method and section 2.3 describes in particular the double light source steady-state photocapacitance (DLSS) measurements. In section 2.4 the experimental apparatus and the experimental method are described. The results are presented in section 2.5 and a discussion is in section 2.6.

2.2 Principle of Photocapacitance

A Schottky diode possesses a depletion region, that is, a region of high resistivity adjacent to the metal. Consider an n-type diode with a shallow donor of concentration N_d and a deep centre of concentration N_T that produces a deep level in the upper half of the band gap.

The differential capacitance of the depletion region is given by

$$C=\{qk/(2(V_{bi} - V))\}^{1/2}(N_d + sN_T)^{1/2} \qquad 2.1$$

In equation 2.1 V_{bi} is the built in potential and k is the dielectric permittivity of the host semiconductor. We have replaced N_T by sN_T where s is the charge of the impurity with respect to the lattice. For

Ni d^9 in GaP,s is -2.Suppose we change the impurity occupancy by an amount Δn_T, then the fractional change in the depletion layer capacitance is

$$\Delta C/C = \Delta n_T/(2(N_d + s N_T))$$

If we make the approximation of there being much more of the centres giving the shallow level than those giving the deep level,then $N_d + sN_T$ will be approximately equal to N_d.This implies that any change in the occupancy of the deep centre will be small compared to N_d.Under this approximation the above equation can be simplified to

$$\Delta C/C = \Delta n_T/2N_d \qquad 2.2$$

Making the above approximation leads to the simple result that the change in the occupancy of the deep centre is directly proportional to the capacitance change of the depletion region.In photocapacitance the change in the occupancy of the deep level is brought about by shining light on the diode.

The sign of the capacitance change can tell us which band is involved in the optical process.In the case considered above,the sign of the capacitance will be positive because we are taking electrons from the deep centre and leaving a net positive charge behind.

A further advantage of using photocapacitance lies in the fact that,apart from a Debye length at the edge of the depletion region,the capture of free electrons by the deep centre can be neglected.The main disadvantage of using photocapacitance is that it is time

consuming.One good spectrum can take a month or two to take.

To measure the differential capacitance of the diode a small ac signal is applied to the diode.The applied frequency of this signal must be such that we are only measuring the photocapacitance that is due to the "bulk" defects and not to the surface defects.These surface defects are found to be "slow responders" (Many et al (1965) and their contribution to the total capacitance of the diode can be eliminated if we apply a frequency larger then 100kHz."Bulk " defects are those that are found in the bulk of the semiconductor away from the surface.

2.3 DLSS Method

In this section we will describe the advantages of using two beams of light to study the optical parameters of deep centres in semiconductors.In the two beam experiment,a pumping light ("second light source") is used to fix the initial occupancy of the deep centre and then a monochromatic light is used to perturb the occupancy of the deep centre to produce an optical cross section spectrum for electrons or holes.One advantage of using two light beams is to make one of the optical cross sections (either electrons or holes) negligible in the experiment.To show this,consider the diagram shown in figure 2.2.If the effect of the second light source was such that it emptied the impurity centre of electrons, then $e_n^o n_T$ will be negligible compared to $e_p^o p_T$ and so the monochromatic light will only measure the hole emission constant. Here n_T is the concentration of electrons localised at the impurity centre,p_T is the hole occupancy of the impurity centre,e_p^o is the optical hole emission constant and e_n^o is the

optical emission constant for electrons. Hence by fixing the initial occupancy of the deep centre one can study e_n^o and e_p^o separately, even when they are of nearly equal magnitude. If many centres are present in the band gap of the material, then the second light can be used to fill one centre with electrons or holes and the monochromatic light can be used as before.

Figure 2.2 shows an infinitesimal region of the depletion region. A light source is filtered to lie in the energy range $E_T - E_v < h < E_g$ thus ensuring that the deep centre is initially occupied mainly by electrons. A monochromatic light of much lower intensity than the first light is then used to perturb the occupancy of the deep level.

When the second light is switched on the rate equation describing the change in the impurity electron occupancy is

$$\dot{n}_T = -(e_{ns}^o + e_{ps}^o)n_T + e_{ps}^o N_T \qquad 2.3a$$

In steady-state

$$n_T = e_{ps}^o N_T/(e_{ps}^o + e_{ns}^o) \qquad 2.3b$$

When the monochromatic light is switched on in addition to the second light, the steady-state change in the impurity electron occupancy will be given by

$$n_T = e_{ps}^o N_T/(e_n^o + e_{ns}^o + e_{ps}^o) \qquad 2.3c$$

The steady-state change in the impurity electron occupancy produced by the monochromatic light alone is given by subtracting 2.3b from 2.3c. This is given by

$$\Delta n_T = \{e^o_{ps} N_T / (e^o_{ns} + e^o_{ps})^2\} e^o_n \qquad 2.3$$

To derive equation 2.3 we have made use of the condition $e^o_{ns} + e^o_{ps} >> e^o_n$. In equation 2.3 we have the result that the steady-state change in the capacitance is proportional to the optical emission constant. The optical emission constant divided by the incident flux is the optical cross section.

2.4 Experimental Detail

The experimental apparatus for measuring the capacitance is shown in figure 2.3. The bridge is a specially constructed one and it has been used for photocapacitance work previously. Consequently it has been characterised (Szawelska (1980)). The important result of this characterisation is that the off-balance signal observed on the chart recorder is directly proportional to the change in the capacitance.

The diode was fabricated by H. Szawelska . Szawelska and Allen (1982) have described how this diode was fabricated. The diode was connected to a cold finger using pressure contacts. The cold finger was connected to a bath in a home-made cryostat. In the bath ice and an acetone - CO_2 mixture were used to give temperatures of 0^oC and -76^oC

respectively.The temperature was measured on a CRL 207 digital thermometer.

To the diode a 400kHZ signal with a p-p value of 18mV was applied.This signal ensures only bulk traps are able to follow the applied signal and that the diode can be represented by its small signal equivalent circuit.

The procedure for producing a DLSS spectrum was to balance the dark capacitance of the diode.Then a light from a 60W tungsten-halogen lamp ,after passing through Kodak Wratten filter 23A and Ealing filter 263053,was shone on the diode.This filtered light lay in the energy interval (1.8,2.0)eV. The off-balance signal produced by this light (the "second light source"),was monitored on the chart recorder until a steady signal was observed.The bridge was rebalanced to offset this large capacitance change.Light from a Bausch and Lomb monochromator is then used to excite electrons from the deep level into the conduction band and the resulting off-balance signal produced by the monochromatic light is monitored on the chart recorder until a steady signal is observed.The monochromatic light is blocked by closing a shutter.Once a steady signal is observed with the diode in the dark,the wavelength of the monochromator is changed and the procedure outlined above is repeated. The automated photocapacitance method is described in the next chapter.

The monochromator uses a diffraction grating to produce the monochromatic light. To remove the second order wavelengths, a Grubb Parsons Si filter was placed at the exit of the monochromator for photon energies between (0.6,0.9)eV,while for photon energies between

(0.9,1.3)eV a Grubb Parsons GaAs filter was placed. The band pass of the monochromator for wavelengths between 1.98 μm and 1.40 μm (0.60eV to 0.90eV) was 0.01 μm and for wavelengths between 1.39 μm and 0.98 μm (0.9eV to 1.30eV) it was 0.013 μm.

One method of ensuring the second light source was of a greater intensity than the monochromatic light was to measure the photocurrent produced by the two light sources.This was done by connecting the diode to a Keithley 616 electrometer.The flux of the monochromatic light was measured in relative terms by connecting a Hilger Schwartz thermopile to a Keithley 155 null detector microvoltmeter.

One of the main difficulties of doing any experiments,which is most certainly true for photocapacitance,is the noise in the signal that we are trying to observe.To reduce this noise,various steps were taken.The noise caused by the coaxial cables picking up noise was reduced by making the lengths of these cables as short as possible.Mains-borne "spikes" that are caused by electrical equipements being turned on and off were reduced by operating the signal generator and the pre-amplifier from a mains line conditioner. The pre amplifier had in addition a mains filter to reduce the mains noise even further.(It was also found that the best time to run the photocapacitance experiments was at night when the mains-borne noise was the least.) From the pre amplifier the signal was fed into a passive RLC band pass filter with the centre frequency of the filter at 400kHz.Finally to reduce the effect of the stray radiation,we worked from outside the dark room and only entered it when it was necessary to change the wavelength of the monochromator.

2.5 Results

The results of the DLSS experiments are shown in figures 2.4 to 2.7.Figures 2.4 and 2.5 show a band in the DLSS spectrum at $0^{o}C$ and $-76^{o}C$ respectively.This band is due to photothermal excitation of an electron from a ground state of a deep level.The kinetics describing this situation are shown in appendix 2A.In figure 2.4 a large onset in the spectrum occurs at 0.70eV. A reason for this large onset can be given if we assume the charge state of the nickel is d^{9}.The zpl of Ni d^{9} is 0.664eV (Kaufmann et al (1979)) and a 31meV phonon has been shown to exist in n-type GaP (Kaufmann et al (1979)). This large transition is due to the optical transition to the first excited vibronic level.The band at the lower temperature shows additional peaks at 0.72eV and 0.76eV.For single phonon participation,additional peaks are expected to occur at 0.73eV and 0.76eV.This is in reasonable agreement with the experimental data.The full width at half maximum is 0.095eV at $-76^{o}C$ compared with 0.17eV at $0^{o}C$.

Szawelska and Allen (1982) and Yang et al (1984) have also observed this band in their photocapacitance experiments.The band was not resolved by them and they assumed the band to have a Gaussian shape to do further analysis . A band seen in say absorption experiments that does not show any structure,and has a Gaussian shape is a classic example of a system that shows evidence of strong electron- phonon coupling.Thus the value of the number (the Huang Rhys S) which indicates the level of the coupling has been overestimated both by Szawelska and Allen (1982) and by Yang et al (1984).

Figure 2.6 is the spectrum showing the photoionisation of the Ni d^9 impurity over a wider spectral range.There is a photoionisation threshold near 0.9eV and a second threshold near 1.2eV.The dip seen in figure 2.6 is shown on an expanded scale on figure 2.7.The position of the dip corresponds to the $^3T_1 - {}^3T_1$ transition of isolated Ni d^8.Since the $d^9 - d^8$ level lies $\sim$ 0.9eV below the conduction band then the $d^8 - d^9$ level lies $\sim$ 1.35eV above the valence band.In a process involving a photothermal excitation of a hole to the valence band from d^8 (and thereby converting it into d^9) the order of 1.24eV energy is supplied by the photons and the remainder is supplied through phonon absorption.Ni d^8 is produced from photoionisation of Ni^9 and then the photoionisation of d^9 competes with the internal transition of d^8 which results in the d^8 converted into d^9.

For photoionisation a model has been proposed by Allen (unpublished).In this model the initial wavefunction of the localised electron is an evanascent one and its final wavefunction is that of a plane wave.The result of the calculation is,near the threshold of photoionisation,the optical cross section varies with photon energy as

$$\sigma(h\nu) \sim (h\nu)^{-1}(h\nu - h\nu_o)^{3/2}$$

Figure 2.8 shows a graph of $(\sigma h\nu)^{2/3}$ vs $h\nu$.From this graph a photoionisation threshold of (0.88 ± 0.01)eV is obtained.This threshold is significantly different from the threshold found by Szawelska et al (1981) from their absorption and photocapacitance data.The apparent discrepancy in the threshold values can be explained by noting that over a large range of Ni concentration,Ni complexes can form (Ennen and Kaufmann (1980) and Baranowski et al (1982)).A nickel

related centre will have a large value of the optical cross section because of the reduced symmetry around this complex.This nickel related centre may occur in "small" concentration but its absorption coefficient is greater than that for Ni d^9.In the absorption spectrum reported by Szawelska et al (1982) for GaP:Ni a bump was seen which roughly correlated with the zero phonon $^2T_2$ - ^2E electron transition of Ni d^9 in n-type GaP.The value of the photoionisation threshold found from the rising part of the absorption spectrum was smaller then the photoionisation threshold found from the DLSS data The absorption spectrum reported by Szawelska et al therefore has the two effects superimposed;the rising part of this spectrum being dominated by the Ni related centre.

Szawelska et al (1982) noted the difference between the absorption and the photocapacitance spectra of nickel in n-type GaP.This difference was tentativly suggested to be related with the electric field in the depletion region of the Schottky diode. The difference in the two spectra can be understood if there is a nickel related complex and the Ni d^9 in n-type GaP. In the transient photocapacitance technique, the optical cross section and the impurity concentration are measured separately whereas in the absorption experiments we measure the product of these two quantities.In light of what has been said above we can say that the photocapacitance experiments have measured the properties of the Ni d^9 while the rising part of the absorption spectrum is dominated by the nickel related centre. Thus we can say that there are two charge centres present;one centre that dominates the absorption experiment ,reported by Szawelska et al, (the nickel related centre) and the Ni d^9 that dominates the photocapacitance experiments.

2.6 Discussion

The band seen in the DLSS experiments is an internal transition of Ni d^9 as shown by the structure of the band. This structure is resolved and is probably due to a 31meV phonon involved in the photothermal process. Although two other groups (Szawelska and Allen and Yang et al) have observed this band in their photocapacitance experiments ,they have not been able to resolve the structure of this band.

A previously unseen feature in the electron optical cross section is the appearance of a dip at 1.24eV.This dip can be explained by assuming the charge state of the nickel in n-type GaP when the diode is in the dark is Ni d^9. When a photon of energy 1.24 eV is incident on the diode,internal transitions of Ni d^8 will be competing with the photoionisation of Ni d^9 into d^8.Since the d^9-d^8 level is 0.9eV below the conduction band then the d^8-d^9 level will be 1.35 eV above the valence band.The incident photon energy supplies 1.24eV and the and $\sim$ 0.1eV will be supplied by phonon absorption.Thus in a photothermal process involving an electron from the valence band some of the Ni d^8 will be converted into Ni d^9 again. This dip is a strong evidence that the charge state of the nickel in n-type GaP is d^9.

We showed above a photoionisation threshold that occurs at 0.88eV.This is the energy required to convert Ni d^9 into Ni d^8 with an electron in the conduction band.Our value of the d^9 - d^8 energy level of Ni is slightly higher than that reported by Yang et al (1984).This is because our value of the photoionisation threshold is found at a

higher temperature than Yang et al.

In conclusion, the charge state of the nickel in n-type GaP is d^9 and the $d^9 - d^8$ energy level of the nickel impurity is 0.88eV below the conduction band. The band seen in the DLSS spectrum is consistent with the internal transition of Ni d^9.

Appendix 2A

Diagram 2.9 show a small region of the depletion region with a deep level that possesses an excited level and a ground state. The various symbols are now defined. The symbol "e" stands for emission with the superscript "o" for the optical and "t" for the thermal processes. The subscript n is for the change in the occupancy of the deep level caused by the monochromatic light and "ns" as that caused by the secondary light source. A further quantity that needs to be defined is c^* which is the probability of an electron in the excited state being captured by the ground state.

We can write down the rate equations for the electrons in the ground state and in the excited state when only the secondary light source is shone on the diode, in obvious notation, as

$$\dot{n}_{Tg} = = e^{o}_{ps} p_T + c^* n_{Te} - e^{o}_{ns} n_{Tg}$$

$$\dot{n}_{Te} = -(e^{t} + e^{o}_{1ns} + c^*) n_{Te}$$

If the lifetime of the excited level is large then n_{Te} will be approximately zero. Thus

$$n_{Tg} = e^{o}_{ps} N_T / k_1 \qquad (1)$$

where $k_1 = (e^{o}_{ps} + e^{o}_{ns})$. When the monochromatic light is shone on the diode the rate equations for the two states become

$$\dot{n}_{Tg} = -(k_1 + e^o_n)n_{Tg} + e^o_{ps}N_T + (c^* - e^o_{ps})n_{Te}$$

$$\dot{n}_{Te} = -(e^o_{1ns} + e^t + c^*)n_{Te} + e^o_n n_{Tg}$$

In the last two equations we have used the relation $N_T = n_{Tg} + n_{Te} + p_T$. In steady-state the last two equations give

$$N_{Tg}/N_T = e^o_{ps}k_2/D_1$$

$$n_{Te}/N_T = e^o_n e^o_{ps}/D_1$$

Where $k_2 = e^t + e^o_{1ns} + c^*$ and $D_1 = (k_1 + e^o_n)k_2 - [(e^o_{ps} - c^*)e^o_n]$. Thus the total change in the electron occupancy produced by the monochromatic light and the secondary light is

$$n_T/N_T = e^o_{ps}(e^o_n + k_2)/D_1 \qquad (2)$$

Subtracting (1) from (2) we get the change in the electron concentration produced by the monochromatic light alone

$$\Delta n_T/N_T = \{[k_2 - c^* - e^o_{ns}]/(k_1^2 k_2)\}e^o_n$$

When there is direct photoionisation of the impurity centre then e^t and c^* can effectively be put to zero at low temperatures. Then the change in the electron concentration produced by the monochromatic light is

$$\Delta n_T/N_T = \{e^o_{ps}/(e^o_{ps} + e^o_{ns})^2)\}e^o_i$$

References

S.A Abagyan,G.A Ivanov and G.A Koroleve

Sov Phys Semicond 10,1056(1979)

J W Allen and G L Pearson

Stanford Electronics Report no.5115-1 (1967)

J M Baranowski,J W Allen and G L Pearson

Phys Rev 167,758(1967)

J M Baranowski,Z Liro and M Jezewski

Proc of the 16th conference on Semiconductors (Montpellier)

(1982)

S G Bishop,P J Dean,P Porteous and DJ Robbins

J Phys C13,1331(1980)

H Ennen and U Kaufmann J Appl Phys 51,1615(1980)

H Ennen,U Kaufmann and J Schneider

J Appl Phys L13,335(1981)

S Fung and R Nicholas J Phys C15,7355(1983)

H Grimmeiss and C Ovren J Phys E14,1031(1980)

W Hayes,R F Ryan,C L West and P J Dean

J Phys C12,L815(1979)

Z Liro and J M Baranowski J Phys C15,4599(1982)

U Kaufmann,W H Kochel and J Schneider

Phys Rev B19,3343(1979)

U Kaufmann and J Schneider Sol Stat Comm 25,1113(1979)

A Many,Y Goldstein and H Grover "Semiconductor Surfaces"

North Holland Publ. Comp.,Amsterdam (1965)

M S Saidov,K Abdrimov,A S Saidov and V G Makarenko

Sov Phys Semicond 17,332(1983)

H R Szawelska PhD thesis (1980) St Andrews University

H R Szawelska,J M Noras and J W Allen

J Phys C14,4141(1981)

H R Szawelska and J W Allen (1982) unpublished

Y Ueda,J R Nichlas,J M Spaeth,U Kaufmann and J Schneider

Sol Stat Comm 46,127(1983)

X-Z Yang,L Samuelson and H G Grimmeiss

J Phys C17,6521(1984)

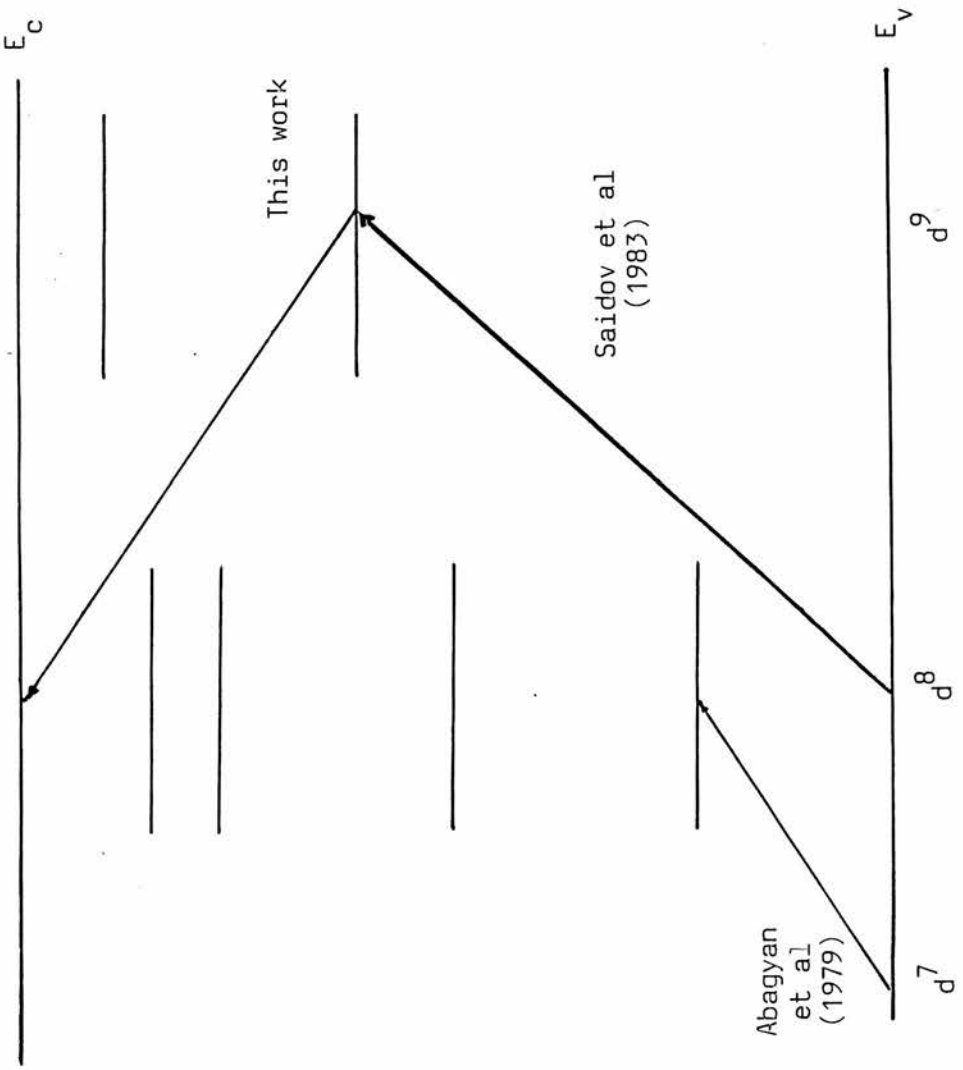

Fig 2.1 Summary of nickel transitions in GaP.

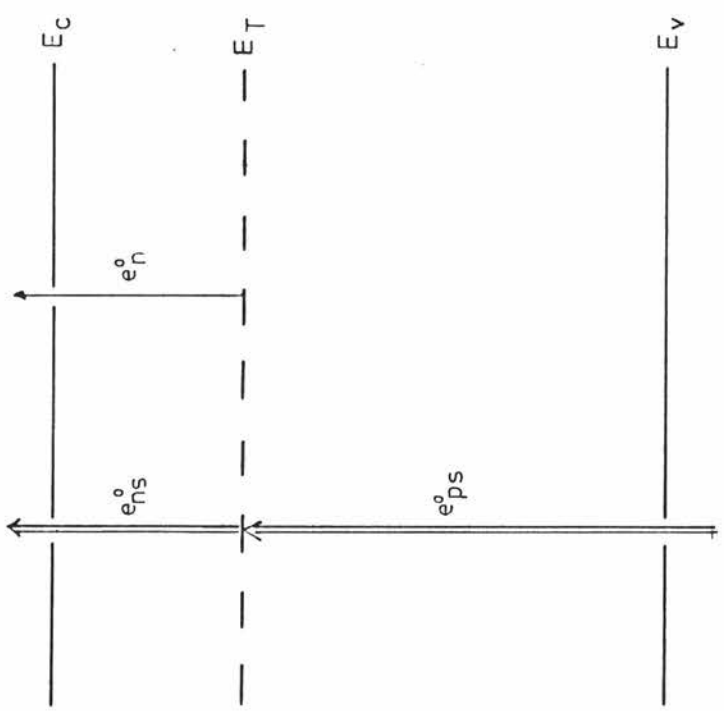

Fig. 2.2 Principle Of A DLSS Experiment

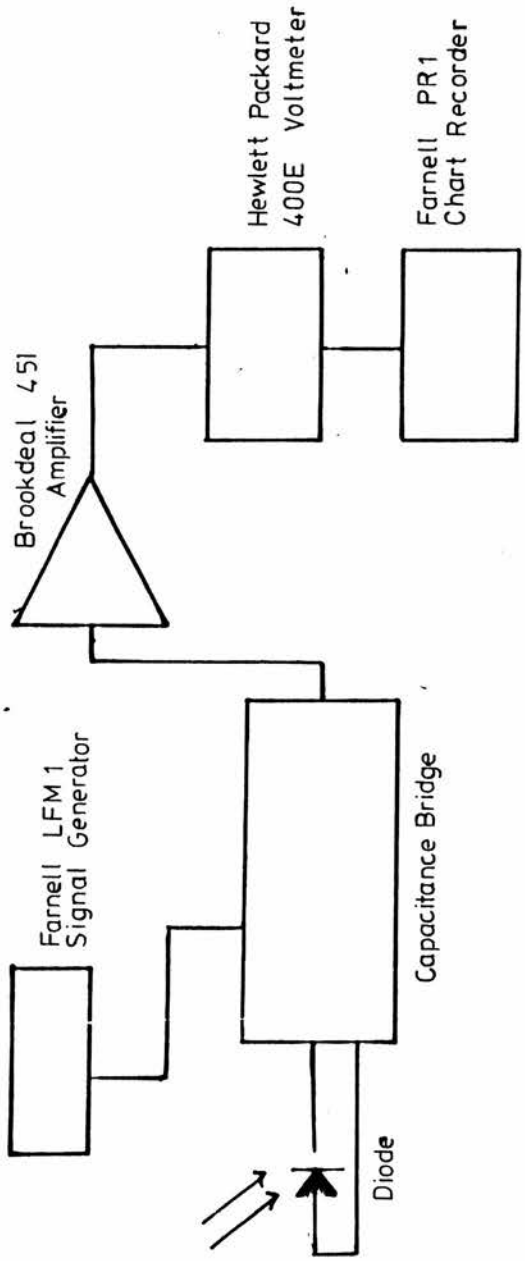

Fig. 2.3 Schematic Diagram Of Experimental Apparatus

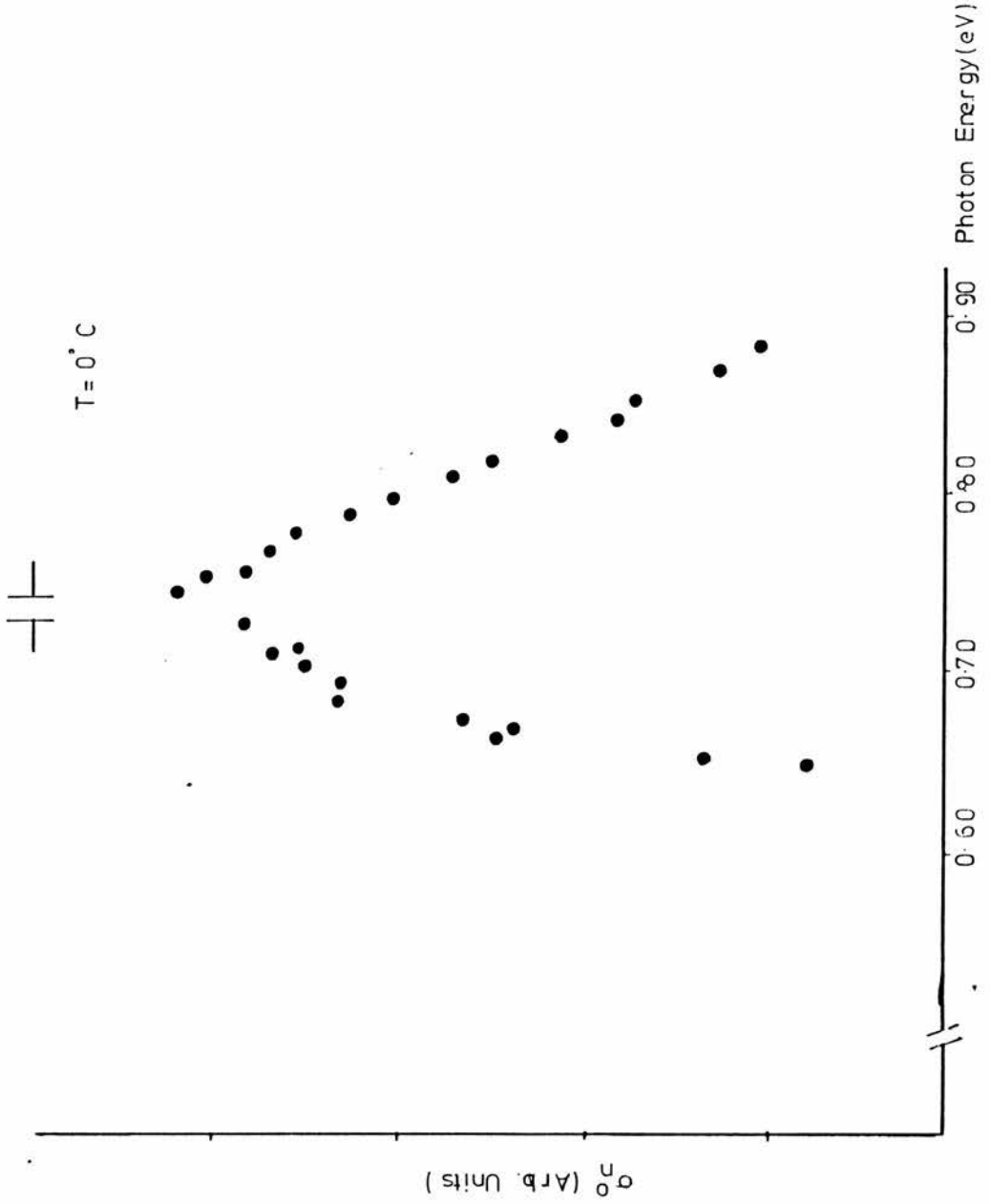

FIG 2.4

DLSS Spectra at 0°C

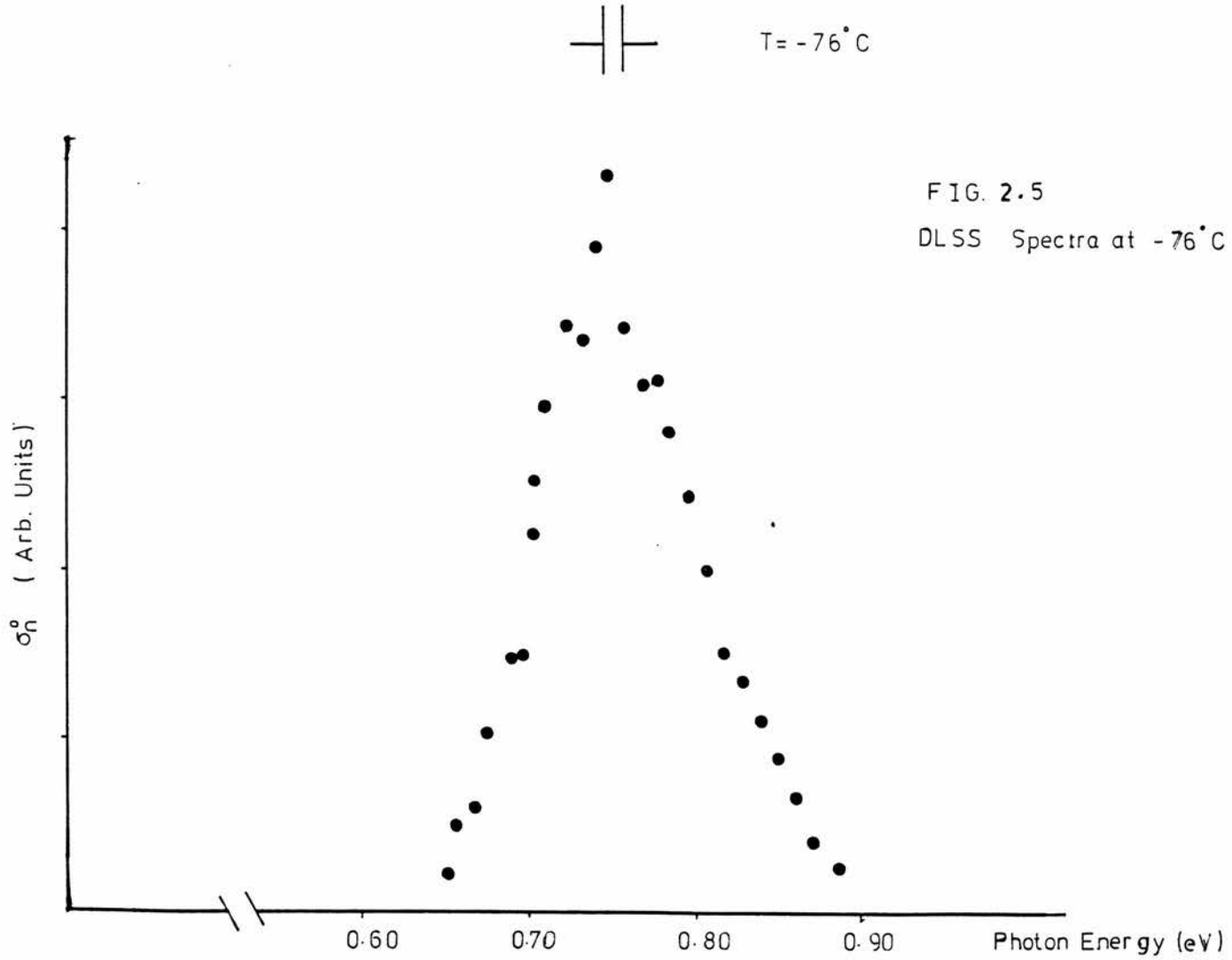

FIG. 2.5
DLSS Spectra at -76°C

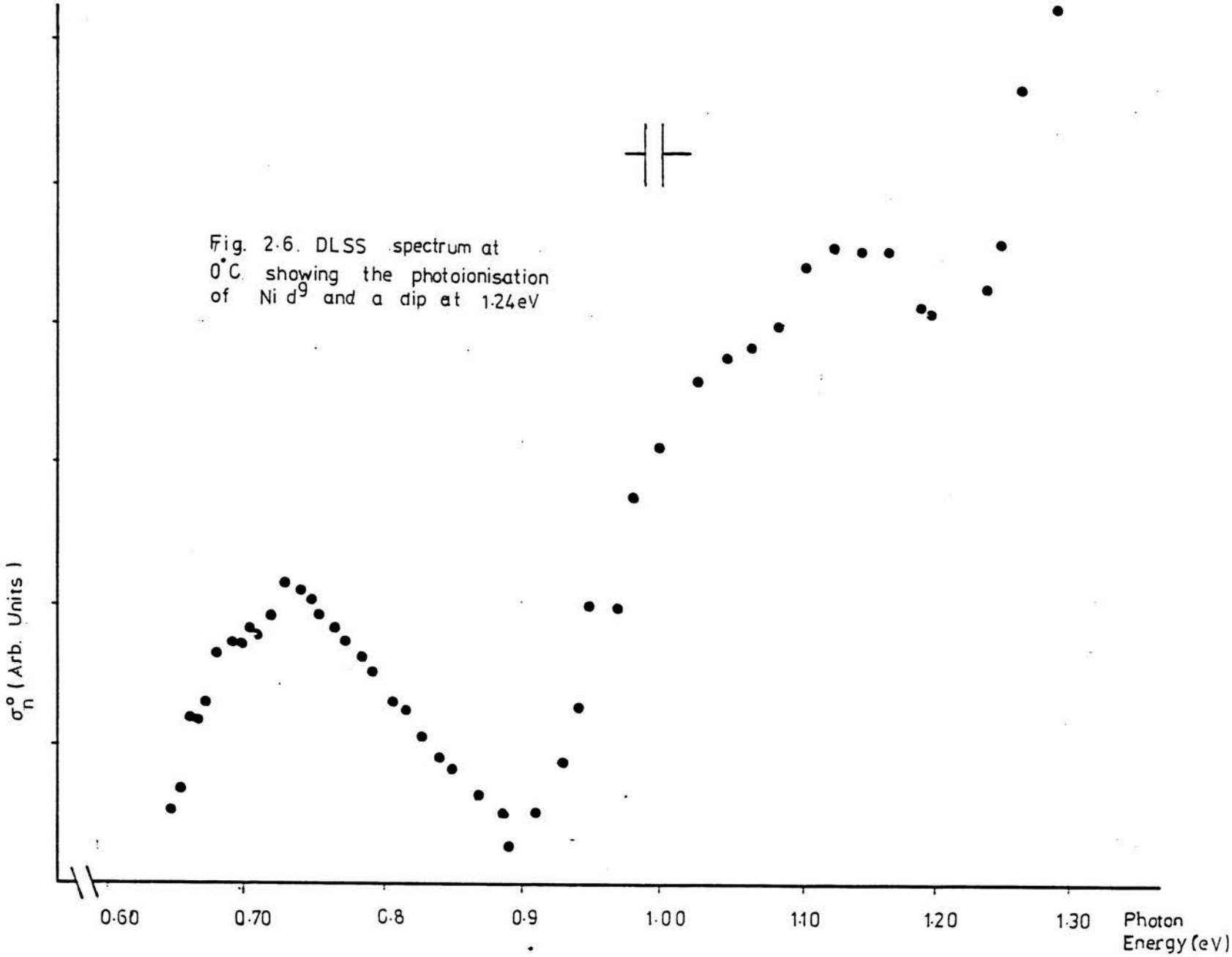

Fig. 2·6. DLSS spectrum at 0°C showing the photoionisation of Ni d^9 and a dip at 1·24eV

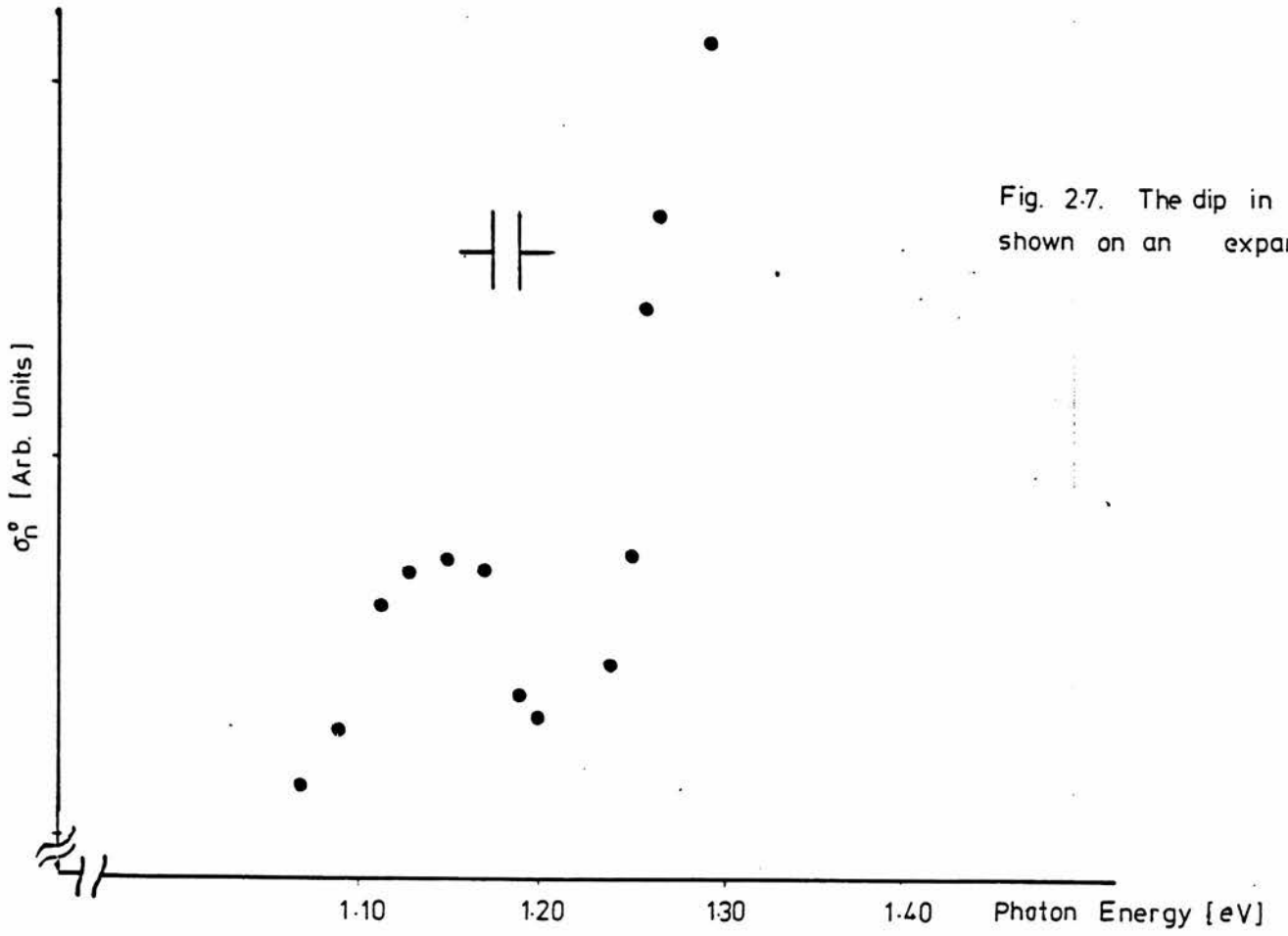

Fig. 2·7. The dip in fig. 2·6 shown on an expanded scale.

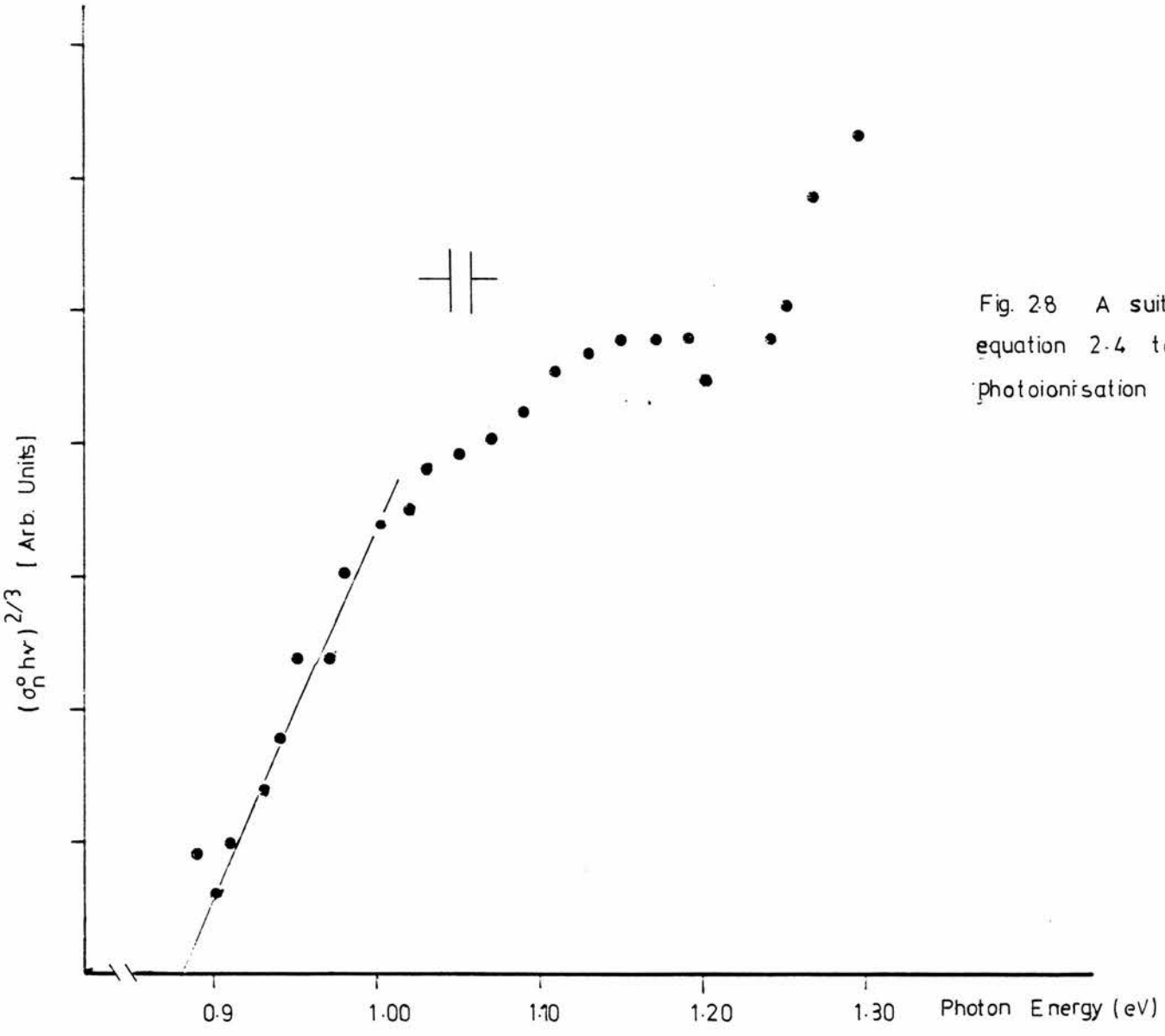

Fig. 2·8 A suitable plot of equation 2·4 to find the photoionisation threshold

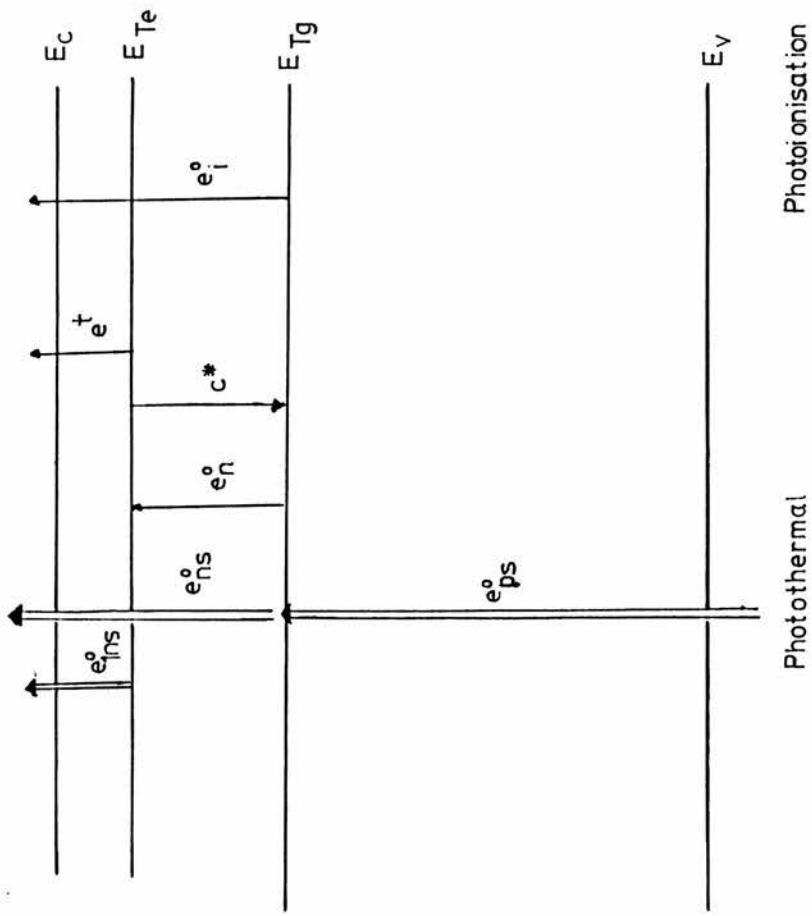

Fig. 2.9. Transitions involved in a DLSS experiment when a two level impurity exists in the upper half of the band gap.

3 The automated capacitance method

In this chapter a method of automating the photocapacitance (PC) is presented.This method was initially developed for the DLSS photocapacitance method that was used to study nickel in GaP.Modification of the program for the transient photocapacitance method is indicated .The automated method described here is also ideally suited for other photo-experiments,such as photoconductivity.The over-all view of the automated system is shown in figure 3.1.

This chapter is divided into three sections.Section 3.1 explains what the human operator does in the photocapacitance experiments.This section also establishes the principle of automating the PC experiment.In section 3.2 the various boards developed will be described and section 3.3 will describe how all these boards are connected together to form the complete automated system. We conclude this chapter with some experimental plots of PC transients and the measured points using the automated system.

3.1 PC under human control

In this section we will describe how the PC spectrum is taken by the human operator.The flow chart describing the steps for one transient of the DLSS method is shown in figure 3.2a.The modification to this flow chart for carrying out the transient photocapacitance method is indicated. The human operator follows a repetitive pattern

of opening the shutter,waiting for a steady signal to appear on the chart recorder and recording the steady state values of the signal;the shutter will then be closed and the wavelength of the monochromator will be incremented.He will do this for each wavelength of interest.

The method described is repetitive and hence it is ideal for microprocessor control.In figure 3.2b the flow chart in more mathematical terms is described.

The condition "is the trace steady" now reads "if two consecutive readings from the voltmeter lie within a specified interval then the trace is steady". The rest of the steps in figure 3.2b are the same as in figure 3.2a but now these steps will be under computer control.

We have not mentioned in the above chart flows how reading the temperature of the sample will be made.The temperature is only read occasionally and this can be achieved in the automated PC method by utilising a counter. Once this counter reaches a specified value then the temperature reading will be taken and the counter will be put to zero.The counter will then be incremented.

3.2 Sub-systems to automate the PC method

In this section the various circuit boards (sub-systems) needed to make the automated system will be described.Figure 3.1 is a schematic diagram of the system constructed.We see that the system is developed around the PET$^{(TM)}$ microcomputer.

Most of the boards developed used the serial-to-parallel converter.The method of synchronising the serial data from the 6522 VIA (which is the USER port of the PET) is presented in appendix 3B.In section 3.2.1 the interface developed to place a bias on the diode is described.This sub-system is the least complex of the interfaces developed.An understanding of this interface will help to understand the other two major interfaces.Section 3.2.2 describes the temperature - PET interface.This interface is assembled around the control and readout logic model 207 (CRL 207).In section 3.2.3 the most complex interface developed is described.This interface was to take serial four bit data into the PET.An interface,based on the IEEE 488 bus,was purchased from Glen Creston Limited to automatically select the wavelength of light emerging from the exit of a Spex 'Minimate' monochromator.Finally an interface to open and close a shutter will be presented in section 3.2.4.In section 3.3 the interconnection of all these sub-systems is made.

3.2.1 Bias control

There are cases in photocapacitance when there is a need to put a bias on the diode.The case which we mean here explicitly is the transient photocapacitance method.In this method,a forward bias pulse is used to fill the deep centre (with electrons) after the monochromatic light has emptied the centre of electrons.

The interface developed is the most easily understandable one .It employs a serial-to-parallel converter (SPC),a digital-to-analogue converter (DAC) and an amplifier.The action of the serial to parallel converter is described in some detail in appendix 3B.The control line CB2 is also used for the temperature and the voltmeter interfaces.Furthermore,we cannot employ the MR (master reset) to control when the SPC works (as this trick,as will be shown later, has already been used with the other two interfaces).One method of controlling when this SPC works is to AND the CB2 line and the line that controls the MR of the SPC.This method will then ensure that data will be input into the SPC when we want data to enter it.

Once the required bit pattern on the SPC has been achieved then the enable line of the DAC will be changed and an analogue representation of the digital data will appear at the output of the DAC.

This analogue signal can then be amplified to the maximum bias that we wish to apply to the diode.The amplifier we have chosen is a low noise bifett opp-amp with feedback to give the amplifier a gain of 1.9.The software to drive this interface is described in figure 3.3.The complete diagram of the bias interface is shown in figure 3.4.

3.2.2 The temperature interface

In order to understand how this interface works,an understanding of the output from the the CRL 207 is required.The CRL 207 is a microprocessor based temperature indicator.The displayed reading is isolated from the input and made available on the output port of the unit in parallel form.By this we mean the displayed reading is presented as four bit words,ie each digit is four bits long.In addition there is a bit that indicates whether the data is valid and another bit that signifies the sign of the reading.(The displayed reading is in degree centigrade.)

In carrying out the photocapacitance experiments it is highly unlikely that the temperature range of interest will span a few hundred degree centigrade. Thus we only need to look at three digits at any time,which will be sufficient to indicate this temperature range.The interface developed for reading the temperature indicator is shown in figure 3.5.Data on the output port of the CRL 207 is only valid for 0.7s before it is updated and the new temperature is displayed and made available on the output port.Thus the parallel data from the CRL must be latched and then this reading can be processed. The latched parallel data is routed to a 16 bit multiplexer.The 12 bit data from the multiplexer can then be multiplexed out by the control lines s_o to s_3 permuting through all combinations.Simple software can then be used to convert this serial data to the displayed reading.The flow chart to read the temperature indicator is shown in figure 3.5a and the software is presented in figure 3.5b.

3.2.3 The voltmeter interface

This interface was developed to convert the analogue signal from the output of the Hewlett-Packard hp 400E to a digital representation using a precision analogue-to-digital convertor (ADC).The precision ADC is the Analogic AN2574 which has effectively 18 bit resolution.The Analogic AN2574 incorporates a precision ADC,display drivers,display unit and an output port.On the output port the displayed data is presented as a serial 4 bit data,as shown in appendix 3C.(This figure is reproduced with kind permission from Analogic Limited.)

Thus the output port presents data as a four bit word at a time corresponding to the display digits.The digit that is represented as a four bit word is denoted by the logic level of the digital strobe lines D_0 to D_3. If the logic level of the strobe is HIGH,then the digit corresponding to the strobe value will be presented as a four bit word on the 4 data lines.Thus if D_0 is HIGH then the least significant digit will be presented on the 4 bit data lines.As the strobes go through all the four full digits sequentially, then each displayed digit is presented sequentially on the four bit data lines.

The interface developed was able to convert this complex data transfer into bit serial data transfer.This serial data is processed under simple software control to read the digital reading displayed by the analogic.The circuit design for reading the displayed reading on the AN2574 is shown in schematic form in figure 3.6 and the actual wire diagram is shown in figure 3.7.

To understand how this interface works let us work from the analogic side of the interface.The output from the analogic presents data on the "data" lines for 0.8ms before this data is changed and the next digit is placed on the data lines.

The interface must be able to latch the data for a particular digit and then read the value of this digit.This must be done for each of the four full digits. To do this,the digit strobes are fed through one port of the 2x4 bit multiplexer and the output from this part of the multiplexer is taken to the clock input of a shift register.One of the outputs from this shift register is used to control a latch.The inputs to this latch come from the 4 bit digit data representing the value of the digit strobe.

To read a particular digit the following procedure was found to be convenient.The A side of the 2x4 bit multiplexer (MUX) is disabled and the B side of the MUX is enabled.The address lines s_o and s_1 are given values to take a particular digit strobe to the input of the shift register(SR). The D_n inputs on the SR are taken low so that the latch will be transparent to the digit inputs (the digit value).Then the D_n are taken low and thus data will be latched.The B side of the MUX is now disabled and the address lines s_o and s_1 go through all possible combinations to read the bits of the four bit word.Simple software is then used to convert these bits to the number displayed on the analogic display.

The function of the other components on the board will now be described. The SPC has already been described. The first three bits from the SPC go to latch (latch$_1$) and from the output of latch$_1$ they go to the enable lines of the MUX and to the SR's D_n inputs. The fourth bit is used to look at the value of the 1/2 digit. The 1/2 digit is either HIGH or LOW and thus there is no need to go through the above complex procedure. We need an OR gate so that we can either look at the 1/2 digit and the full digits sequentially. If the control line from latch$_1$ is held LOW then the output from the AND gate will be LOW and the data being read will be the four digits. If both ports of the MUX are disabled and the control line to the AND gate is HIGH then the output from the OR gate will reflect the 1/2 digit.

The full flow chart diagram showing how data is read is shown in figure 3.8a and the BASIC version of this flow chart is shown in figure 3.8b. In BASIC The typical time to read the analogic display was 9 seconds. This time of reading can be improved by employing a system that has a "fast" BASIC then the PET or by using the machine code facilities on the PET.

3.2.4 The shutter interface

The mechanical design of the shutter is shown in figure 3.9. It is basically just a rotary solenoid. A blackened copper-nickel plate was fastened on this solenoid. By energising the coil we could move the metal plate across the aperture of the monochromator. This shutter, although primitive, is ideal for the photocapacitance work. The

shutter interface (developed by the electronics workshop in the Physics department) is simply a power supply with a control line from a TTL gate.A HIGH on this TTL gate will open the shutter and LOW will close the shutter.The circuit diagram showing the design of the shutter interface is shown in figure 3.10.

3.3 Interconnection of the various sub-systems

The interconnection of the various sub-systems developed above is shown in schematic form in figure 3.11.The right hand side of this figure is the USER port and PA0 through PA7 constitute the 8 bits of this port.

The temperature interface and the voltmeter interface both use the SPC and multiplexers to process the data from their respective units.We can decide from which of the two interfaces we want to take data. This is accomplished using simple hardware.The component which do this function is the inverter labelled I.If the voltmeter interface is enabled then the temperature interface will be disabled.(That is,if the MR is high on one of the SPC's then it must be LOW on the other SPC.)

The outputs from the temperature interface and the voltmeter interface are ORed together;this ensures we can take the output from the two interfaces into a single bit on the VIA.The control line (clock),CB2,connects the three interfaces as shown.

The inverters and the OR gate in figure 3.11 were made on a separate circuit board.This extra buffering ensures an extra protective layer between the interfaces and the PET VIA.(A 20p chip is a lot quicker,and cheaper,to replace than a computer!)

The various sub-systems made were written in modular form so that they could be used on their own or in a much larger program.In figure 3.12 we have shown how the rise (and decay) of a transient in a DLSS experiment can be digitised. We can see from this figure that the "digital transient" and the "analogue transient" are in very good agreement with each other.The data in figure 3.12 is for GaP:Ni.The use of the system to do experimental work will be presented else-where.

In conclusion,the system developed above is capable of carrying out optical experiments on semiconductors under microprocessor control.

Appendix 3A

In this appendix we will describe how the Commodore PET communicates with devices that are external to it.On the PET there are two input/output (I/O) ports:the so-called USER port (based on the 6522 versatile interface adaptor (VIA)) and the IEEE port.

The IEEE port is designed for connecting devices that use the IEEE 488 bus interface (or the general purpose interface bus(as named by its inventors - Hewlett Packard)).On this port we can connect a printer,disc drives or any device that makes use of the IEEE 488 bus.In particular a total of 15 devices can be connected to the IEEE port.The speed of the system will then by limited by the slowest device.One caution in using the Commodore version of the IEEE device is that a "timing error" will occur if no data is received in 0.7seconds. (This feature is not part of the true IEEE 488 interface.)The IEEE port therefore needs no further interfaces and allows the user to connect directly to any device that operates on the IEEE 488 bus principle. The Glen Creston stepper motor control is based on this interface.

The USER port,on the other hand is,a much more useful in the sense that its properties can be used by the user.There are two sides to this port-the A side and the B side.The B side is used in the timing control of the IEEE port.Thus useful interfacing can only be done with the A side of this port.The A side of the port is 8 bits long.These bits can be configured in the output mode or in the input mode.In addition to these bits there are two very useful bits for use

in cases where the data from the PET must be synchronised.These bits are called CB2 and CA1.The CB2 line can be used in the input and in the output mode whereas the the CA1 line can only be used in the input mode. The use of the VIA is therefore to treat it just like any other memory location in the computer.Data can be written to this port whence lines PA0 to PA7 will be transmitting data or we can receive data from the VIA port,whence data will be input into VIA from external devices.The memory map of the 6522 VIA,as applicable to the PET,can be found in the book by Hampshire (1980)

In conclusion,the I/O ports of the PET can be used to communicate with instruments that use a standard interface (the IEEE 488 bus) or to communicate with interfaces tailored to the specification of the user (the USER port).

Appendix 3B

The interface developed to make use of the USER port made extensive use of the serial-to-parallel convertor(SPC).In this appendix we will describe how serial data from the USER port was converted into parallel bits (this effectively gives us more lines to connect to various units).

The SPC converts serial data into n bit parallel bit data.For the 74164 SPC n is 8.Diagram 3B.1 is a schematic diagram of the 74164 and the truth table associated with it.This diagram also shows the timing sequence to convert the serial data to parallel form.

To convert serial data into parallel data ,the MR (master reset) is set HIGH and data at the input pin of the SPC will be right shifted on the positive transition of the clock.This suggests that some form of synchronisation must be done between the serial data input and the clock signal.The clock signal must only change when there is data on the input of the SPC.

To do this the CB2 line on the USER port is configured as an output line and is used as a clock signal.It can be toggled up and down using software.On one line of the USER port (ie one of the PA0-PA7 lines) the data to be converted into parallel form is placed.This line is connected to the input of the SPC. The CB2 line is toggled up and down and the data on the input pin of the SPC will be right shifted.This is done for the required parallel bit pattern.

References

N.Hampshire "PET Revealed" Nick Hampshire Publishing (1980)

C.L Hallmark "the Master IC Cookbook TAB (1980)

Texas TTL Data book

PET manual (version 4.0)

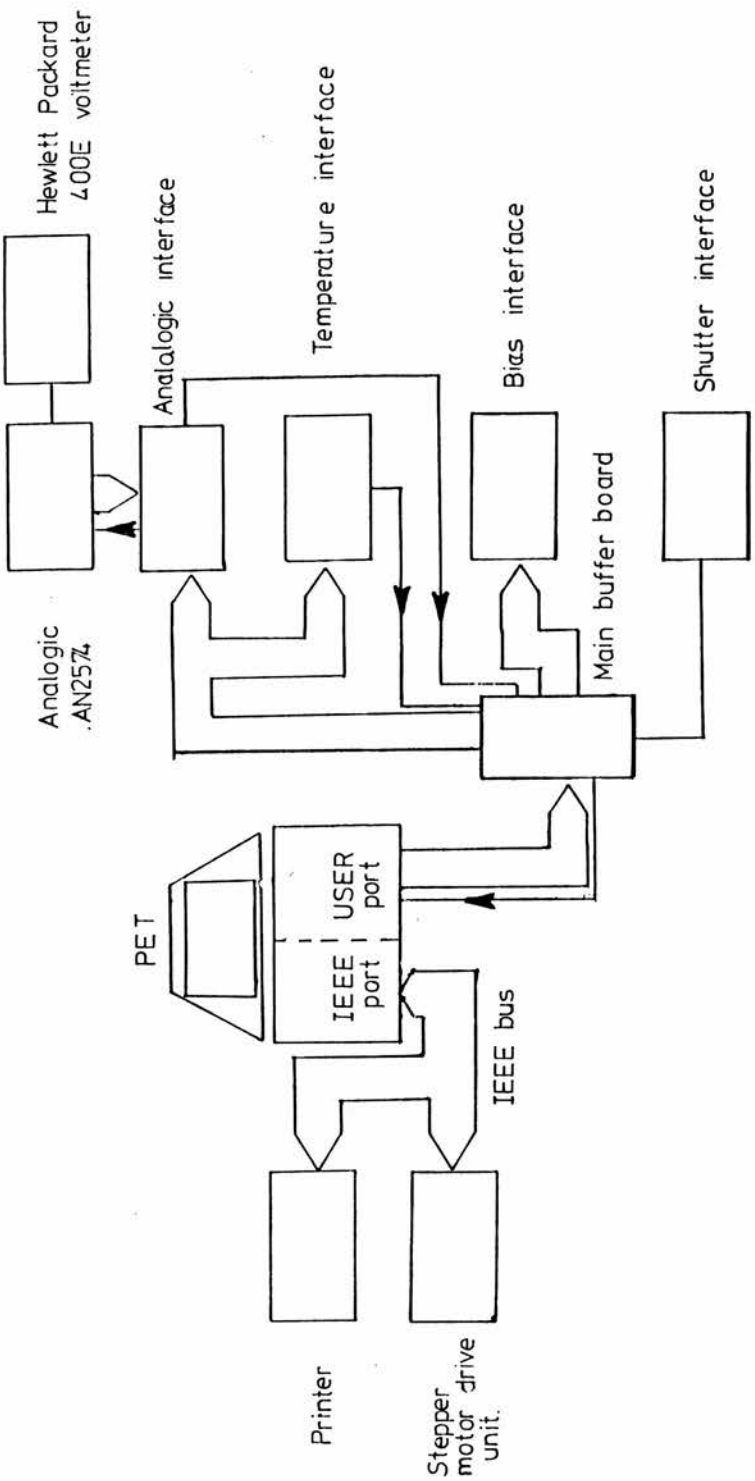

Fig 3-1. Simplified diagram of how the interfaces and external devices are connected to the I/O ports of the PET. Arrows indicate data flow.

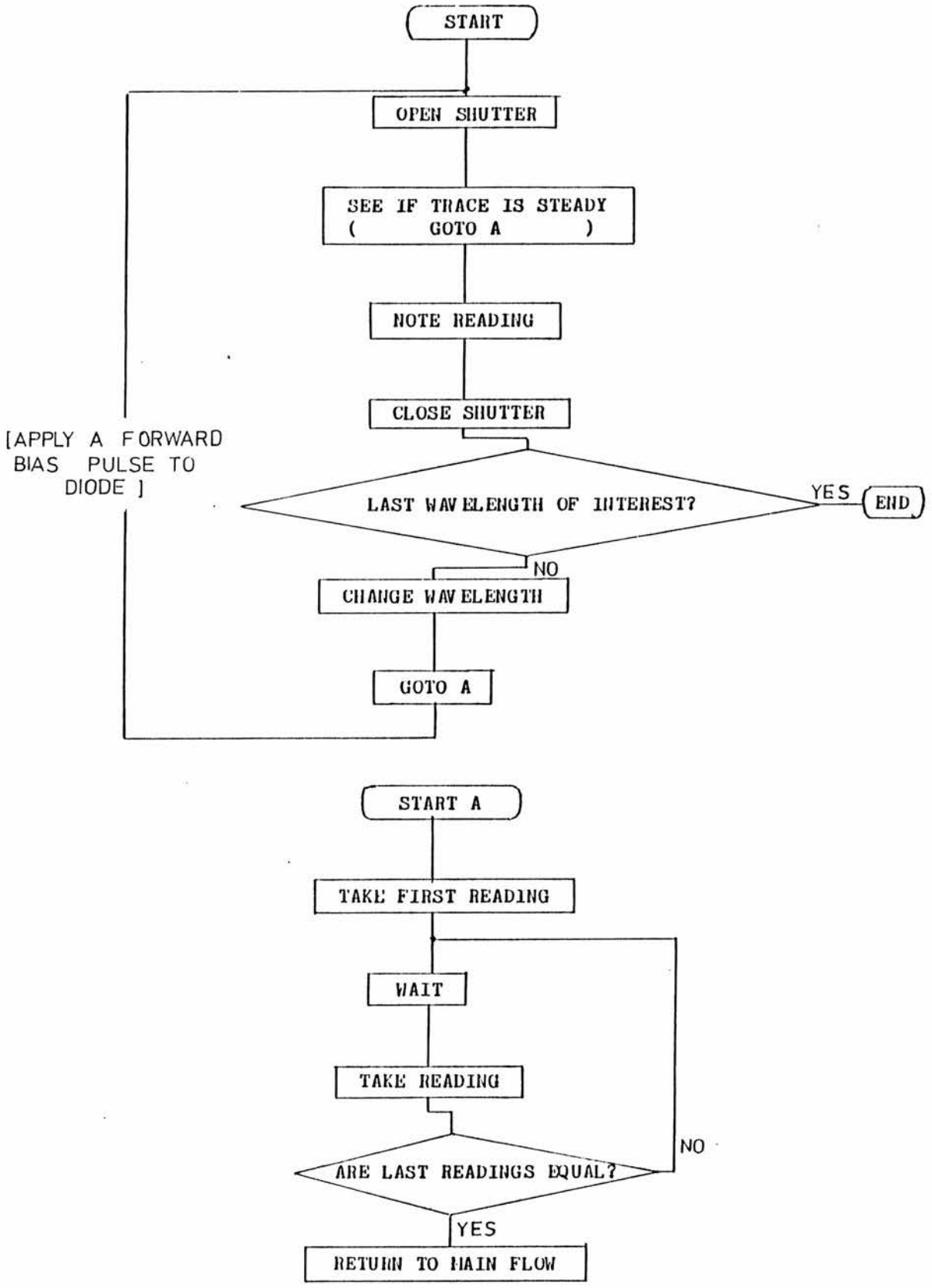

Figure 3.2a. Photocapacitance under human control

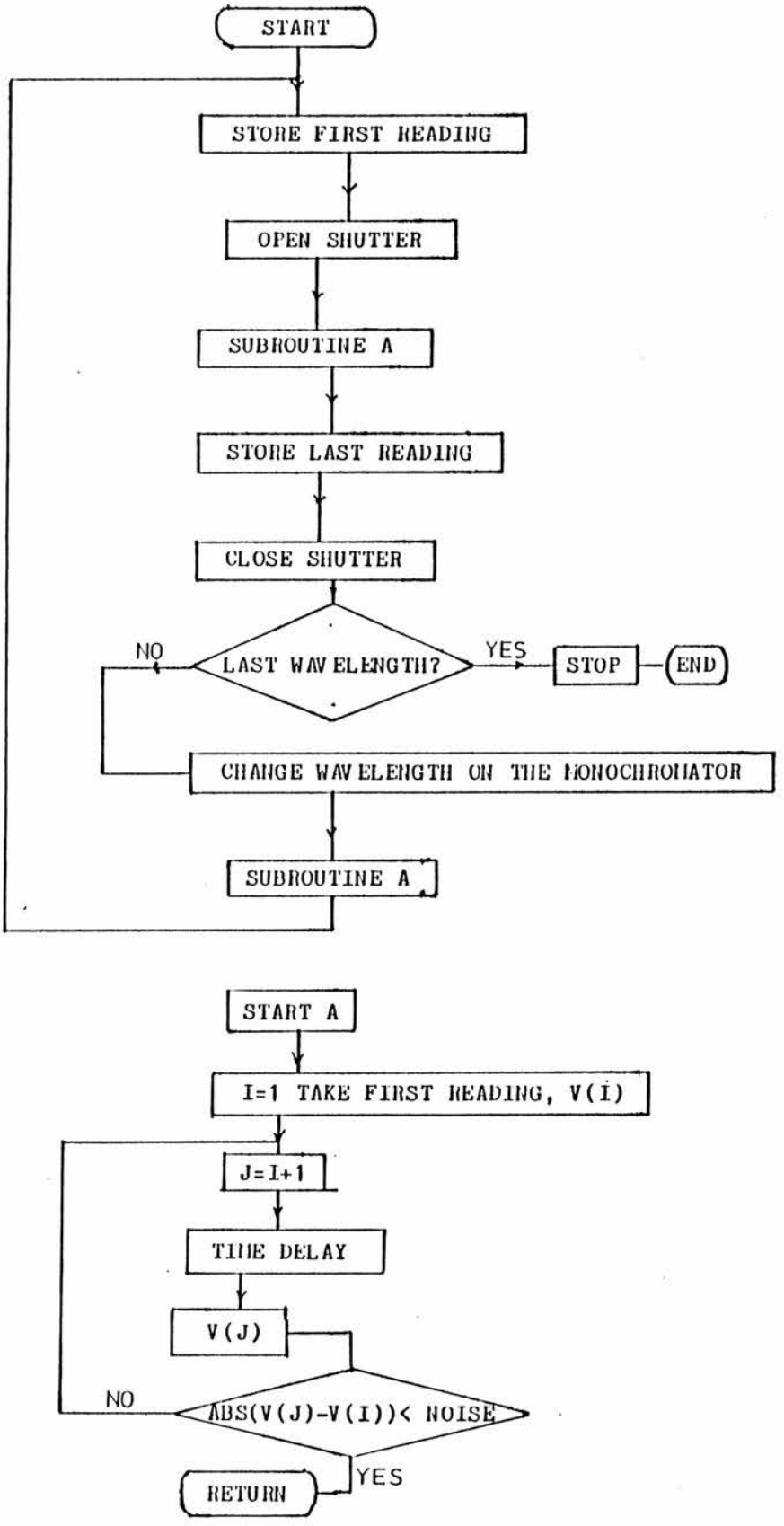

Figure 3.2b. Photocapacitance under microprocessor control

```
1 REM
5 A4=59471:A8=59468:A9=31:Z3=192:Z4=224
0 POKE59459,247
0 POKE59467,PEEK(59467)AND227
6 GOSUB400
7 POKEA4,1
0 PRINT"■BIAS WHICH CAN BE APPLIED TO THE DIODE ARE THE FOLLOWING":PRINT:PRINT
0 PRINT:PRINT:PRINT"0=NULL":PRINT"1=(1/4)FULL":PRINT"2=(1/2)FULL"
5 PRINT"3=(3/4)FULL)":PRINT"4=FULL"
8 IFN>4THENGOSUB400
0 PRINT"PLEASE INPUT ONE OF THE ABOVE NUMBERS":INPUTN:IFN>4THEN60
0 IFN=0THENGOTO85
0 GOSUB500
5 POKEA4,080
0 END
00 FORI=1TO4:FORJ=1TO2:GOSUB1000:POKEA4,016:GOSUB2000:NEXTJ:NEXTI:RETURN
00 FORI=1TON:FORJ=1TO2:GOSUB1000:POKEA4,048:GOSUB2000:NEXTJ:NEXTI:RETURN
000 POKEA8,PEEK(A8)ANDA9ORZ4:RETURN
000 POKEA8,PEEK(A58)ANDA9ORZ3:RETURN
ADY.
```

Fig. 3.3 Software to drive the bias interface.

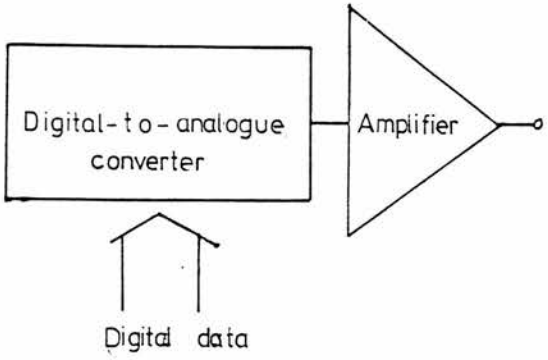

Principle of digital to analogue conversion

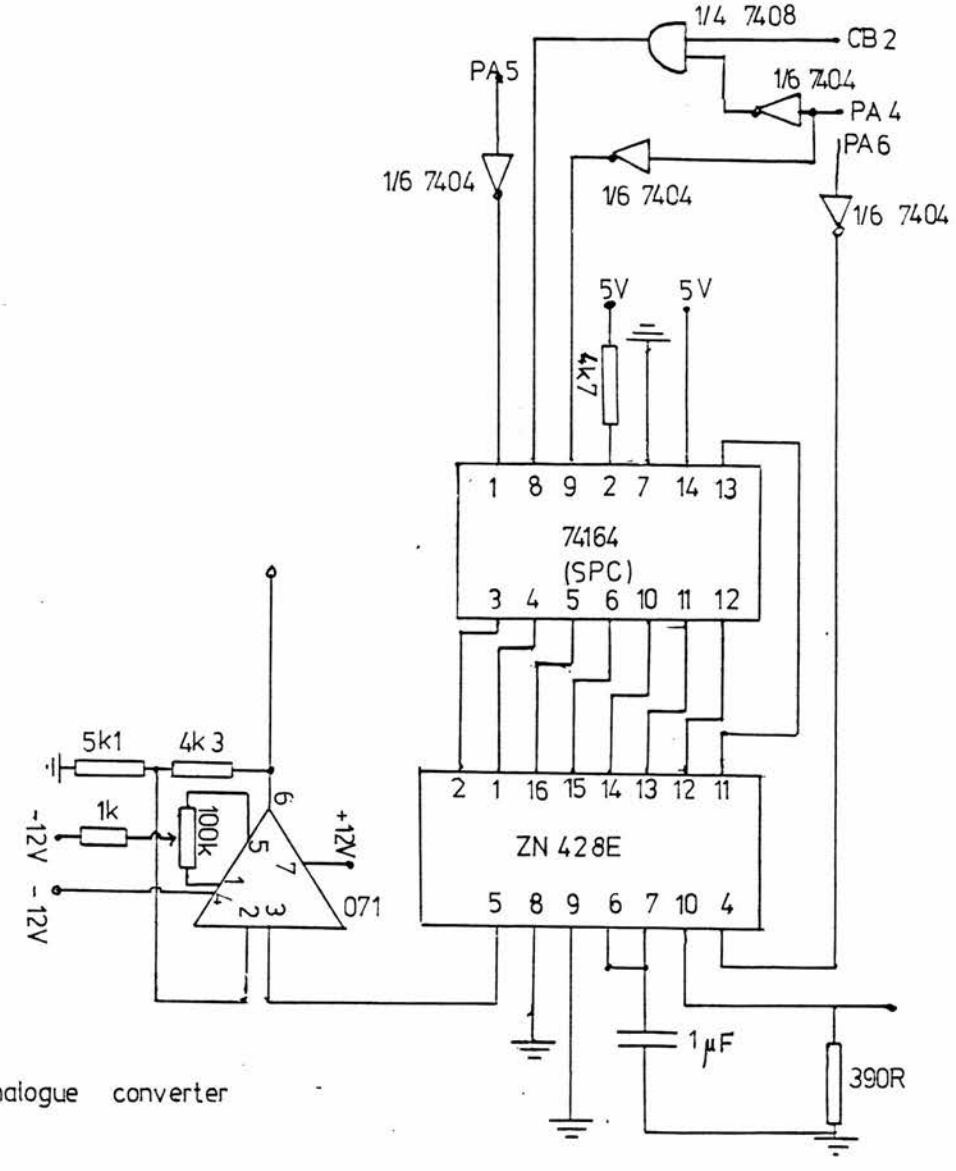

Fig. 3.4. Actual digital-to-analogue converter

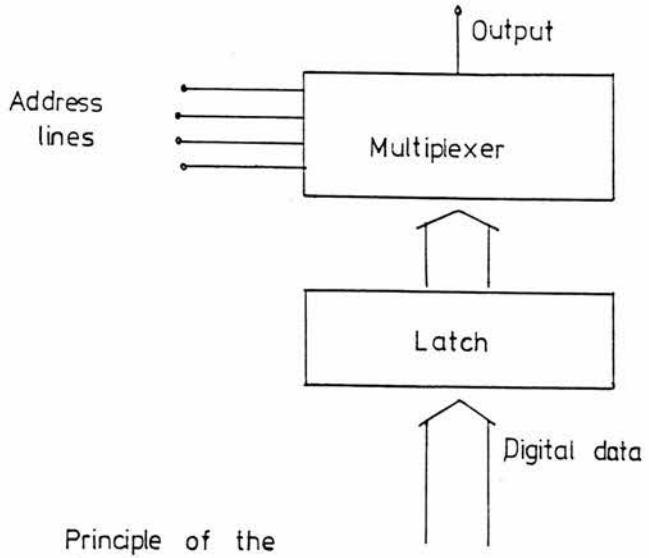

Principle of the temperature interface

Design of the temperature interface

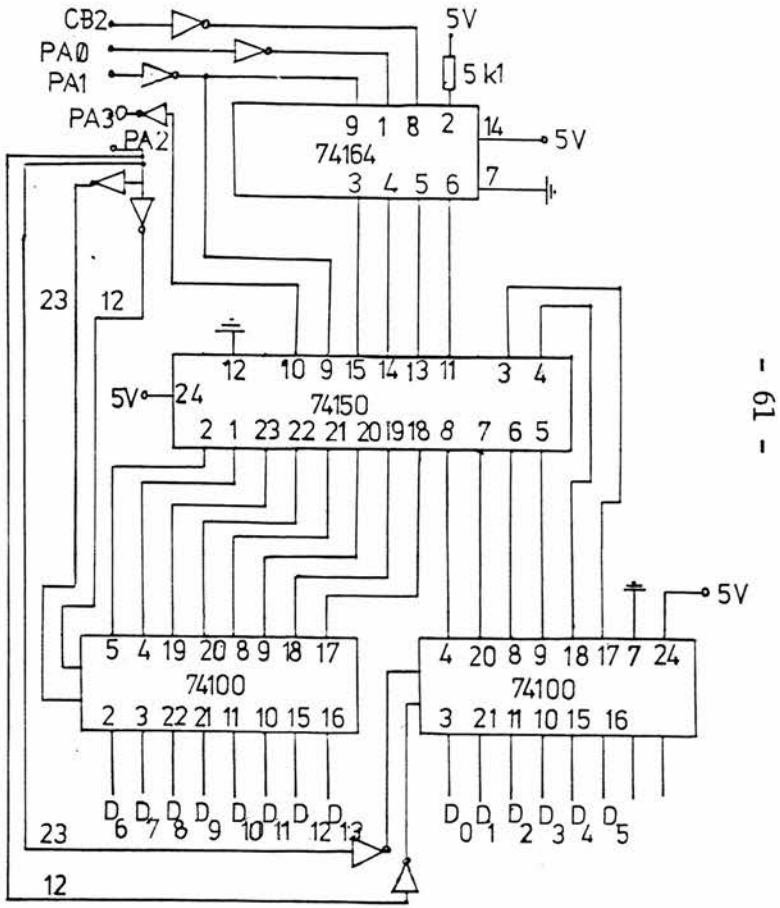

Fig. 3.5. The temperature interface

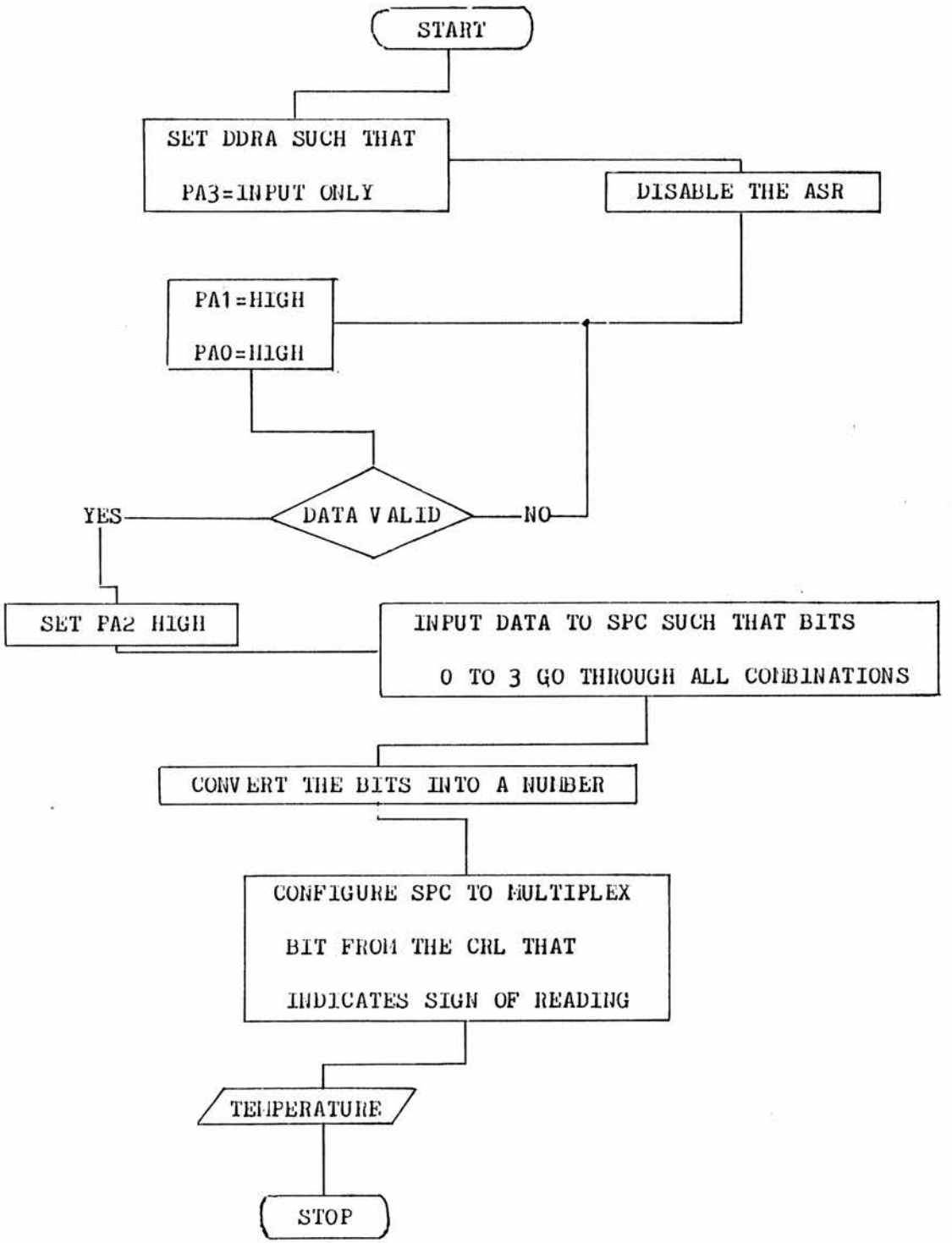

Fig.3.5a.Flow chart to read the temperature display

```
READY.

 10000 REM OUTCLOCK SUBROUTINE
 10005 REM"OUTCLOCK17"
 10010 A=59459:A1=1:A2=2:A3=3:A4=59471:A6=59467:A5=59468:AA=31:Z1=31:Z2=227
 10020 Z4=224:A0=0:Z3=192
 10030 POKEA,247
 10032 S=0:N=0
 10040 POKEA6,PEEK(A6)ANDZ2:REM DISABLE THE SHIFT REGISTER OF THE ACR
 10046 POKEA4,A3
 10048 GOSUB14000:GOSUB14000:GOSUB10700
 10050 IF L=0THEN10046
 10100 S=0
 10110 GOSUB15000:GOSUB14000:GOSUB10700:S=S+L:PRINTL
 10120 GOSUB15000:GOSUB15000:GOSUB10700:S=S+2*L:PRINTL
 10130 GOSUB15000:GOSUB16000:GOSUB10700:S=S+4*L:PRINTL
 10140 GOSUB15000:GOSUB13000:GOSUB10700:S=S+8*L:PRINTL:N=N+S :S=0
 10150 GOSUB16000:GOSUB14000:GOSUB10700:S=S+L:PRINTL
 10160 GOSUB16000:GOSUB15000:GOSUB10700:S=S+2*L:PRINTL
 10170 GOSUB16000:GOSUB16000:GOSUB10700:S=S+4*L:PRINTL
 10180 GOSUB16000:GOSUB13000:GOSUB10700:S=S+8*L:PRINTL:N=N+10*S:S=0
 10190 GOSUB13000:GOSUB14000:GOSUB10700:S=S+L*2:PRINTL
 10200 GOSUB13000:GOSUB15000:GOSUB10700:S=S+L*1:PRINTL
 10210 GOSUB13000:GOSUB16000:GOSUB10700:S=S+L*4:PRINTL
 10220 GOSUB13000:GOSUB13000:GOSUB10700:S=S+L*8:PRINTL:N=N+100*S:
 10230 GOSUB14000:GOSUB13000:GOSUB10700:IFL=0THENN=(-N):PRINTN;" °C"
 10240 IFL=1THENPRINTN;" °C"
 10249 PL=0
 10250 RETURN
 10700 IFPEEK(A4)-22<=0THENL=0
 10705 PRINTPEEK(A4)
 10710 IF(PEEK(A4)-27)>=0THENL=1
 10720 RETURN
 11000 POKEA5,PEEK(A5) AND AA OR Z4:REM CB2 HIGH
 11010 RETURN
 12000 POKEA5,PEEK(A5)AND AA OR Z3:REM CB2 LOW
 12020 RETURN
 13000 REM SUBROUTINE FOR PRODUCING TWO HIGHS
 13100 FORI0=1TO2:GOSUB11000:POKE A4,4:GOSUB12000:NEXTI0:RETURN
 14000 REM SUBROUTINE FOR PRODUCING TWO LOWS
 14100 FORI0=1TO2:GOSUB11000:POKE A4,5:GOSUB12000:NEXTI0:RETURN
 15000 REM SUBROUTINE FOR PRODUCING LH
 15100 GOSUB11000:POKE A4,5:GOSUB12000:GOSUB11000:POKEA4,4 :GOSUB12000:RETURN
 16000 REM SUBROUTINE FOR PRODUCING HL (IN THAT ORDER)
 16100 GOSUB11000:POKE A4,4:GOSUB12000:GOSUB11000:POKE A4,5:GOSUB12000:RETURN

READY.
```

Fig 3·5b The sofware for the temperature interface

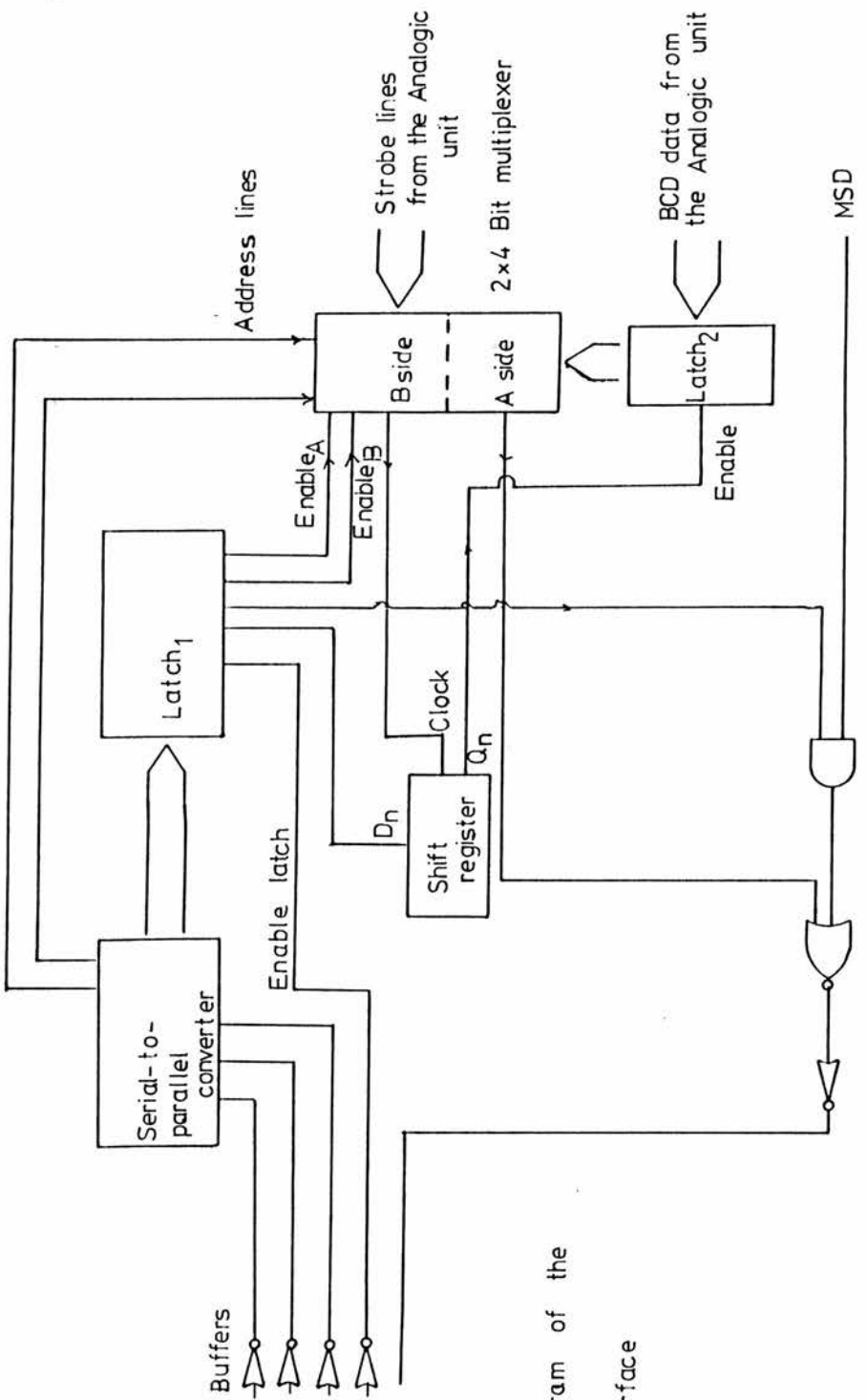

Fig. 3.5 Schematic diagram of the Analogic interface

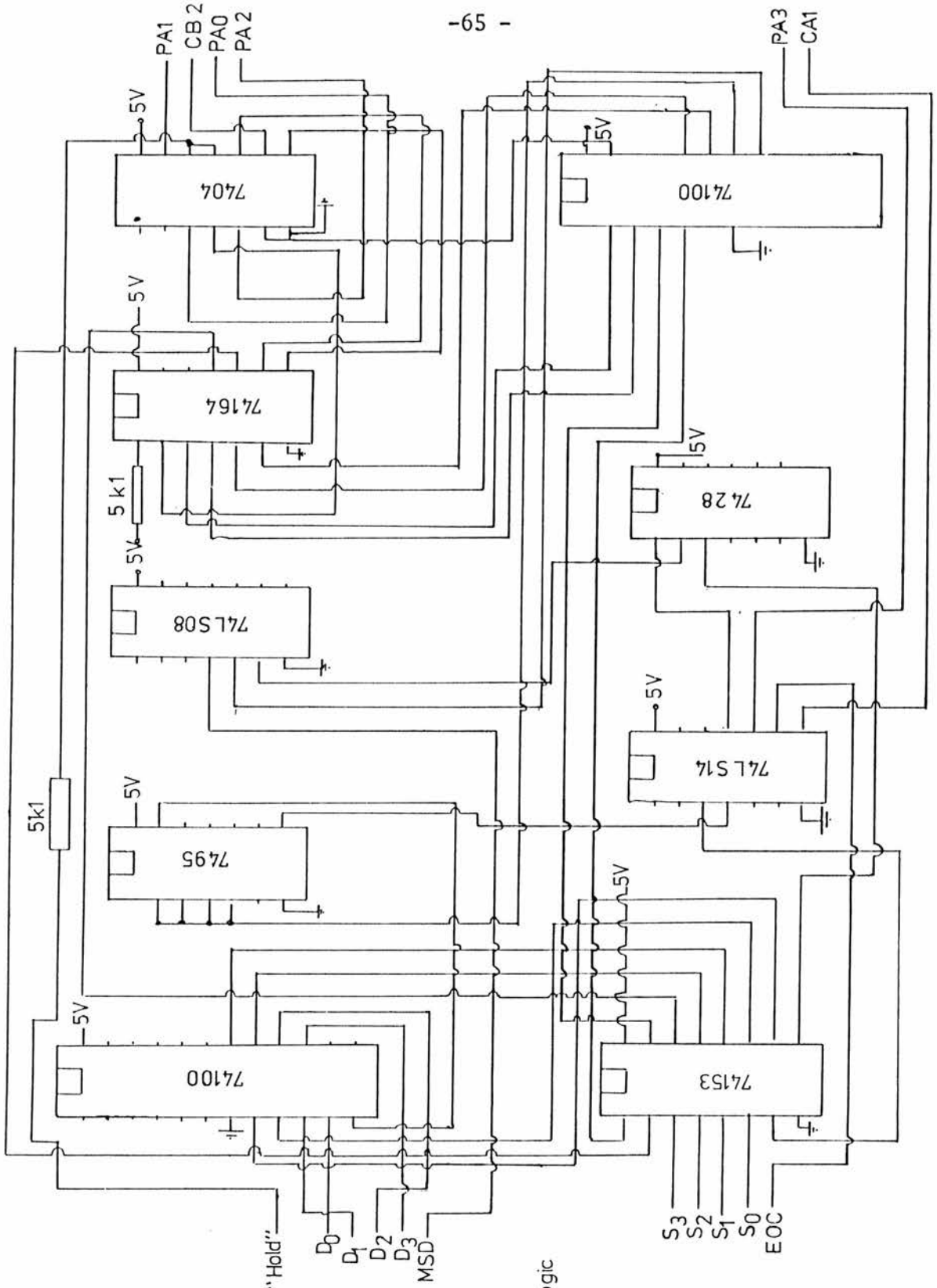

Fig. 3.7 Actual circuit diagram for the Analogic interface.

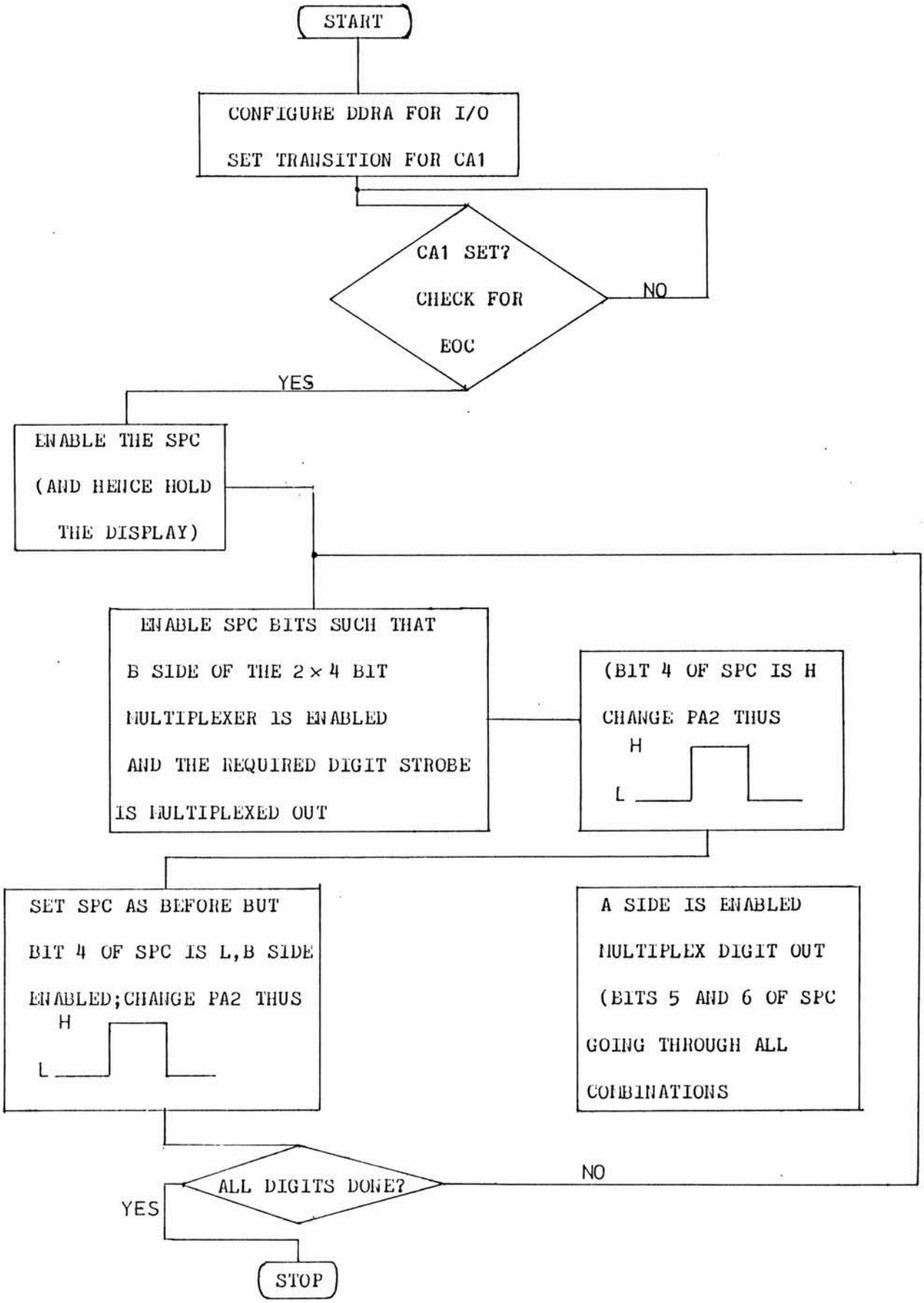

Fig. 38a. Flow chart for reading the Analogic display

```
READY.

 10 REM ***** ANALOGIC10*****
 14 OPEN2,4,2
 15 OPEN4,4,1
 16 PRINT#2,"AAAAAAAAAAAAAAAAAA AAAAAAA AAAA"
 17 PRINT#4,"READING"CHR$(29)"STEP"
 20 PRINT"INPUT TIME BETWEEN READINGS IN SECONDS"
 25 INPUTS
 26 PRINT"J"
 30 A=59459:A1=1:A2=2:A3=3:A4=59471:A5=59468:A6=59467:A7=59468:A9=30:Z2=227
 40 Z3=192:Z4=224:B1=5:B2=7:B6=59457
 50 POKEA,247
 55 DIMX(1000):I=1
 60 POKE(A6),PEEK(A6)ANDZ2
 70 L=PEEK(B6)
 80 POKE(A7),PEEK(A7)AND254
 90 POKEA6,PEEK(A6) AND A3
 100 IFPEEK(59469)AND A2 THEN120
 105 POKEA4,5
 110 GOTO100
 120 VOLT=0:BIT=0
 130 POKEA4,0:POKEA4,2
 140 GOSUB3000:GOSUB3000:GOSUB6000:GOSUB6000:POKEA4,2:POKEA4,6
 142 GOSUB3000:GOSUB3000:GOSUB3000:GOSUB6000:POKEA4,2:POKEA4,6
 144 GOSUB3000:GOSUB3000:GOSUB3000:GOSUB5000:POKEA4,2:POKEA4,6:GOSUB7000:
 145 VOLT=VOLT+0.01*BIT:BIT=0
 150 GOSUB3000:GOSUB5000:GOSUB6000:GOSUB6000:POKEA4,2:POKEA4,6
 160 GOSUB3000:GOSUB5000:GOSUB3000:GOSUB6000:POKEA4,2:POKEA4,6
 170 GOSUB3000:GOSUB5000:GOSUB3000:GOSUB5000:POKEA4,2:POKEA4,6
 171 GOSUB7000:VOLT=VOLT+0.1*BIT:BIT=0
 180 GOSUB3000:GOSUB6000:GOSUB6000:GOSUB6000:POKEA4,2:POKEA4,6
 183 GOSUB3000:GOSUB6000:GOSUB3000:GOSUB6000:POKEA4,2:POKEA4,6
 185 GOSUB3000:GOSUB6000:GOSUB3000:GOSUB5000:POKEA4,2:POKEA4,6
 187 GOSUB7000:VOLT=VOLT+BIT:BIT=0
 190 GOSUB3000:GOSUB4000:GOSUB6000:GOSUB6000:POKEA4,2:POKEA4,6
 195 GOSUB3000:GOSUB4000:GOSUB3000:GOSUB6000:POKEA4,2:POKEA4,6
 198 GOSUB3000:GOSUB4000:GOSUB3000:GOSUB5000:POKEA4,2:POKEA4,6
 200 GOSUB7000:VOLT=VOLT+10*BIT
 220 GOSUB3000:GOSUB3000:GOSUB5000:GOSUB4000:POKEA4,2:POKEA4,6
 230 GOSUB700
 240 VOLT=VOLT+100*L
 242 X(I)=VOLT
 243 PRINT#4,X(I)CHR$(29)I
 244 T=TI
 246 IFTI<=T+60*STHEN246
 247 IFABS(X(I)-X(I-1))<=.09THEN250
 248 I=I+1
 249 GOTO60
 250 PRINT#2,"AAAAAAAAAAAAAAAAAAAAAA":PRINT#2,"ZZ"
 251 PRINT#4,"TIME BETWEEN READINGS=";S+9;"SECS"
 254 PRINT#2:CLOSE2:PRINT#4:CLOSE4:END
 700 IFPEEK(A4)-22<=0THENL=0
 710 IFPEEK(A4)-29>0THENL=1
 720 RETURN
 1000 POKEA7,PEEK(A7)ANDA9ORZ4
 1100 RETURN
 2000 POKEA7,PEEK(A7)ANDA9ORZ3
 2100 RETURN
 3000 FORK=1TO2:GOSUB1000:POKEA4,7:GOSUB2000:NEXTK:RETURN
 4000 FORJ=1TO2:GOSUB1000:POKEA4,6:GOSUB2000:NEXTJ:RETURN
 5000 GOSUB1000:POKEA4,7:GOSUB2000:GOSUB1000:POKEA4,6:GOSUB2000:RETURN
 6000 GOSUB1000:POKEA4,6:GOSUB2000:GOSUB1000:POKEA4,7:GOSUB2000:RETURN
 7000 GOSUB3000:GOSUB3000:GOSUB3000:GOSUB5000:GOSUB700:BIT=BIT+L
 7100 GOSUB3000:GOSUB5000:GOSUB3000:GOSUB5000:GOSUB700:BIT=BIT+2*L
 7200 GOSUB3000:GOSUB6000:GOSUB3000:GOSUB5000:GOSUB700:BIT=BIT+4*L
 7300 GOSUB6000:GOSUB4000:GOSUB3000:GOSUB5000:GOSUB700:BIT=BIT+8*L:RETURN
READY.
```

Fig 3.8 Software for the voltmeter interface

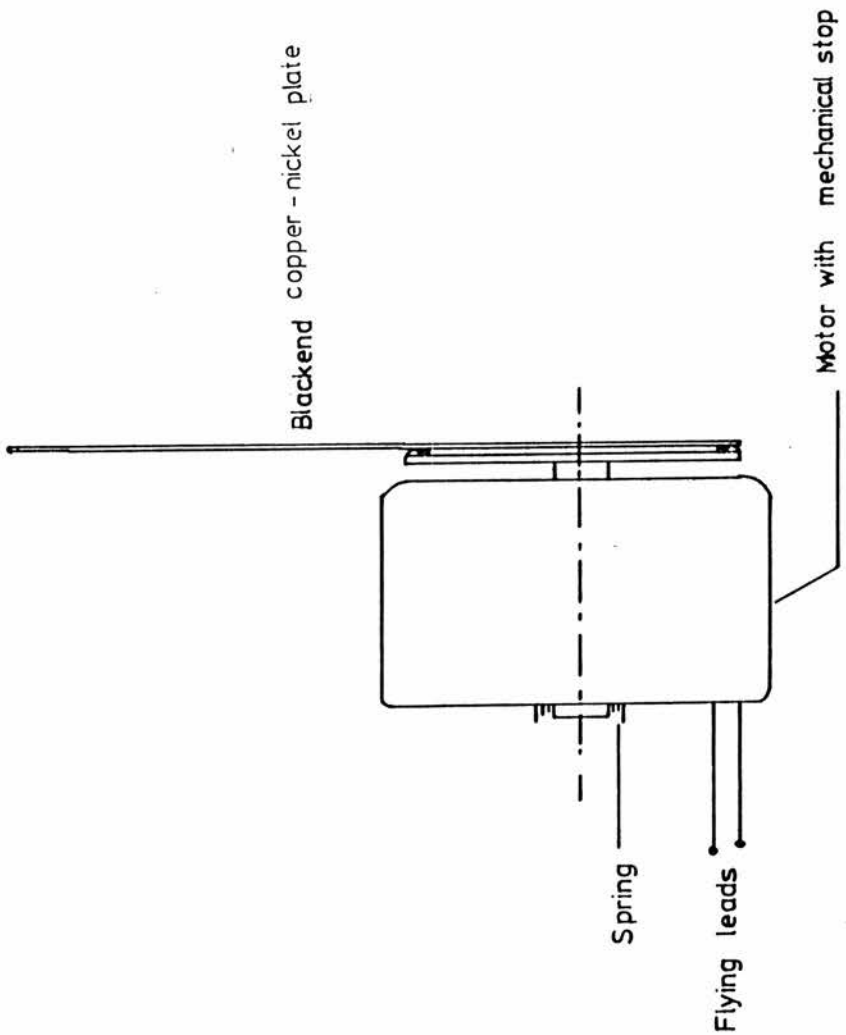

Fig 3.9. Shutter design

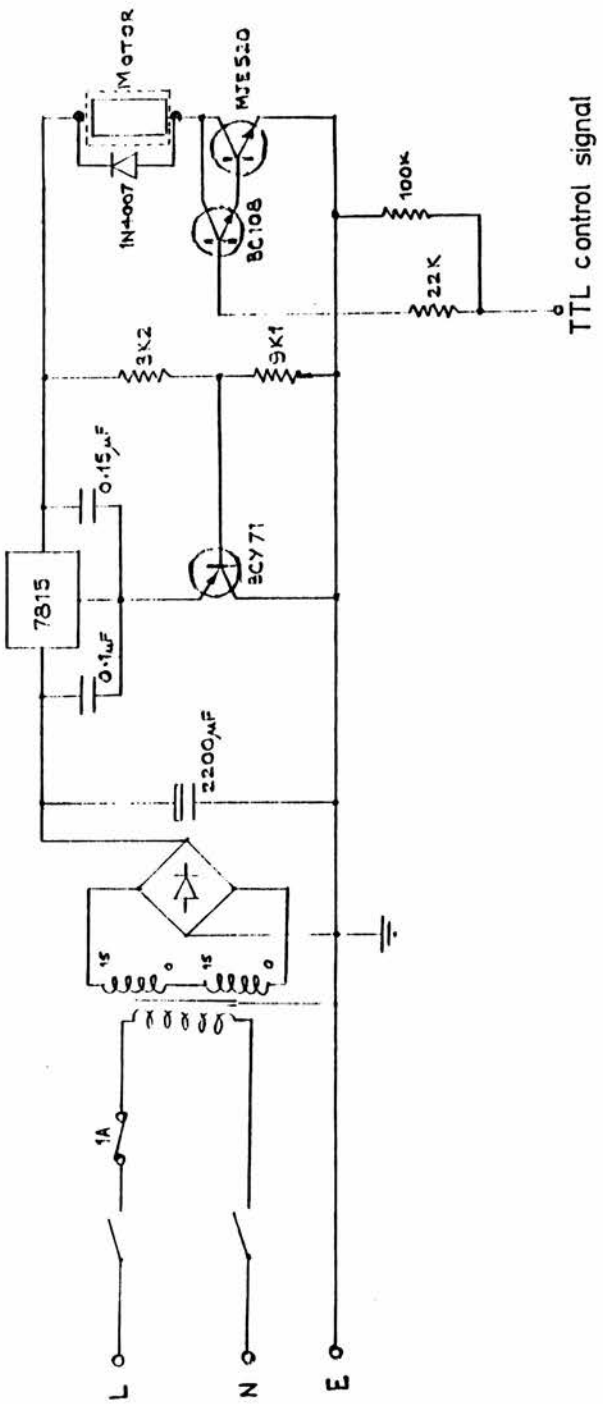

Fig. 3.10. The shutter interface.

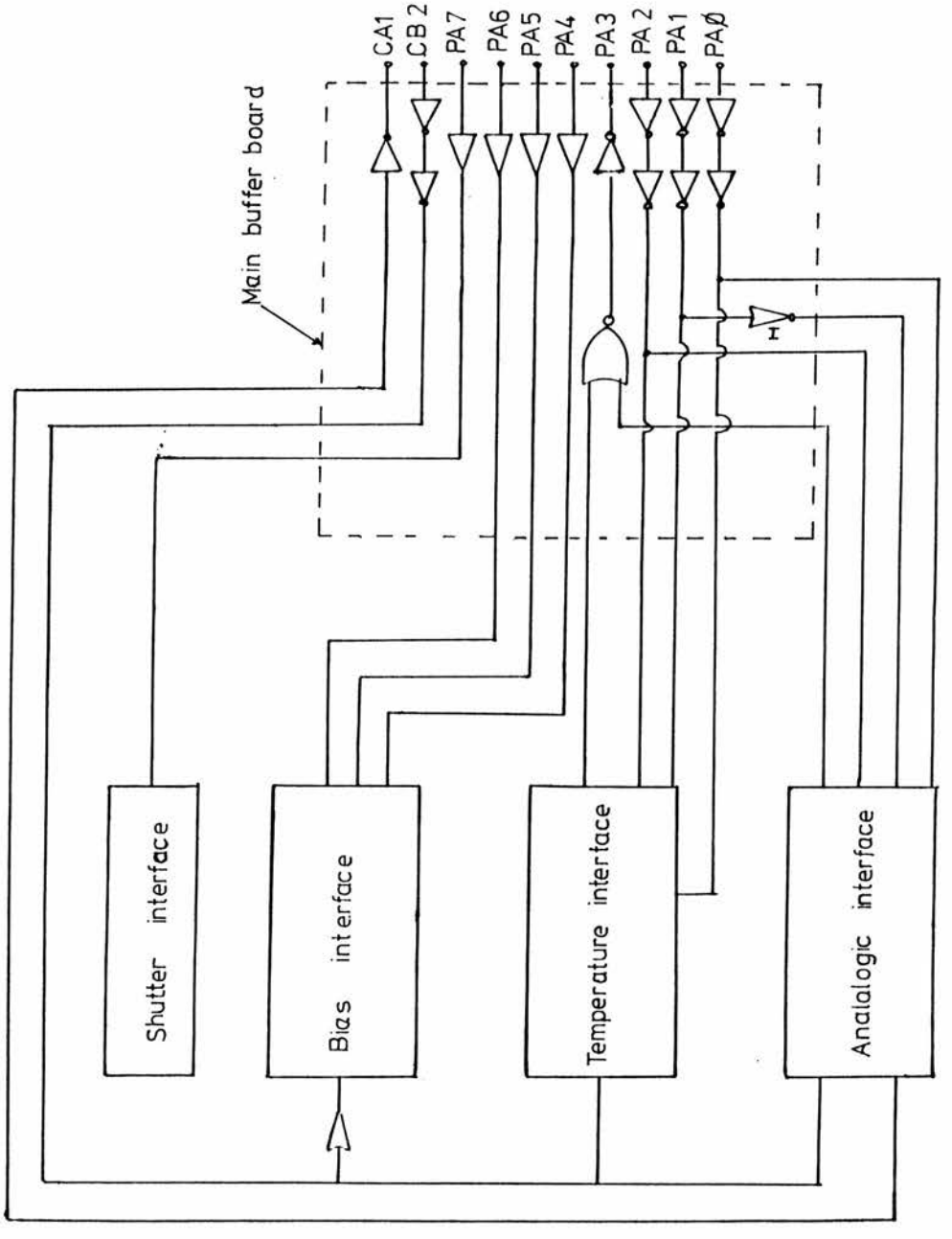

Fig. 3.11 Interconnection of the developed interfaces to the main buffer board

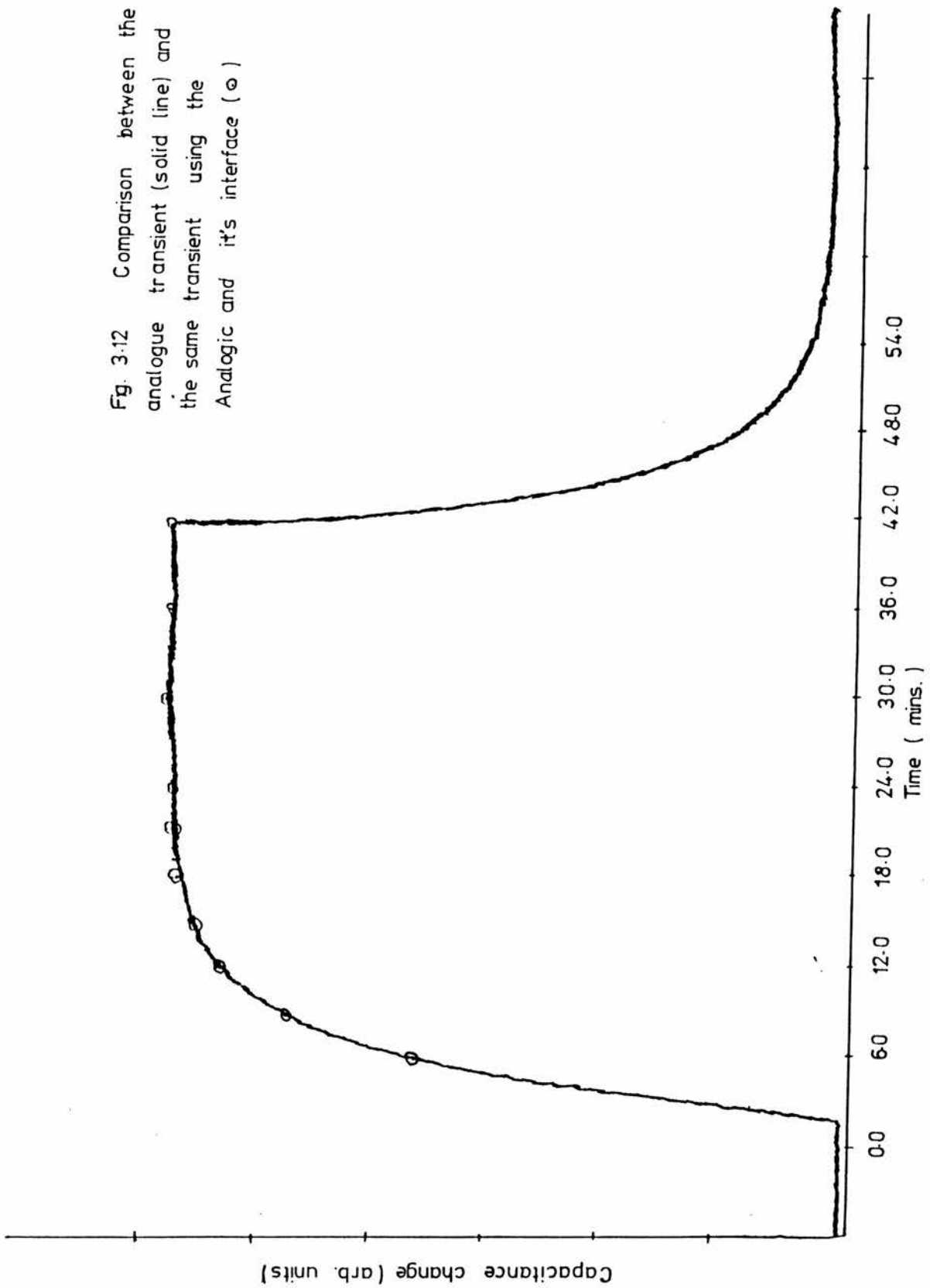

Fig. 3.12 Comparison between the analogue transient (solid line) and the same transient using the Analogic and it's interface (o)

employing a free running clock

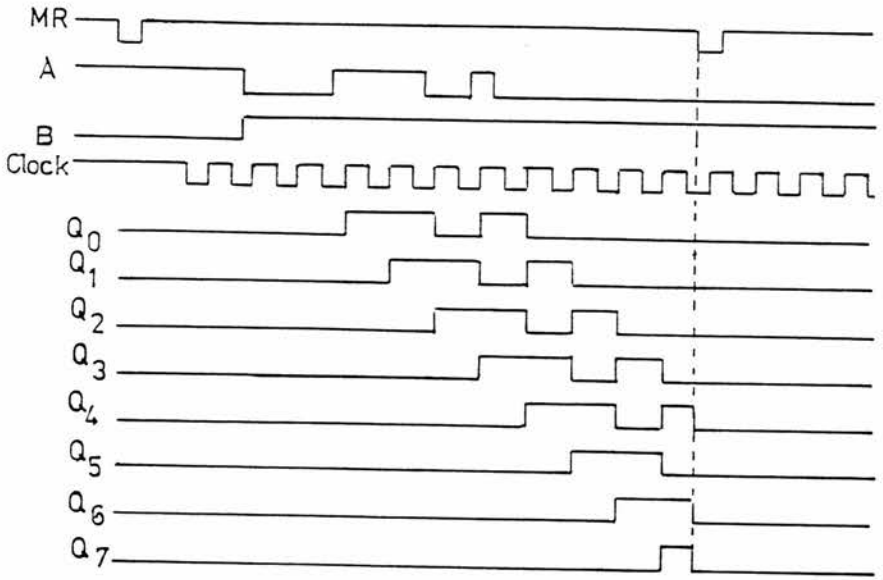

Figure 3B.1

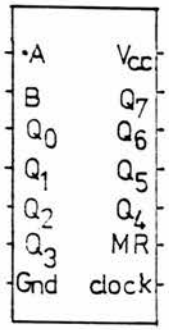

Pin identification
of the 74164

Function table

MR	Clock	A	B	Q_0 $Q_1 \cdots Q_7$
L	X	X	X	L L L
H	L	X	X	Q_{0o} Q_{1o} Q_{7o}
H	↑	H	H	H Q_{0n} Q_{6n}
H	↑	L	X	L Q_{0n} Q_{6n}
H	↑	X	L	L Q_{0n} Q_{6n}

X Don't care
L Digital low
H Digital high
↑ Low to high clock transition
Q_{io} State of the respective outputs before MR and clock changed state
Q_{in} State of the respective output one step prior to the ↑ clock transition

Appendix 3C

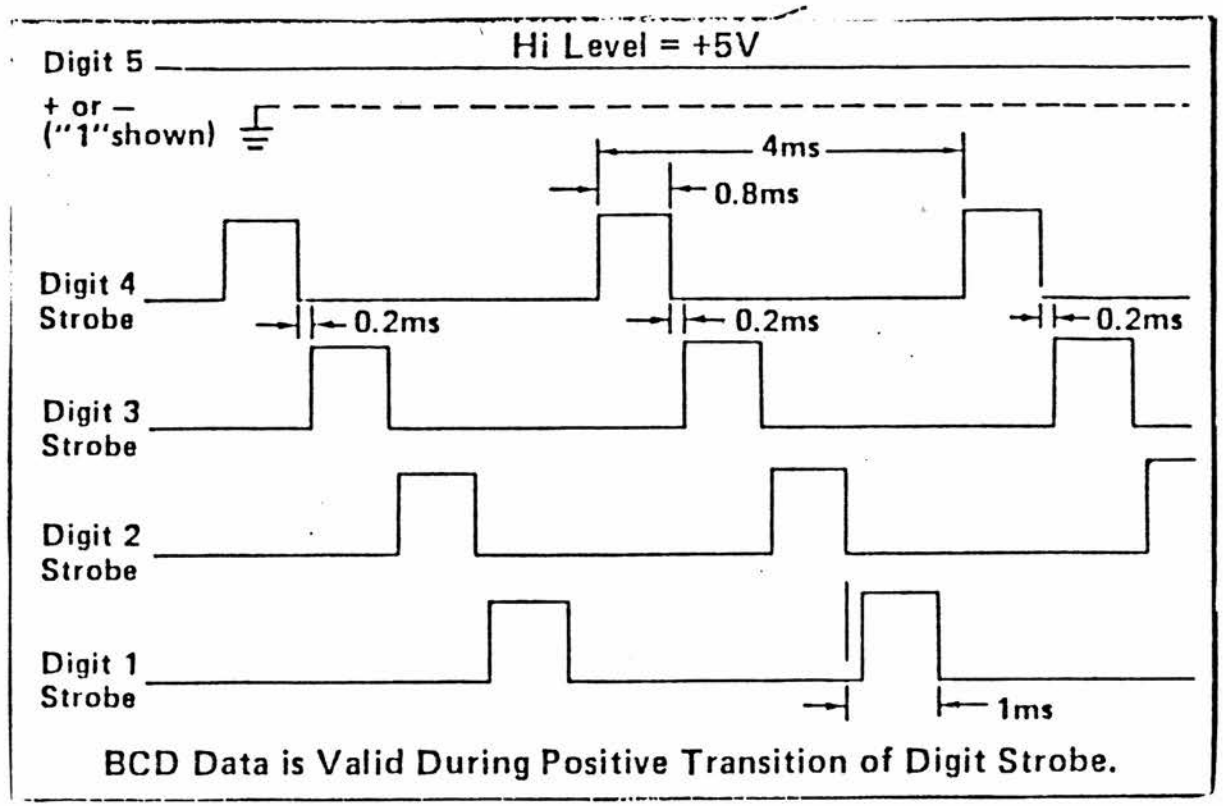

Display timing diagram for serial data

4 Thin film electroluminescent devices:optical and electrical investigations

Introduction

Thin films of ZnS:Mn fabricated in thin film electroluminescent device (TFED) form will become important commercially as they offer great potential for fabricating flat screen monitors,large area displays and other optical displays (see Theis (1981)). Most of the published data concerning the TFED is devoted to the luminescent properties of the Mn centre in ZnS,while very little published data is concerned with the optical and the electrical properties of the TFED.

The optical and electrical properties of a dc TFED were studied using a capacitance bridge and a frequency response analyser respectively. The structure of the (dc)TFED is a sandwich consisting of a back aluminium electrode-ZnS:Mn-transparent electrode (almost always a conducting oxide). The phosphor in these devices is almost always semi-insulating, as the mechanism for the electroluminescence is the impact excitation of the Mn centre by "hot" electrons. The hot electrons are produced by applying high electric field to the TFED. The optical experiment carried out was an exploratory experiment to find any residual impurities that produced energy levels in the band gap of the semi-insulator. In this experiment, a specially constructed capacitance bridge was used.When light was shone on the TFED ,a "capacitance" change was observed. This "capacitance" change reflects the change in the free carrier concentration,that is,the

resistance change of the TFED.

The reason for this is that the capacitance bridge represents the TFED as an equivalent circuit consisting of a series combination of a capacitor and a resistor. As the true equivalent circuit of the TFED is not a series combination of a resistor and a capacitor,the capacitance measured by the capacitance bridge contains terms from the true resistance of the device.Thus when we shine light on the TFED,we are in fact measuring the resistance change of the TFED,that is,a photoconductive effect,and not a photocapacitive effect. The conclusion that we are not observing photocapacitance when we shine light on the TFED can also be inferred from the fact that no depletion region exists in the semiconductor.Typical parameters for the TFED substituted into the formula giving the depletion width for a Schottky contact shows that the "depletion region" of the TFED is much larger than the thickness of the semiconductor layer.Suda et al (1979) have carried out an optical experiment on a "moderately doped" ZnS:Ag with the semiconductor sandwiched between a transparent electrode and an aluminium contact.They modelled their experimental data by assuming a depletion region could be defined in their sample.From the above discussion it is clear that the depletion region will be much larger than the thickness of the semiconductor and hence no "photocapacitance" will be seen. The capacitance associated with the TFED is the geometrical capacitance.In our experiment the rise in the "capacitance" when light is shone on the TFED is modelled on the basis that we are observing a photoconductive process. We carried out a second experiment to find the equivalent circuit of the TFED.The equivalent circuit representation of the TFED is important,as many

electrical characteristics of the device can be analysed more simply by representing the device as an equivalent circuit consisting of capacitors and resistors. It is shown that the simple impedance picture of the TFED is not applicable when light is shone on the device .This is because the resistor and capacitor representing the equivalent circuit of the TFED become frequency dependent for frequencies less than 100kHz This experiment also shows that the equivalent circuit of the TFED is not a series combination of a resistor and a capacitor when light is shone on the device. In this chapter,optical and electrical investigations on semi-insulating films of ZnS:Mn fabricated in TFED form were carried out.For the optical experiments,two devices ,differentiated only whether the sputtering of the ZnS was in an atmosphere of argon (the non-hydrogenated device), or in an atmosphere of argon and hydrogen (the hydrogenated device) were studied using the capacitance bridge described in chapter 2.

The optical investigations revealed that both the devices have the same deep centre which produces a deep level located at 2.49eV below the conduction band. The hydrogenated device has another impurity in the band gap.

The non-hydrogenated device was studied further to find the equivalent circuit for the device. When the TFED was in the dark it was found that the ZnS layer can be regarded as a capacitor with a leakage resistor .These two components are in series combination with the contact resistance. When light was shone onto the device,the same equivalent circuit is useful but the leakage resistance and the capacitance become frequency dependent.The frequency dependence of the two components is explained on the basis that a novel form of hopping

conduction is taking place.

The chapter is organised into three sections.Section 1 describes the optical experiments and section 2 describes the electrical measurements.These sections are self contained and they can be read independently of each other. Finally in section 3 some concluding remarks on the two sections are made.

Section 1 Optical characterization

4.1.1 Introduction

In this section , optical investigations of highly resistive films of ZnS:Mn films, fabricated in a thin film electroluminescent device (TFED),performed using the capacitance bridge described in chapter 2 are described.

For the non-hydrogenated device,the rise of the off balance signal produced by shining light on the TFED showed that the transient could be fitted to an exponentially increasing function. The inverse rise time of the transient was found to be directly proportional to the incident flux of photons.This property was used to calculate the photoionisation threshold of the impurity. For the hydrogenated device,the rise of the transient was complicated and it could not be described as simply as for the non-hydrogenated device.For both the devices,the photoionisation threshold was found to be 2.49 eV below

the conduction band. For photon energies larger than 3.1eV, the hydrogenated device showed a quenching effect whereas the non-hydrogenated device did not show any such effect. The cause of this quenching is the recombination of the excited carriers with a deep centre in the band gap.This recombination centre is of concentration less then 10^{12} cm^{-3} (this concentration being the limit of the capacitance bridge sensitivity (Szawelska (1980)).

4.1.2 Experimental method

The basic structure of the device consisted of a Corning glass substrate followed by a thin layer of Cd_2SnO_4 (a conducting oxide).On top of this was a layer of the sputtered ZnS:Mn.An aluminium contact was placed on top of the ZnS.The Cd_2SnO_4 made contact with the entire ZnS:Mn phosphor while the aluminium contact was in strips such that ten "pixels" were defined on the glass. These devices were made at RSRE,Malvern (UK).

To the aluminium contact a modified croc clip with a flying lead was attached,while the contact to the conducting oxide consisted of a swab of silver paste to which a flying lead was attached. The silver paste was left for 12 hrs to dry.Once these contacts were made then the TFED was connected to the capacitance bridge described in chapter 2.

Monochromatic light from a Spex "minimate" spectrometer fitted with a 250W lamp was incident on the glass side of the TFED using the optical arrangement shown in figure 4.1.The exit slit of the monochromator corresponded to a band pass of 200Å . An Ealing 263038 filter was placed at the exit of the monochromator to eliminate the higher order wavelengths.To reduce any low frequency vibrational noise,the optical bench rested on a sandwich of two hard board planks and air filled polythene.

The shutter used to block the light had to have the special property that it did not produce any excessive vibrational noise.The camera type shutter proved to be inadequate as did the shutter constructed for the automated capacitance bridge.The final design of the shutter is shown in figure 4.2.The basic design is that of a low inertia motor to which a blackened sheet of copper-nickel alloy is attached with Araldite.To block and unblock the monochromatic light,an appropriate pulse from the pulse generator was used to rotate the motor.The above design of the shutter effectively implied that we could not use the automated capacitance bridge described in the previous chapter.

The flux of light incident on the TFED was measured in relative terms using a Hilgar Schwartz thermopile connected to a Keithley 155 null micro voltmeter.

To obtain a spectrum,the capacitance bridge was first balanced with the TFED in the dark.Light from a monochromator was shone on the TFED and the resulting off balance signal (OBS) was observed on the chart recorder.The OBS is found to be directly proportional to the "capacitance change" (Szawelska (1980)).However as discussed in the introduction, the "capacitance change" actually reflects the resistance change of the device when light is shone on it. Once a steady OBS was observed on the chart recorder, the monochromatic light was blocked,and the OBS returned to its dark value. The wavelength on the monochromator was decreased and the above procedure was repeated.

From the chart recordings,the inverse rise time of the transient was calculated using the method due to Mangelsdorf (1959).An example of this calculation is shown in figure 4.3. For the Mangelsdorf method to be applicable,the OBS must increase exponentially.Figures 4.4a and 4.4b show that it is only the final part of the OBS that is increasing exponentially.In the calculation of the inverse rise times only the final part of the trace was used in the calculation. (A more complete discussion on the rise of the OBS will be presented in a latter section.)

In the optical experimental study,two pixels from each device were studied.Since the two pixels from each device showed similar behaviour,results will be presented for only one pixel from each device.

4.1.3 Results

For one of the devices (the non-hydrogenated one),a current-voltage experiment was carried out.The experiment showed the device to be highly insulating when it was in the dark(even with room lights on) with a resistance of greater than $10^{11}\ \Omega$. But when UV light from a P W Allen UV lamp was shone onto the device the I-V data showed Ohmic behaviour up to 10V.The resistance of the device in this case was found to be $10^{9}\ \Omega$. The dark capacitance of the hydrogenated device was typically 926pF while for the non-hydrogenated device it was typically 626pF.

The large resistance of the device implies that the ZnS has a deep level.Additionally we can say that there is no band bending at the aluminium ZnS:Mn interface.If the depletion region did exist it would be much larger than the thickness of the semiconductor layer(which is $\sim 1\mu m$). This conclusion is in disagreement with the work carried out by Suda et al (Suda et al (1979)) on ZnS:Ag who model their experimental data by assuming a depletion region to be defined. Typical parameters for their sample will reveal that once again the depletion region will be much larger than the sample thickness.

When the peak-to-peak signal applied to the device was changed by an order of magnitude (from 18mV to 180mV) no appreciable change in the dark capacitance of the device was observed.For all the data reported 18mV was applied to the device.

Figure 4.5a shows the variation with photon energy of the steady state value of the OBS divided by the flux of light incident on the non-hydrogenated device ($\Delta V/\phi$) .Figure 4.5b shows the spectrum of the inverse rise time of OBS divided by the incident flux of photons.Figures 4.6a and 4.6b are the corresponding figures for the hydrogenated device.

Figures 4.5a and 4.6a show that the steady state OBS is similar for both the devices although the non-hydrogenated device does not show any quenching of the OBS above 3.1eV(at this photon energy we are still well away from the conduction band edge).Further comparison of the two figures show that the hydrogenated device has the larger value of $\Delta V/\phi$. We can normalise the $\Delta V/\phi$ spectrum for the two devices to investigate whether the same impurity exists in both the devices.This is done in figure 4.7. In this figure,we have normalised the results of the hydrogenated device to those of the non-hydrogenated device at S". Figure 4.7 shows that the rising part of the $\Delta V/\phi$ is identical for both the TFEDs.A difference in the two spectra is seen for photon energies in excess of 3.10eV. The hydrogenated device shows a quenching effect.The cause of this quenching could be the presence of another impurity.

It was mentioned above that the inverse rise times were obtained by the Mangelsdorf method.In carrying out this analysis only the final part of the chart recording was used for the calculation.The reason for this is clear if the form of the rise of the transient is modelled. For the purpose of modelling the rise of the OBS and for obtaining information about the possible rise times,various neutral

density (ND) filters were used to vary the incident flux on the TFEDs.The wavelength of the exciting light was 0.46 μm for the hydrogenated device and 0.39 μm for the non-hydrogenated device.The wavelengths were chosen where the change in the OBS was the largest;for the hydrogenated device,this effectively implied that the chosen wavelength must be greater than where the quenching effect appears.

To describe the form of the rise in the OBS,we essentially have to find the appropriate solutions to the following equation:

$$\dot{n}_c = -e_n^o n_T + Cn_c(N_T - n_T) \qquad 4.1$$

Here n_c is the concentration of electrons in the conduction band,e_n^o is the optical emission constant for electrons,C is the capture probability for electrons in the conduction band,N_T is the total concentration of the impurity of which n_T are occupied by electrons.This equation assumes that a single deep level exists in the band gap.

In in the limit when the impurity is completely occupied by electrons when the TFED is in the dark then

$$n_c(t) = N_T(1 - \exp -t/\tau) \qquad 4.2$$

where $\tau^{-1} = e_n^o$. Thus equation 4.2 predicts that

$$\tau^{-1} = e_n^o = \sigma\phi$$

that is a plot of τ^{-1} vs ϕ (where ϕ is the flux of light incident on the TFED) should yield a straight line.Furthermore the rise in the OBS will be an exponentially increasing function.

An alternative solution to equation 4.1 when the second term cannot be neglected is

$$n_c = (1/2C)[-e_n^o + \tanh\{(\Delta /2C)(t - k)\} \qquad 4.4$$

where $\Delta^2 = (e_n^o)^2 + 4e_n^o CN_T$ and k is a constant of integration.Equation 4.4 can be approximated by an exponentially increasing function for large values of $\Delta /2C(t - k)$.

Figure 4.8a 4.8b show the rise in the OBS for the non-hydrogenated device for two different ND filters.An attempt has been made to fit the experimental data to the models presented above. These figures show that the rise in the OBS can be best described by equation 4.2. This conclusion is further supported if we plot τ^{-1} found from the final part of the trace using Mangelsdorf's method against ϕ we get a straight line.This is shown in figure 4.9.Hence figure 4.5b shows for the non-hydrogenated device $(\tau\phi)^{-1}$ $(h\nu)$ is the spectral dependence of the electron cross section.

We can use this information to find the photoionisation threshold for the impurity present in the non-hydrogenated device.In chapter 2 we showed that a model for the impurity photoionisation is

$$\sigma (h\nu) \sim (h\nu)^{-1}(h\nu - h\nu_o)^{3/2} \qquad 4.5$$

In figure 4.10 we have plotted a graph of $((\tau\phi)^{-1}h\nu)^{2/3}$.From a least squares analysis,a photoionisation threshold of (2.49 $\pm$ 0.25)eV is obtained.

For the hydrogenated device a similar analysis of fitting the rise in the OBS for different ND filters was carried out.Figure 4.11a and 4.11b show the fit to the rise of the OBS to equations 4.2 and 4.4.It is seen that neither of the models gives a complete agreement with the experimental data.Equation 4.4 gives a better description to the data at the start of the OBS but the latter part is described better by equation 4.2.Thus the inverse rise time for the hydrogenated device does not give good information as in the non-hydrogenated device.Accordingly if we take the final part of the OBS then the spectral dependence of $(\tau\phi)^{-1}$ reflects the optical cross section for electrons.Since we have shown above in figure 4.7 that the same impurity exists in both the devices we need not plot a graph of $(\tau\phi)^{-1}(h\nu)$ for the hydrogenated device

A further analysis can be made from the general equation describing the rise of the OBS (equation 4.2).If the impurity occupancy does not change appreciably when light is incident on the TFED then the steady state change in the OBS will reflect the optical emission constant for electrons.To test this a graph of $((\Delta V/\phi)h\nu)^{2/3}$ was plotted and a photoionisation threshold of 2.49$\pm$ 0.03eV was found for both the devices.It seems therefore,that the occupancy of the deep centre does not change appreciably when light is shone on the TFED.

4.1.4 Discussion

We reported earlier that the dc conductivity of the TFED increased by at least two orders of magnitude when UV light was shone on the device. Furthermore, the I-V curve for this device showed Ohmic behaviour up to 10V. A further conclusion from this experiment is that the OBS reflects the change of photoconductivity rather then a change of photocapacitance.

The rise of the transient when monochromatic light was shone onto the device was modelled to show that the OBS increased exponentially for the non-hydrogenated device only. This property was used to find the photoionisation threshold of the deep centre which was found to be 2.49 ± 0.25 eV below the conduction band. For the hydrogenated device the rise of the OBS was complicated and neither of the models presented above was able to model the rise of the OBS. A comparison of the spectrum of $((\tau\phi)^{-1})$ for the two devices showed, however, that the same deep centre existed in both the hydrogenated and the non-hydrogenated device.

The value of the photoionisation threshold of 2.49 ± 0.25 eV was found from the spectrum of $(\tau\phi)^{-1}$. If the occupancy of the deep centre does not change appreciably when a perturbation is applied to the TFED, the steady state value of the OBS reflects the optical emission constant (this, of course, assumes that only a single deep centre exists in the band gap). This hypothesis was used to find the photoionisation threshold of the deep centre from the spectrum of $(\Delta V/\phi)$ for the non-hydrogenated device. The photoionisation threshold

found from this spectrum was within experimental error the same as that found from the spectrum of $(\tau\phi)^{-1}$.

Therefore,at this point we can conclude that the photoionisation threshold of the impurity of the deep centre is 2.49 $\pm$ 0.25 eV below the conduction band and that its occupancy does not change appreciably from the dark occupancy of the deep centre.

Some speculation of the nature of the deep centre will be made here briefly.It is known by the researchers in the field of TFEDs that copper diffuses rapidly in ZnS and that complexes of copper can almost always be found (G Muller - private discussion).In fact in earlier work, TFEDs were doped intentionally with copper as this was found to promote good electroluminescence.Thus there is a possibility that the deep centre observed in the optical experiments is a copper related complex.Alternatively,the deep centre could be associated with a lattice defect such as a point defect. The effect of hydrogenating the TFED is to produce other deep level(s) in the band gap.These extra deep levels act as recombination centres when monochromatic light is shone on the device.

4.1.5 Conclusion on the optical experiments

A deep centre with a photoionisation threshold of 2.49 $\pm$ .25eV below the conduction band occurs in both the hydrogenated and the non-hydrogenated device. When monochromatic light is shone onto the device,very little change in the occupancy of the deep centre is produced.The only difference between the hydrogenated and the

non-hydrogenated device was that the hydrogenated device showed a quenching of the steady state value of the OBS for photon energies in excess of 3.1eV.The deep centre observed could be a copper related complex or it could be a native defect associated with the lattice.

Section 2

4.2 Equivalent circuit of the TFED

In this section we will show that the equivalent circuit of the TFED is the capacitance of the ZnS in parallel with the leakage resistance of the ZnS. These two components are in a series combination combination with the resistance of the contacts. This simple picture of the TFED will be shown to be inadequate when light is shone on the device.Furthermore,when light is "on",the device can be modelled if the resistance of the device has a frequency dependence.This frequency dependence of the resistance is explained on the basis that "multiple trap controlled hopping" is the process that gives rise to the dispersive nature of the resistance of the device.

4.2.1 Experimental method

The apparatus for measuring the capacitive and the resistive parts of the TFED consisted of a Solatron frequency response analyser (FRA) linked to a Tektronix 4006 computer.

The FRA was first tested for reliability by connecting a 3600pF low loss silver mica capacitor to it and measuring the capacitance of the capacitor over six orders of frequency (1Hz to 1MHz).The silver mica capacitor was chosen for its low loss factor of $\sim 10^{-3}$ over the frequency range of 60 HZ to 1 MHz (Terman (1943)),ie over this frequency range we should not expect to see any dispersion in the capacitance of the capacitor.Figure 4.13 shows that the frequency response of the capacitor is flat except in the frequency range from 100kHz to 1MHz.This behaviour is consistent with the specification of the FRA which states that the useful range of the FRA is from 10^{-5}Hz to 10^{5} Hz.

Two experiments were done with the TFED.In one experiment,the TFED was placed in a darkened plastic box for at least thirty minutes and then the frequency response of the TFED was measured over the frequency range of 1Hz to 1MHz.The results of this experiment are shown in figure 4.14a for frequencies between 1Hz and 1MHz.The case when the TFED is in the dark is called "dark case". It is seen in figure 4.14a that the dark capacitance of the TFED is constant within the frequency range [1,100k]Hz. The rise in the capacitance of the TFED above 100kHz shows a behaviour similar to that of the silver mica capacitor. It follows that the data above 100kHz can safely be neglected.All the data presented in later sections will only be

presented in the frequency range [1,100k]Hz.

In the second experiment, light from a 250W lamp was passed through a lens to form an image on the TFED which covered slightly more than one pixel. Light was left on for 5 minutes and with the light continuously on the TFED ,the FRA was logically started from the computer to start gathering data.The situation when there is light on the TFED is referred to as "light on" case.

To find the resistive and the capacitive parts of the TFED the FRA assumed that the equivalent circuit of the TFED could be represented as a series combination of a capacitor and a resistor (C_s and R_s) as shown in figure 4.16b.

4.2.2 Results

The dispersion of R_s and C_s when the TFED is in the dark is shown in figure 4.14a and 4.15a respectively.The frequency dependence of C_s has been mentioned in the previous section.Variation in $R_s(f)$ shows that above 1kHz the resistance of the device stays constant at 815Ω .Below 1kHz, R_s increases as the frequency is decreased as a power law.

When light is shone onto the device ("light on"), R_s and C_s show the dispersion seen in figure 4.15a and 4.15b.In contrast to the case when the TFED is in the dark, C_s shows dispersion;it increases as the frequency is decreased in a non linear fashion at low frequencies,while at high frequencies the value of C_s tends to a constant value.The behaviour of R_s,however, is similar to that when

the TFED is in the dark. The difference between R_s when the TFED is in the dark is that with the light on R_s shows three distinct regions in the dispersion: above 40kHz R_s stays constant, while below this frequency, there are two regions of power law behaviour.

To analyse the above results, consider the equivalent circuit of the TFED shown in figure 4.16a. In terms of the parameters R_s and C_s, it is straight forward to show that:

$$R_p = [1 + 4\pi^2 f^2 C_s^2 (R_s - R)^2]/\{4\pi^2 (R_s - R) f^2 C_s^2\} \qquad 4.6$$

$$C = C_s/[1 + 4\pi^2 f^2 C_s^2 (R_s - R)^2] \qquad 4.7$$

The R_s and C_s have been converted into R_p and C using equation 4.6 and 4.7 and the results of these calculations when the TFED is in the dark are shown in figures 4.17a for R_p and 4.17b for C respectively. By comparing figure 4.17b with 4.15b it is seen that C_s - C stays constant and since C is constant then

$$R_p = \frac{1}{2\pi f\sqrt{[C(C - C_s)]}} \qquad 4.8$$

Equation 4.8 therefore predicts that R_p should be directly proportional to the inverse of frequency. A least squares analysis on figure 4.17a shows that the slope of the line is -1.0 ± 0.1. Hence the equivalent circuit shown in figure 4.16b is the correct equivalent circuit when the TFED is in the dark.

Using equation 4.6 and 4.7, R_p and C were also calculated when light was shone onto the device. The results of these calculations are shown in figure 4.18 for R_p and 4.17b for C. For R_p we notice that for frequencies larger than 4kHz $R_p \propto f^{-0.86}$, while below 4kHz two power laws are observed where the exponents have values of -0.63 and -0.26. The power laws seen in figure 4.18a are not consistent with the simple impedance picture of the TFED, as the impedance picture implies that the capacitance and the resistance of the device should be independent of frequency. It is seen in figures 4.18 that the resistance of the TFED varies as a power law. Such power law behaviour in the conductance is well known in amorphous semiconductors where the ac conductivity, σ_{ac}, varies as a power law of frequency. Hopping conduction in a-ZnS has recently been observed by Iida and Suzuki (1983).

To explain the frequency dependence of the resistance of the TFED we shall propose that "multiple trap controlled hopping" (see Schmidlin (1977), Pfister and Scher (1978) and Tiedje and Rose (1980)) as a possible process that gives rise to the dispersion in R_p and C.

The phenomenon of hopping conduction is well known in amorphous semiconductors, although it is less well known in crystalline and polycrystalline semiconductors. Conventional hopping involves a electron (or hole) tunnelling between different donor (acceptor) sites. The tunnelling depends on the overlap integral, that is, on the the overlap of the wavefunction of the electron (hole) between its present site and other sites that are removed from it spatially. To observe hopping conduction we must go to low enough temperatures so

that the electrons can be frozen onto the donor states.

Hopping conduction has been described by Mott and co-workers (Mott and Davis (1979))where it is the overlap in the wavefunction of the carrier between different energy states that gives rise to hopping.Scher and Lax(1973)) have described hopping conduction using the continuous time random walk formalism.

The hopping conduction observed by us is ultimately connected with the kinetics of photoconductivity,ie,with the capture and release of carriers from traps. This is the main reason for preferring the multiple trap controlled hopping conduction (MUTCOHC). To understand the main features of MUTCOHC,consider what may happen to an electron excited optically from a deep level.In figure 4.19,we have shown a schematic diagram of a semiconductor with a deep level and "shallow" donor levels below the conduction band.The shallow donors have a distribution of ionisation energies with respect to the conduction band. The shallow donors are also assumed to be distributed randomly in the lattice. Indicated in figure 4.19 is the path of an electron excited optically from the deep level and the subsequent path following capture and thermal release from the shallow centres. The electron excited optically into the conduction band will be "free" until it is captured by a (vacant) site on a donor.The electron will remain on that site until one of three possible mechanisms can remove it to another site.The simplest possibility is that the electron can be thermally emitted into the conduction band. This is process "1" in figure 4.19.The electron can tunnel between different donor sites that are separated spatially ("2" in figure 4.19) ,or,if the donor sites also differ in energy then phonon assisted tunnelling can take place

between the two donor sites ("3" in figure 4.19). The end result of the electron tunnelling between different donor sites and or the conduction band is that it executes a random walk amongst the donor sites. The life of the electron on the donor will be terminated when it is trapped by a deep centre. Hopping conduction amongst the shallow donors is expected to be more dominant than hopping conduction amongst the deep levels.The reason is that the wavefunction for shallow levels is spread out whilst the wavefunction for electrons localised at deep levels have a localised wavefunction. Hence the probability for an electron to tunnel between different donor sites is expected to be large for electrons at shallow levels. It should be mentioned that MUTCOHC has primarily been used for explaining the transient photoconductivity following a flash of light on one surface of the semiconductor. It can in principle be adapted to the case when we have a steady state situation with the light on. When light is shone on the semiconductor,the rate equations for electrons excited into the conduction band,n_c, and the occupancy change of the deep centre are

$$\dot{n}_c = g + \sum_j n_i r_i - n_c \sum_i w_i \qquad 4.9$$

$$\dot{n}_i = n_c w_i - n_i r_i \qquad 4.10$$

Here n_c is the concentration of electrons excited into the conduction band,g is the generation rate of the excited carriers, n_i is the electron occupancy of the ith trap,w_i is the capture rate for the ith trap,r_i is the (thermal) release rate of the ith trap.In steady state,we have

$$n_c = g \; / [\sum_i w_i (1 - r_i^{-1})] \qquad 4.11$$

Now g was kept constant during the course of the experiment, and if w_i is slowly varying in time (compared to the time of the experiment) then n_c will be varying in time. Thus in the Fourier transform of n_c the real and the imaginary parts of the transform will show variation in frequency.

Jonscher (1983) has interpreted the MUTCOHC as a delayed reaction between the applied signal and the carrier corresponding to the signal. This is intuitively clear when capture and release of the carrier from a trap are involved. An excited carrier which is captured by a trap will spend some time in the trap before it is thermally released from the trap.

As far as we are aware, there has only been one paper on some form of hopping conduction occurring in ZnS based TFEDs (Szuba and Polewska (1982)). It was concluded by these authors that hopping conduction was due to an amorphous structure within their device. It is difficult to infer some amorphous structure occurring in their sample as the device structure has not been clearly specified. In our device, however, there was no evidence from the electron diffraction pattern study carried out by Cattel and Cullis (1982) that the ZnS had an amorphous structure. In fact the sputtered ZnS deposited onto a glass substrate was in the cubic phase and that it was polycrystalline with a grain size between 100 and 200 Å.

Before leaving the subject of hopping conduction, various authors are advancing their own theories as the "correct" theory at the expense of omitting all the other theories and experimental data. One prime example of this behaviour is the work of Jonscher and co-workers. They are advancing the proposition that if χ' and χ'' are the real and the imaginary parts of the dielectric susceptibility respectively then

$$\frac{\chi''(\omega)}{\chi'(\omega)-\chi'(\infty)} = \cot(n\pi/2) \qquad 4.12$$

In figure 4.20, we have plotted a graph of $C(f) - C(\infty)$ with the dark capacitance of the TFED taken as the high frequency limit of the capacitance. In the same figure, we have indicated the experimentally obtained exponents from a least squares analysis, n, and that obtained from the use of the Kramers-Kronig relationship, n', in brackets. It is seen from figure 4.20 that n and n' agree with each other only in the frequency interval from 10Hz to 5kHz. Outside this frequency range there is very little correlation between n and n'. The reason for this poor correlation is that the Kramers-Kronig relationship cannot be used for functions which vary with frequency as f^{-m}, where m is a positive quantity less than one. There are two reasons why the Kramers-Kronig relationship cannot be used for such functions. In the first case, there is a singularity at zero frequency and secondly, the frequency response of the dielectric susceptibility is not known from $-\infty$ to $+\infty$. The correlation between n and n' in the frequency range [10,5k]hZ in figure 4.20 is purely accidental and thus the relationship indicated in equation 4.12 is also accidental. The relationship in equation 4.12 is therefore not a consequence of the

Kramers-Kronig relationship; it is to be regarded as an empirical relationship which is sometimes observed experimentally.

4.2.3 Discussion

The equivalent circuit of the TFED in the dark is a parallel combination of a resistor and a capacitor (representing the ZnS as a dielectric with a leakage resistance)in series with a resistance of the contacts.The same equivalent circuit is useful when light is shone onto the device but the resistor and the capacitor become frequency dependant and the simple impedance picture of the TFED breaks down.The frequency dependence is associated with a type of hopping conduction involving the band states and states in the band gap of the ZnS. We believe that this is the first time that this kind of behaviour is seen in a II-VI semiconductor.

It could be argued that when electrons are excited from the deep level, they can form a small polaron.Since conduction by a small polaron is believed to be that by hopping then the existence of the small polaron in ZnS can explain the frequency dependence of R_p and C. This view is unlikely,as substituting typical parameters for ZnS as quoted by Mach and Muller (1982) into the formula for the Frohlich coupling coeffecient,we find that α turns out to be less then unity,hence no small polaron can form in ZnS.Space charge within the dielectric will also not influence the capacitance and the resistance.This is because we have measured the differential capacitance of the device and it can be shown that such effects can be neglected.

In conclusion,hopping conduction in ZnS:Mn is a possible mechanism to explain the dispersion in the capacitance and resistance of the TFED.

Section 3

The hydrogenated and the non-hydrogenated device have the same defect that gives rise to a deep level located at 2.49eV below the conduction band.The hydrogenated device has additional deep levels in the band gap.

In the electrical measurements we have found that the equivalent circuit of the TFED is only valid when the TFED is in the dark as the capacitance and the resistance of the TFED become frequency dependent when the light is on the device.The frequency dependence of R_p and C is associated with a novel form of hopping conduction.

References

J Appel Sol Stat Phys 21,193(1968)

A F Cattel and A G Cullis Thin Sol Films92,211(1982)

S Iida and S Suzuki J Non Cryst Sol 59-60,633(1983)

A K Jonscher "Dielectric relaxation in solids" Chelsea dielectric press,London 1983

P C Mangelsdorf J Appl Phys 30,442(1959)

R Mach ad G Muller Phys Stat Sol (a) 69,11(1982)

N F Mott and E A Davis "Electronic processes in non crystalline materials" Oxford,Clarendon 1979

G Pfister and H Scher Adv Phys 27,747(1978)

H Scher and M Lax Phys Rev B7,4491(1973)

F W Schmidlin Phys Rev B16,2362(1977)
Sol Stat Comm 22,451(1977)

T Suda,K Matsuzaki and S Kurita J Appl Phys 50,3638(1979)

S Szuba and W Polewska Phys Stat Sol(a) 71,65(1982)

H R Szawelska PhD thesis (1980) St Andrews university

T Tiedje and A Rose Sol Stat Comm 37,49(1980)

F E Terman "Radio engineers handbook" New York Mcgraw Hill 1943 page 11

D Theis J Lumin 23,191(1981)

Fig. 4.1 Schematic diagram of the experimental arrangement to study the TFEDs.

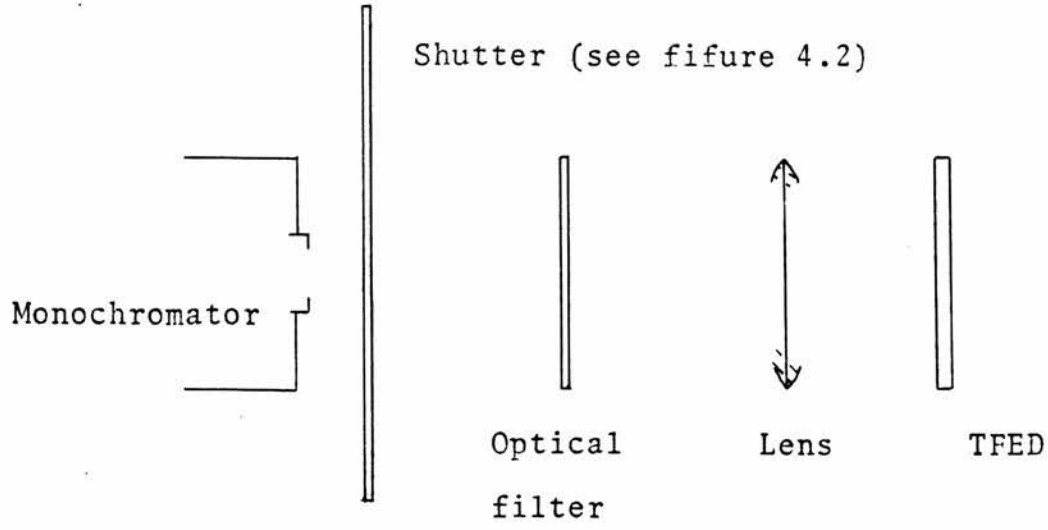

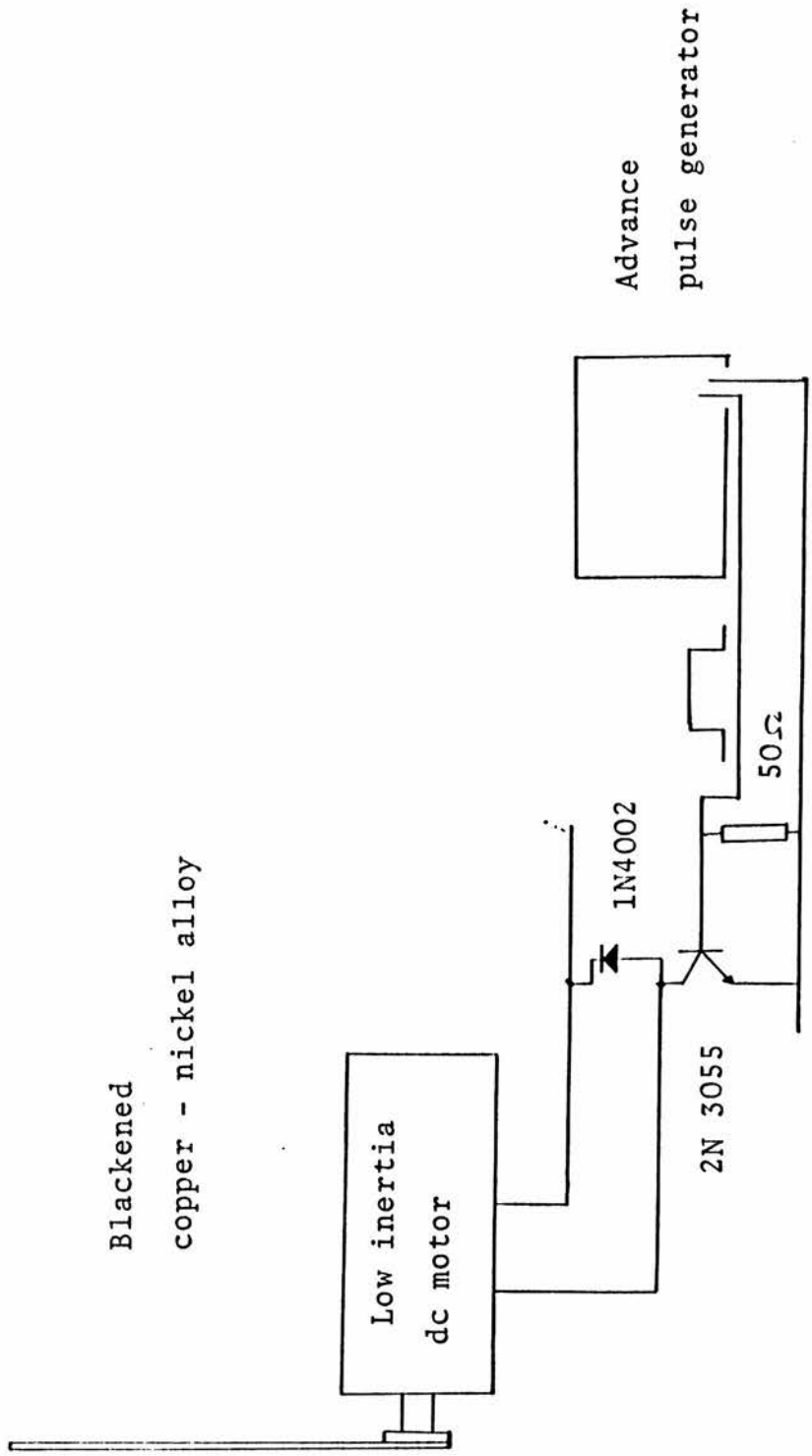

Fig. 4.2 The design of the shutter

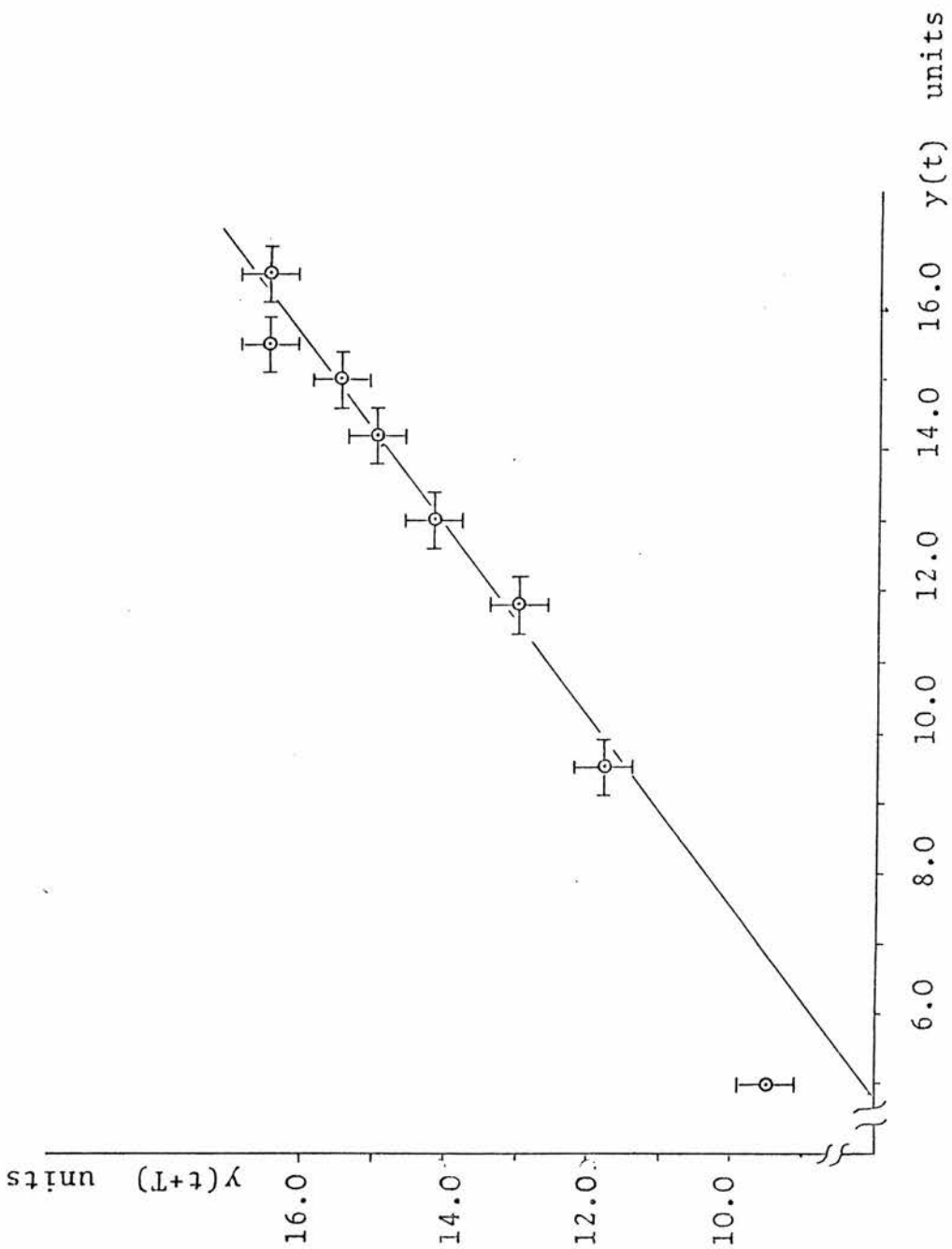

Figure 4.3 An example of a Manglesdorf plot to find the inverse rise time.The experimental points are for the hydrogenated device. λ=0.51 µm

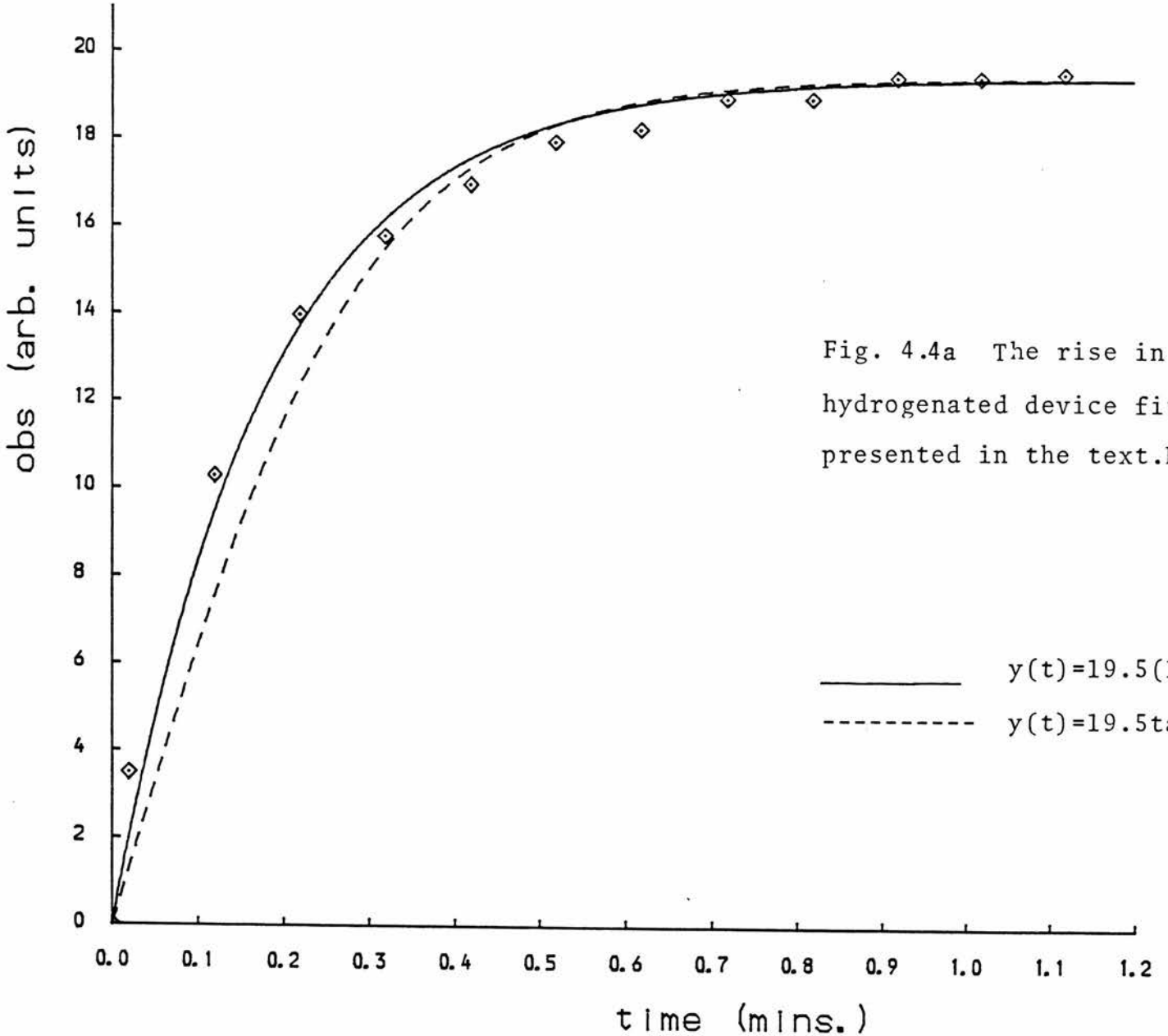

Fig. 4.4a The rise in the OBS of the non hydrogenated device fitted to the two models presented in the text.ND=0.6

———— y(t)=19.5(1-exp-5.55t)

---------- y(t)=19.5tanh(3.4t)

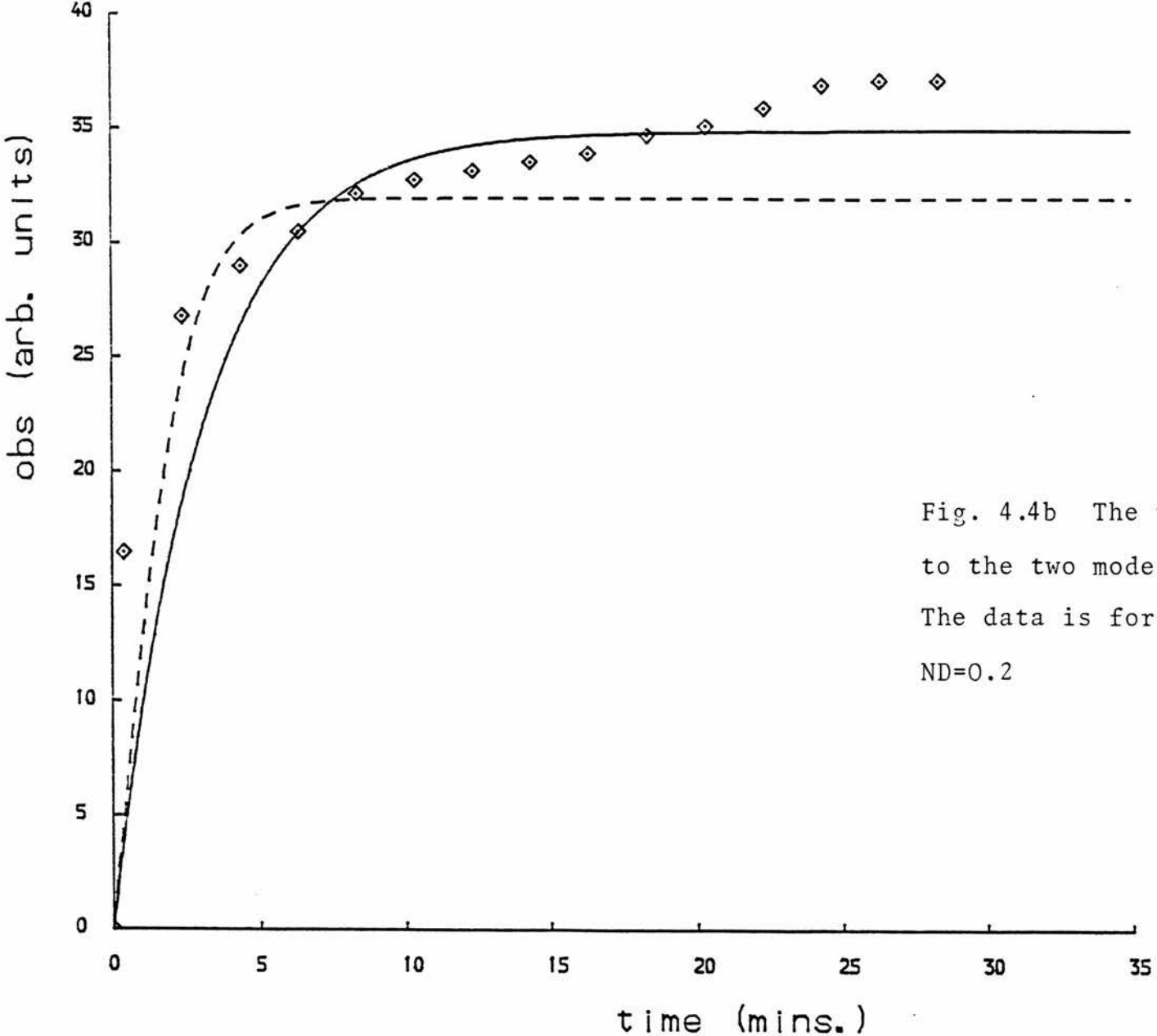

Fig. 4.4b The rise in the OBS fitted to the two models presented in the text. The data is for the hydrogenated device. ND=0.2

The inverse rise time and the steady state value of the OBS divided by the photon flux for the hydrogenated device.

Fig. 4.5a

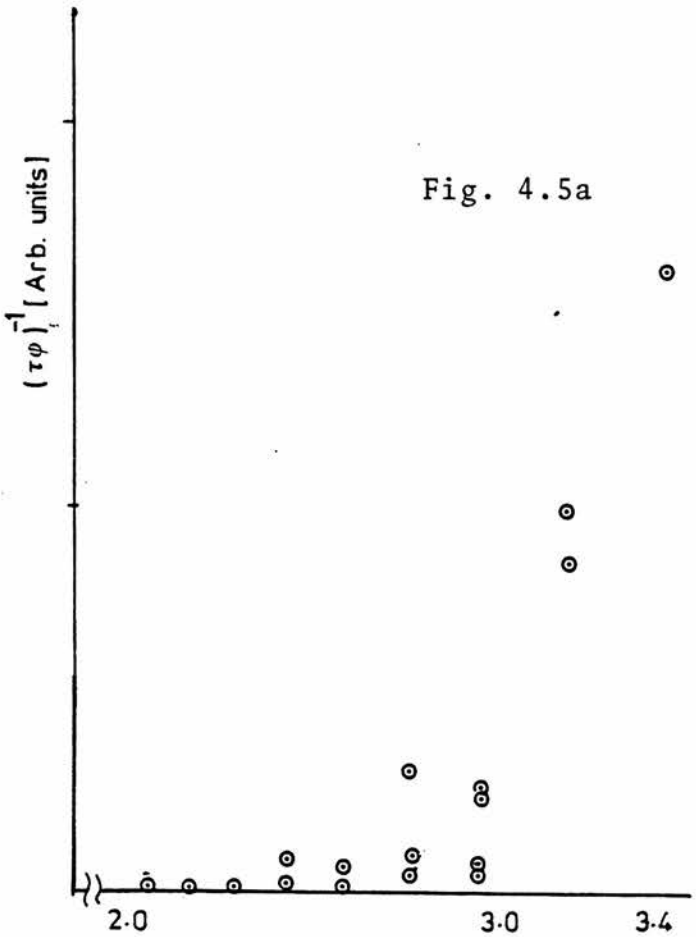

Fig. 4.5b

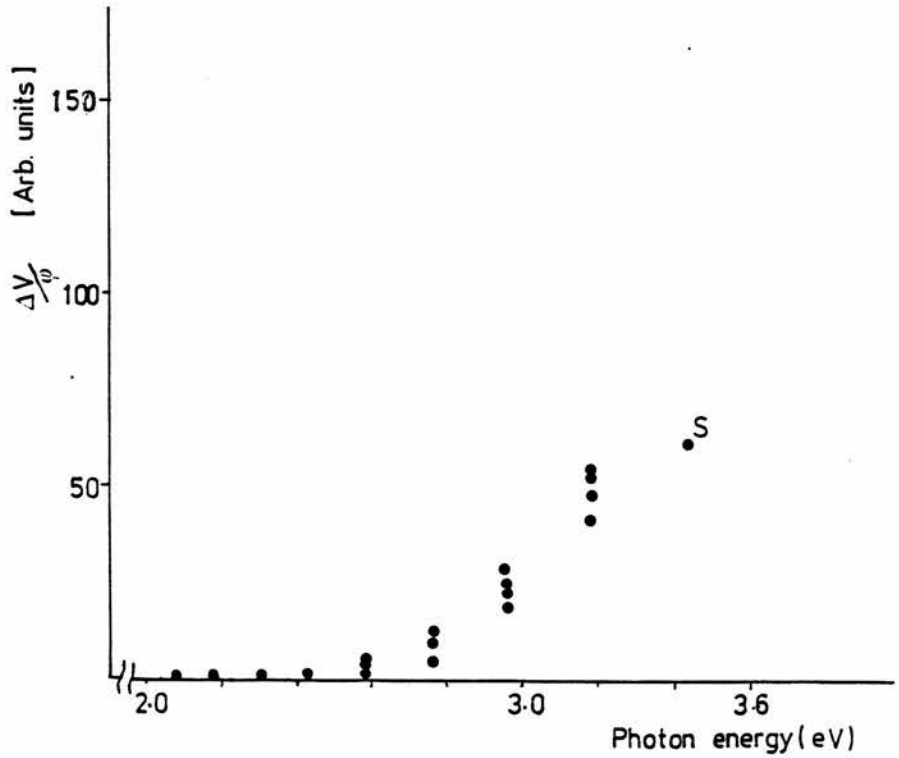

The inverse rise time and the steady state value of the OBS divided by the photon flux for the non hydrogenated device.

Fig. 4.6a

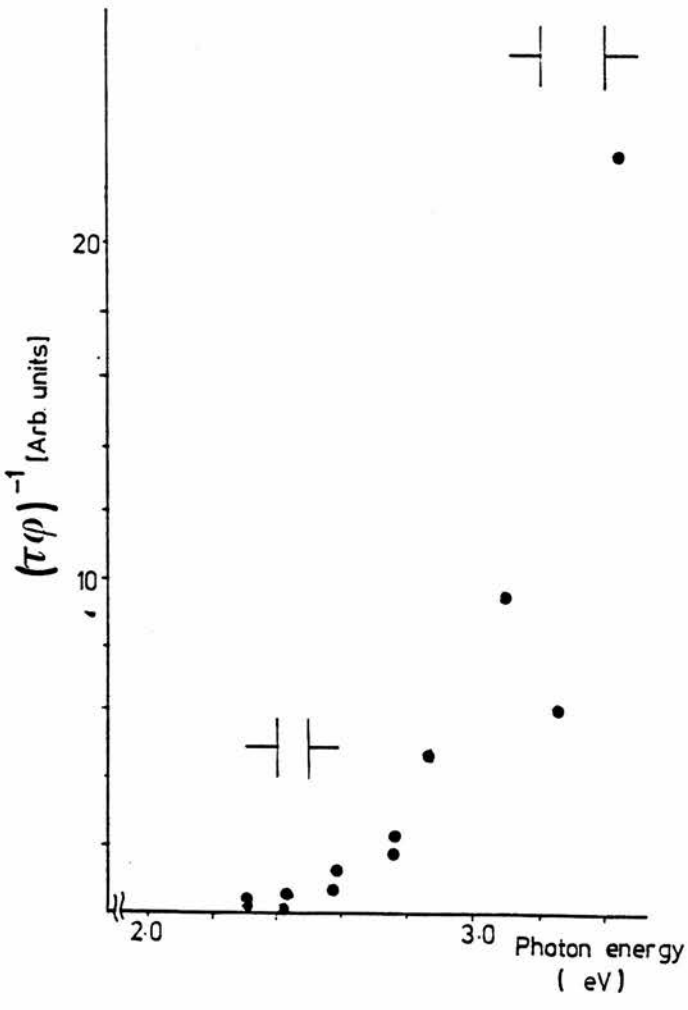

Fig. 4.6b

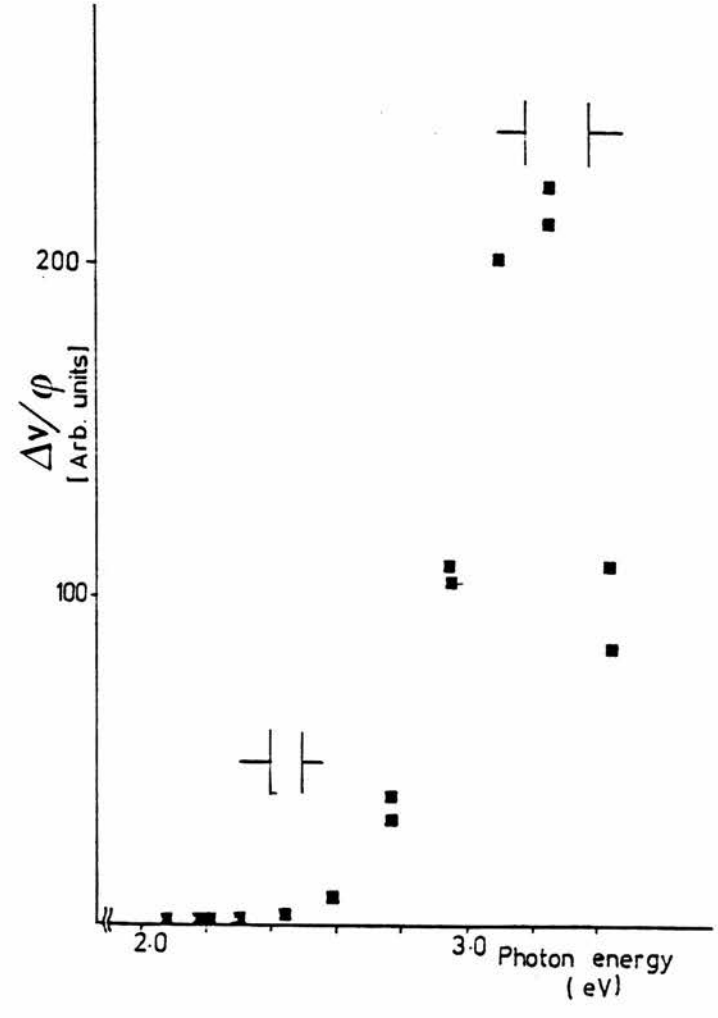

Fig 4.7 Comparison of the $(\Delta V/\varphi)$ spectrum for the non-hydrogenated and hydrogenated TFED's. The spectra are normalised at S'

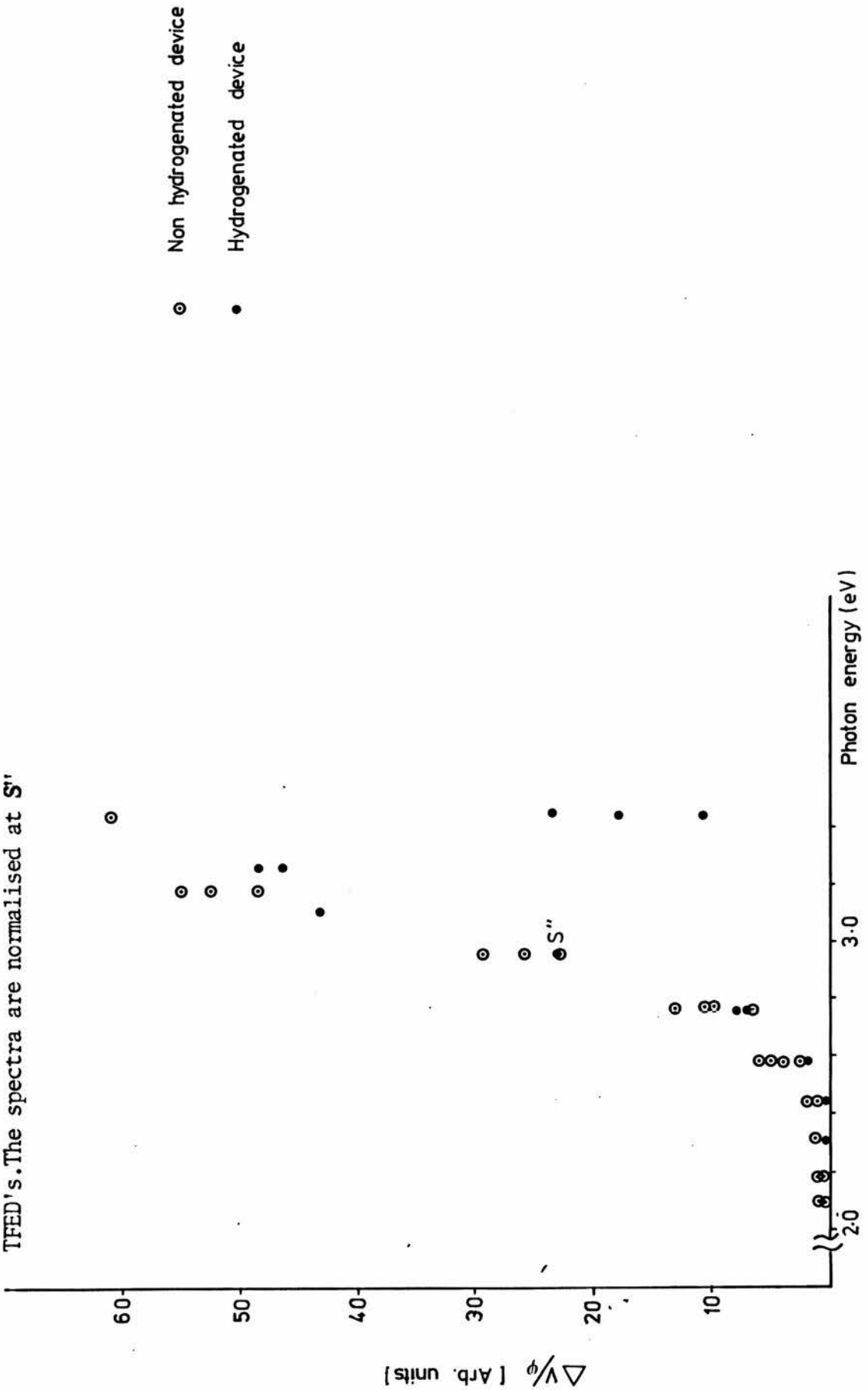

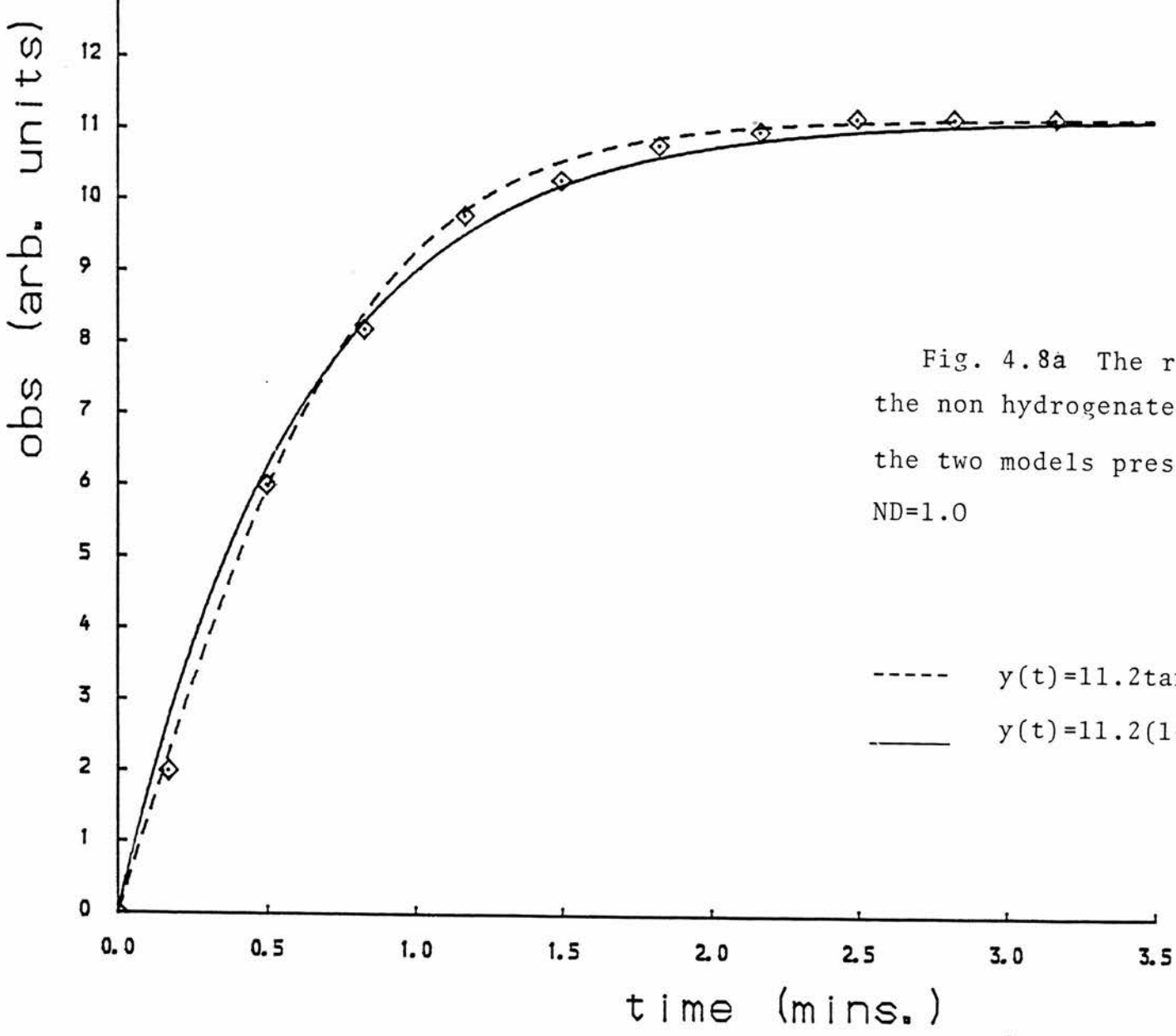

Fig. 4.8a The rise in the OBS for the non hydrogenated device fitted to the two models presented in the text. ND=1.0

----- $y(t)=11.2\tanh(1.13t)$

_____ $y(t)=11.2(1-\exp-1.65t)$

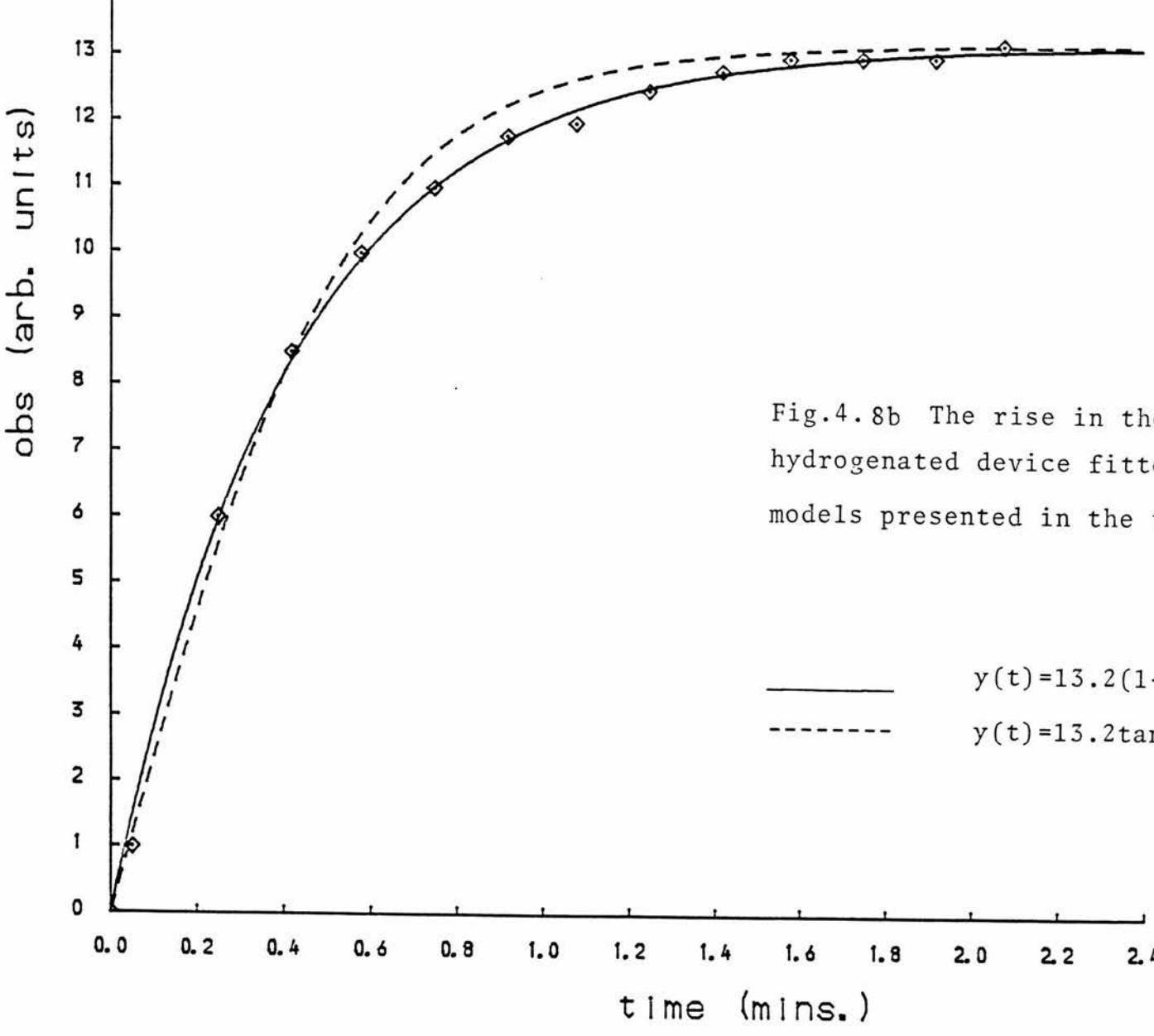

Fig.4.8b The rise in the OBS for the non hydrogenated device fitted to the two models presented in the text.ND=0.4

———— $y(t)=13.2(1-\exp-2.4t)$

-------- $y(t)=13.2\tanh(1.8t)$

Fig. 4.9 Inverse rise time calculated from the Manglesdorf method as a function of increasinf photon flux for the non hydrogenated device. λ=0.39 µm

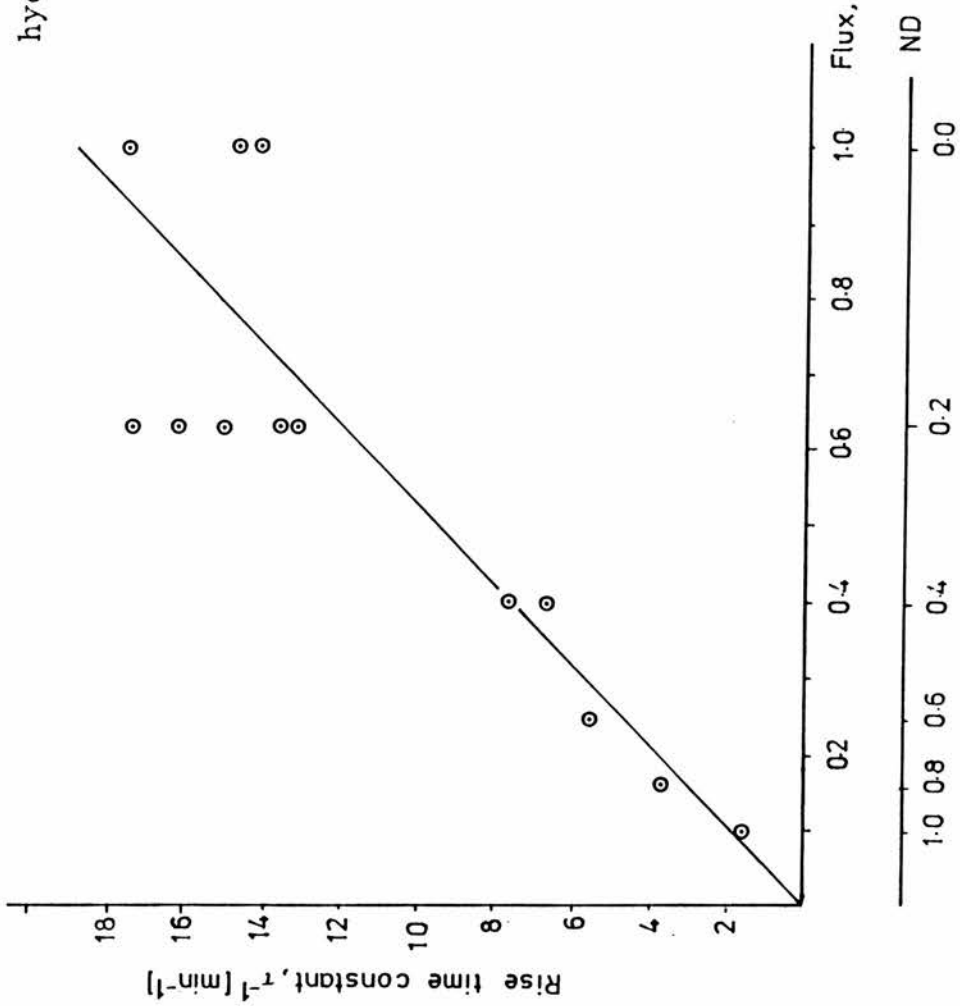

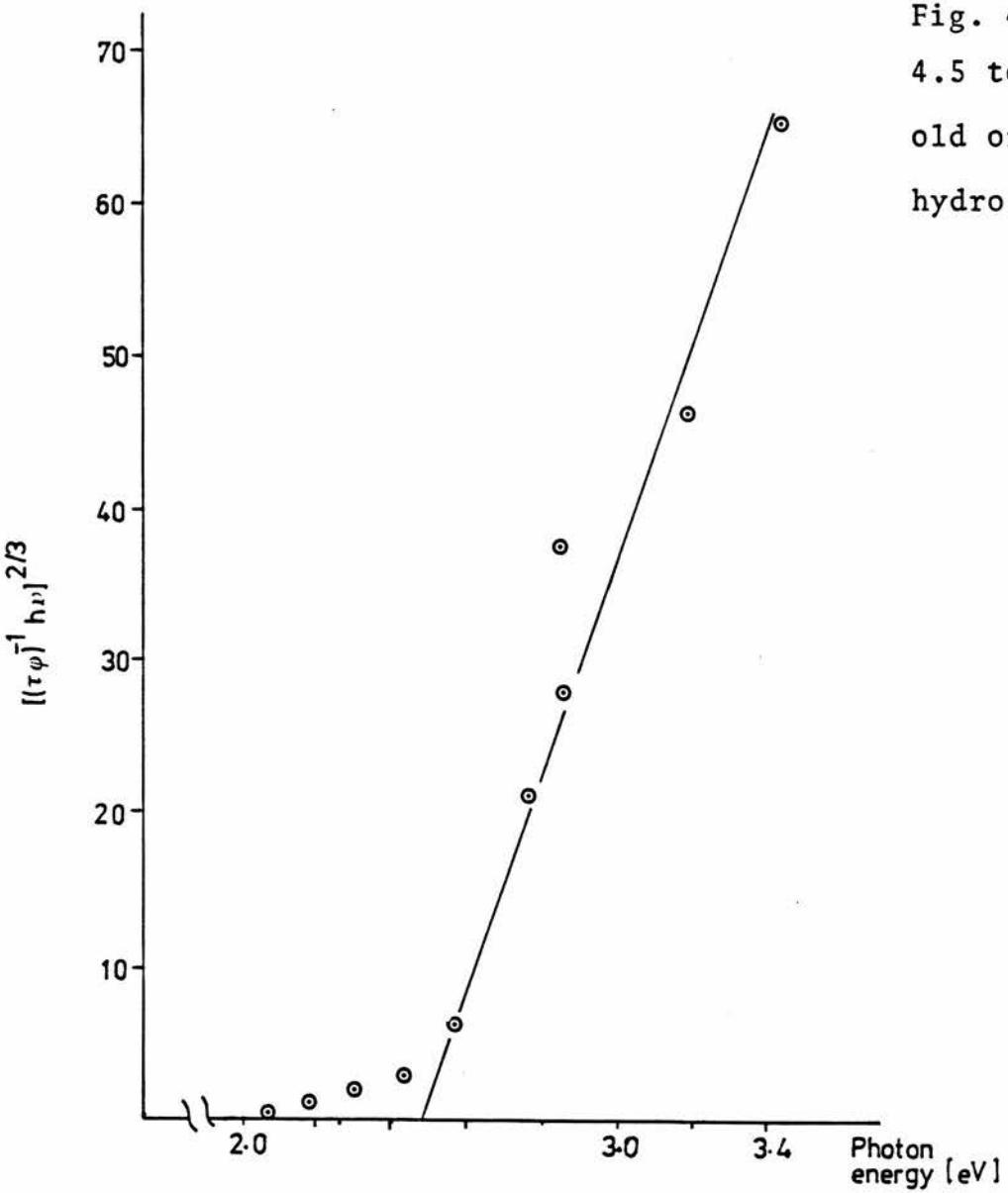

Fig. 4.10 A suitable plot of equation 4.5 to find the photoionisation threshold of the deep centre in the non-hydrogenated device

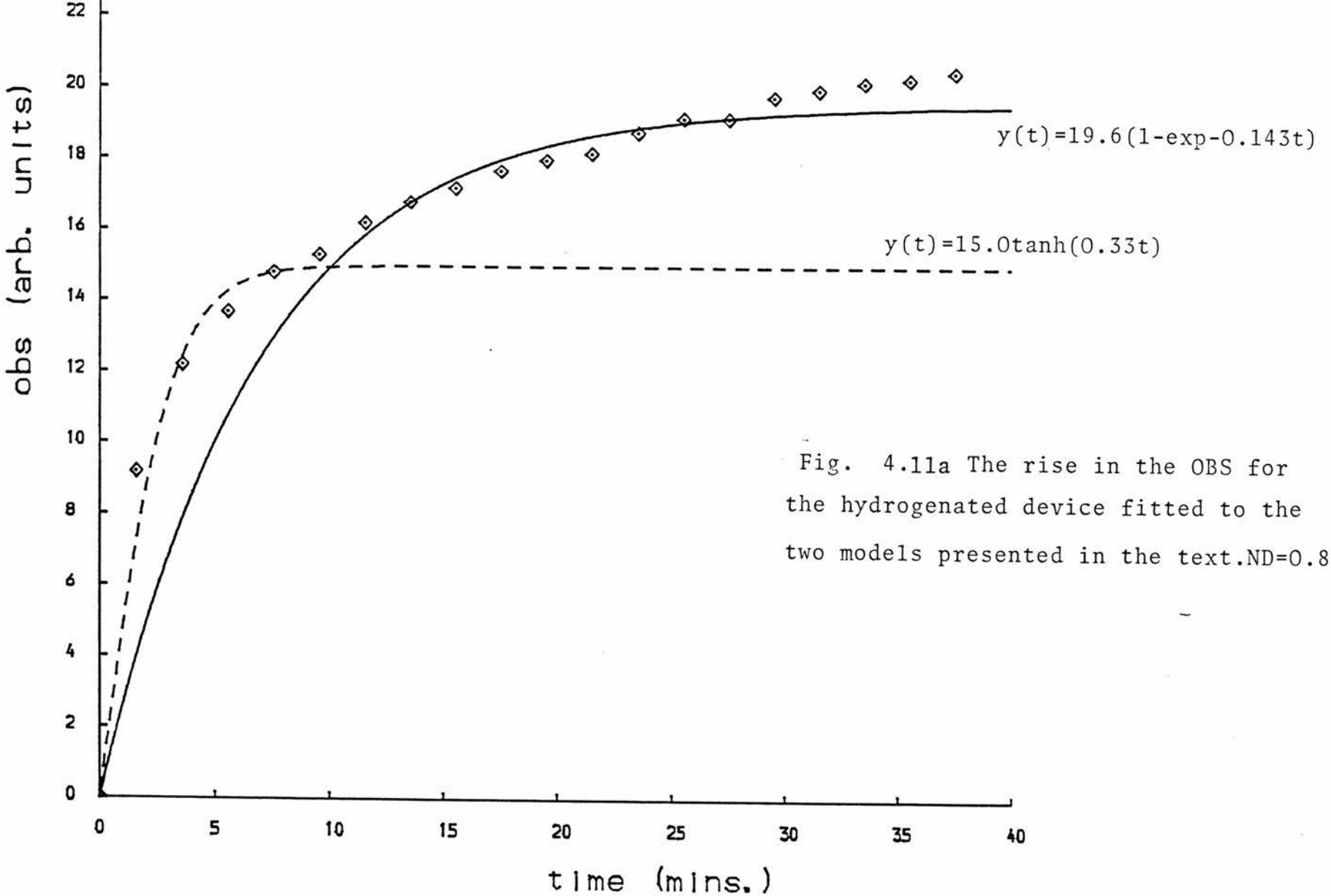

Fig. 4.11a The rise in the OBS for the hydrogenated device fitted to the two models presented in the text.ND=0.8

Fig.4.11b The rise of the OBS fitted to the models presented in the text.Hydrogenated device.ND=0.4

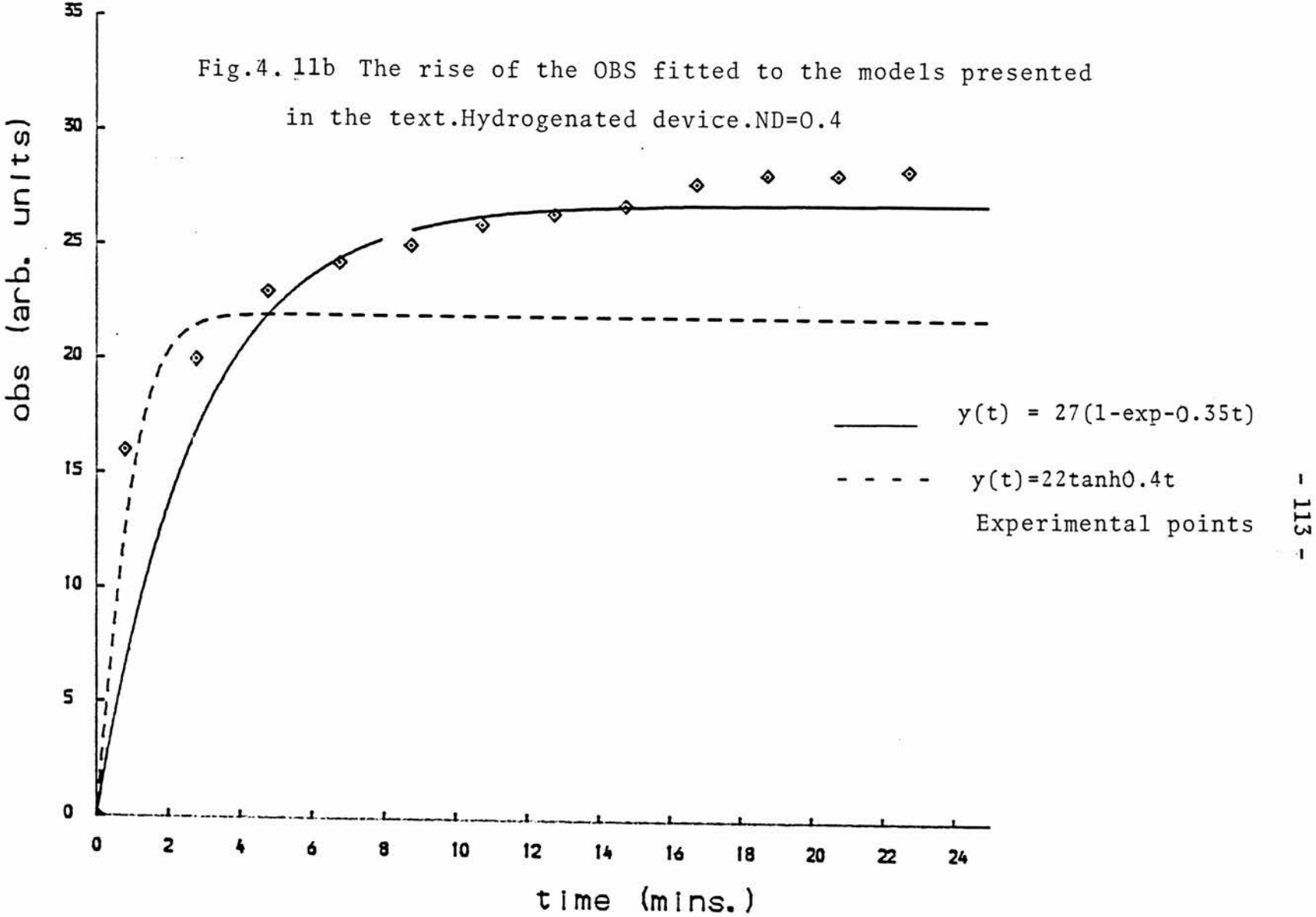

Fig. 4.12 The inverse rise time calculated from the Manlesdorf method as a function of increasing photon flux for the hydrogenated device. λ =0.46

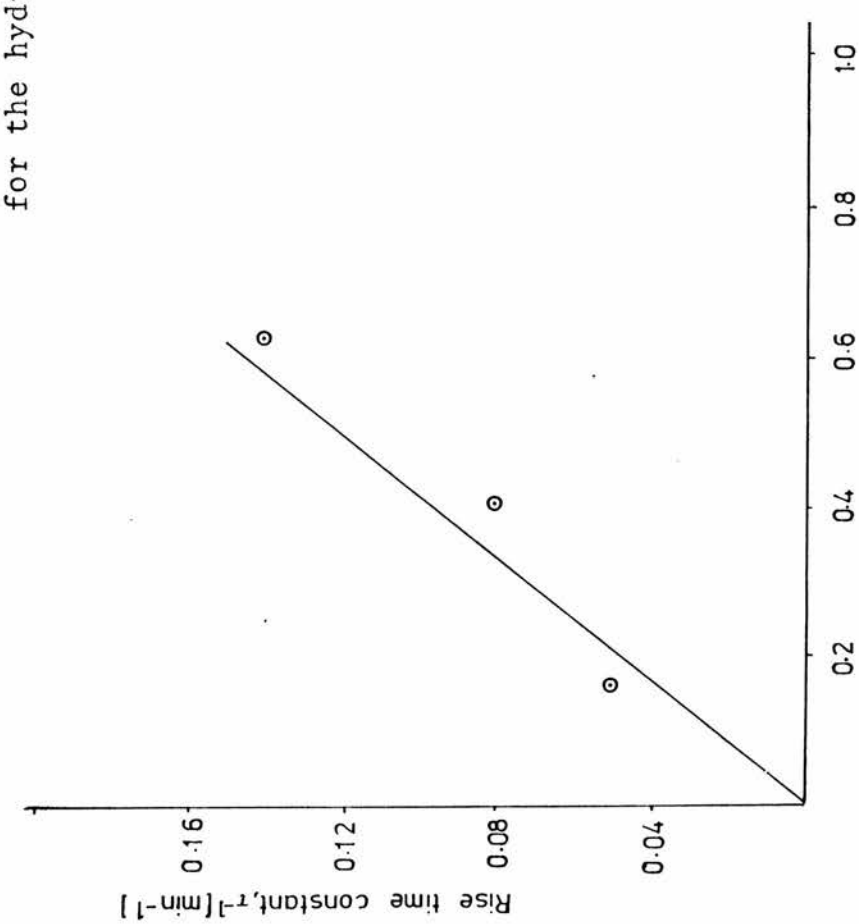

Fig. 4.13 The response of the FRA to a low loss 3n6 silver mica capacitor.

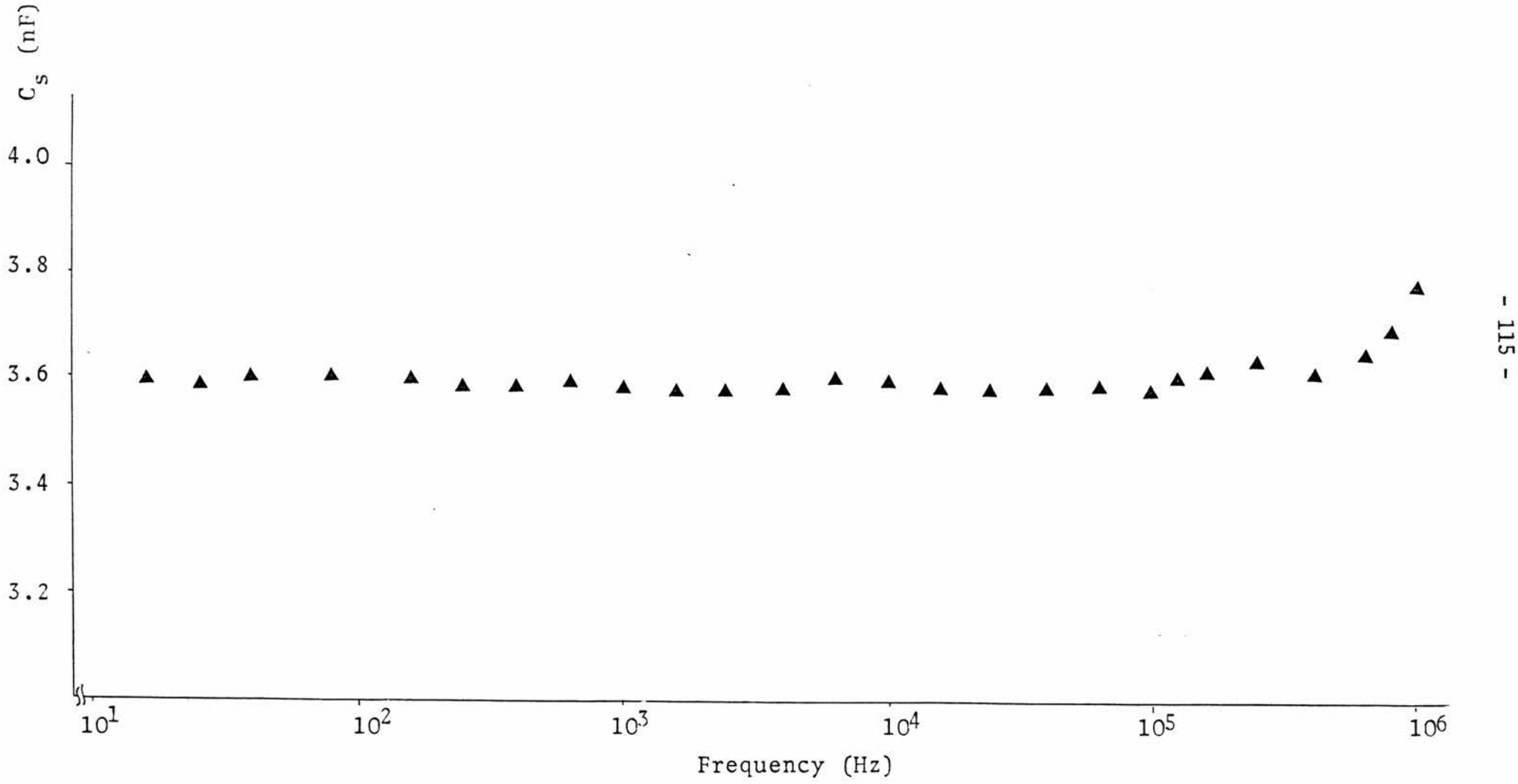

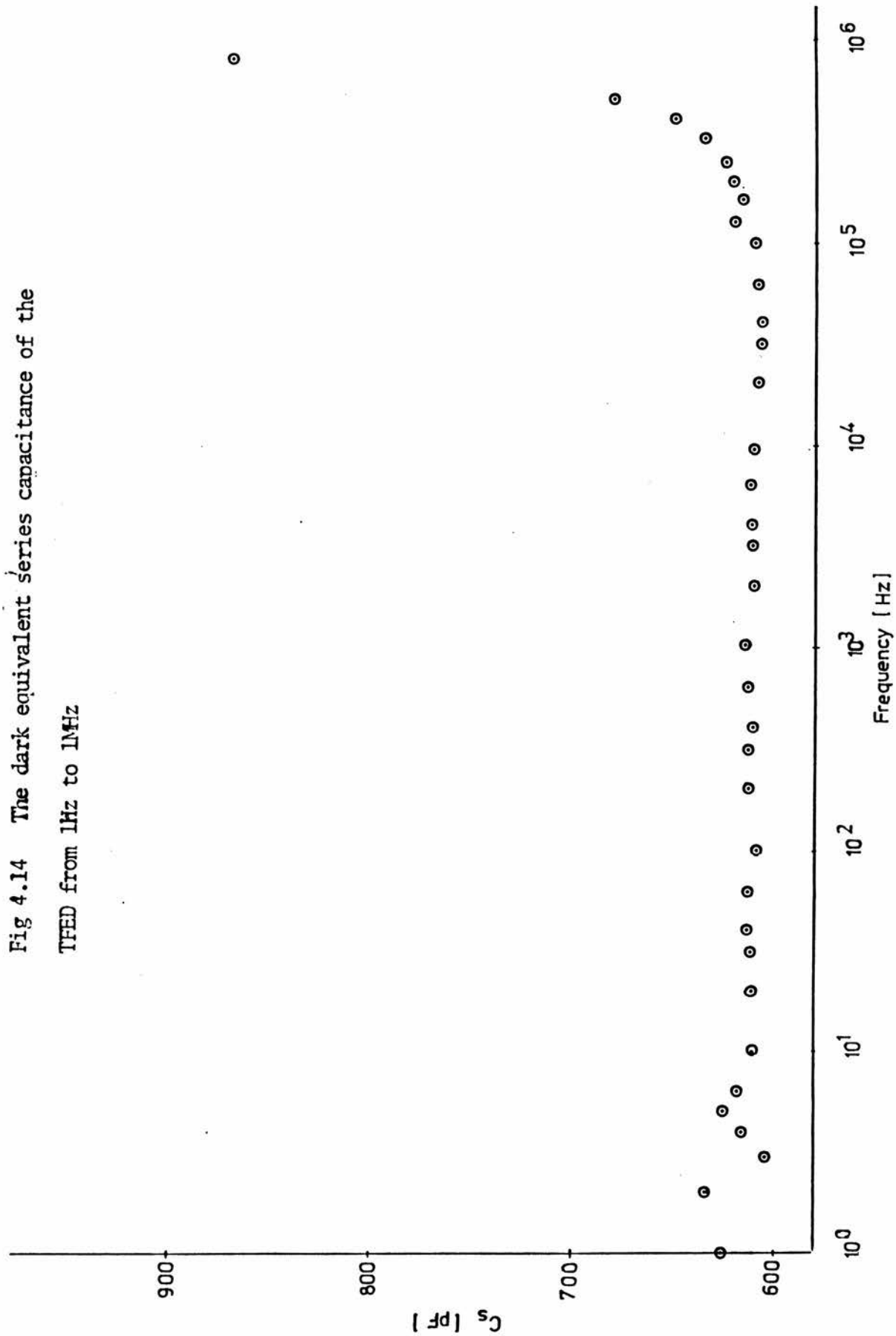

Fig 4.14 The dark equivalent series capacitance of the TFED from 1Hz to 1MHz

Fig. 4.14a TFED's dark equivalent seies resistance as a function of frequency.

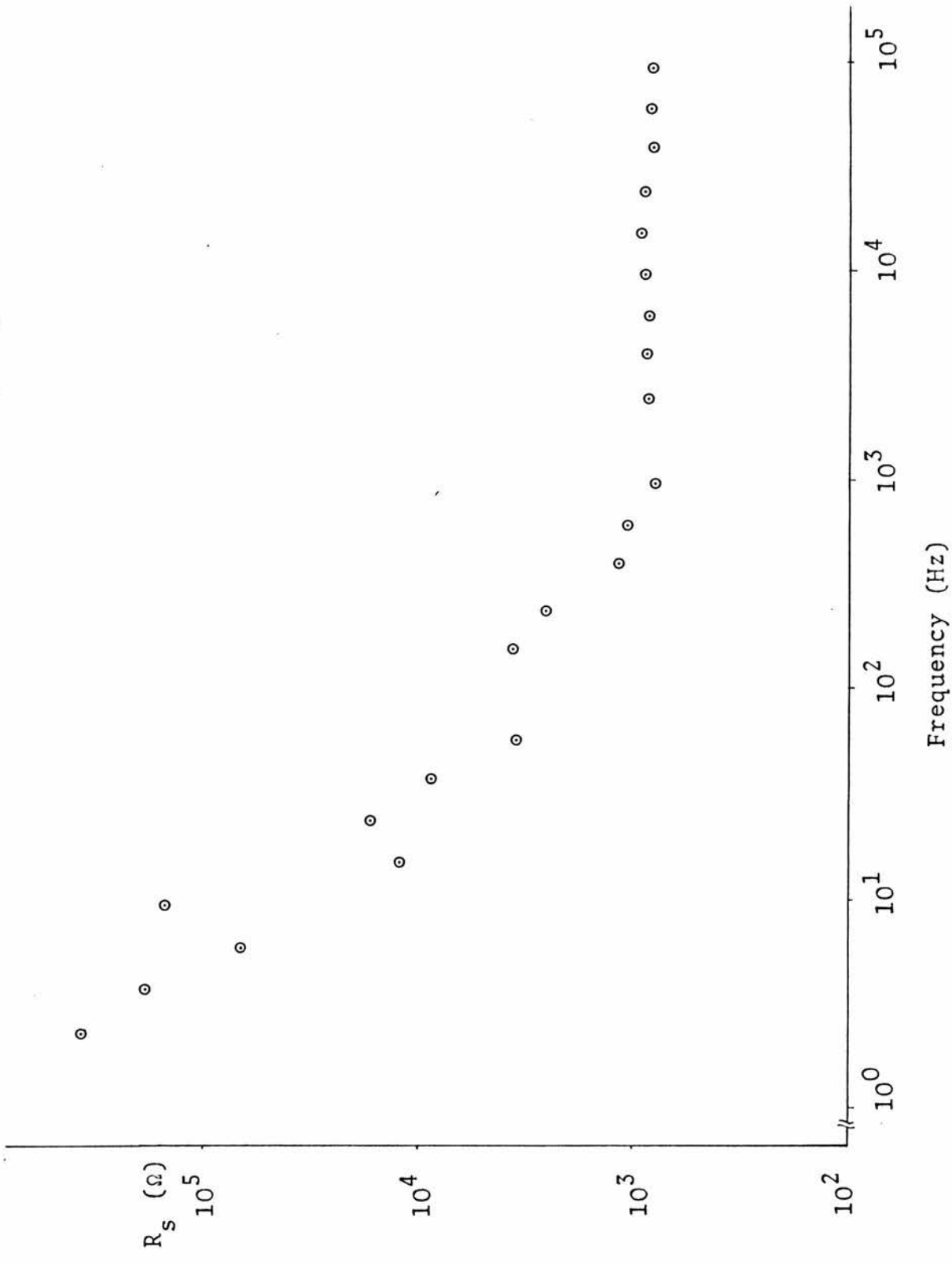

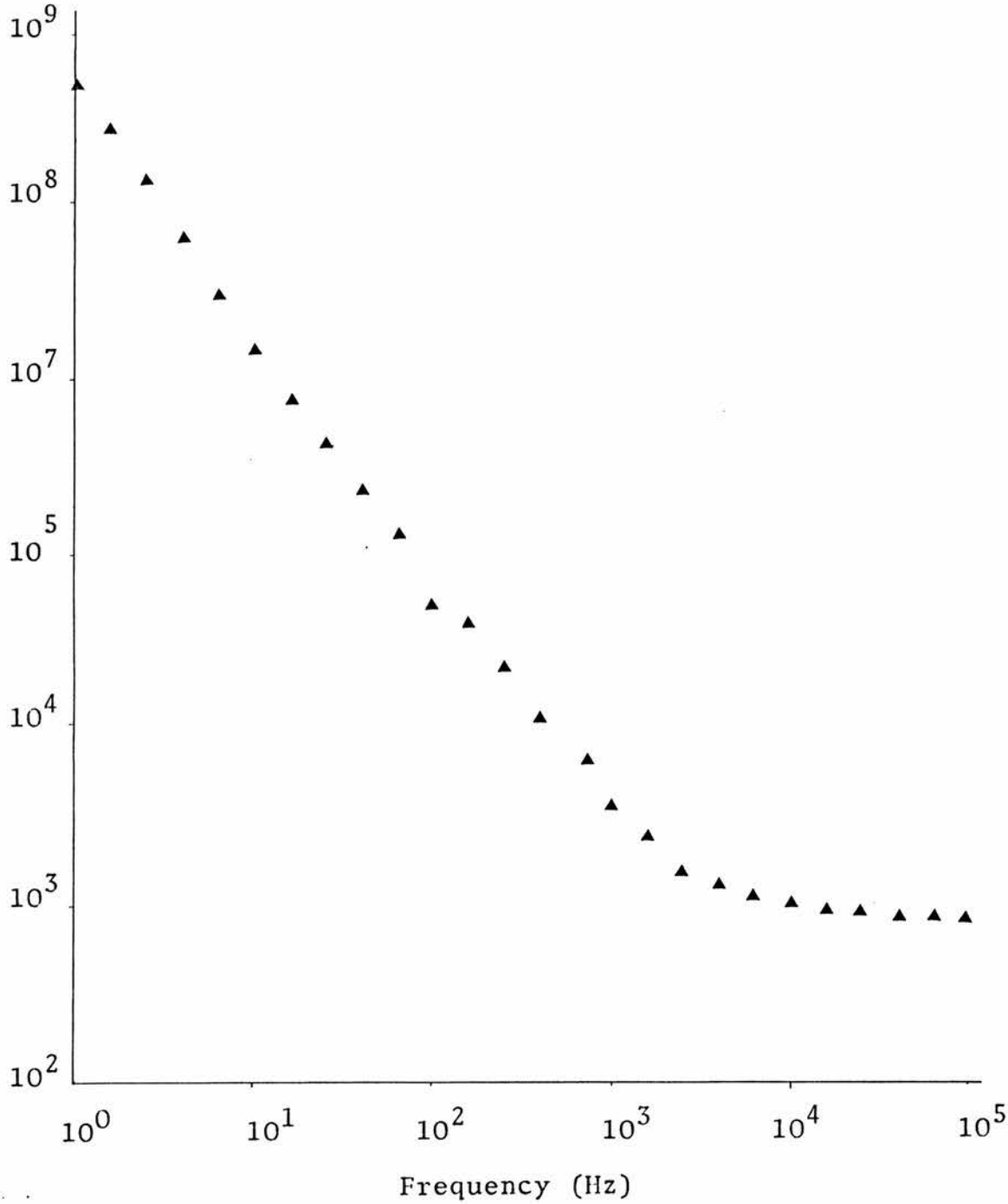

Fig. 4.15a The equivalent seies resistance of the TFED when light is on on the TFED.

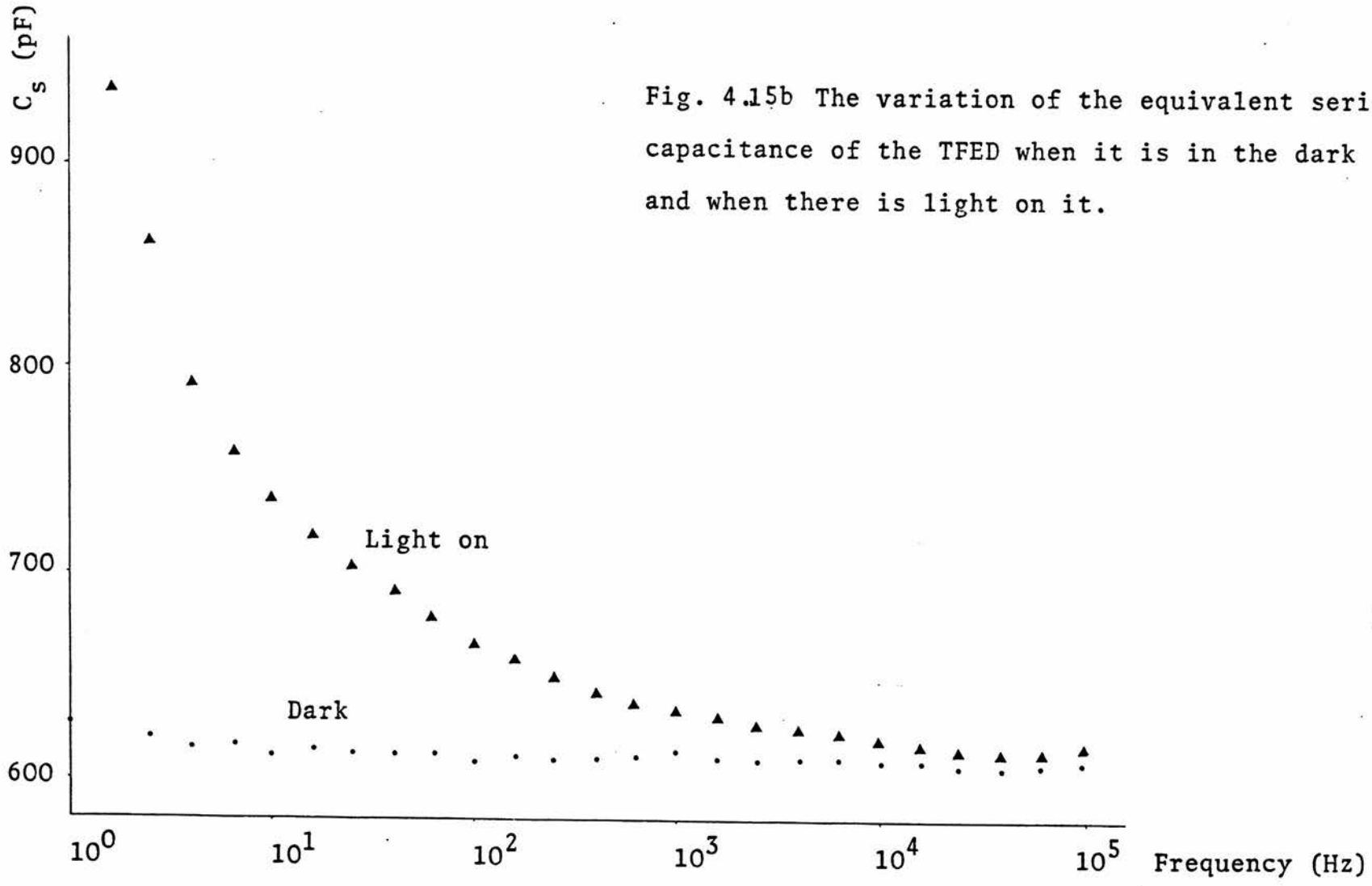

Fig. 4.15b The variation of the equivalent series capacitance of the TFED when it is in the dark and when there is light on it.

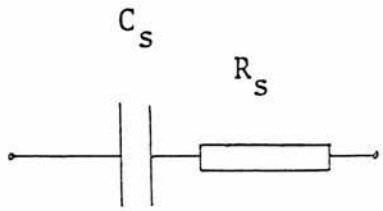

Fig 4.16b The equivalent circuit assumed by the FRA for an element of the TFED.

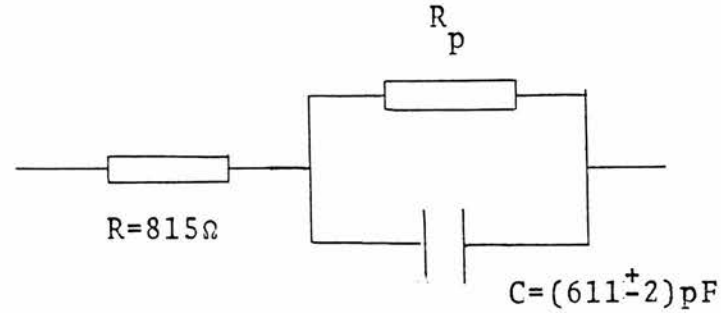

Fig.4.16a The circuit proposed as the equivalent circuit of the TFED.

Fig. 4.17a A graph showing that when the TFED is in the dark, R_p obeys equation 4.8

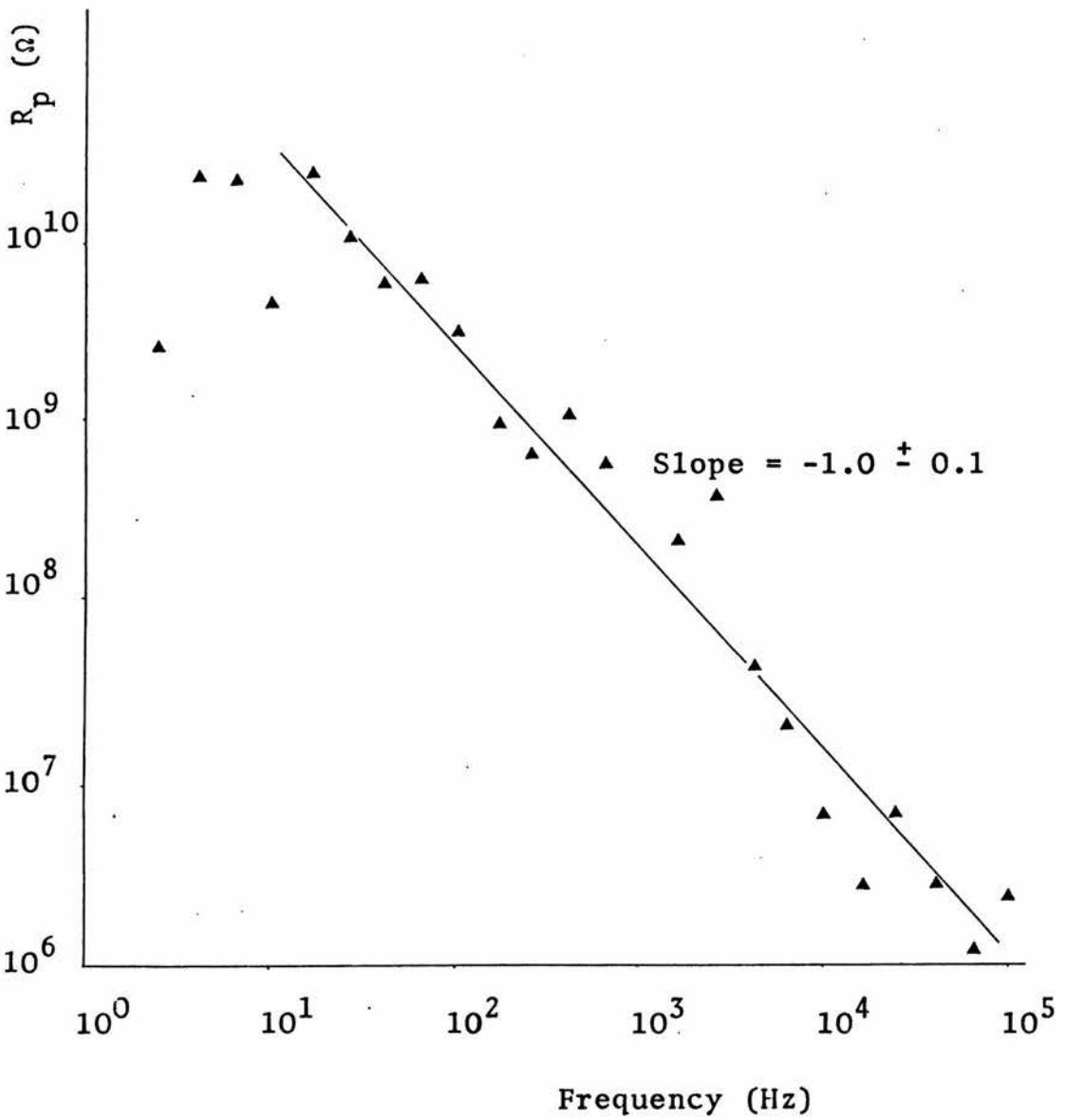

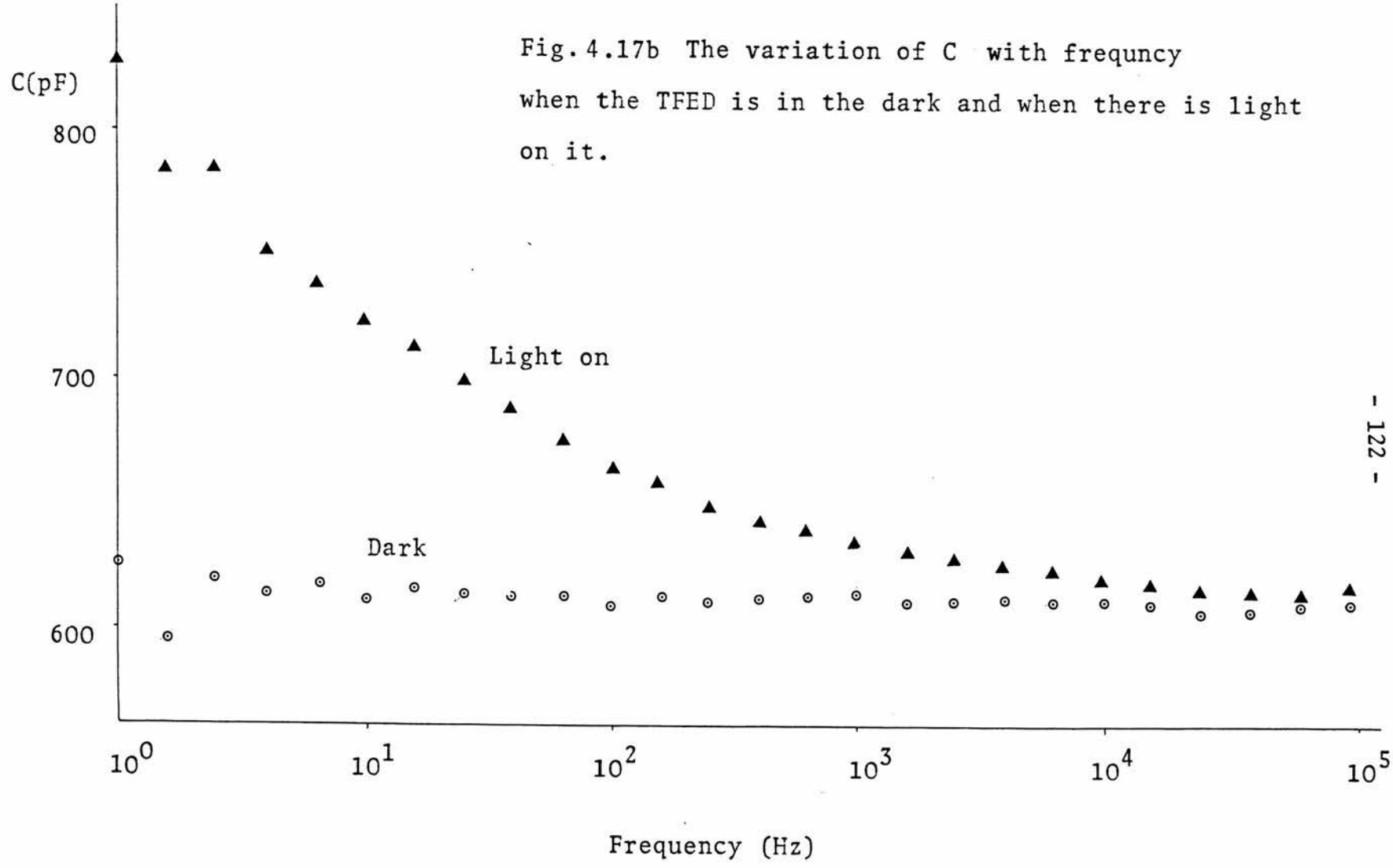

Fig. 4.17b The variation of C with frequncy when the TFED is in the dark and when there is light on it.

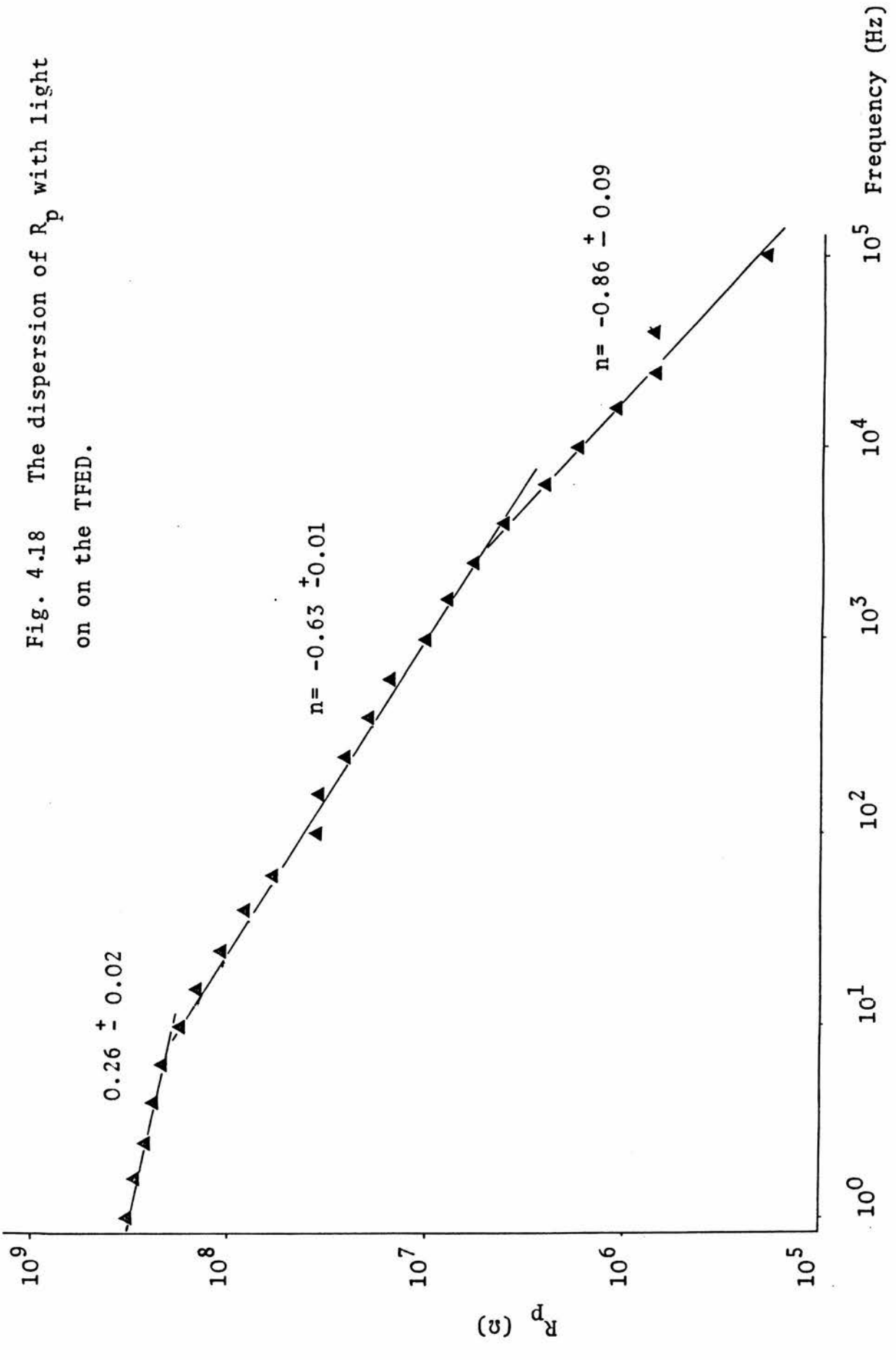

Fig. 4.18 The dispersion of R_p with light on on the TFED.

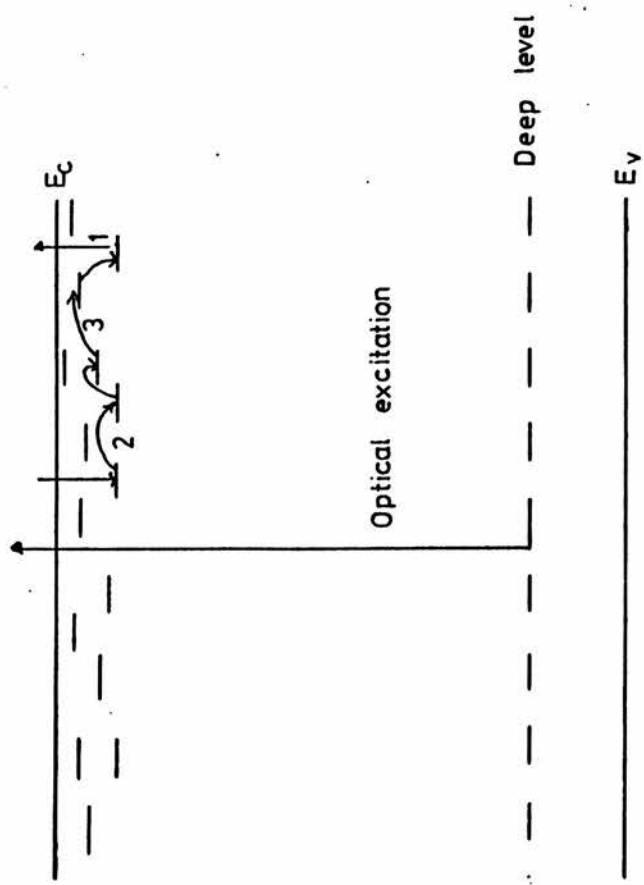

Fig. 4.19 Phyisical interpretation of the process that is giving rise to the dispersion in R_p and C.

Fig. 4.20 A plot of C-C(∞)with light on.The dark capacitance was taken as the value for C(∞).

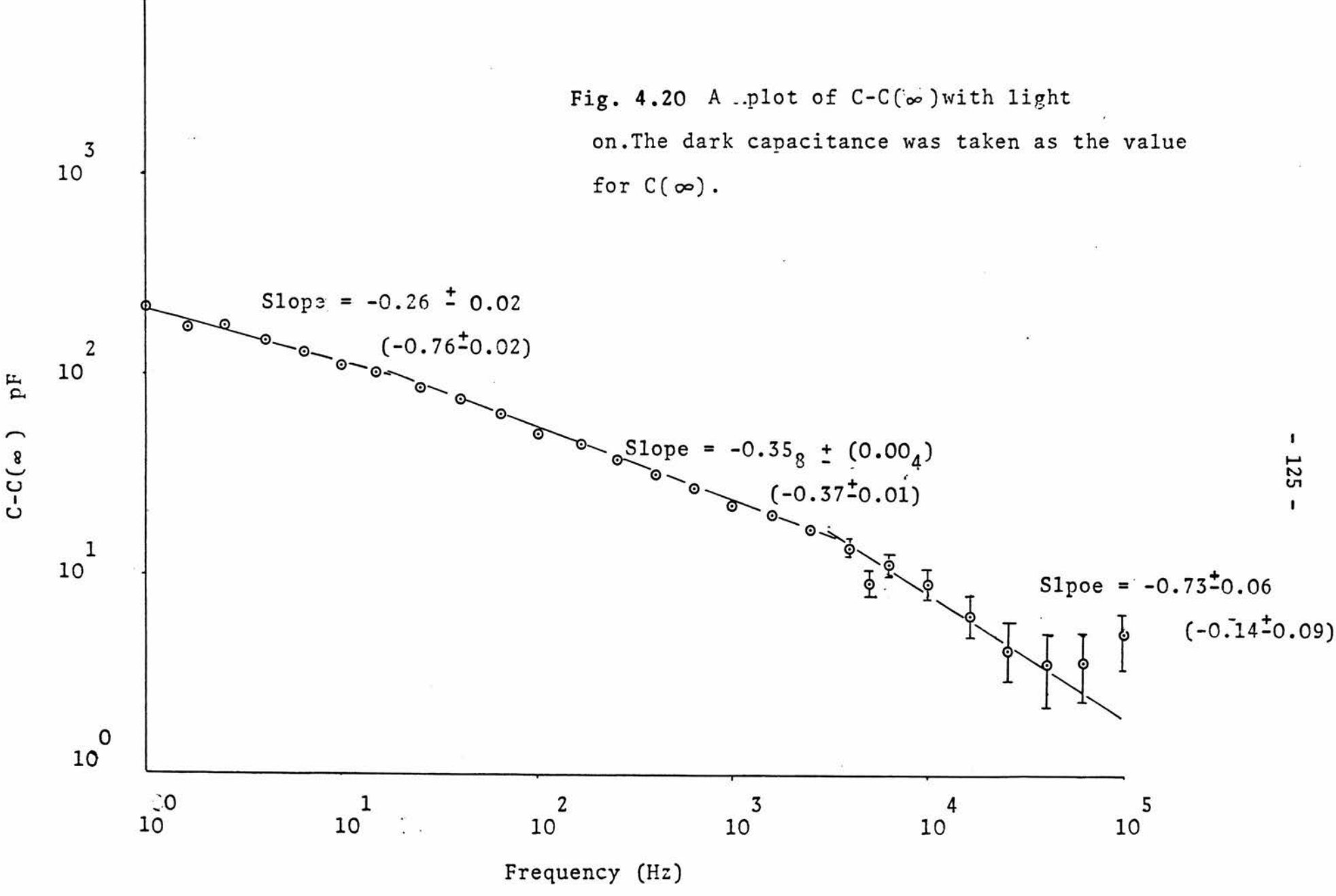

5 Hopping conduction in ZnSe:Mn

5.1 Introduction

ZnSe is a II - VI semiconductor that has a direct band gap of 2.7eV at room temperature.It is usually found to grow in a polycrystalline form although there are techniques available for growing bulk single crystal ZnSe (de Kock (1980)).The wide band gap of the material implies that it can be used as a suitable host material for producing luminescence in the visible region.The main difficulty of producing p-type-ZnSe for fabricating commercial p-n junction LEDs may be overcome by ion implantation of suitable acceptors(Yamaguchi et al (1977)). ZnSe has been studied extensively for the reasons mentioned above by techniques such as photocapacitance,photoconductivity and ESR.

Since the first publication of hopping conduction in crystalline Si by Pollak and Geballe (1961) there have been many publications of hopping conduction in other semiconductors.ZnSe is one of the more important semiconductors with possible applications in the optoelectronic industry.Hence there are some publications of hoping conduction in this material as well.We list here the work done on hopping conduction in ZnSe to date. Hopping conduction in ZnSe has been observed by Rentzsch et al (1979),Timchenko and Nedeoglo (1981),Mathur et al (1979) and in a-ZnSe by Lim and Brodie (1977). Rentzsch et al studied electrical properties of undoped, low resistivity,thin films of ZnSe grown by evaporating ZnSe onto a quartz

substrate. They found ac conductivity to exist in the films where the real part of the ac conductivity obeyed the relationship that $\sigma_{ac} \propto f^s$ where $s \in [0.6, 0.8]$. For films which were annealed at temperatures larger than 550°C the ac conductivity was found to occur at frequencies larger than 100kHz. One further result from their work was the absence of the variable range hopping (that is the dc conductivity did not vary with temperature as $\exp -T^{-1/4}$). Timchenko and Nedeoglo (1981), however, observed in their single crystals of n-type ZnSe (grown by annealing in liquid Zn at 900°C and with Ga as the dopant), variable range hopping (that is the dc conductivity was proportional to $\exp -T^{-1/4}$). Timchenko and Nedeoglo found that their experimental results agreed with a theory to explain variable range hopping that was based on percolation theory. A further result from these authors work is that, like Rentzsch et al, at low temperatures a conductivity of the form $\sigma_{dc} \propto \exp -T^{-1/2}$ is observed. A small inconsistency in the work of Timchenko and Nedeoglo is that the value of the activation energy at high temperatures does not correspond with the value calculated from the parameters of their sample. Mathur et al studied hopping conduction in vapour phase grown n-type ZnSe which was heavily doped with In. These authors interpreted their results in terms of the Mott model (see for example Mott and Davis (1979) for a description of this model). A major objection to using the Mott model to interpret the data of Mathur et al is that the dispersion parameter s (in $\sigma_{ac} \propto f^s$) is found to be temperature dependent (this point was not observed or discussed by Mathur et al). The temperature dependence of s is in contradiction with the Mott model of hopping conduction which effectively points to a s that is independent of temperature. The temperature dependence of s will be discussed in a later chapter.

A conclusion from the above literature survey is that the hopping conduction observed (both dc and ac) is strongly dependent on the method of preparing the sample. All the authors mentioned above carried out their experiments with the sample in the dark.

This chapter reports on the experimental work carried out on two samples of highly resistive ZnSe cut from the same ingot.The samples were characterised by photoconductivity and then the ac properties of the samples were studied.Photoconductivity experiments revealed the presence of a deep level with a photoionisation threshold of 2.01eV below the conduction band and also the existence of shallow levels below the conduction band. The ac properties of the sample showed that when the sample was in the dark no dispersion in the equivalent series capacitance (ESC) was seen. When light is shone on the sample, the ESC shows dispersion.The dispersion in the ESC is interpreted in terms of hopping conduction .

The chapter is presented in 5 sections. In section 5.2,we give a brief description of sample preparation and the method of putting contacts on the sample. Section 5.3 describes the photoconductivity data of the samples while in section 5.4 the ac properties of the samples are presented.The results of the above sections are discussed in the context of a form of hopping conduction in section 5.5 and finally a conclusion is presented in section 5.6. The work carried out on ZnSe is a continuation of the work carried out on the thin film electroluminescent devices presented in the previous chapter.

5.2 Sample preparation

Two samples of ZnSe were cut from the same ingot with a Universal wire saw.The samples were washed in toluene and then hand polished to a thickness of 0.41mm for sample 1 and 0.73mm for sample 2.The samples were further cleaned in toluene and left to dry before contacts were made to the sample. The type of contacts made depended on the experiment to be performed. For the ac measurements, the contacts covered the entire face of the sample,while for photoconductivity measurements,a guard ring arrangement of contacts were used. The material used for making the contacts was silver paste.

5.3 Photoconductivity

Both samples were characterised by photoconductivity using the experimental arrangement shown in figure 5.1.Light from an ac driven lamp (50Hz) was focussed by a lens to the entrance slit of a Zeiss SPM2 mirror monochromator.The slit widths of the monochromator were adjusted to give a band pass of 5nm. Monochromatic light emerging from the exit slit of the monochromator was made to be directly incident on the sample without additional use of lenses.The photoconductive response of the sample is measured by using the circuit of figure 5.1a. Initial measurements of the resistance of the samples using this circuit showed them to have resistance in excess of $10^{10}\ \Omega$. The circuit shown in figure 5.1a measures a combination of the surface and bulk current.However,when light is shone on the sample bulk photoconductivity is measured.This will become apparent when we compare the spectrum of the photoconductivity with the spectrum of the

electron optical cross section for the so-called M centre. The current flowing in the sample is measured by measuring the voltage across the $10^9\ \Omega$ resistor by a high input impedance voltmeter (such as the Keithley 602 solid state electrometer which has an input impedance of greater than $10^{14}\Omega$). The method of replacing the current meter by a fixed resistor was to decrease the response time of the system to 1ms. This response time is much smaller than when the electrometer is operating in the current mode. A reason for this is that when the electrometer operates in the ammeter mode the response time is controlled by the capacitance of the the cables feeding the electrometer and also by the inherent large rise times of the electrometer itself when it operates as an ammeter. As stated above,the voltage developed across the $10^9\ \Omega$ resistor is measured by a Keithley 602 solid state electrometer.From the unity gain output of the Keithley 602,the voltage developed across the $10^9\Omega$ resistor (the 'signal') is taken to a Keithley 160 digital multimeter (DMM) .The signal is further taken from the output of the DMM to a Kipp and Zonen BD8 single channel (or a Farnell PR1) chart recorder and to a Nicolet digital storage oscilloscope fitted with option 206. We took the output from the unity gain of the electrometer to the DMM prior to the chart recorder to make reading the scale of the electrometer easier.All experiments were done at a temperature of $[24,26]^{o}C$.

The relative flux of light incident on the sample was measured by placing a silicon solar cell at the exit of the monochromator and measuring the voltage developed across its terminals with a Keithley 160 DMM when light was shone on the solar cell.

The method of obtaining the photoconductivity spectrum of the samples is as follows. A sample is placed in darkness and light at a fixed wavelength is made incident on it.This produces a resistance change of the sample and the voltage developed across the $10^9 \Omega$ resistor is monitored until a steady-state trace is seen on the chart recorder.The shutter is closed and the sample allowed to reach dark equilibrium.The shutter is opened and the above procedure is repeated for a different wavelength. For a few wavelengths,the decay of the photocurrent was monitored on the digital storage oscilloscope.

The typical rise in the photoconductivity for samples 1 and 2 are shown in figures 5.2 and 5.3 respectively.For sample 1 the photoconductivity goes through a a minimum before increasing to a steady state value. For sample 2,it is seen there is a kink in the initial rise of the photoconductivity before the photoconductivity (PC) reaches a maximum. The PC then goes through a minimum and further increases very slowly with time to reach a steady-state value. The figures also show the resulting PC when an additional UV light is also incident on the samples.The reason for irradiating the sample with UV light is explained later.

The above rise in the PC can be understood in terms of a model where the semiconductor (or a semi-insulator) has at least two centres which produce a deep level and shallow levels. In the discussion that follows,we will assume that the transitions involve the conduction band only. The requirement of the shallow levels is the rate of thermal emission of electrons from the shallow level to the conduction band be much less than the rate of optical generation of electrons

from the deep level. Models to describe the rise of the PC are described in appendix 5A.It is shown in that appendix,that if the semiconductor which we have studied is one that has a deep level and at least two shallow levels,then when electrons are excited from the deep level into the conduction band,they will be captured by the shallow centres and thermally emitted at a rate that depends,amongst other factors, on the energy difference of the shallow level from the conduction band.If one of the shallow levels is "sufficiently deep" and the other is "shallower" then it is shown in appendix 5A that the PC will reach a maximum,decrease to a minimum and then increase slowly to reach a steady-state value.The main features of the rise of the PC for both samples can be understood in terms of this. In the modelling of the rise of the PC,we assumed that one shallow centre is thermally emitting electrons at a rate much less than the optical rate and the other centre thermally emits electrons at a rate that is less than or the order of the optical rate. For sample 2 we observe a kink in the initial rise of the PC.This kink can be produced by a number of mechanisms,some of which will be discussed here. We can discount the kink observed in the initial rise of the PC to be caused by the optical generation of holes from the shallow levels.A reason for this is that the shallow levels are expected to be the order of 0.2eV below the conduction band and thus the contribution of the photoexcited holes to the measured PC is not expected to occur until photons of energy 2.4eV are incident on the sample. The kink,however, was observed throughout the spectral region that was studied. We showed in appendix 5A that the models described therein could describe the post-kink rise of the PC.However, none of the models considered in appendix 5A could reproduce the kink.It is shown in appendix 5A that the model where the semiconductor has two shallow levels and a deep

level gives a much better fit to the experimental rise of the PC.The kink may be produced by the optically excited electrons recombining with holes via some other level in the band gap.Once this centre is "filled up" the recombination process may decrease and the model described in appendix 5A then describes the temporal behaviourof the PC.If the above description of the rise of the PC is plausible,then,when above-band gap light is shone on the sample prior to the monochromatic light,we will fill one of the centres with electrons and thus reduce the capture rate of free carriers by one of the shallow centres. To test this explanation light from a P W Allen UV lamp was first shone on the sample.The UV light was left on until a steady-state trace was seen on the chart recorder.Light from the monochromator was then made incident on the sample and the resulting PC produced was monitored on the chart recorder. We showed in figure 5.2 that for sample 1 the dip in the PC disappears when UV light is shone on it prior to the monochromatic light,and in figure 5.3,it was shown that for sample 2,the kink in the initial rise of the PC was removed when UV light is made incident on it.This experiment,therefore,gives support to the above description for the rise of the PC.

For sample 1 the magnitude of the photocurrent was greater than that of sample 2.The magnitude of the photocurrent is governed by the lifetime of the photoexcited electron.The lifetime is governed by the recombination centres from which we can deduce that the lifetime for photoexcited electrons is larger in sample 1 than for electrons in sample 2.The spectrum of the steady-state PC divided by the photon flux ($\Delta V/\phi$) for both the samples is shown in figure 5.4. The sets of data for the two samples have been normalised at P.Figure 5.4 shows

that there is a close correlation in the two spectra of $(\Delta V/\phi)$,from which we can speculate that the same deep centre probably exists in both samples.For sample 1,the post-dip PC was used to find the inverse rise times from a least squares analysis of Mangelsdorf plots (see the previous chapter for an explanation of Mangelsdorf plots).It is assumed that the final part of the rise of the PC is governed by the deep level and that the form of the final part of the transient can be described by an exponentially increasing function where the inverse rise time of the transient is set equal to the optical emission constant for electrons from the deep level.A similar assumption is also made when the additional UV light is also incident on the sample. The rise time constant of the PC when UV light is also switched on is equal to the rise time constant of the post-dip PC when only the monochromatic light is switched on.A varification of this is shown in figure 5.5.Figure 5.5 shows that for sample 1 the post-dip rise of the PC is essentially governed by the deep centre.(This statement is not in contradiction with the model presented in appendix 5A as it was shown that these models only approximately describe the rise of the PC.)The spectrum of the inverse rise times divided by the photon flux $((\tau\phi)^{-1})$ is shown in figure 5.6.Figure 5.6 shows structure for photon energies at 2.10eV while for photon energies larger than 2.25eV $(\tau\phi)^{-1}$ increases without further structure.

To gain further insights into the meaning of the inverse rise times,the photocurrent was measured for different photon flux incident on the samples at a fixed wavelength.The inverse rise times are only measurable for sample 1, while for sample 2 the steady-state PC (Δ V) is more readily measured. To vary the flux of light incident on the sample,neutral density filters were placed at the entrance slit of the

monochromator.For sample 1 the inverse rise times,calculated from the final part of the rise of the transient using the Mangelsdorf method, were plotted for different flux,while for sample 2,ΔV was plotted for different flux.A graph of τ^{-1}vsϕ is plotted for sample 1 in figure 5.7 and for sample 2,ΔV vs ϕ is plotted in figure 5.8.Figure 5.7 shows that the inverse rise time is directly proportional to the photon flux, that is,assuming the post-dip PC is governed by the deep centre then the inverse rise time constant reflects the optical emission constant for electrons. For sample 2,ΔV increases as a non-linear function of photon flux.The solid curve drawn through the experimental points in figure 5.8 is explained in appendix 5B.Thus for sample 1 the inverse rise time divided by the photon flux reflects the optical cross section for electrons,while for sample 2 the square of the steady-state PC reflects the optical cross section for electrons. A spectrum of $(\Delta V)^2/\phi$ for sample 2 is shown in figure 5.9.

Further analysis in the case of sample 1 can be made by comparing the spectrum of $(\Delta V/\phi)$ and $(\tau\phi)^{-1}$.The reason for comparing these spectra is to gain information about the magnitude of the occupancy change of the deep centre when light is shone on the sample.If the occupancy of the deep centre is not perturbed appreciably from the dark occupancy,then the steady-state PC reflects the optical emission constant for electrons (this,of course,assumes that a single centre is responsible for the PC).We have obtained an e_n^o from the post-dip PC transient and also from the steady-state PC .Thus if the above reasoning is correct, there should be a strong correlation between the spectrum of $(\tau\phi)^{-1}$ and $(\Delta V/\phi)$.Figure 5.10 shows a strong similarity between the two mentioned spectra for sample 1.For sample 1,therefore,when light is shone on it,the occupancy of the deep centre

is only perturbed from the dark occupancy.By implication,the statement concerning the occupancy of the deep centre when light is shone on sample 1 will also be true for sample 2 as we have shown that that the same deep centre exists in sample 2.

To find the photoionisation threshold of the impurity,we will use the model due to Allen (see chapter 2).In this model the optical cross section near the photoionisation threshold varies as

$$\sigma \sim (E_p)^{-1}(E_p - E_{pt})^{3/2}$$

where E_p is the photon energy and E_{pt} is the photoionisation threshold energy.For sample a graph of $((\tau\phi)^{-1}h\nu)^{2/3}$ against photon energy is plotted in figure 5.11. From a least squares analysis,the photoionisation threshold is calculated to be (2.09 ± 0.26)eV. For sample 2, a graph of $[(\Delta V)^2/\phi)h\nu]^{2/3}$ is plotted as a function of energy in figure 5.12. A least squares analysis on figure 5.12 yields a photoionisation threshold of (2.01 ± 0.02)eV. The photoionisation thresholds for sample 1 and 2 confirm what was shown experimentally above (in figure 5.4) that the same deep centre exists in both the samples.

At this point we can say there is a deep centre located approximately 0.6eV above the valence band.A few speculations can now be made on the nature of the deep centre. Grimmeiss et al (1976) have studied copper doped ZnSe and have found a copper related complex (the so-called M centre).In figure 5.13,we have shown the optical cross section for electrons for the M centre (as reported by Grimmeiss et al) and the steady-state PC for sample 1.Although the data for the M centre and the steady-state PC spectrum do not exactly match we can

see that there is reasonable agreement between the two spectra.

The decay of the PC after steady-state PC had been established was investigated for different wavelengths.If the rise in the photoconductivity can approximately be described by conventional theory,then the decay of the PC should be equally described by conventional theory.That is,we should expect the decay of the photoconductivity to be described by some combination of exponentials. From figures 5.14 and 5.15,it is seen that if the dark value of the photocurrent is subtracted from the measured PC,then the PC decays approximately as a power law. This is a rather surprising result.We further observe from figures 5.14 and 5.15 that the photocurrent starts to decay 0.1s after the light has been blocked off.We expect the photocurrent to decay after a time the order of the recombination time of the electrons. The form of the decay of the photocurrent suggests that a new behaviour is being observed here.

It is known in the study of amorphous semiconductors that the PC after flash illumination, is governed by the photoexcited carriers being captured by progressively deeper density of states (a simple model explaining this is due to Tiedje and Rose (1980)). The prediction of the model is that the PC decays as a power law.The model due to Tiedje and Rose assumes that the density of states below the mobility edge in an amorphous semiconductors is exponentially decreasing.

It is known in polycrystalline semiconductors that the bands bend exponentially at the intergranular regions (Matare' (1984)).This is interpreted as due to exponentially decreasing density of states at the inter-granular regions.These density of states are concerned mainly with the density of states for free carriers and not with the density of states within the band gap. In the temporal dependence of the photocurrent we showed the possible existence of shallow levels below the conduction band.We expect these shallow levels to have an energy distribution. These shallow levels then take the place of the density of states below the mobility edge and one can then use Schmidlin's theory(1977) to find out the shape of the decay of PC. We did not have sufficient information of the distribution of the shallow levels to carry out such study.

5.4 AC properties of the samples

In this section,experimental data concerning the equivalent series capacitance (ESC,or C_s) of the samples will be presented.It will be shown that when the samples are in the dark,the ESC is essentially independent of frequency while when light is shone on the sample the ESC shows dispersion. The form of this dispersion is that $C_s \propto f^{-n}$ where f is the frequency of the applied "small signal" and n is a positive number less than unity. The exponent n will be shown to be dependent on temperature and on the frequency of the light incident on the sample.

The experimental arrangement used to measure C_s, the significance of which is indicated below, is shown in figure 5.16. At the heart of system used to measure the capacitance and the resistance of the sample is a General Radio 1615A capacitance bridge operated in the "3 TERM" mode. The small ac signal (18-25mV) applied to the bridge was from a Farnell LFP1 signal generator. The detector output from the bridge is fed into the 'input' of a Brookdeal 9501 lock-in amplifier. The 'reference signal' to be applied to the lock-in amplifier was derived from the signal generator after being amplified by a Brookdeal 450 low noise amplifier. The output from the lock-in amplifier is taken to a Telequipment D1010 oscilloscope and a Farnell TM2 voltmeter.

To measure the capacitance and resistance using the capacitance bridge, the bridge has to be operated in a mode where it assumes that the sample can be represented either as a parallel combination of a resistor and a capacitor or as a series combination of a resistor and a capacitor. The accuracy of the bridge is better when the sample is represented as a series combination of a resistor and a capacitor, R_s and C_s respectively. Hence these were the measured quantities in the experiments.

The procedure of obtaining a reading for R_s and C_s at a fixed frequency is as follows. All decade capacitance and D levers on the capacitance bridge are first put to zero. The signal fed into the lock-in amplifier is maximised as suggested in the manual for the lock-in amplifier. After this, the bridge is balanced in the normal way. Once a reading has been obtained for C_s and R_s, the decade

capacitance and D levers on the bridge are again put to zero and the above procedure is repeated for a different frequency. To test whether this procedure was valid,the ESC of a 270pF silver mica capacitor was measured from 20Hz to 100kHz with the capacitance bridge operating in the '3 TERM' mode. The 3 TERM measurement measures the 3 terminal capacitance of the sample. The advantage of this method is that the capacitances due to the cables connecting the sample to the bridge can be neglected.The error introduced by using long cables is now due to the inductance of the cables.Thus in the experiments all cables were kept as small as possible. The frequency dependence of the silver mica capacitor is shown in figure 5.17.The figure shows that for frequencies larger than about 50Hz,the ESC stays constant, while below this frequency,the ESC decreases.The frequency dependence of the ESC of the silver mica capacitor is consistent with the specification of the capacitance bridge; that the useful frequency range is from 50Hz to 100kHz.For frequencies less than 50Hz,special detection techniques must be used to determine the balance point. When the ESC and frequency are plotted on a double logarithmic graph paper,the variation of ESC for frequencies less than 50Hz will be "smoothed out". In figure 5.17,in the region where the ESC stays constant,we find from standard statistical analysis,that the ESC of the capacitor is (256 $\pm$ 1)pF,ie the standard error in the measured ESC is less than 1/2%.

When the samples were connected to the bridge,using the method shown in figure 5.16,only the ESC of the sample could be measured,ie only C_s. A reason why only C_s could be measured is because the value of R_s was such that no dissipation factor could be measured using the bridge. Thus all the data to be presented below will for C_s only.

Two exploratory experiments were done when the sample was in the die cast aluminium box (see figure 5.16).In the first case,the sample was considered to be in the dark when a lid was placed on the die cast aluminium box. As shown in figure 5.18,C_s there stays constant for frequencies larger than 40Hz.The decrease of C_s for frequencies less than 40Hz has been explained above. In the second case the lid was removed and the sample was exposed to normal room lights for at least 10minutes.The dispersion in C_s produced in this case is shown in figure 5.19.It is seen in this figure that C_s is proportional to f^{-n} where n is found from a least squares analysis to be 0.28 ± 0.01 for sample 1 and 0.33 ± 0.01 for sample 2. For frequencies larger than 50Hz when the sample is in the dark,where C_s is independent of frequency, we can calculate a value for the dielectric permittivity for ZnSe. In standard notation,the capacitance of a parallel plate capacitor is given by $\varepsilon\varepsilon_o$ A/d.For sample 2 the area was estimated by placing the sample on a graduated graph paper and photographing it using a combination of close up lens. The area was approximately found by counting the mm^2 squares.The thickness of the sample was measured with the travelling microscope. Using these techniques,we find that the the dielectric permittivity of sample 2 is $(0.73 \times 4.63 \times 10^{-12})/(8.85 \times 10^{-15} \times 35) = 10.1$.The value obtained for ε is within 10 % of the quoted value of 9.1. The main reason for the apparent large value of ε is that measured capacitance,C_s, contains some stray capacitance.For our experiments the stray capacitance is expected to be the order of 0.5pF.

The temperature dependence of n was investigated using the arrangement shown in figure 5.20.The sample was placed in a copper block which had a hole drilled in it.The copper block rested on an aluminium block which in turn rested on a Griffin hot-plate. Located approximately 2cm above the copper block was a small 5W tungston lamp which was continuously left on while the temperature was varied. When the temperature,as measured by a CRL 207 temperature indicator,reached a constant value,the capacitance - frequency data was taken and plotted on a double logarithmic graph paper and a least squares analysis was used to find the exponent n. Some typical graphs for sample 1 are shown in figure 5.21. Note in figure 5.21 that at high temperatures C_s tends to a high frequency limit which is nearly equal to the dark capacitance of the sample. In figure 5.22 n is plotted as a function of increasing temperature.It is observed that for sample 1,the temperature dependence of n can be described by the empirical relationship that $n = (3.3 \pm 0.2)x10^{-3}T - (0.72 \pm 0.05)$, while for sample 2 $n=(3.1 \pm 0.2)x10^{-3} - (0.67 \pm 0.09)$. A glance at figure 5.22 shows that for a given temperature,the value for n is greater for sample 1.

For sample 2,the dependence of n upon photon energy and photon flux incident on the sample was investigated. Some typical dispersion of the ESC when light of different photon energy is incident on sample 2 are shown in figure 5.23. The dependence of n upon photon energy is shown in figure 5.24. We observe that as the photon energy increases,n slowly decreases. A possible dependence of n on photon flux incident on the sample was investigated.To do this the wavelength of the light incident on the sample was kept constant(λ=0.56μm) and

the flux of light incident on the sample was varied with neutral density filters as before. The resulting dispersion produced in the ESC is shown in figure 5.25. We see that as the photon flux increases, the value of the dispersion parameter decreases.

5.5 Discussion

The ESC measured in the experiments is directly proportional to the real part of the dielectric susceptibility. It has been shown above that the dispersion of C_s can be described by a power law when light is shone on the sample. Furthermore, no dispersion of C_s is seen when the sample is in the dark. The dispersion of C_s will now be interpreted in terms of hopping conduction.

Hopping conduction competes with band conduction. The contribution of hopping conductivity to the total conductivity can be made more dominant by freezing the free carriers onto shallow donors and acceptors. Alternatively, one can work with insulating (or semi-insulating) materials where it should be possible to observe hopping conduction at room temperatures.

In our experiments, when the sample is in the dark, all the electrons will be at the deep level. The wavefunction of electrons occupying the deep level is of a localised nature. Thus the hopping probability, which can physically be thought of as due to the overlap of the wavefunction of an electron at two different sites, will be small. Hence hopping conduction involving the deep centres will only be measurable at low temperatures where the currents produced by this

process will become relatively large compared with that produced by electrons in the conduction band.Normally the magnitude of the current produced by hopping conduction is orders of magnitude less than currents produced by free carriers. This argument explains the absence of dispersion in C_s when the sample is in the dark.

When light is shone on the sample,electrons will be excited from the deep level into the conduction band. The electrons will be free before they are captured by a shallow centre. The trapped electron will remain at the site of the shallow centre before it is thermally emitted into the conduction band. Then following the arguments similar to those used to describe hopping conduction in ZnS:Mn,we can infer that hopping conduction of electrons amongst the shallow centres and the conduction band is highly probable.In the previous chapter the dispersion in the resistance and capacitance of the TFED was interpreted in terms of a model due to Scher and Lax (1973).We have indicated above that the dispersion of C_s is connected with the photoconductive process of capture and thermal emission of electrons amongst a distribution of shallow donor levels and the conduction band. Thus we should use the model of Scher and Lax to interpret the dispersion of C_s. We cannot use the model of Scher and Lax, as presented in their paper, to the present case for the reason that n is temperature dependent.The model of Scher and Lax points to a temperature independent n. In our experiments,we found that the temperature dependence of n can be described by the empirical relationship

$$n = \text{const.}T - 0.8 \qquad 5.1$$

In a related field of decay of photocurrent after flash illumination,it has been found that the decay of the photocurrent can also be described by the continuous time random walk formalism (see for example Pfister and Scher (1978)). An electron which is thermally released from a shallow centre and captured later into an empty site on a shallow centre after the electron has been "free" in the conduction band will execute a random walk amongst the shallow centres. Scher (1977) has shown that if a suitable form of the energy distribution of the shallow levels produced by the shallow centres is made then the distribution function, $\psi(t)$,which describes the (mathematical) nature of the random walk for this case,can be shown to decrease with time as a power law. The resulting distribution function can then be substituted into the general formula for the complex diffusion coefficient derived by Scher and Lax.In principle this procedure can reproduce the temperature dependence of n seen in our experiments (equation 5.1).The procedure mentioned above is ad-hoc; that is if the right assumption is made then the right answer will be obtained. At present we do not have sufficient detail concerning the nature of the shallow levels to form a concrete model.The nature of the hopping conduction has been understood in terms of the random nature of the thermal emission of electrons from shallow centres into the conduction band and the subsequent capture of the electrons into the vacant sites on the shallow centres.The pictorial representation of the hopping considered here is that shown in figure 4.19.

It was mentioned that as the photon energy of the incident light on the sample increased, n decreased to a steady value. This behaviour can be understood in qualitative terms. Electrons excited optically from the deep level, once they are captured by the shallow centres, will occupy a shallow level that depends on the number of electrons excited into the conduction band. We will assume the shallow centres that produce shallow levels below the conduction band are distributed in energy. When the number of electrons excited optically is "small" then the captured electrons are expected to occupy the deeper lying shallow levels. As the number of electrons excited into the conduction band increases, the shallow levels that lie close to the conduction band will become occupied. We hypothesize that the dispersion parameter, n, is controlled by the thermal emission of electrons from the shallow levels. Then at photon energies near the photoionisation threshold, the number of electrons excited into the conduction band are expected to be "small" and, according to our postulate, the value of n to be large. The dispersion parameter n tends to a constant value for photon energies approaching the band edge presumably because the shallowest level is more than a few kT away from the band edge. The relative number of electrons excited into the conduction band can be taken to be described by figure 5.3. The behaviour of n on photon flux can also be understood in terms of the above model. For low photon flux incident on the sample, the number of electrons excited into the conduction band will be "small" and thus the value of n to be "large". When the incident flux of photons is "large" then the dispersion parameter is expected to have a "small" value.

We noticed in figure 5.22 that although the temperature dependence of n for samples 1 and 2 was similar,n had a larger value in sample 1 than in sample 2 for a given temperature.This observation can be understood in qualitatitive terms.We have indicated that n is connected with the thermal release/capture of electrons between the conduction band and a distribution of shallow centres.It was further observed in the photoconductivity analysis that the shallow centres in sample 2 produced shallow levels which were deeper than in sample 1.We expect n to be related with the energetic distance of the shallow levels from the conduction band and thus we further postulate that that n should be large if the shallow levles are "close" to the conduction band and n to be "small" if the shallow levels are "further away" from the conduction band.

5.6 Conclusion

A model of semi-insulating ZnSe is one that has a distribution of shallow levels and a deep level. The PC showed the presence of a deep level with a photoionisation threshold of 2.01eV below the conduction band.We also conclude from the PC experiments the existence of shallow levels below the conduction band.The shallow levels were found to control the form of the rise of the PC.One surprising result from the PC measurements was that the decay of the photocurrent showed an approximate power law behaviour if the dark value of the photocurrent was subtracted from the observed photocurrent.

In the electrical measurements, the ESC of the ZnSe showed a power law dispersion behaviour only if there was light shone on it. When the ZnSe was in the dark the ESC was independent of frequency. A value of the dielectric permitivity found from the ESC when the sample was in the dark was within 10% of the accepted value. The ESC of ZnSe showed a power law dispersion behaviour only when light was made incident on it. We interpret the dispersion of the ESC in terms of electrons hopping between a distribution of shallow states and the conduction band. The dispersion parameter, in $C_s \propto f^{-n}$, was found to increase with temperature according to an empirical relationship of the form $n = \text{const.}T(K) - 0.7$. The dispersion parameter was also found to be dependent on the photon energy and the photon flux of the light incident on it. The dependence of n on the photon energy and photon flux was understood in qualitative terms of thermal emission of captured electrons from a distribution of shallow states.

Appendix 5A. Mathematical models for the rise of photoconductivity

In the main text it was mentioned that the quenching of PC was connected with the fact that the electrons captured by the shallow centre are thermally emitted from the shallow centre at a rate which is much less than the optical rate. In this appendix, we will show how to describe this model mathematically. Figure 5A.1 shows a schematic diagram of a semiconductor which has a deep level and a shallow donor level below the conduction band. The rates which are to be considered are indicated in the figure. Specifically, it will be assumed that the deep level and the shallow level do not communicate with each other directly but only indirectly through the conduction band. Using the symbols defined in figure 5A.1, we can write down the rate equations for electrons in the conduction band and for the electrons occupying the shallow and the deep levels when light is shone on the sample as:

$$\dot{n}_1 = -(e_1^t + e^o)n_1 + c_1 n_c (N_1 - n_1) \qquad 5A.1$$

$$\dot{n}_2 = -e_2^t n_2 + c_2 n_c (N_2 - n_2) \qquad 5A.2$$

$$\dot{n}_c = (e^o + e_1^t)n_1 + e_2^t n_2 - n_c(c_1(N_1 - n_1) + c_2(N_2 - n_2)) \qquad 5A.3$$

The material that we have studied should correctly be called a semi-insulator. Thus we can make the following approximations to the above three equations. We expect the deep centre to be fully occupied by electrons when the sample is in the dark, hence $N_1 - n_1$ can be put

to zero.Furthermore,as the Fermi level is expected to be away from the shallow level,thus $N_2 - n_2$ can be put to equal N_2.Finally when the sample is in the dark,that is at time t=0,we can put $n_1(0) = N_1, n_2(0)=0$ and also $n_c(0) = 0$.Using these approximations ,the above three equations can be simplified to

$$\dot{n}_c = -(e_1^t + e^o)n_1 \qquad 5A.4$$

$$\dot{n}_2 = -e_2^t n_2 + c_2 N_2 n_c \qquad 5A.5$$

$$\dot{n}_c = (e_1^t + e^o)n_1 + e_2^t n_2 - c_2 N_2 n_c \qquad 5A.6$$

Taking the Laplace transforms of the above equations (where the ~ indicates a Laplace transform of the variable from the time domain to the s domain) ,we have

$$s\tilde{n}_1 = -(e_1^t + e^o)\tilde{n}_1 + N_1 \qquad 5A.7$$

$$s\tilde{n}_2 = -e_2^t\tilde{n}_2 + c_2 N_2 \tilde{n}_c \qquad 5A.8$$

$$\tilde{n}_c = (e_1^t + e^o)\tilde{n}_1 + e_2^t\tilde{n}_2 - c_2 N_2 \tilde{n}_c \qquad 5A.9$$

Solving equations 5A.7 and 5A.8 for $\tilde{n}_1$ and for $\tilde{n}_2$ in terms of $\tilde{n}_c$ and substituting into equation 5A.9,we have after a little algebraic manipulation that

$$\tilde{n}_c = k_1 N_1((s + e_2^t)/(s(s + k_2)(s + k_1))) \qquad 5A.10$$

In equation 5A.10, $k_1 = e_1^t + e^o$ and $k_2 = e_2^t + c_2N_2$. To derive the above equations, we have made use of the initial conditions described above. Making use of the extensive tables of inverse Laplace transforms (see for example Erdeyli et al) we get that

$$n_c(t) = N_1k_1(e_2^t/(k_1k_2) +$$

$$(e^t - k_1)\exp -k_1t/(k_1(k_1 - k_2))$$

$$+ c_2N_2\exp -k_2t/(k_2(k_2 - k_1))) \qquad 5A.12$$

In the final expression of n_c which was used for modelling purposes, e_1^t was put to zero. The form of n_c predicted by the above equation is plotted in figure 5A.2. Also shown in figure 5A.2 are experimental points for the rise of the PC for sample 2. It is seen that although equation 5A.12 gives a reasonable fit to the experimental data, the fit is not good. Note further that the maximum in the experimental points and the theoretical points do not match. The fit to the experimental data was made such that the thermal rate e_2^t was less than the optical rate. We can modify the model presented above to two more cases. In the first case suppose that there are two deep levels and a single shallow level. For the second case, we assume that there are two shallow levels and only a single deep level. Consider the first case. Let the electron emission constants for

electrons for the two centres of concentrations N_1 and N_2 be e_1^o and e_2^o respectively. Then following the arguments and the method used to derive equation 5.12 it is straight forward to show that the rise of $n_c(t)$ will be given by

$$n_c(t) = e_1^o N_1[\{(e_3^t/be_1^o) +$$

$$[(e_3^t - e_1^o)/(e_1^o - b)]\exp(-e_1^o t)$$

$$+ C_3N_3/(b(b - e_1^o))\exp-bt)\}$$

$$+N_2e_2^o\{e_3^t/(be_2^o) +$$

$$(e_3^t - e_2^o)/(e_2^o - b)\exp(-e_2^o t)$$

$$+ [C_3N_3/(b(b - e_2^o))]\exp-bt\} \quad 5A.13$$

In equation 5A.13 e_1^t and e_2^t (the thermal rates for electrons for the deep centre 1 and 2 respectively) have been put to zero. The symbols C_3 and e_3^t are, respectively, the capture probability of free electrons and e_3^t is the thermal emission rate of electrons from the shallow centre and $b = e_3^t + C_3N_3$. It is apparent that equation 5A.13 can be adjusted so that it coincides with the maximum in the experimental PC. However, the form of equation 5A.13 is similar to that of 5A.12 and thus it cannot predict the slow rise in the PC after the PC has reached a minimum.

The slow rise in the PC following the minimum can be reproduced by assuming that we have a single deep centre, which is excited optically, and two shallow levels below the conduction band. Let the centre that produces the deep level have an optical rate for electrons be e_1^o and its concentration be N_1. For the shallow centres, let them have concentrations N_2 and N_3 with thermal rates e_2^t and e_3^t and the capture probabilities for electrons C_1 and C_2 respectively. Then making the same approximations as those used to derive equation 5A.12 and making use of the tables of Laplace transforms it is straightforward to show that in this case the rise of the PC will be given by

$$n_c(t) = N_1 e_1^o \{e_3^t e_2^t / (e_1^c \alpha_1 \alpha_2)$$

$$+ [(e_2^t - e_1^o)(e_3^t - e_1^o)/(e_1^o(\alpha_1 - e_1^o)(\alpha_1 - e_1^o))]\exp -e_1^o t$$

$$-[(e_2^t - \alpha_1)(e_3^t - \alpha_1)/(\alpha_2(e_1^o - \alpha_1)(\alpha_2 - \alpha_1))]\exp -\alpha_1 t$$

$$- [(e_2^t - \alpha_2)(e_3^t - \alpha_2)/(\alpha_2(e_1^o - \alpha_2)(\alpha_1 - \alpha_2))]\exp -\alpha_2 t\} \quad 5A.14$$

The α's are found from factorising the quadratic

$$s^2 + s[e_3^t + e_2^t + C_2N_2 + C_3N_3] + e_2^t N_3 C_3 + e_3^t C_2 N_2$$

Some numerical computation showed that equation 5A.14 had some interesting properties. It was found that the size of the peak seen in the initial rise of the PC is governed by the more deeper laying shallow centre. The slow rise thereafter is controlled by the centre that produces the more shallow level. In figure 5A.3 we have plotted

the rise of the PC as predicted by equations 5A.12 and 5A.14.It is seen that the model of equation 5A.14 gives a much better fit to the experimental rise of the PC.We further observe in figure 5A.3 that the maximum in equation 5A.14 coincides with the experimental rise of the PC.In fitting equation 5A.14 to the experimental data we assumed that $e_2^t >> e_3^t$.

We also investigated the possibility of equation 5A.14 also describing the rise of the PC for sample 1 as well.If the rate of thermal emission of electrons from the centres that produce the shallow levels are approximately equal then the rise of the PC shown in figure 5A.4 results.Figure 5A.4 shows a strong similarity to the rise of the PC for sample 1.Hence we arrive at a model of the rise of the PC for both samples with the prominent features of the rise of the PC governed by the location of the shallow levels below the conduction band. Equations 5A.12 to 5A.15 further predicts that the steady-state value of the PC to be independent of the spectral content of the incident light. This was not seen experimentally throughout the entire spectral region that was studied.However, the main features of the quenching of the PC has been described by the models presented above.

Appendix 5B

The variation of the steady-state PC of sample 2

In the previous appendix,we showed that the quenching of the PC was a consequence of the excited electrons captured by shallow centres and then thermally emitted at a rate which was much less than the optical rate.Although the model in appendix 5A was able to reproduce the main features of the time dependence of the PC, it predicted that the steady-state PC was independent of the photon energy.This appendix presents another solution to equations 5A.1 to 5A.3. It was shown in the previous appendix that for sample 2,the PC is governedby the thermal emission of electrons from the shallow centres after the photoexcited electrons have been captured by these centres.If the shallow centres are of sufficiently small concentration,then these centres will be fully occupied by electrons when light has been shone on the sample for a long time.Thus in the steady-state,we can put $n_c = N_2 - n_2$.Hence in steady-state we get from equaion 5A.2

$$c_2 n_c^2 + e_2^t n_c - (e^o n_1 + e_2^t N_2) = 0 \qquad 5B.1$$

In equation 5B.1,e_1^t has been put to zero.The solution to equation 5B.1 is

$$n_c(\infty) = -k_3 \pm [k_3^2 + e^o n_1 + e_2^t N_2]^{1/2} \qquad 5B.2$$

Now $k_3 = e_2^t/c_2$ is the order of unity and $e^o >> e_2^t$, then equation 5B.2 can be approximated to

$$n_c(\infty) \propto (e^o n_1)^{1/2}$$

ie $$n_c(\infty) \propto (\sigma\phi)^{1/2}$$

Thus if we plot the steady-state photoconductivity against the photon flux, , a parabola should be obtained. The fact that this is so has been demonstrated in figure 5.15.

References

A Erdelyi (ed) "Tables of integral transforms" McGraw-Hill New York(1954)

H G Grimmeiss,C Ovren and J W Allen J Appl Phys 47,1103(1976)

P K lim and B E Brodie Can J Phys 55,1461(1977) and ibid 55,1512(1977)

A J R de Kock Handbook of semiconductors 3,247(1980)

H F Matare J Appl Phys 56,2605(1984)

P C Mathur,B R Sethi,P L Talwar,O P Sharma,R P Sharma Phys Lett 73A,234(1979)

N F Mott and E A Davis "Electronic processes in non crystalline materials " Oxford,Clarendon 1979

G Pfister and H Scher Adv Phys 27,747(1978)

M Pollak and T H Geballe Phys Rev 122,1742(1961)

R Rentzsch,I S Shlimak and H Berger Phys Stat Sol(a) 54,487(1979)

H Scher Proc 7th Int Conf amorphous and liquid semicond,Centre for consultancy and liason, University of Edinburgh,Edinburgh,1977 (p197)

H Scher and M Lax Phys rev B7,4491(1973)

F W Schmidlin Phys Rev B16,2362(1977)

T Tiedje and A Rose Sol Stat Comm 37,49(1980)

I N Timchenko and D D Nedeoglo Phys Stat Sol(b)105,55(1981)

M Yamaguchi,A Yamamoto and M Kondo J Appl Phys 48,1961(1977)

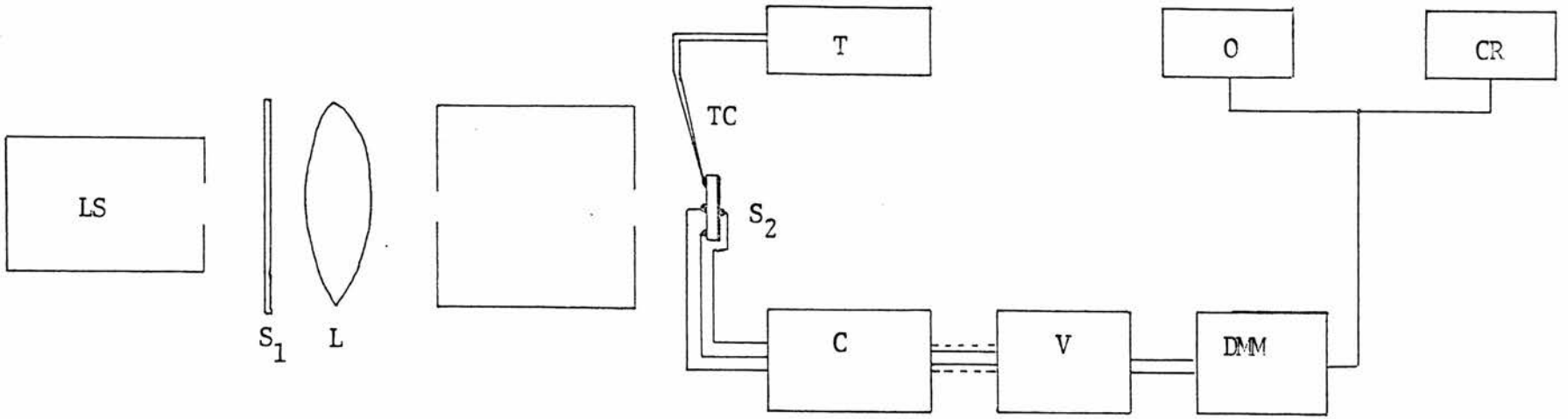

Legend

C	Circuit in figure 5.1a	M	Zeiss SPM2 mirror monochromator	S_2	Sample
CR	Kipp and Zonen BD8 single channel chart recorder	O	Nicolet Instruments digital oscilloscope	T	CRL temperature indicator (model 107)
L	5cm focal length lens			TC	Thermocouple
LS	Light source	S_1	Shutter	V	Keithley 602
				DMM	Keithley 160 digital voltmeter

Fig 5.1 Schematic diagram of the experimental arrangement for studying the photoconductivity of the samples.

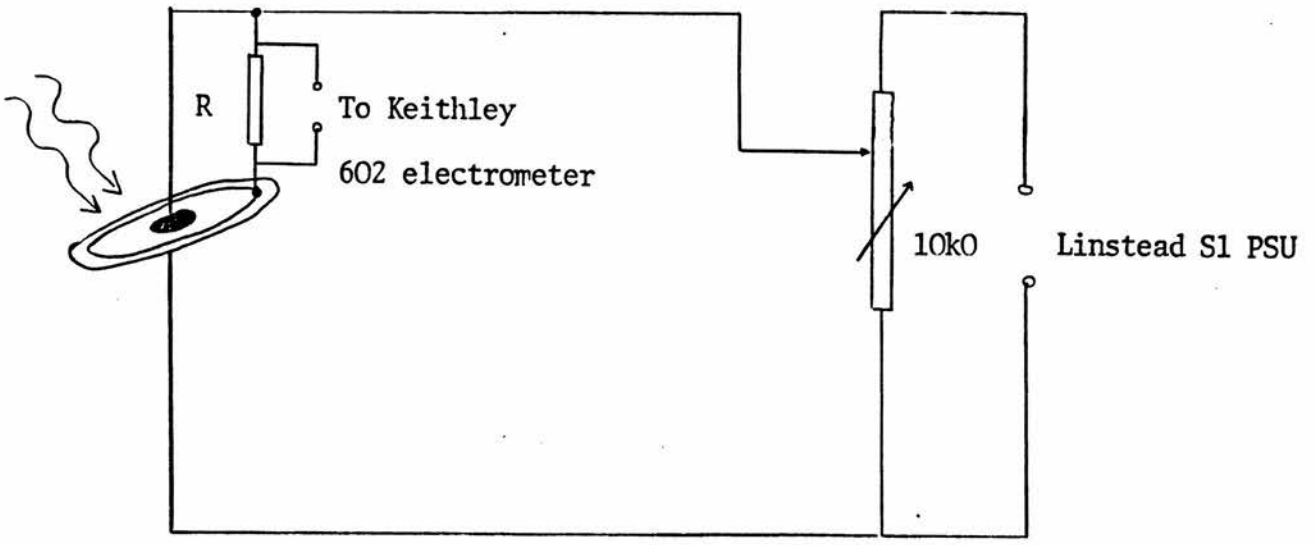

Fig. 5.1a Schematic diagram of the circuit used to measure the photoresponse of the samples.The value of R was $10^9\Omega$

Fig 5.2 Typical rise in the photcurrent for sample 1 for incident monochromatic light and with additional UV light.

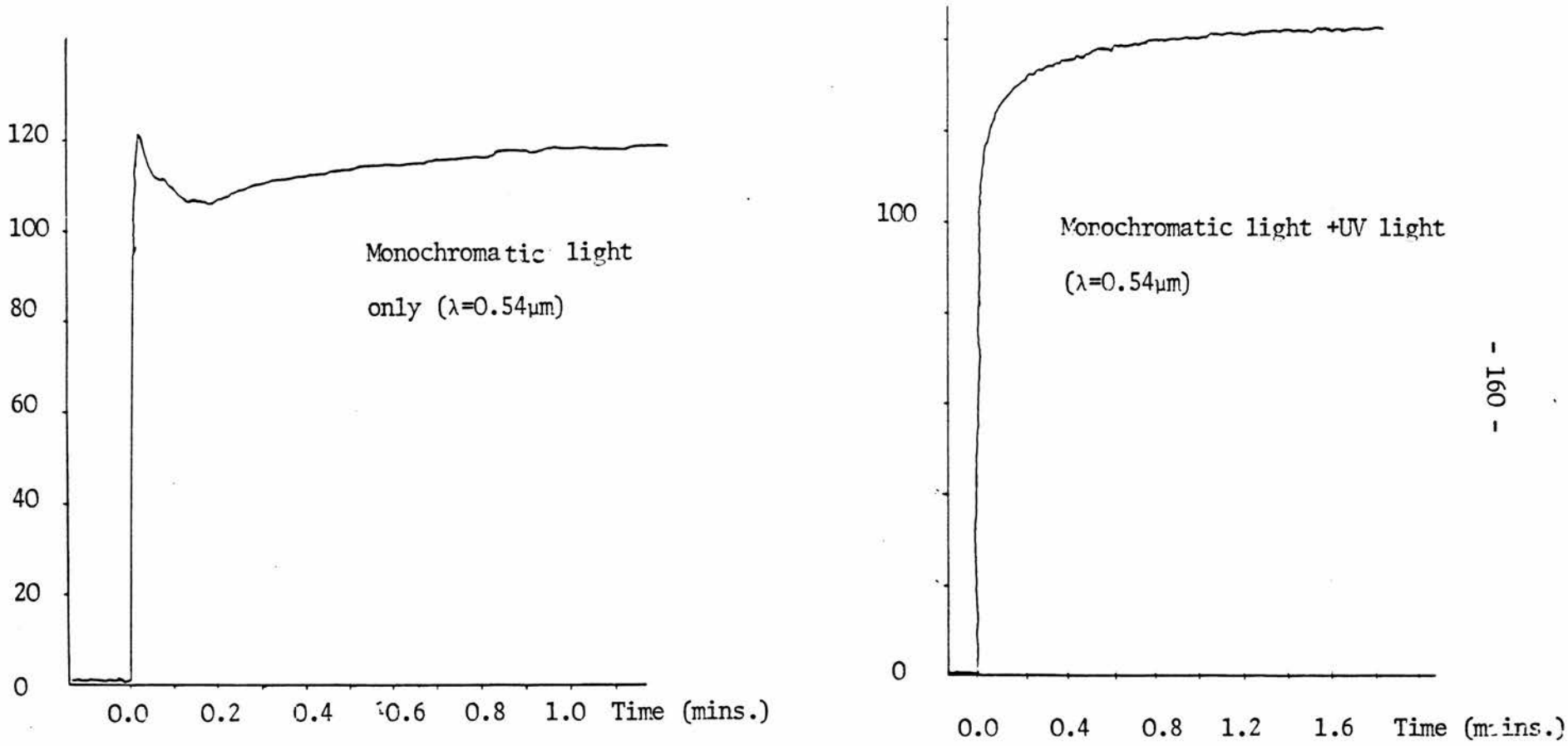

Fig 5.3 Typical rise in the photocurrent for sample 2 for monochromatic light and with additional UV light.

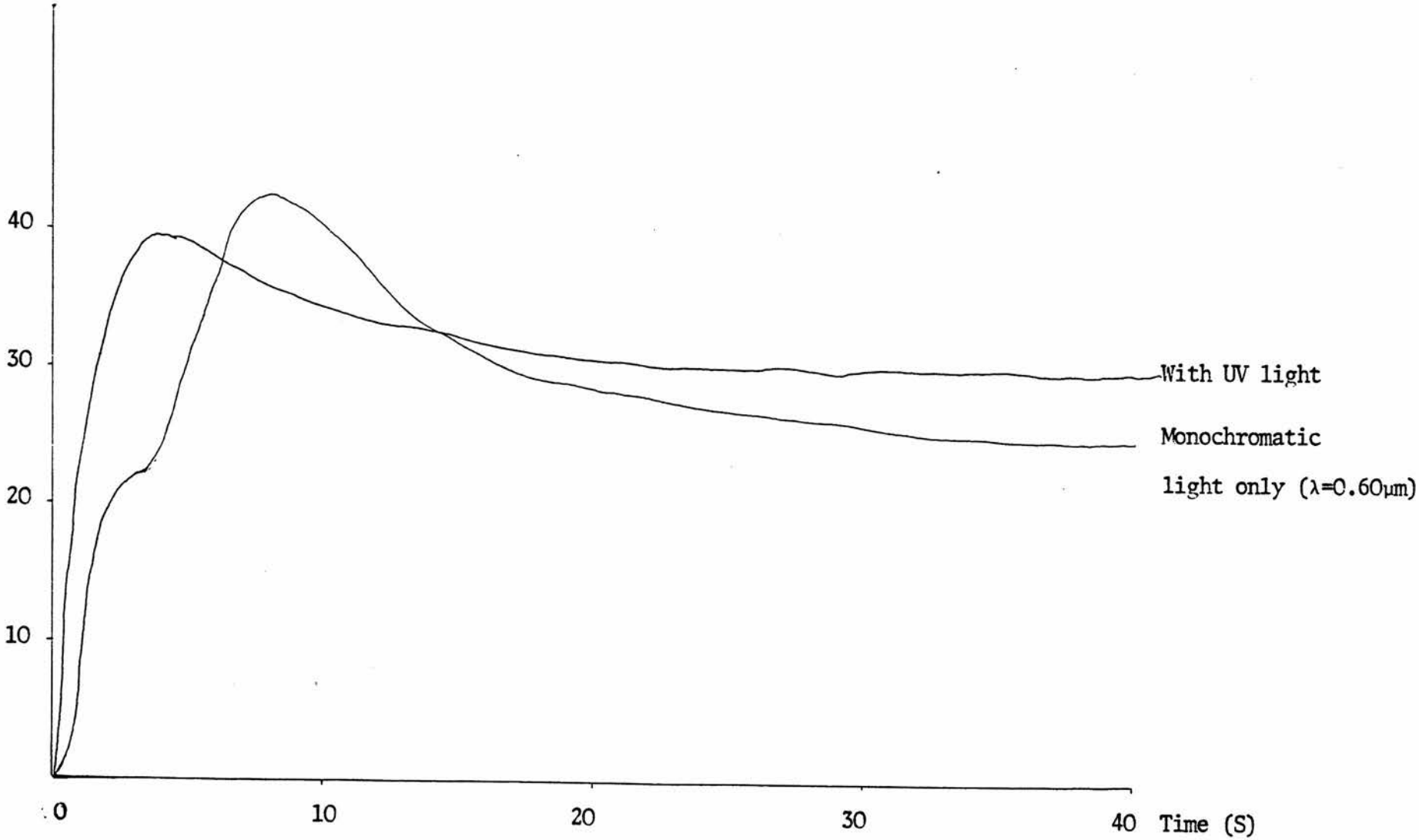

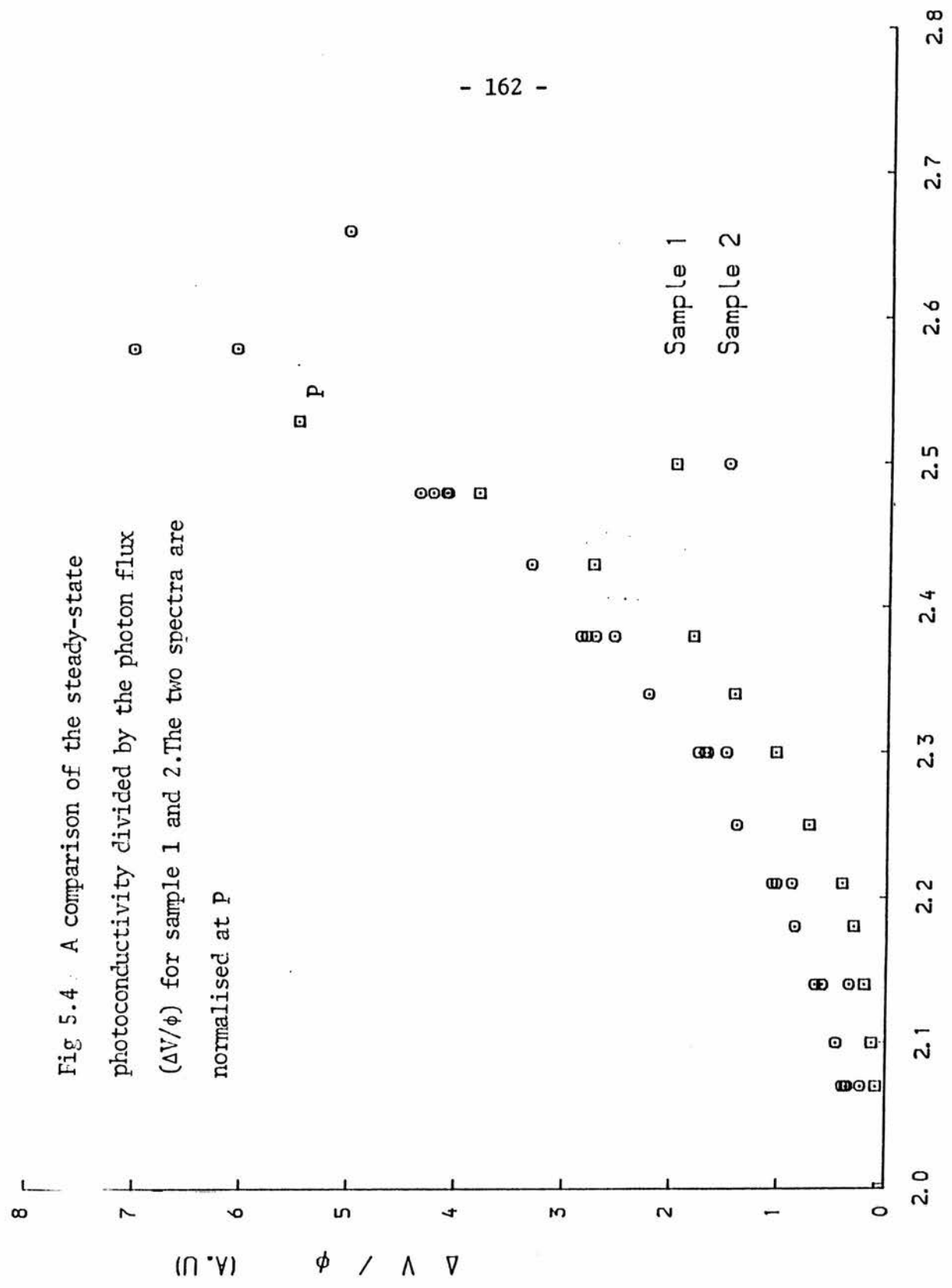

Fig 5.4 A comparison of the steady-state photoconductivity divided by the photon flux ($\Delta V/\phi$) for sample 1 and 2. The two spectra are normalised at P

Fig. 5.5 A comparison of the inverse rise time of the photoconductivity of sample 1 when UV and monochromatic light are incident on sample 1, τ_1^{-1}, and when only monochromatic light is incident, τ_2^{-1}.

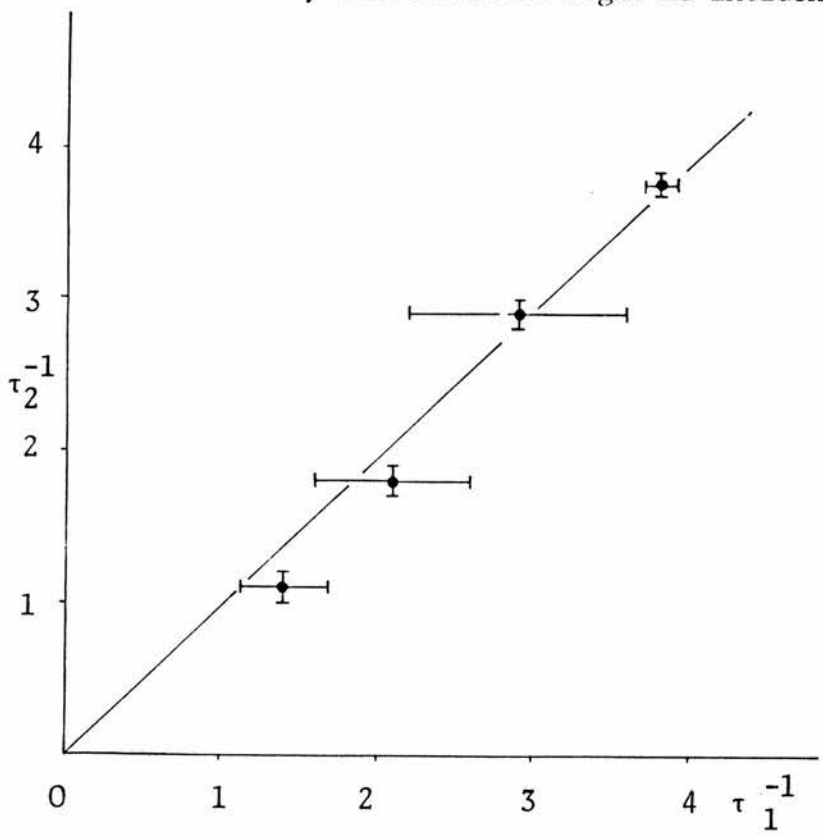

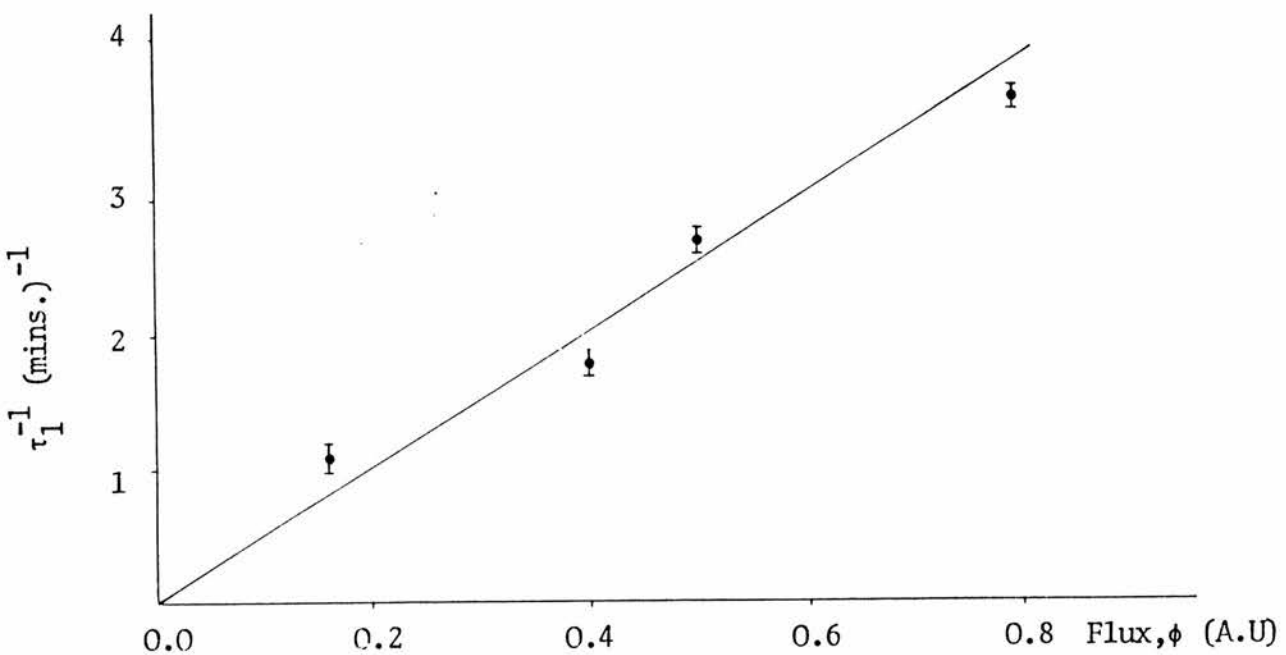

Fig. 5.7 The inverse rise time constant of photoconductivity of sample 1 as a function of increasing photon flux. The UV light was continuously left on.

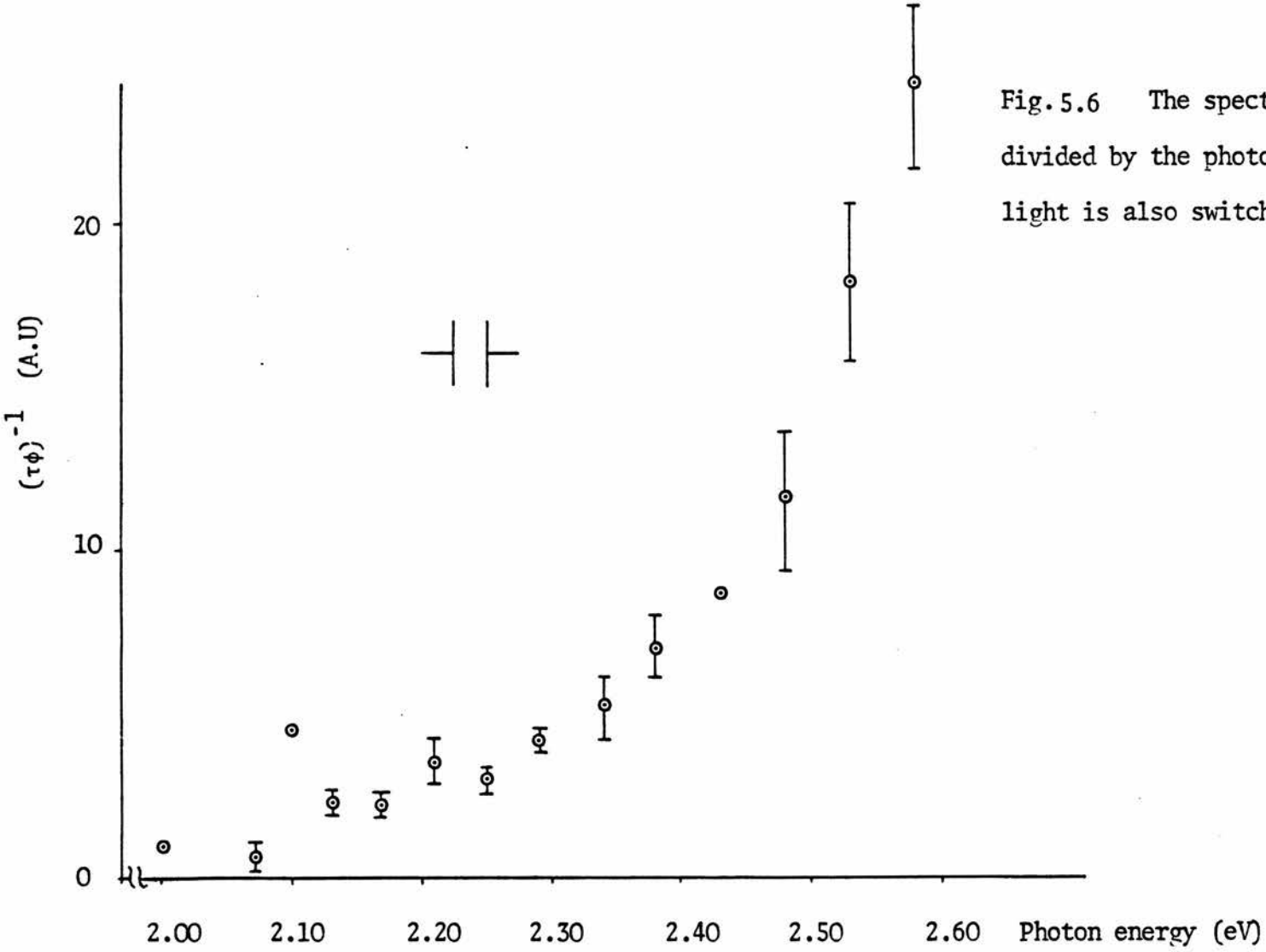

Fig. 5.6 The spectrum of the inverse rise time divided by the photon flux for sample 1 when UV light is also switched on.

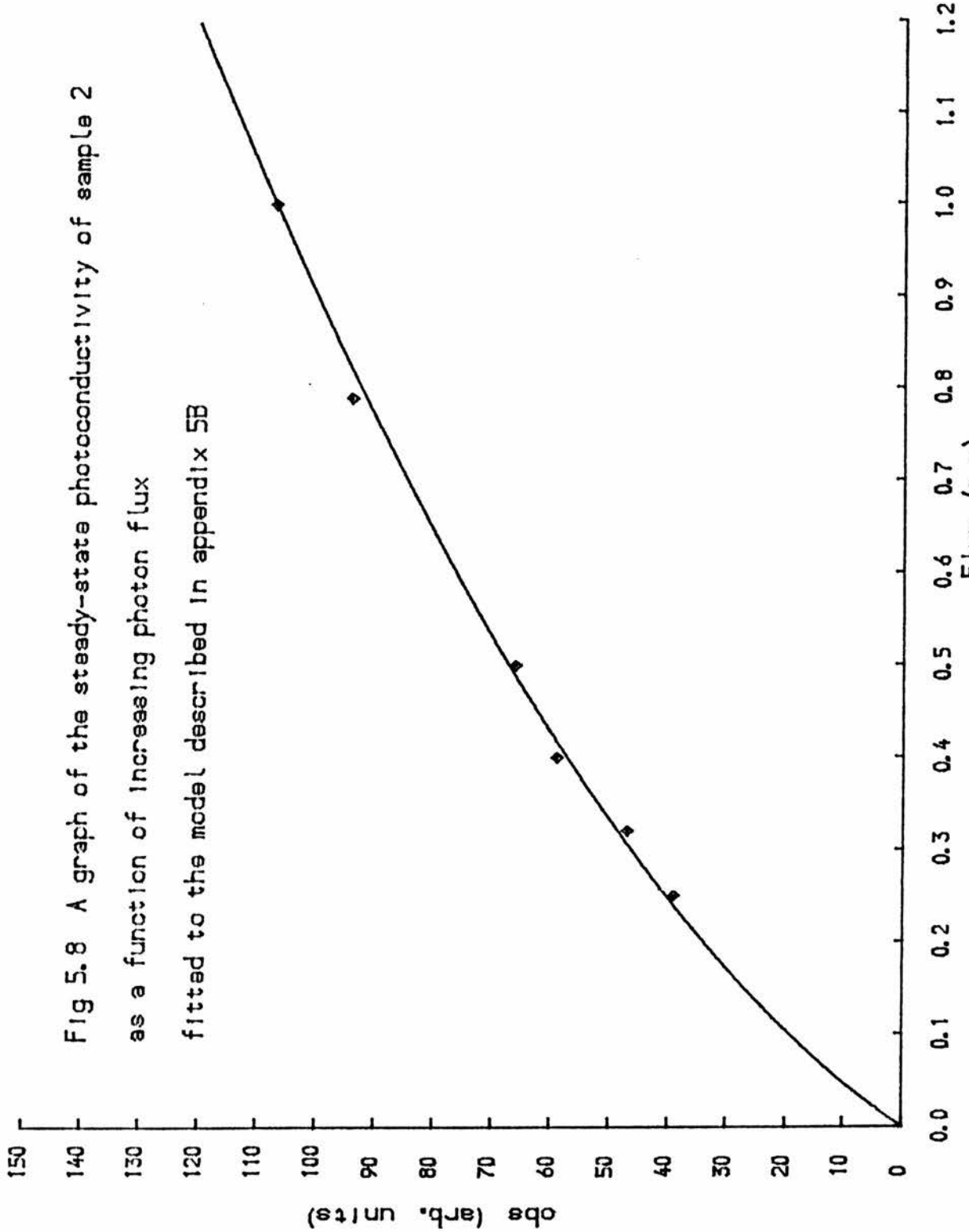

Fig 5.8 A graph of the steady-state photoconductivity of sample 2 as a function of increasing photon flux fitted to the model described in appendix 5B

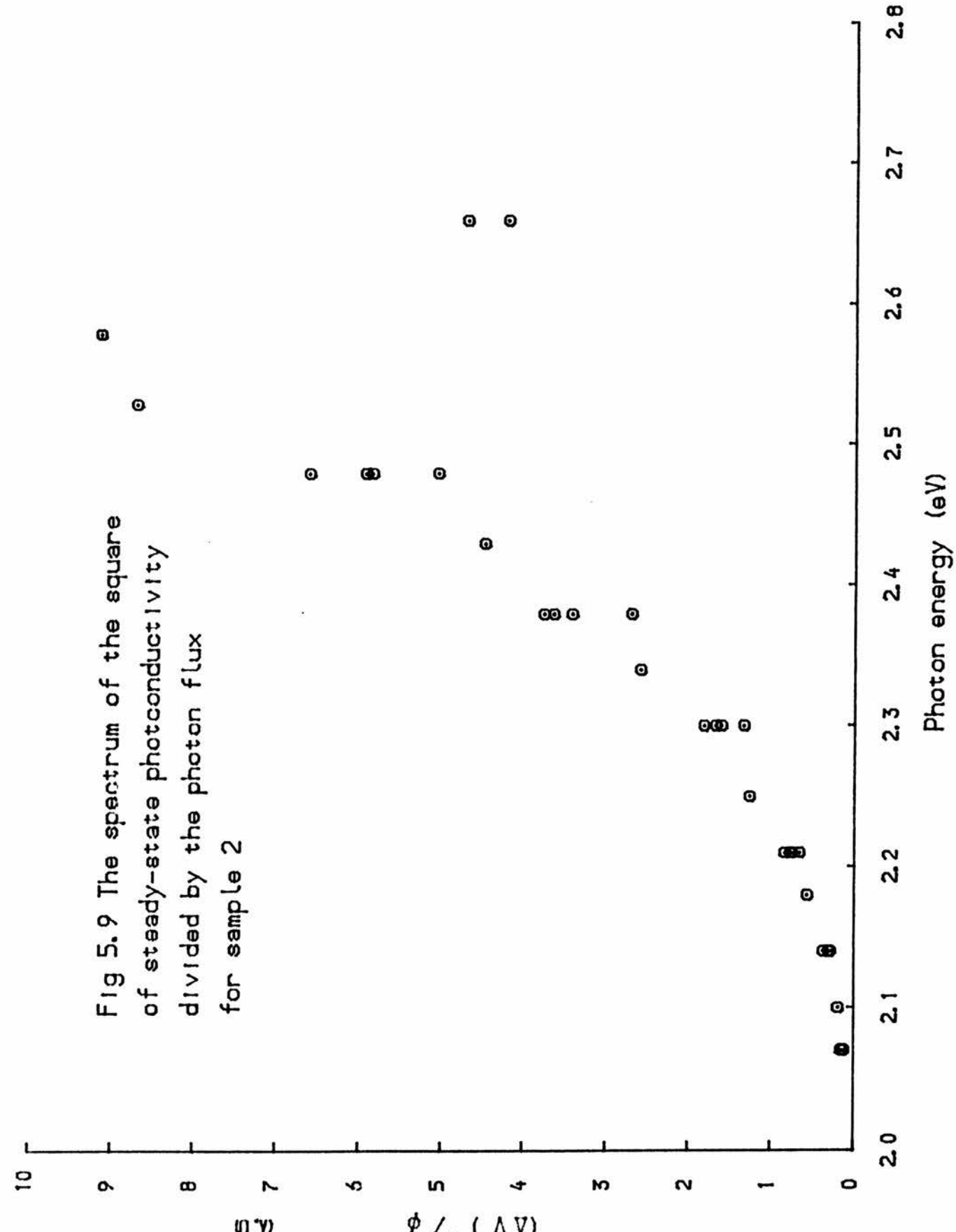

Fig 5.9 The spectrum of the square of steady-state photoconductivity divided by the photon flux for sample 2

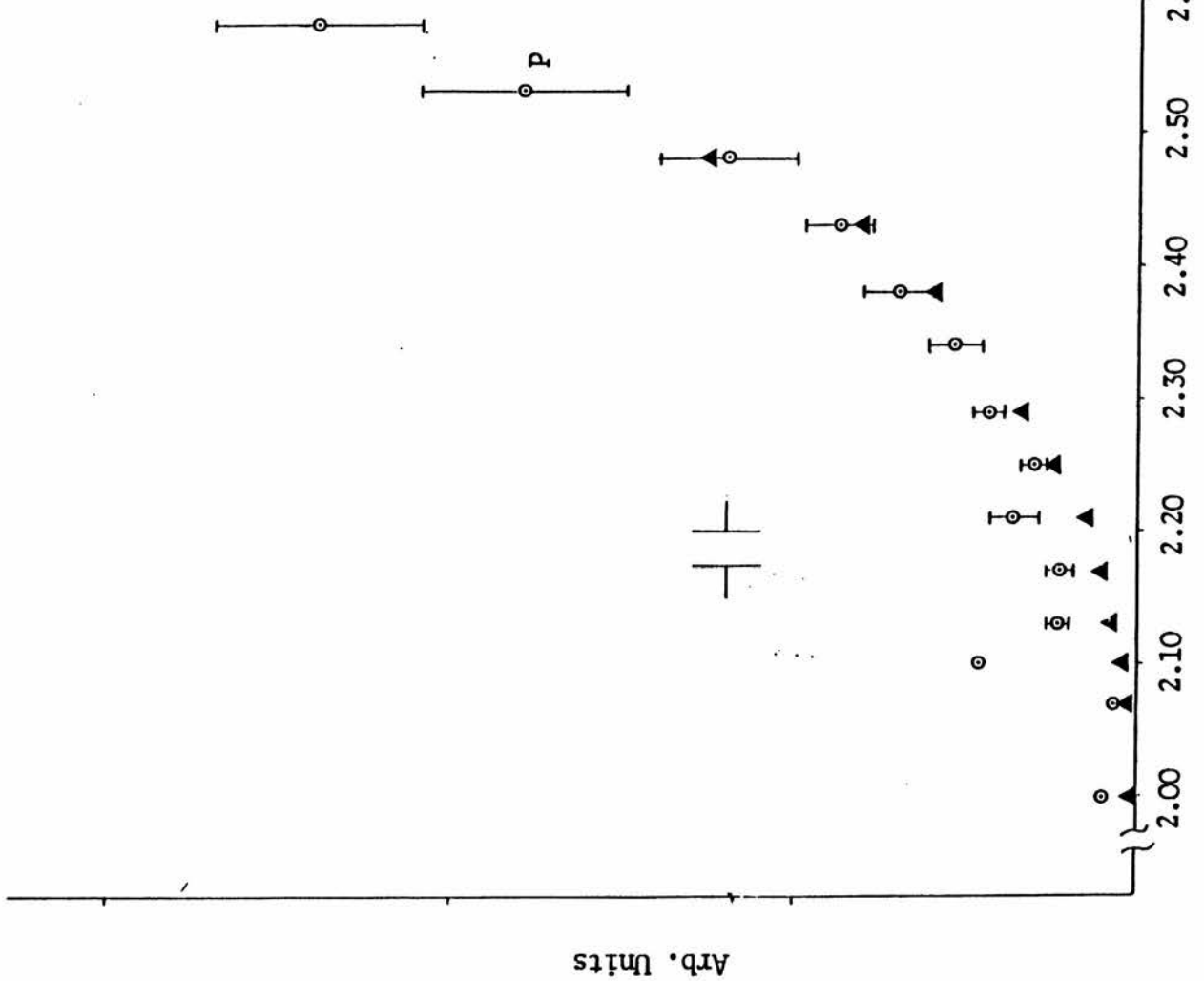

Fig. 5.10 A comparison of $(\tau\phi)^{-1}$ and $(\Delta V)/\phi$ for sample 1. The two sets of data are normalised at P.

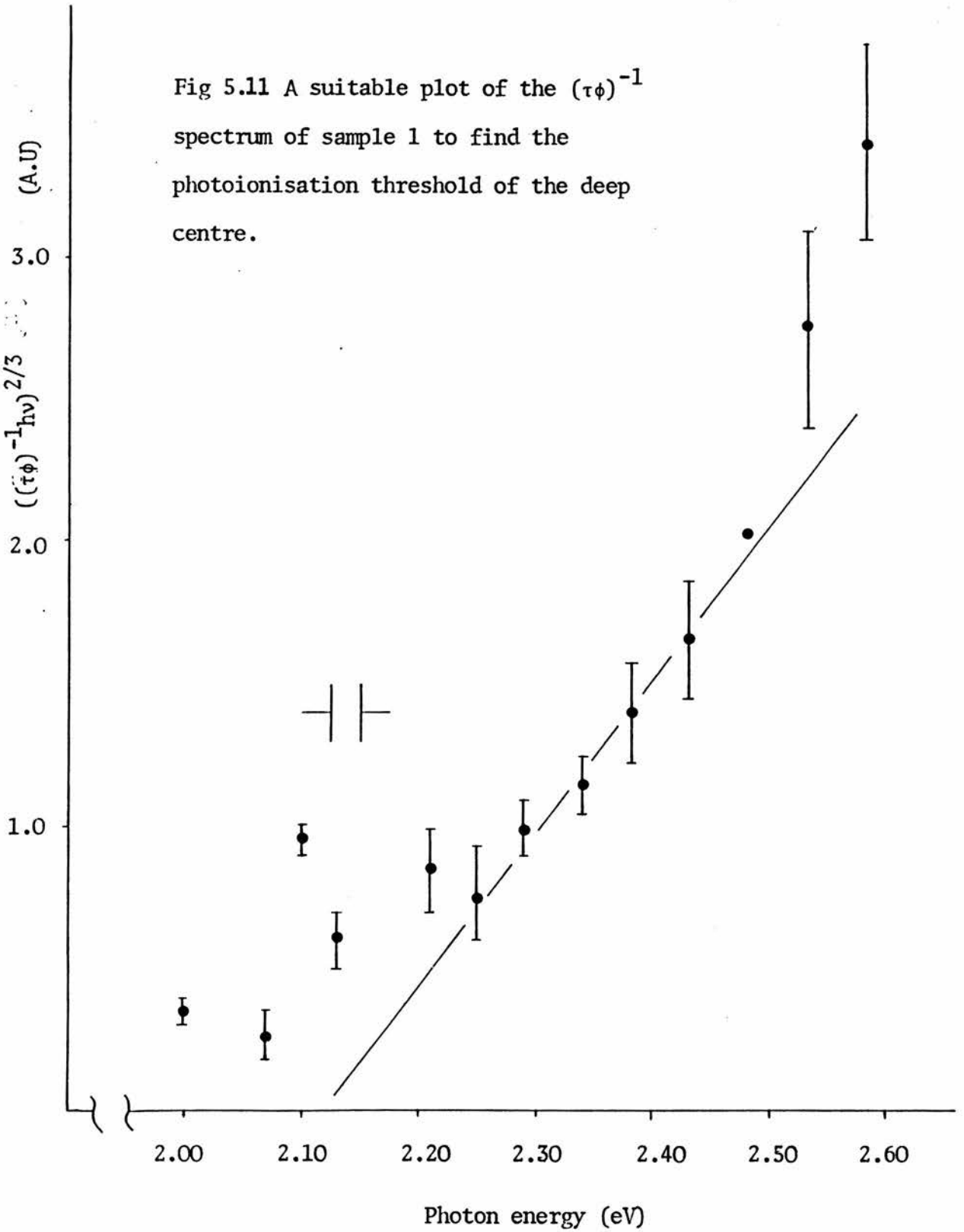

Fig 5.11 A suitable plot of the $(\tau\phi)^{-1}$ spectrum of sample 1 to find the photoionisation threshold of the deep centre.

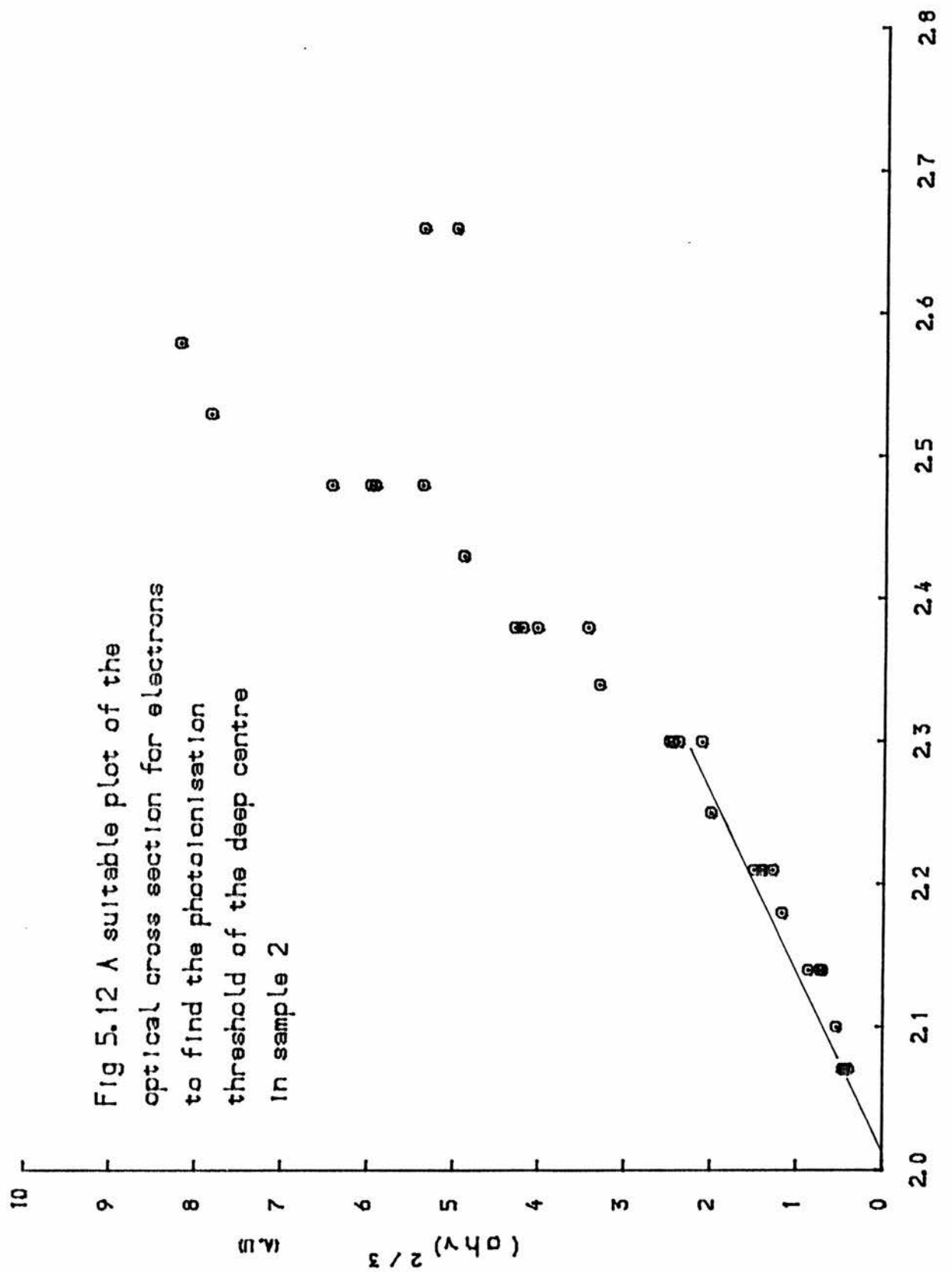

Fig 5.12 A suitable plot of the optical cross section for electrons to find the photoionisation threshold of the deep centre in sample 2

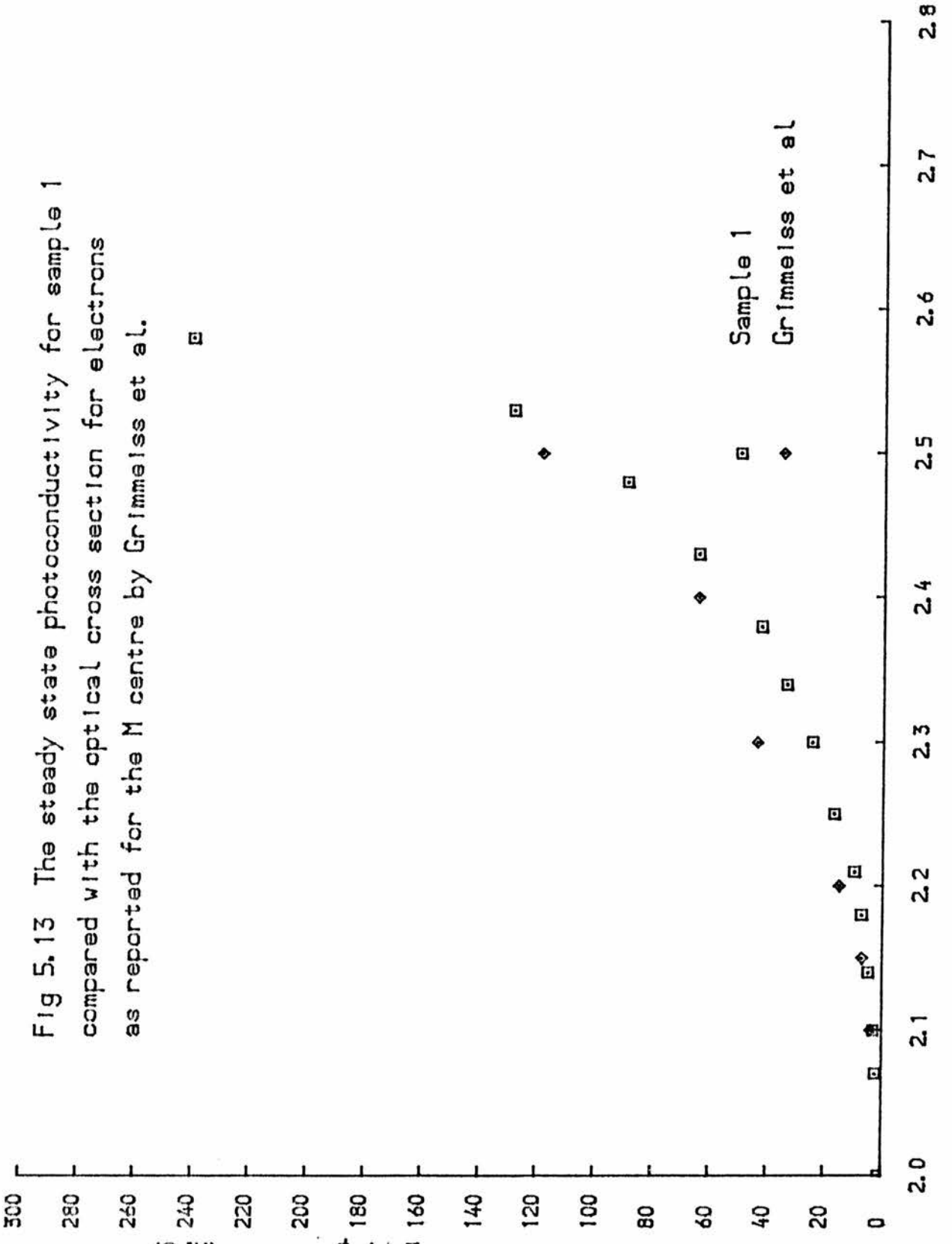

Fig 5.13 The steady state photoconductivity for sample 1 compared with the optical cross section for electrons as reported for the M centre by Grimmeiss et al.

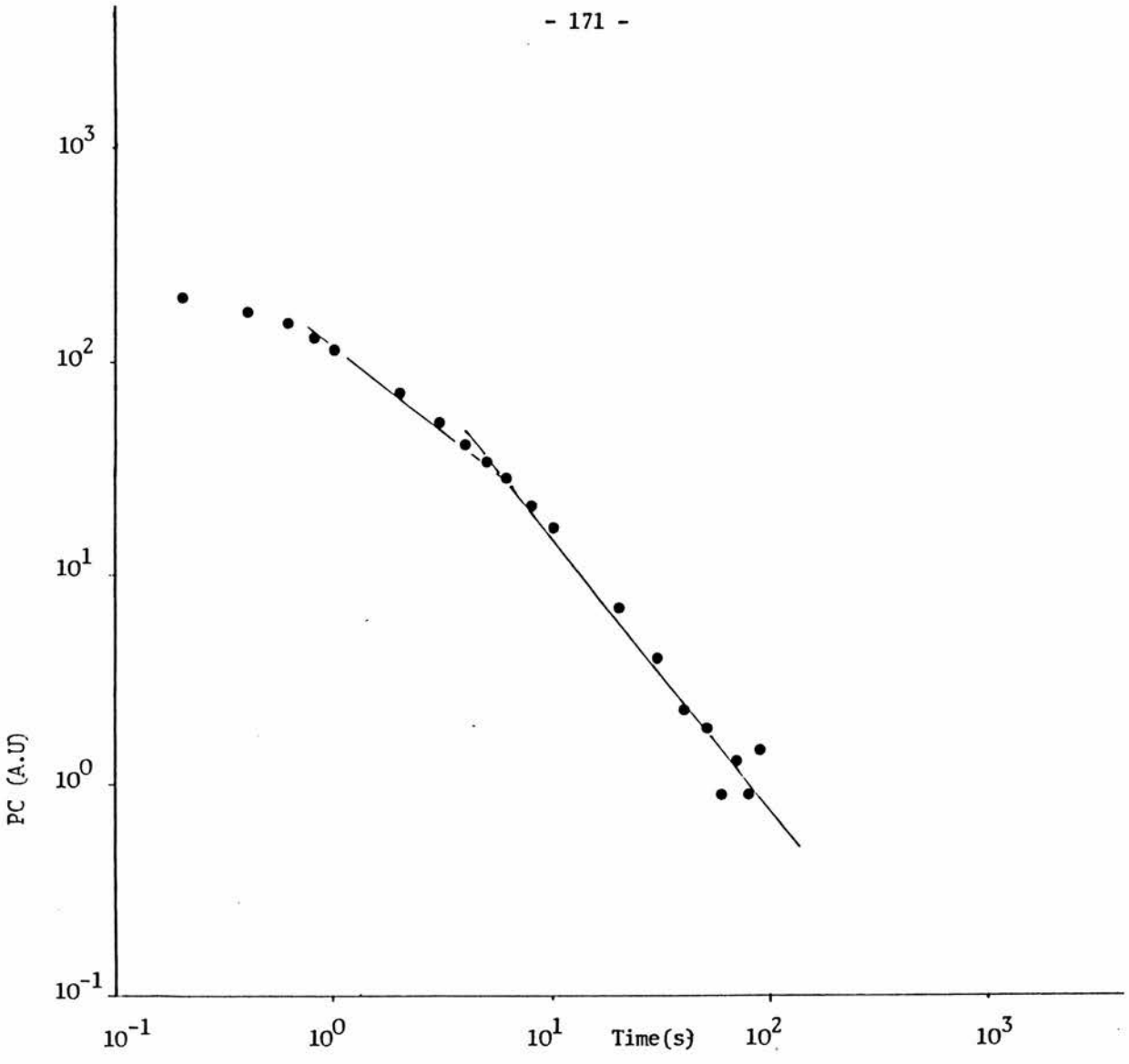

Fig. 5.14 The decay of steady-state photoconductivity of sample 1 with no additional UV light switched on (λ=0.49μm)

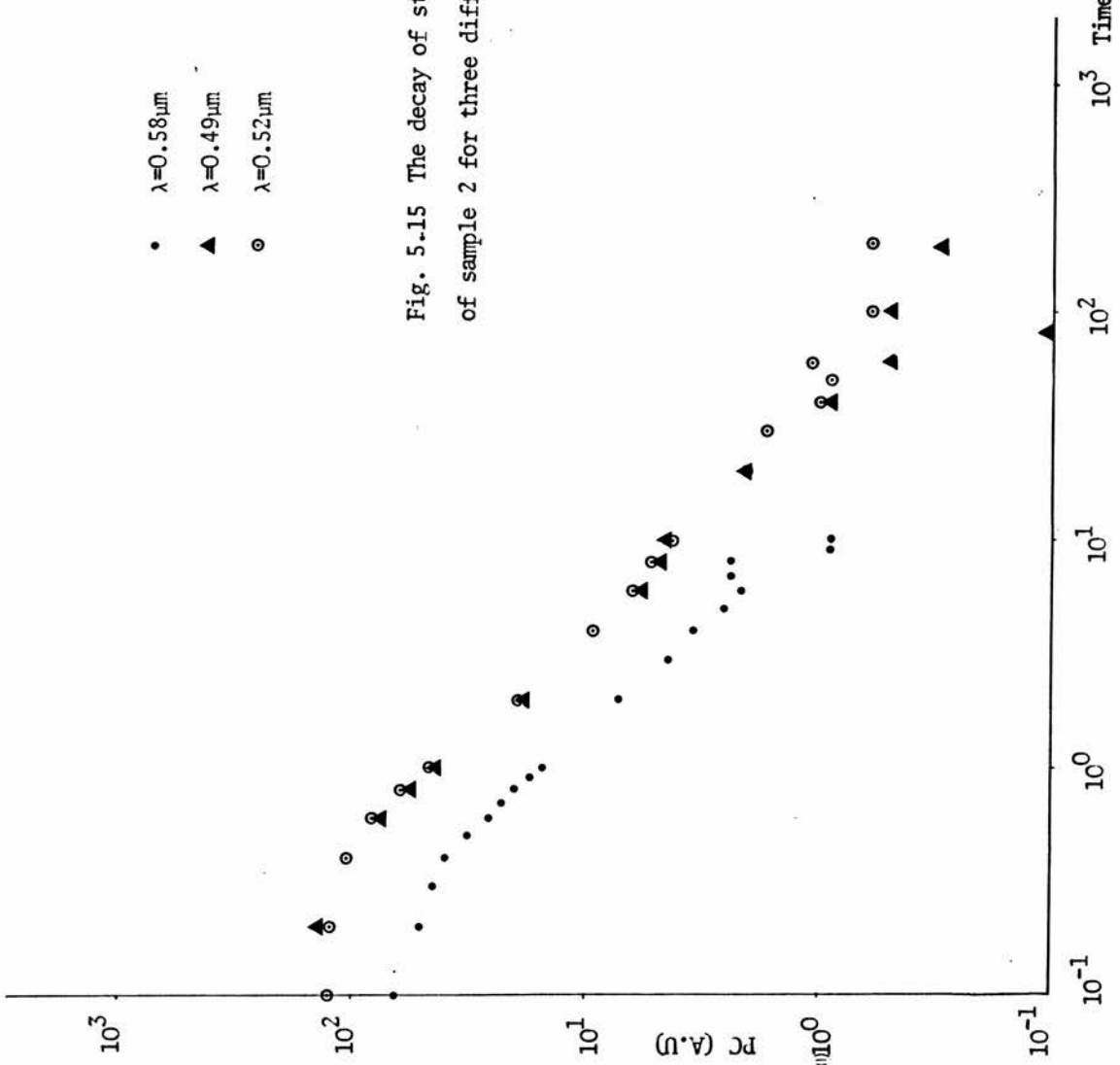

Fig. 5.15 The decay of steady-state photoconductivity of sample 2 for three different wavelengths.

Fig. 5.16 Schematic diagram of the experimental arrangement used for measuring the equivalent series capacitance of the samples. Also shown is a schematic diagram of the method of connecting the sample to the bridge.

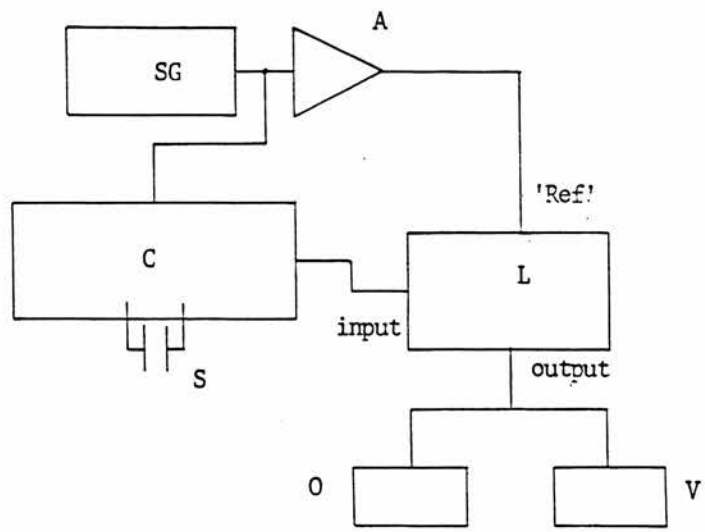

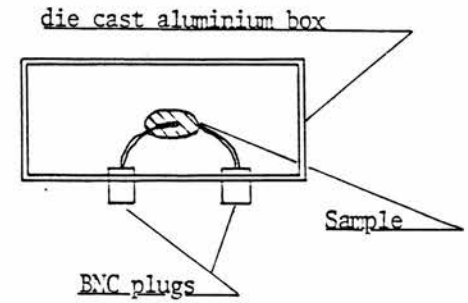

Legend

A Brookdeal 450 low noise amplifier

C General Radio 1615A capacitance bridge

L Brookdeal 9050 lock-in amplifier

O Telequipment D1010 oscilloscope

SG Farnell LFP1 signal generator

S sample

V Farnell TM2 voltmeter

Fig. 5.17 The equivalent series capacitance of a 270pF silver mica capacitor measured over four orders of frequency using the apparatus shown in figure 5.16.

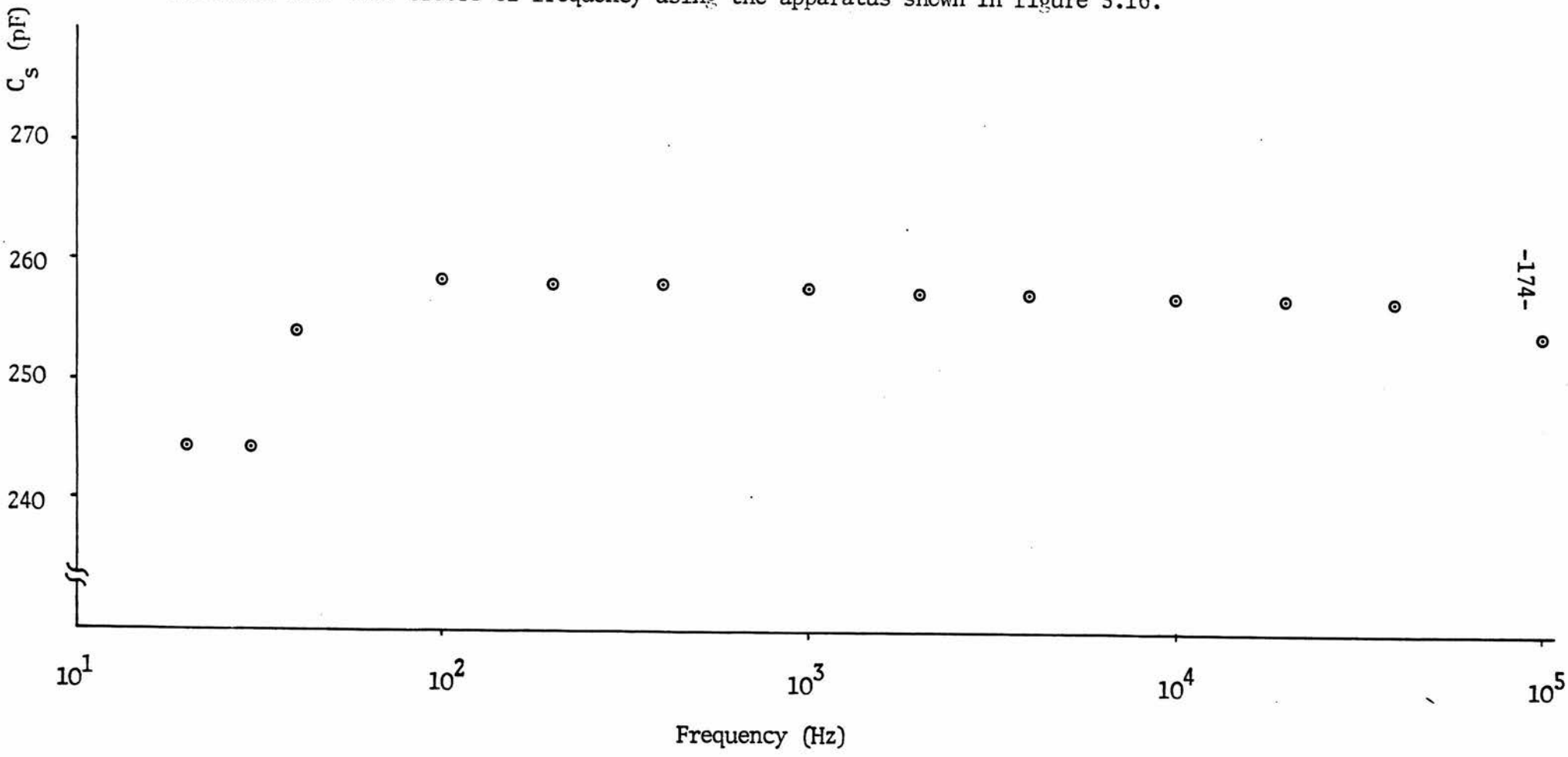

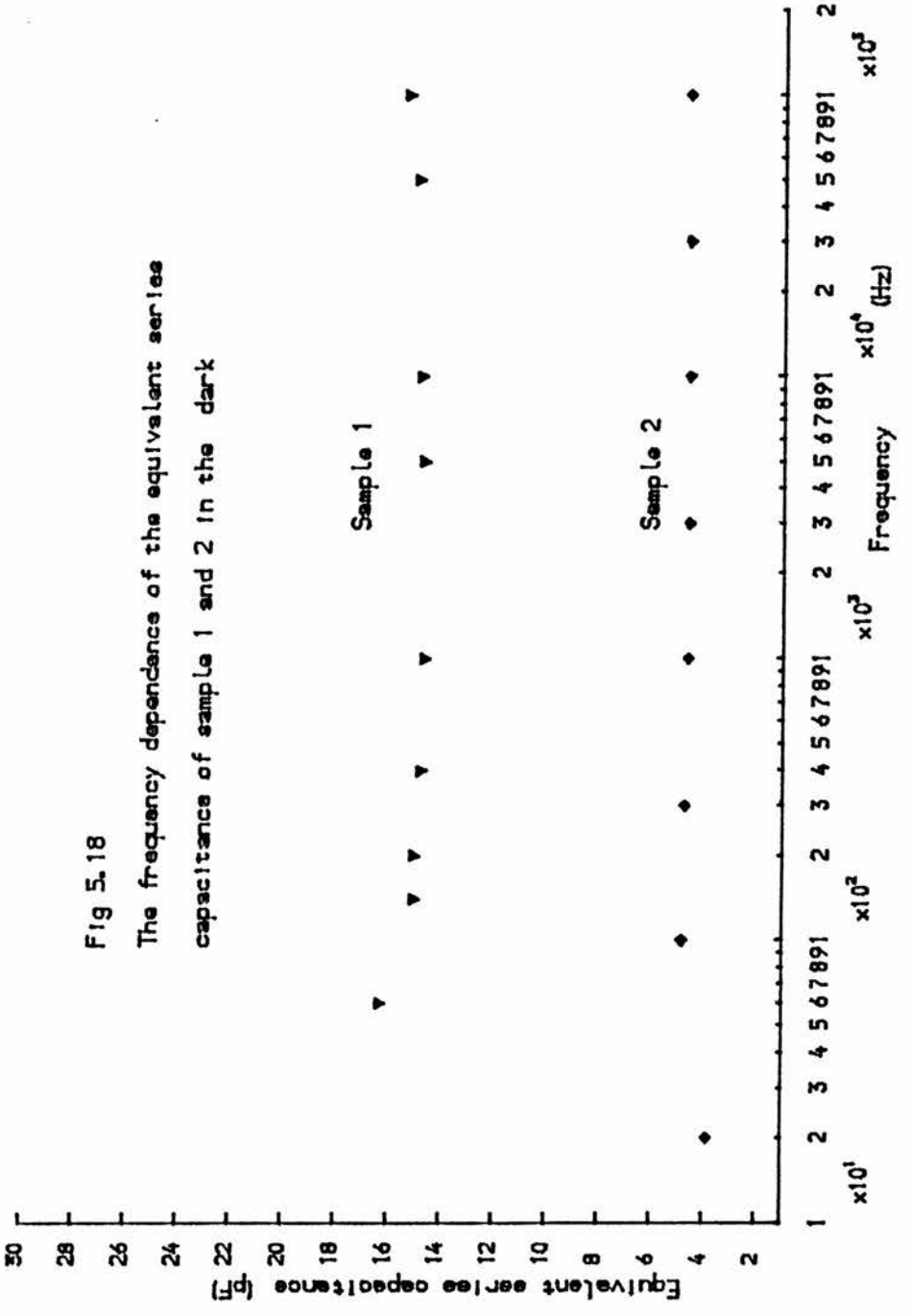
Fig 5.18
The frequency dependance of the equivalent series
capacitance of sample 1 and 2 in the dark
Sample 1
Sample 2
Equivalent series capacitance (pF)
Frequency (Hz)
x10¹
x10²
x10³
x10⁴
x10⁵

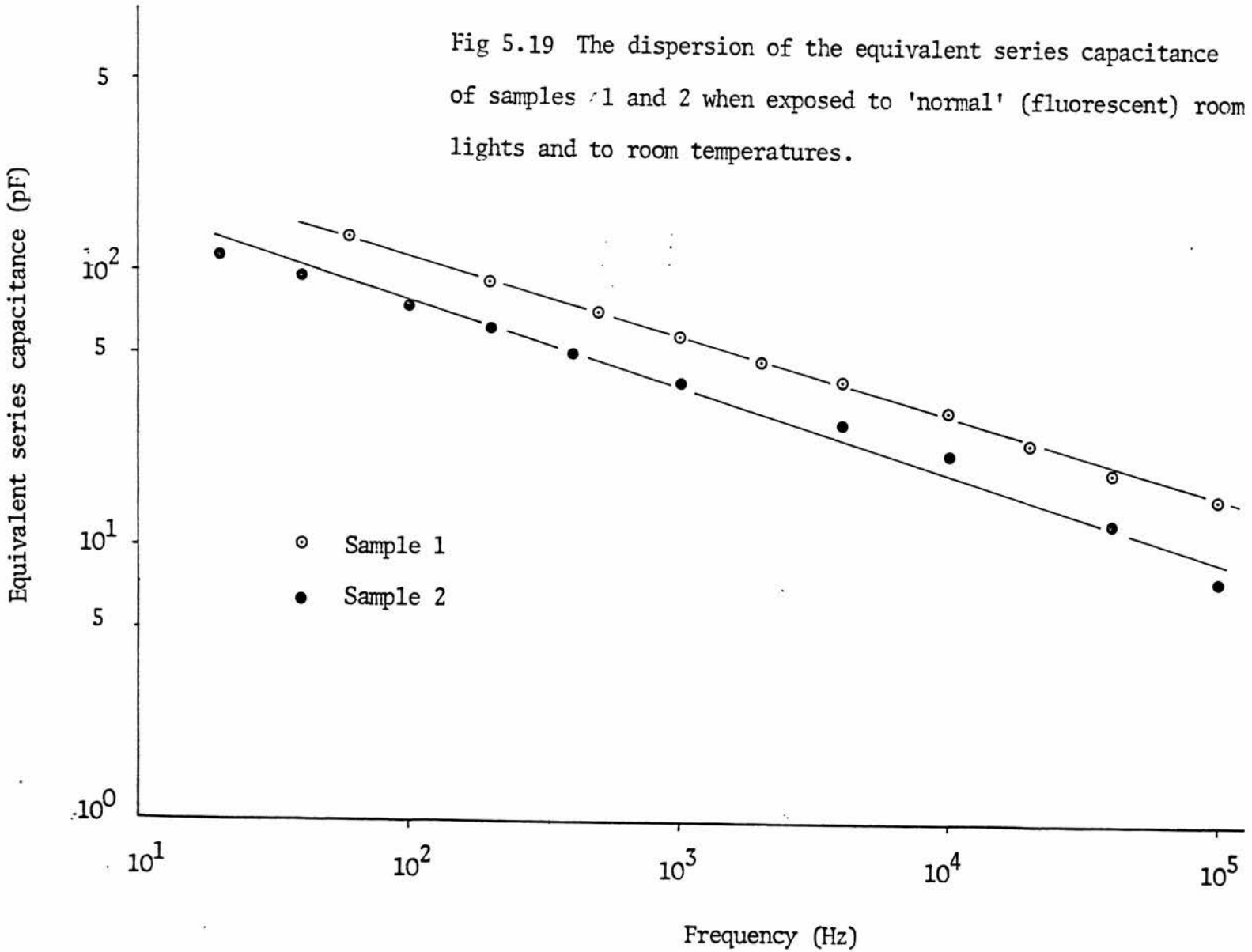

Fig 5.19 The dispersion of the equivalent series capacitance of samples 1 and 2 when exposed to 'normal' (fluorescent) room lights and to room temperatures.

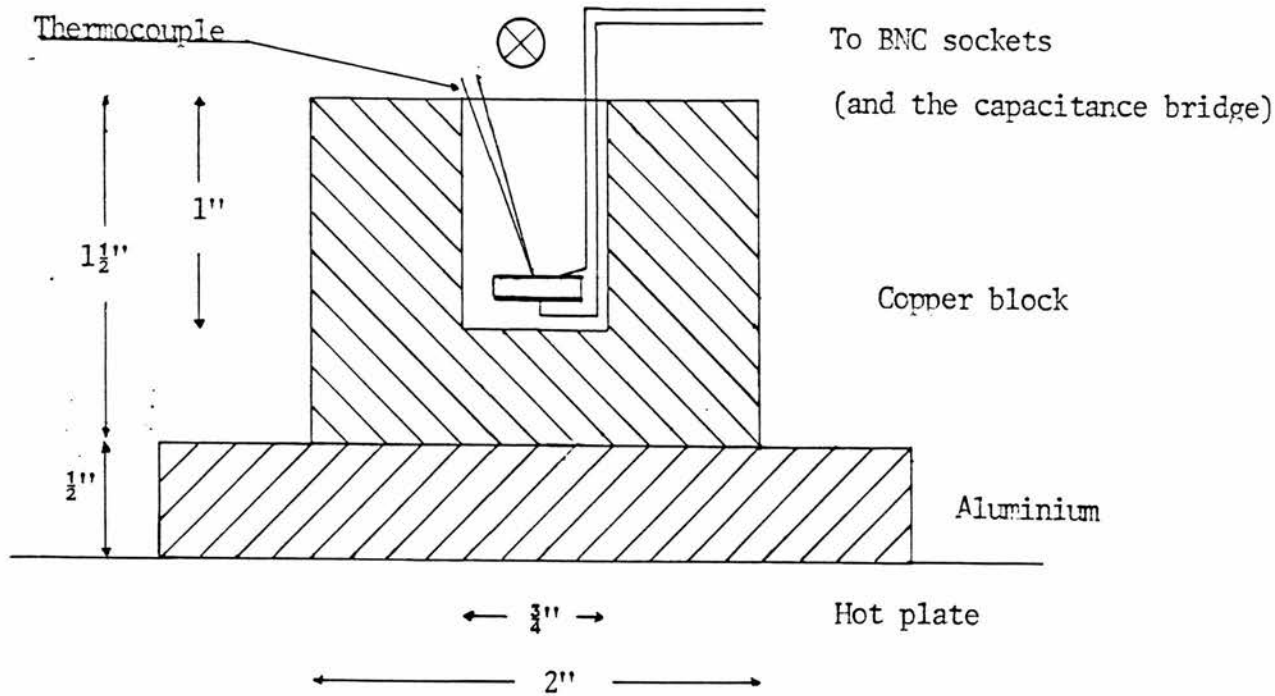

Fig.5.20 Schematic diagram of the method used for observing the dispersion of C_s as a function of temperature and hence for observing the variation of n with temperature.

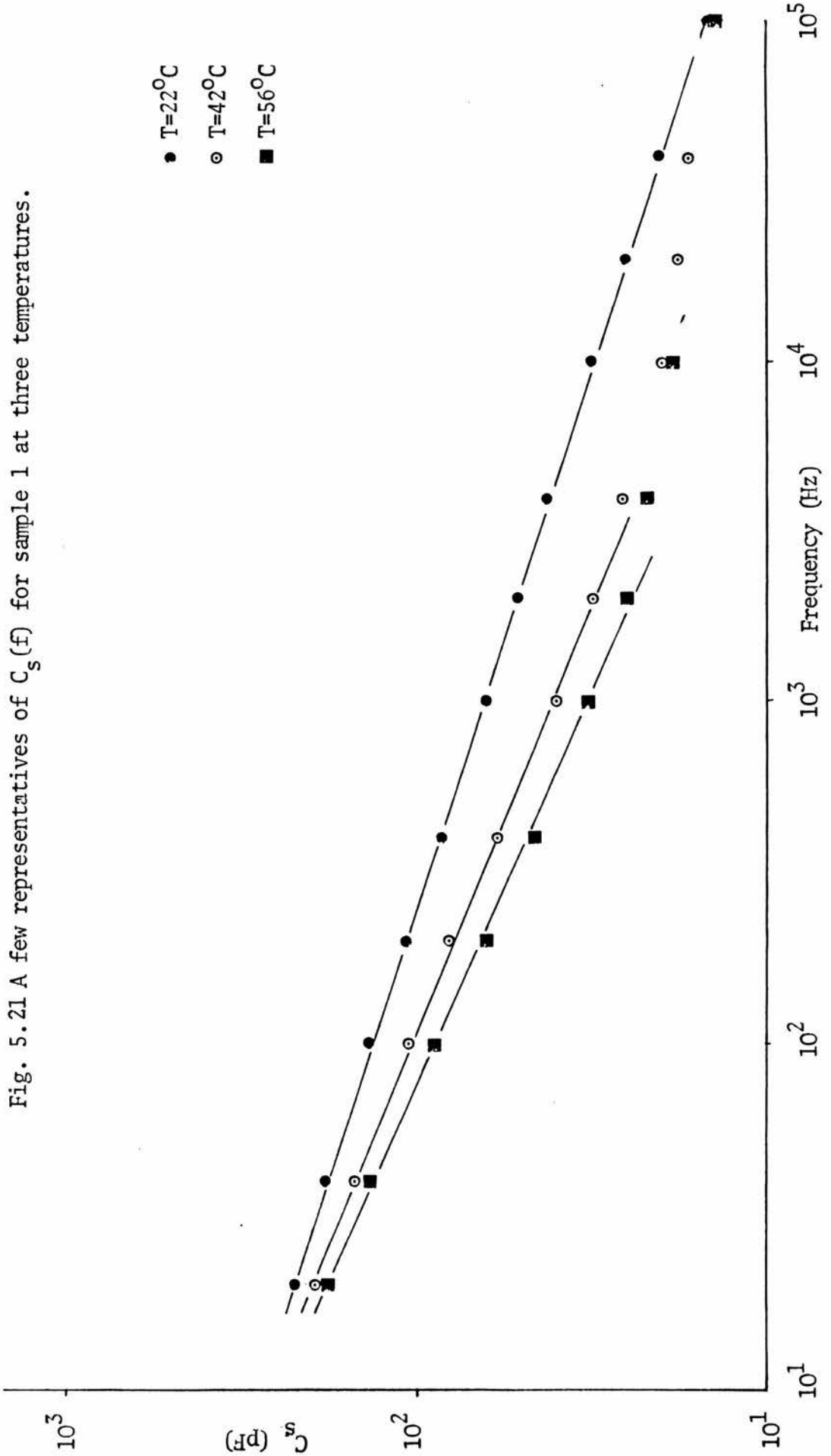

Fig. 5.21 A few representatives of $C_s(f)$ for sample 1 at three temperatures.

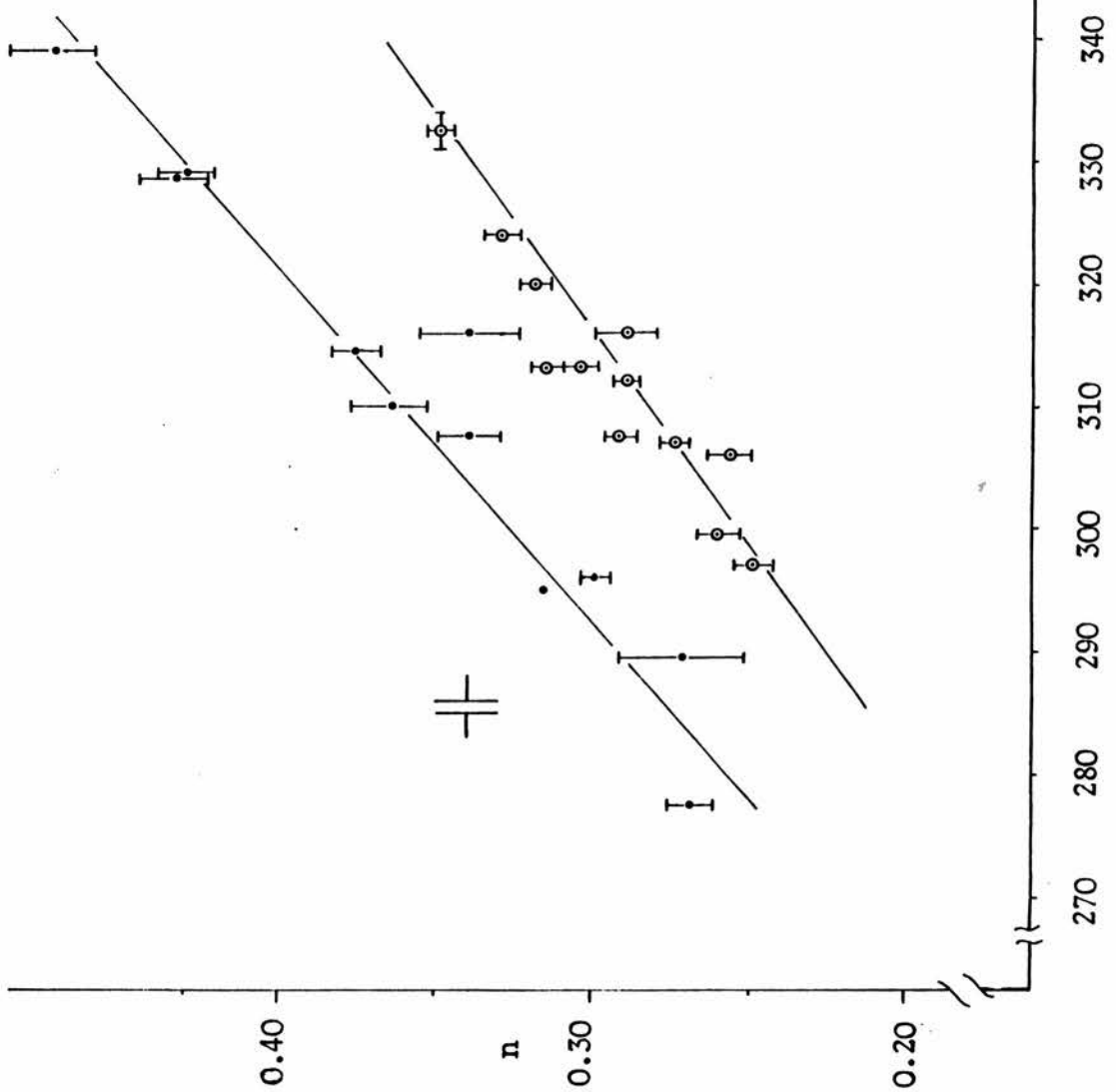

Fig. 5.22 The dependence of the dispersion parameter, n, on temperature.

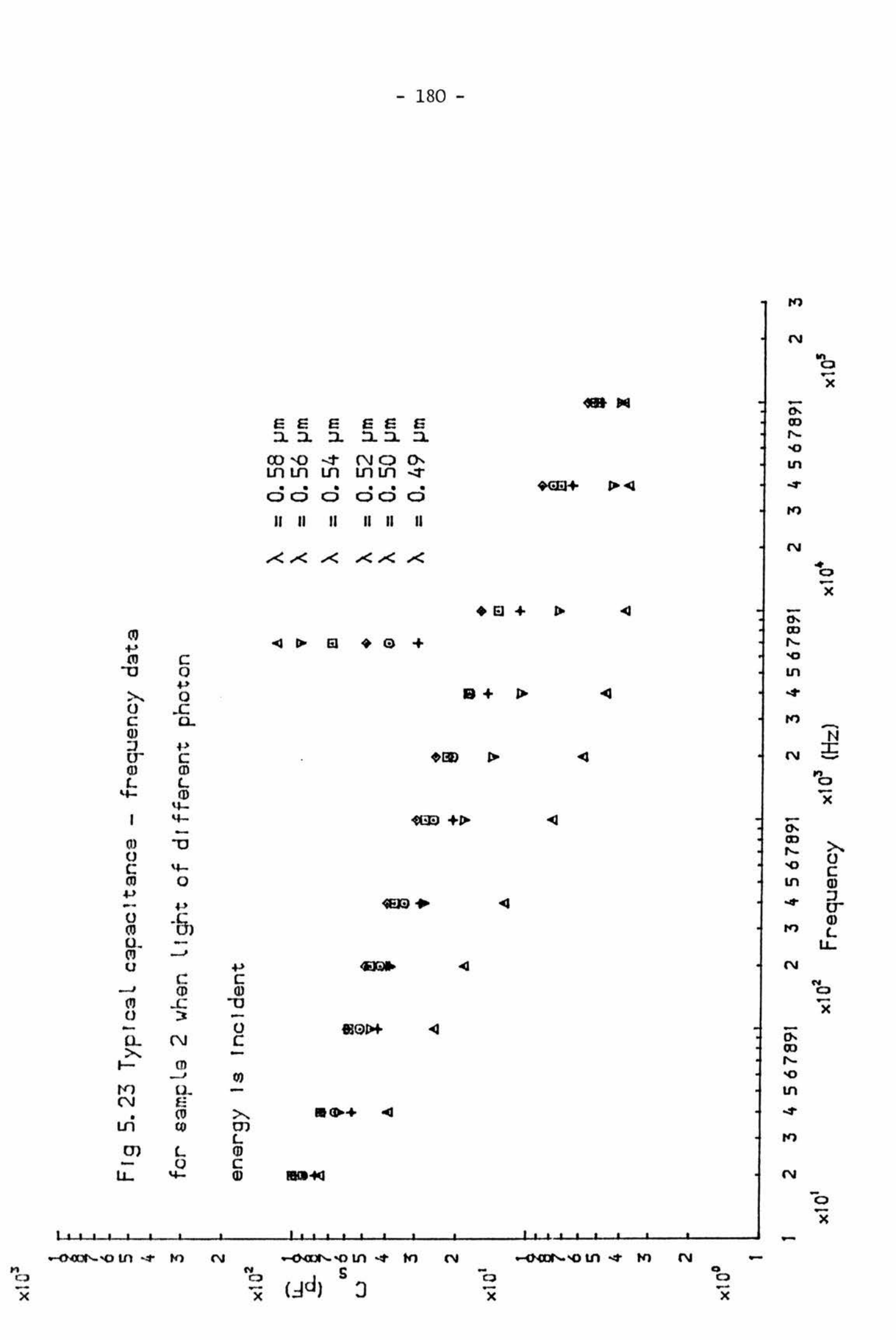
Fig 5.23 Typical capacitance - frequency data
for sample 2 when light of different photon
energy is incident
λ = 0.58 μm
λ = 0.56 μm
λ = 0.54 μm
λ = 0.52 μm
λ = 0.50 μm
λ = 0.49 μm
C_s (pF)
Frequency (Hz)
x10^3
x10^2
x10^1
x10^0
x10^1
x10^2
x10^3
x10^4
x10^5

Fig. 5.24 The variation of the dispersion parameter,n,with photon energy.

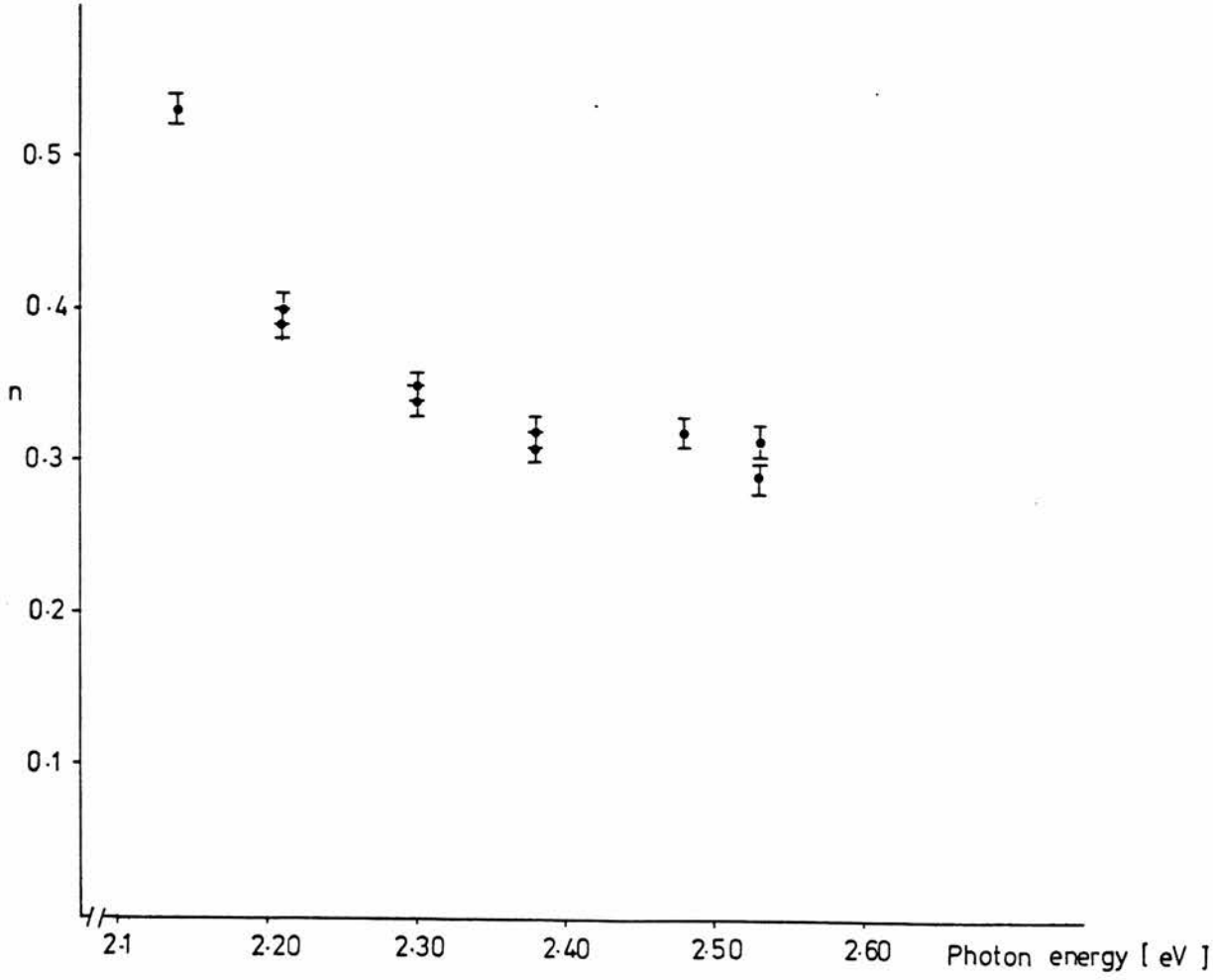

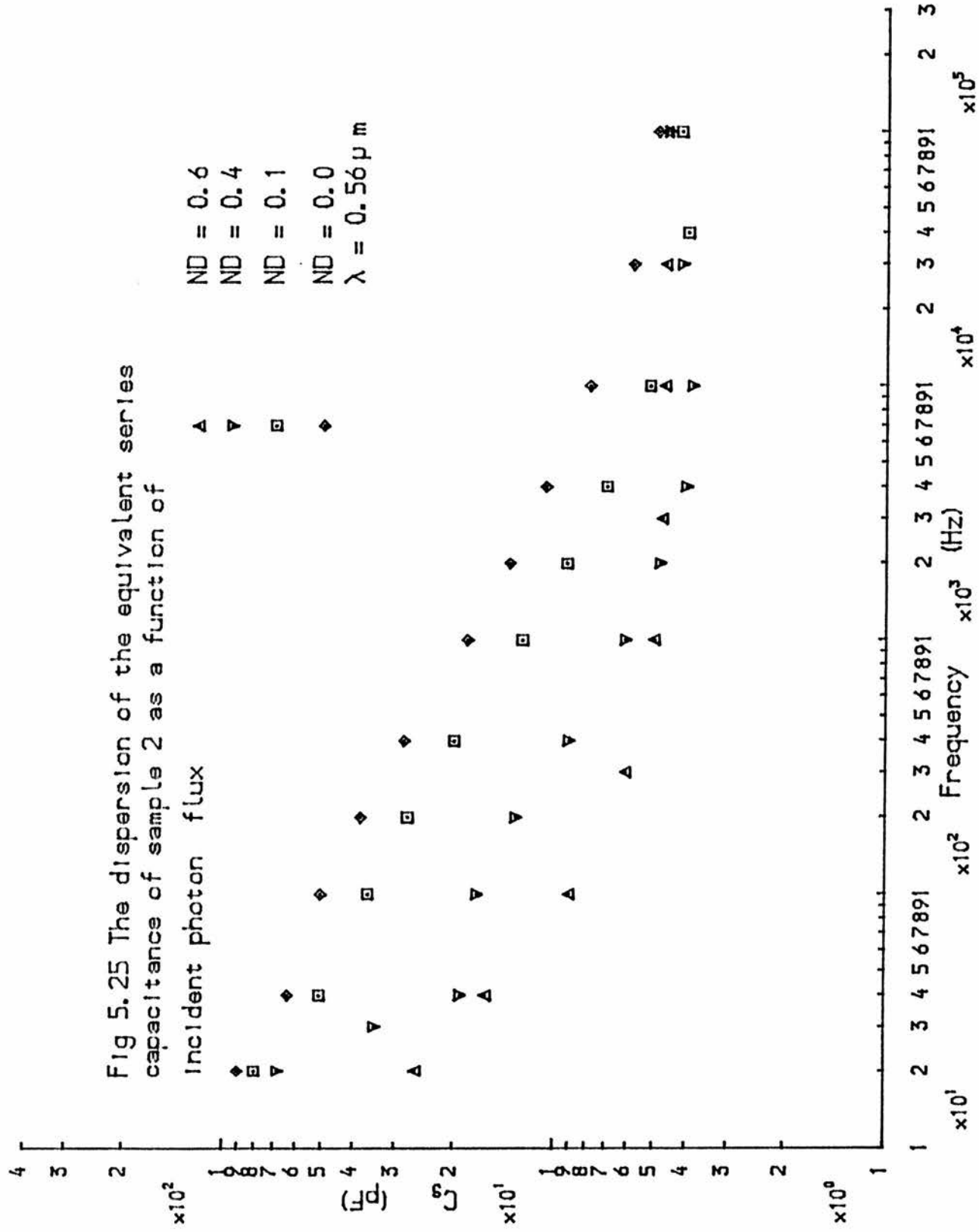

Fig 5.25 The dispersion of the equivalent series capacitance of sample 2 as a function of

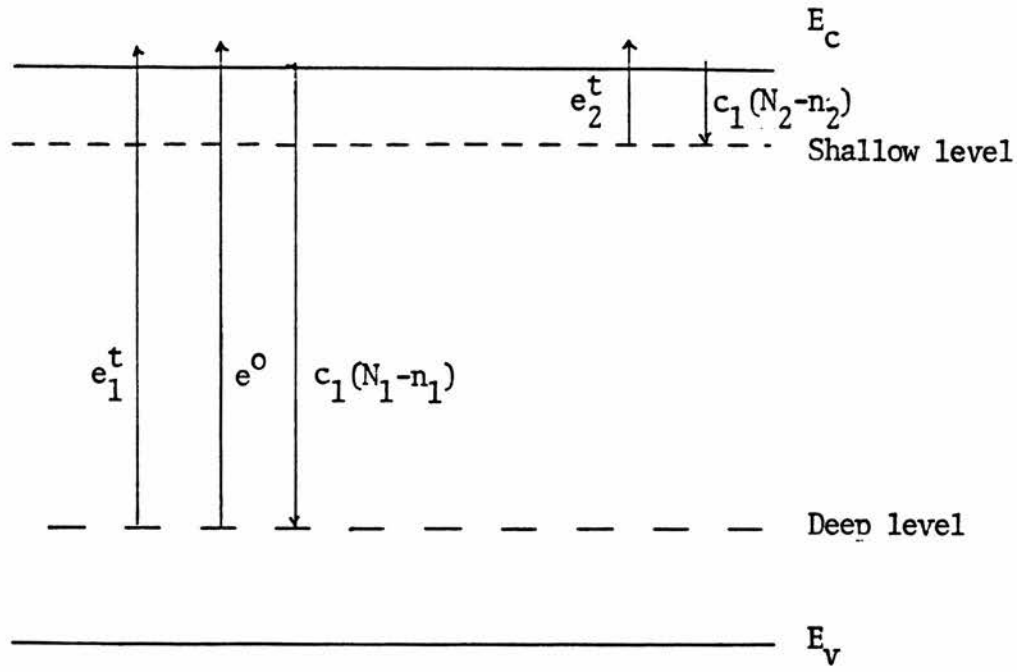

Fig 5A.1 An energy level diagram of a semiconductor with a deep level and a shallow level.The labelled transitions are those considered in appendix 5A to describe the rise in the photoconductivity of sample 2.

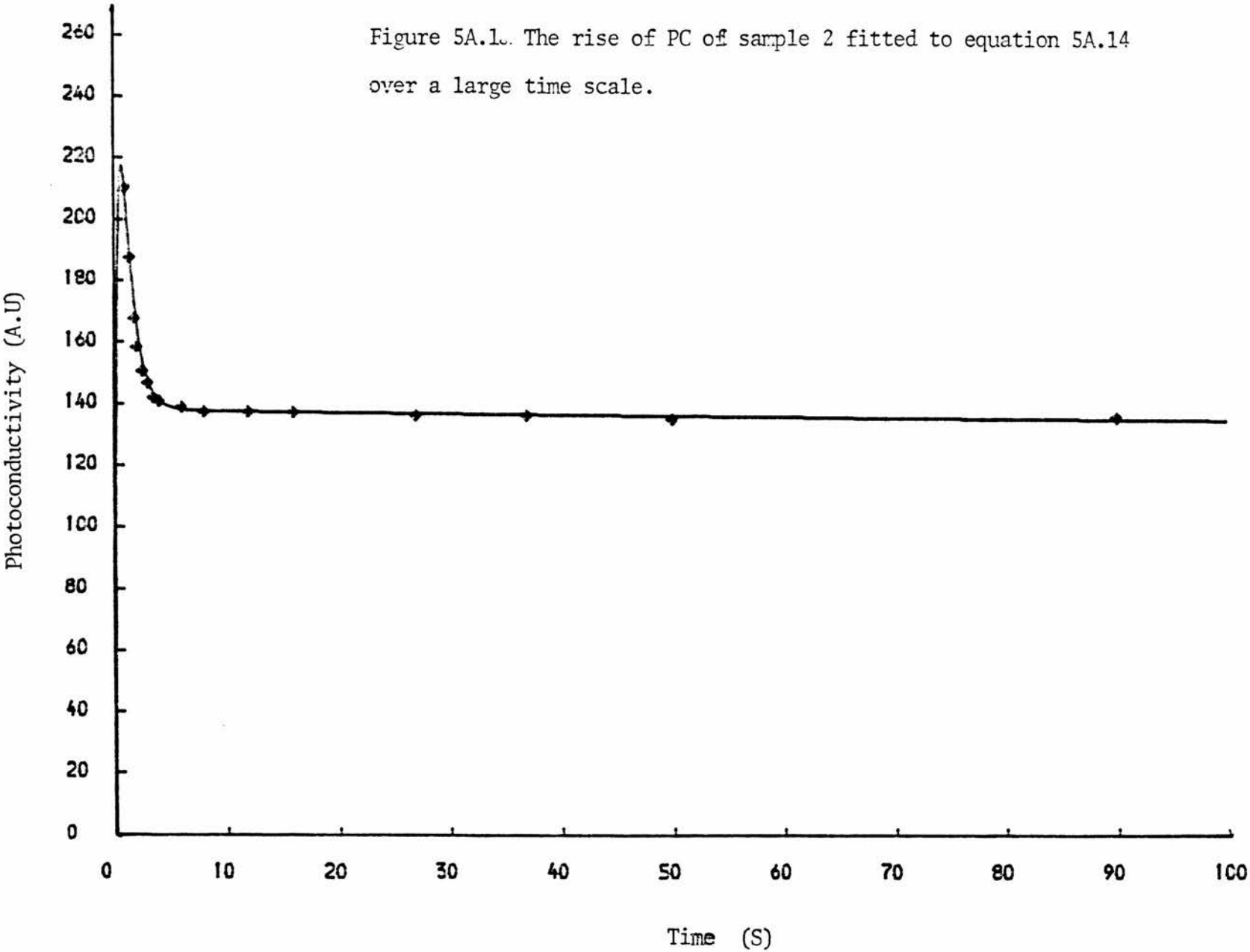

Figure 5A.1. The rise of PC of sample 2 fitted to equation 5A.14 over a large time scale.

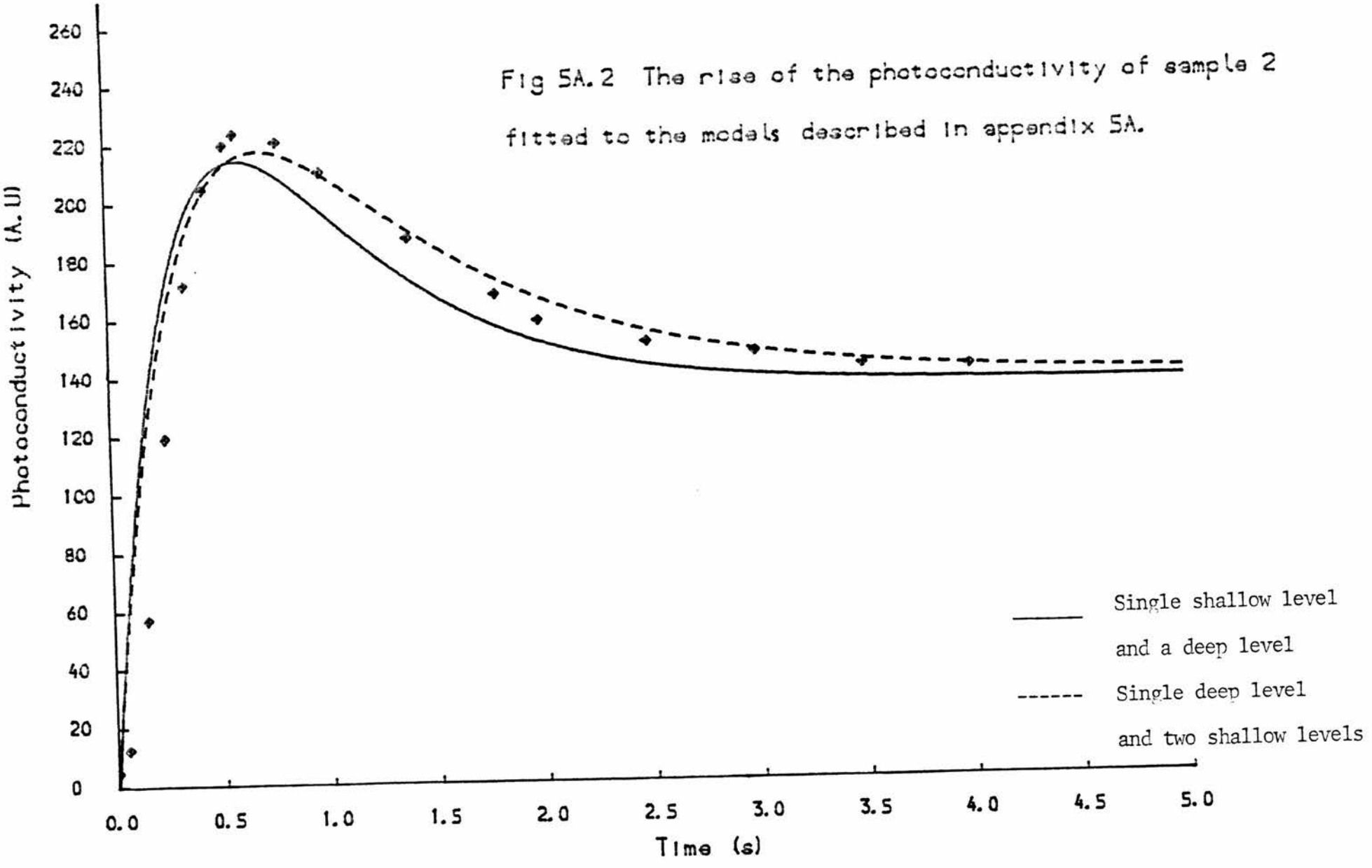

Fig 5A.2 The rise of the photoconductivity of sample 2 fitted to the models described in appendix 5A.

Figure 5A.3 The form of equation 5A.14 when we have a single deep level and two shallow levels which are located at approximately the same energy below the conduction band.

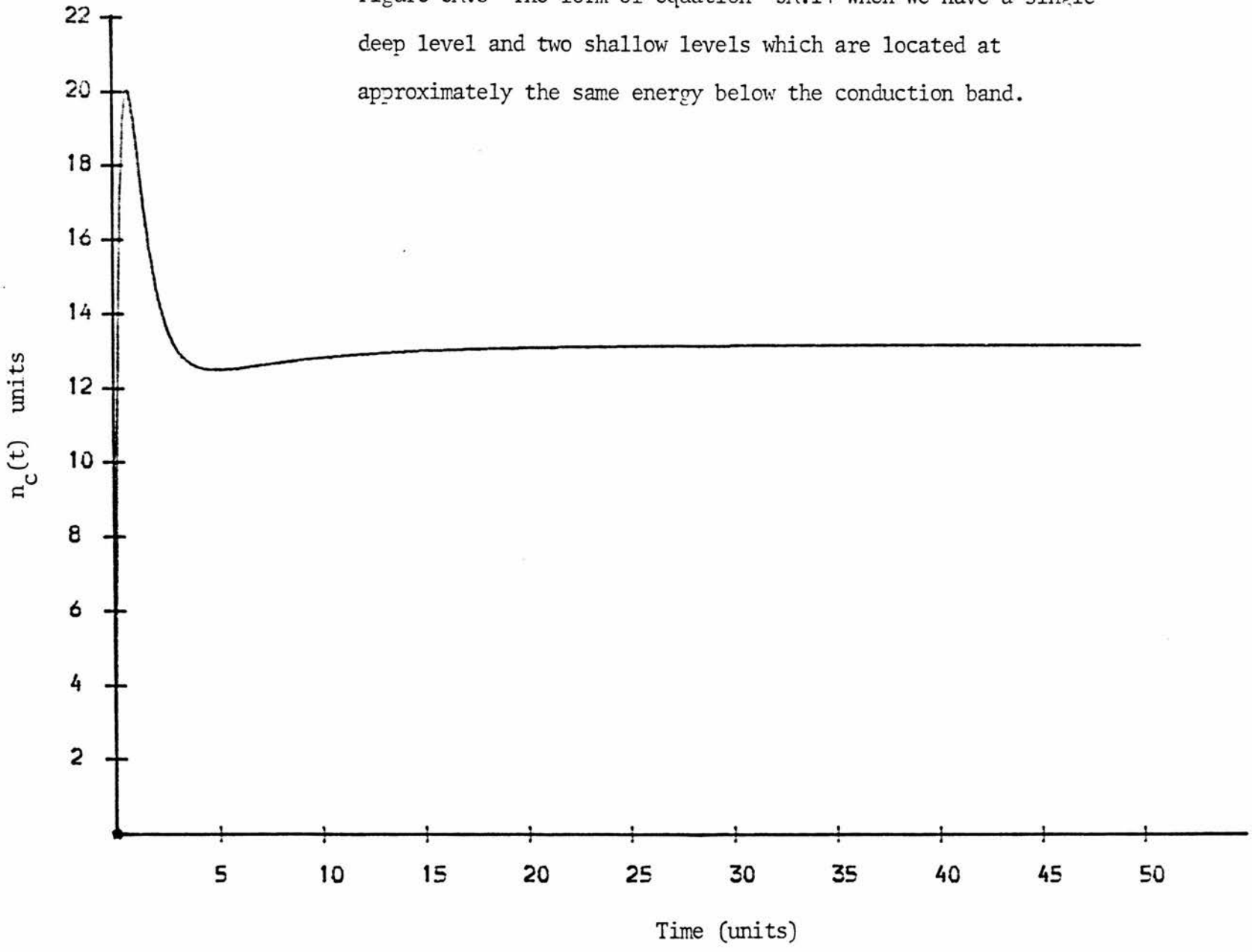

6 Some theoretical models of ac conductivity

There are many models that attempt to describe the ac conductivity seen in a large variety of materials.A large majority of these models are applicable to amorphous and glassy materials.Very few of these models will be applicable to semiconductors that are not heavily doped.It is the object of this chapter to give an over-view of the models that have been used to describe the ac conductivity theoretically.

This chapter is presented in four sections.Section 1 deals with the defects that contribute towards the ac conductivity in the chalcogenide glasses, amorphous materials and semiconductors.In section 2 we give an overview of the models that have been frequently quoted in the literature connected with hopping conduction in semiconductors.The criteria for selecting a sample to observe hopping conduction in a semiconductor will be presented in section 3.A conclusion is presented in section 4. We complete this chapter on the limitations and use of the Kramers-Kronig relationship in appendix 6A.

6.1 Defects that control the ac conductivity

Glasses.such as the chalcogenides (for example As_2S_3) have an important defect known as the 'lone-pair'(see for example Connell and Street[4]). This defect is produced by dangling bonds that together with strong electron-phonon interaction produce a situation whereby one of the dangling bonds can bind two electrons while another

dangling bond is empty of electrons.The two bonds with their electron occupancy are usually labelled D^- and D^+ respectively.The D^- and D^+ are thought to arise from the same defect which is neutral and is denoted by D^o.

In tetrahedrally bonded amorphous semiconductors,the D^+ and the D^- pair arises in a manner similar to the glassy materials.The mutual repulsion between the electrons in the doubly occupied dangling bond is opposed by some form of structural relaxation due to strong electron-phonon interaction (Connell and Street).Other forms of defects that are bound together by Coulombic interaction may occur,for example,between an impurity and a defect.

The D^+ and D^- type of defects can occur in semiconductors but we expect their concentration to be very small compared with that in glassy and amorphous materials.In heavily doped semiconductors the electron wavefunction associated with the electron at the site of a dopant starts to overlap with the site of a neighbouring site of a dopant so that an impurity band can form.Clearly,in such a case it is feasible to consider electrons,for example,tunnelling between the potential wells associated with the impurity sites.The potential wells are separated by a potential barrier.A potential barrier can also be formed by a defect and an impurity which behave as a pair.As the density of the doping decreases.then the number of such pairs will decrease (although they will still occur in small numbers).It therefore follows that the contribution of such defects to the total ac conductivity will decrease in nominally un-doped or lightly doped semiconductors (NULDS).Real semiconductors will always have residual impurities present in small concentrations.Hopping in semiconductors

which have not been heavily doped should be analysed,as it will become apparent later,in terms of an electron hopping over all the impurity sites.

6.2 An overview of the models to describe the ac conductivity

The ac conductivity is related to the dielectric susceptibility via the relationship:

$$\sigma_{ac} = \omega(\chi'' + i\chi') = \sigma'_{ac} + i\sigma''_{ac}$$

where σ'_{ac} and σ''_{ac} are the real and imaginary parts of the ac conductivity respectively.Most of the theories deal with the real part of the ac conductivity,the imaginary part assumed to be related to the real part through the Kramers-Kronig relationship.The use of the Kramers-Kronig relationship will be discussed in appendix 6A.

One of the earliest attempts to describe the form of the ac conductivity was that by Pollak and Geballe[20].They wrote down the rate equations for the occupancy of electrons communicating (for example by quantum mechanical tunnelling with and without phonon assistance) between two impurity sites and summing over all the impurity sites.The resulting equations proved to be intractable.A method of rendering them tractable is to assume that the hopping is confined between pairs of impurity sites.Where the main contribution to the ac conductivity comes from pairs of impurity sites,one usually refers to it as a "pair approximation" (which has been popularised by

Mott and Davis[17]).Within the pair approximation,we can distinguish three possible forms of hopping conduction:correlated barrier hopping (CBH), correlated and non-correlated hopping.In the CBH model,a charge carrier jumps over the potential barrier separating the potential wells associated with the pair defect.The correlated barrier term comes from the fact that the height of the potential barrier is related to the separation of the two defects.An example of CBH is shown in figure 6.1 Correlation effects can be included by considering the effect of the exclusion factor in the rate equations describing the charge transfer from one defect to the other.Uncorrelated hopping can be confined to pairs of defects where the exclusion factor is unimportant. Calculation of σ_{ac} within the pair approximation is straightforward. One centre (pair) will have a mode of χ'' of the Debye type,the mode being characterised by one relaxation time τ.One then formulates the problem according to whether the electron hops over the barrier or whether it tunnels to the other potential minimum with or without phonon assistance.A general expression for the ac conductivity within the pair approximation is of the form (Pollak[20]),

$$N\int_{\tau_1}^{\tau_2} \alpha(\tau,\xi)(1+\omega^2\tau^2)^{-1}\omega^2\tau^2 p(\tau)d\tau \qquad 6.2$$

A distribution of some physical quantity is made so that $p(\tau)$(the probability distribution of the relaxation times) has some explicit form.For hopping over barrier $p(\tau)$ has the form (Elliot[7])

$$d_\tau p(\tau) = (4\ kT\varepsilon_o/4e^2)[4e^2/(\varepsilon_o\{W_m - \ln(\tau/\tau_o)\})]d\tau/\tau \qquad 6.2$$

where W_m is the ionisation energy of the hopping entity.Many theories that model the ac conductivity make use of the expression for the polarizability $\alpha(\tau,\xi)$ which was derived by Pollak and Geballe.The various models which have used the pair approximation are collected in

the review by Long[11]. In table 6.1 we list some of the models which use the pair approximation and others that may have relevance to the semiconductor field. It is clear that a model of the ac conductivity based on the pair approximation will be valid if there are defects in the material that can be considered as pairs.In the chalcogenide glasses and in amorphous semiconductors the pair defect will be connected with the D^+ and the D^-.Furthermore for the chalcogenide glasses,in connection with bi-polaron hopping,Elliot has shown that the temperature dependence of the exponent in the expression for the ac conductivity ($\sigma_{ac} \propto f^s$) varies with temperature as $s = 1 - 6kT/W_m$ where W_m is the activation energy of the bipolaron.In semiconductors.the CBH model may be applicable to heavily doped semiconductors.In such semiconductors,ionised and neutral donor can exist in close proximity to each other so that they are bound together by some mutual interaction.An electron hops from the neutral donor (creating an ionised donor) to the ionised donor.

As the concentration of the dopants decreases.then the probability of such pairs existing in the semiconductor decreases.In the work of Pollak and Geballe for example,the donor concentration of sample 9.for which the ac conductivity data is presented,may not be sufficient to form pair defects.The pair approximation has been extended by Butcher and Summerfield[2].Butcher and later Summerfield extended the work of Miller and Abrahams[15] to the case when an alternating field is applied to the sample.They showed that for the ac case capacitors and voltage generators must be included in the resistor network of the sample which was worked out by Miller and Abrahams for the dc case.An approximation introduced by these authors was the 'extended pair approximation'.ie,the pair approximation

introduced by Pollak and Geballe is valid in the general case even when the centres concerned are separated by large distances. Altnough this approach would be valid to NULDS. the theory developed by tnese authors cannot be used to give an analytical expression for the ac conductivity (without invoking the pair approximation); numerical studies carried out by these authors revealed. however, that the theory is in reasonable agreement with experimental data for Ge as quoted in their papers.

Another approach to describe the form of the ac conductivity in NULDS would to be abandon the pair approximation (for all the simplicity it offers) and to concentrate on the stochastic process of hopping conduction. This line of reasoning was taken up by Scher and Lax[22] (making full use of the mathematical formulation of such a process developed by Montroll and Weiss[16]). Scher and Lax used the continuous time formalism of a random walk (CTRW) by a walker on a lattice of impurity lattice sites. Specifically they found a general expression for the complex diffusion coefficient which can be written down in terms of a mathematical function ψ that describes the nature of the random walk. There have been other forms of ψ (ref 25) other than the one derived by Scher and Lax. The main criticism of the CTRW model is that the dc limiting value of the ac conductivity is not in reasonable agreement with experimental data (Long), altnough the agreement with the ac conductivity is good (the CTRW model has been further refined by Odagaki and Lax[18])

A sensitive test to observe which theory may be applicable to one set of experimental data is to plot the temperature dependence of s.This simple test will be valuable when it has not been possible to fully characterize the sample(as for example in semi-insulating samples where it is difficult to carry out Hall effect measurements to determine the carrier concentrations and mobility).If,for example.one looks at the work of Mathur et al[12],an inspection of their data on the ac conductivity of ZnSe heavily doped with Indium revealed that s had a temperature dependence.The temperature dependence of s was not observed by Mathur et al.In figure 6.2 we show the temperature dependence of s for the data of Pollak and Geballe (crystalline Si),Mathur et al(crystalline ZnSe) and Jonscher and Pickup[9] (crystalline GaAs:Cr).In all three cases shown in figure 6.2 the exponent s decreases with increasing temperature .For ZnSe the form of the decrease of s can be expressed by the linear equation

$$s = (0.94 \pm 0.06) - (2.2 \pm 0.2)\times 10^{-3}T$$

In table 6.1 it is indicated that such a temperature dependence of s can exist where an electron jumps over a potential barrier rather than quantum mechanical tunnelling between the two potential wells.The material studied by Mathur et al was heavily doped with Indium.In light of what was said in section 6.1.it would appear that the model of Elliot is applicable to the data of Mathur et al. Knowing this,we calculate W_m to be 0.24eV (which is close to an "activation energy" reported by these authors).The data for Si (taken from the paper by Pollak and Geballe) also shows a s that decreases with temperature although in this case s does not tend to 1 as the temperature tends to zero.It is worthwhile remarking here that any theory that models the ac conductivity and uses the data of Pollak and Geballe for comparison

must explicitly show the temperature dependence of s as seen in figure 6.2.Further note in figure 6.2 that s obtained from the data of Jonscher and Pickup also shows the decrease of s with increasing temperature in a linear fashion (although at high temperatures. s increases again for some unknown reason).It is unclear whether the donor concentration of sample 9 of Pollak and Geballe is sufficient to produce pairs of defects.No concentration of the chromium impurity in GaAs:Cr was reported by Jonscher and Pickup.Thus the linear decrease of s with temperature as seen in figure 6.2 must be taken as an empirical fact which is sometimes observed in non heavily doped semiconductors.The temperature dependence of s as shown in figure 6.2 has not been observed before.

In polycrystalline materials (for example ZnS and ZnSe) the crystal is made up of grains which have interface states.A study of dc hopping conduction in polycrystalline Si,InSb,and CdTe by Sharma at al[23] concluded that the variable range hopping conduction seen in their samples was associated with the amorphous nature of the interface regions between the grains.This approach to describe the variable range hopping in these materials is unlikely as this would imply that the hopping conduction was a two dimensional effect . The dc conductivity observed by these authors obeyed σ_{dc} exp-$(T_o/T)^{1/4}$ rather than σ_{dc} exp-$(T_o/T)^{1/3}$ .thus the model put forward by these authors for the physical origin of the variable range hopping can be discounted.Since we know that polycrystalline materials are granular,a better approach to the origin of the variable range hopping in these materials would to be to acknowledge the fact that the total conductivity will be controlled by the path taken by an electron such that it will experience the least amount of resistance.ie. the dc

conductivity will be adequately described by a percolation theory (see for example Ambegaokar et al [1]).

6.3 Selecting a sample to observe hopping conduction

The early studies on hopping conduction were done at liquid helium temperatures (for example Pollak and Geballe observed hopping in Si at LHT).In all such materials,the material used had shallow donors (for n-type materials) that had an ionisation energy much less than kT at room temperatures.Thus to observe hopping conduction the electrons had to be frozen out onto the donors.Hopping conduction then observed can then be thought to be pictorially described by figure 4.21 (with the optical generation rate put to zero as there are already electrons at the shallow donors).If the shallowest donor is more then a few kT away from the conduction band edge (at room temperatures,this would mean that the donor ionisation energy is more than 27meV away from the conduction band) then it will be possible to observe hopping conduction at room temperatures.The above argument can equally be applied to the case when hopping is thought to be due to holes.Thus to observe hopping conduction at room temperatures,the ionisation energy of the shallowest impurity must be greater than a few kT away from the band edge.However,to observe this form of hopping conduction, electrons,for example,have to be photoexcited so that they will occupy some donor states.This simple principle was used to select the materials to observe hopping conduction in semi insulating ZnSe and ZnS.

6.4 Conclusions

An overview of the models used to describe the ac hopping conduction in a large variety of materials has been presented.For the chalcogenide glasses and the amorphous semiconductors,a "correlated barrier hopping" model of an electron jumping from one potential well to the other adequately describes the ac hopping seen in these materials.This type of model may also describe the ac hopping seen in heavily doped semiconductors.A test of this showed that the hopping conduction seen in heavily doped ZnSe was described by the model of Elliot.However for NULDS the pair approximation breaks down as the number of pairs of defects occurring in the material will be small.For NULDS,the stochastic nature of hopping conductivity (the CTRW model of Scher and Lax) gives perhaps the best insight of hopping conductions.A further conclusion from the literature survey is that the dc hopping conduction in polycrystalline materials is not connected with the possible amorphous nature of the interface states between the grains of the polycrystalline material.The dc conduction in these materials is most likely to be connected with the fact that the grains that make the crystal will have different conductivities and the path that an electron,for example,will take in traversing the material will be such that it will encounter the least resistance.One further surprising result from the above literature survey is that the dispersion parameter,s,is sometimes temperature dependent.The form of this temperature dependence is that s decreases linearly with increasing temperature.

Appendix 6A

Use of the Kramers-Kronig relationship to interpret the ac conductivity

The text book Kramers-Kronig relationship (KKR) is based on the following assumptions (Landau and Lifshitz[10])

(i) The complex dielectric permitivity $\varepsilon(\omega)$ is analytical throughout the entire frequency range. For the sake of mathematical convenience the frequency is taken to be a complex variable,

(ii) $\varepsilon(-\omega^*) = \varepsilon^*(\omega)$

(iii) For real ω im ε changes sign at $\omega = 0+i0$,

(iv) For a real dielectric, $\mathrm{Re}(\varepsilon(\omega)) \to E$ as $\omega \to \infty$, where E is some finite value of the real part of the complex dielectric permitivity. For the imaginary part $\mathrm{Im}(\varepsilon(\omega)) \to 0$ for a dielectric while for metals $\mathrm{Im}(\varepsilon(\omega)) - \frac{\sigma_{dc}}{\omega} \to 0$ as $\omega \to \infty$.

Making use of these assumptions it is straightforward to show (Landau and Lifshitz) that the real and the imaginary parts of the dielectric permitivity are related by the equations:

$$\varepsilon' - E = \pi^{-1} P \int (\varepsilon''(x)/(x - \omega))dx \qquad 6.1a$$

$$\varepsilon'' = \pi^{-1} P \int ((\varepsilon' - E)/(x - \omega))dx \qquad 6.1b$$

where the P indicates that the principal value of the integral must be taken, that is, the value of the integral

$$\lim_{\substack{b\to\infty \\ \rho\to 0}} \int_{-b+\rho}^{b-\rho} f(x)dx$$

exists as the two values (ρ and b) tend to their respective values. Jonscher (1983)[8] has argued that hopping conduction is best described by the relationship given by equation 4.12 (ie $[\varepsilon' - \varepsilon'(\omega)]/\varepsilon'' = \tan(s\pi/2)$). It will be shown here that the relationship given in equation 4.12 only exists as an accident as $\omega \to 0$. If ε'' varies with frequency as f^{-n} (where n is less than unity) and this is substituted into equation 6.1a then ε'-E varies with frequency as f^{-n} if one ignores the fact that the integral has no finite value. It is then observed that the relationship given in equation 4.12 is found. Clearly, the relationship given by equation 4.12 is not a consequence of the KKR and the fact that such relationships are sometimes seen experimentally must be taken as an empirical fact and not as a consequence of the KKR as mooted by Jonscher.

Equations 6.1 are a consequence of the Cauchy principal value theorem (see for example Churchill and Brown[3]). Making use of this theorem we note that there will be a pole at the origin if the dielectric permitivity varies with frequency as a power law of the type f^{-n} where n is positive. Thus we must add a residue of the pole to the right hand side of equation 6.1a (which must be the static value of the dielectric permitivity). For negative frequency the same frequency dependence

of the dielectric permitivity can be used.

We further note that the real part of the ac conductivity,which can be empirically expressed by the relationship $\sigma_{ac} \propto f^{s}$.where s is positive and less than unity,also fails to be analytic at the origin. This follows from the fact that the derivative of σ_{ac} will vary with frequency as f^{s-1}.Since s - 1 is negative the result follows. Thus a concluding remark would be that although the KKR is an important one.its limitations and use must be understood before it is applied.

References

(1) V Ambegaokar,B I Halperin and J S Langer J Phys B4,2612(1974)

(2) P N Butcher Phil Mag B42,799(1980)

(see also: P N Butcher and S Summerfield J Phys C14,L1099(1901)

S Summerfield and P N Butcher J Phys C16,2851(1983)

S Summerfield Phil Mag B52.9(1985))

(3) R Churchill and J W Brown "Complex variables and applications" 4th edition,McGraw-Hill,Tokyo,1984

(4) G A N Connell and R A Street "Handbook of Semiconductors" vol 3,p691,N Holland Publ Co. Netherlands (1980)

(5) L A Dissado and R M Hill Nature 279,685(1979)

(6) J C Dyre Phys Lett 108A,457(1985)

(7) S R Elliot Phil Mag 36.1291(1977)

(8) A K Jonscher "Dielectric relaxation in solids" Chelsea dielectrics press,London 1983

(9) A K Jonscher and C Pickup J Phys C18.L343(1985)

(10) L D Landau and E M Lifshitz "Electrodynamics of continuous media" Pergamon press,Oxford 1960

(11) A R Long Adv Phys 31.553(1980)

(12) P C Mathur,B R Sethi,P L Talwar,O P sharma and R P Sharma Phys Lett 73A.234(1979)

(13) J L Merz,K Nassau and J W Shiever Phys Rev B8.1444(1973)

(14) J L Merz Phys Rev B9,4593(1974)

(15) A Miller and E Abrahams Phys Rev 120,745(1960

(16) E Montroll and E W Weiss J Math Phys 6.167(1965)

(17) N F Mott an E A Davis "Electronic processes in non crystalline solids" Clarendon press,Oxford 1979

(18) T Odagaki and M Lax Phys Rev B24,5284(1981)

(19) G E Pike Phys Rev B6,1572(1972)

(20) M Pollak Phil Mag 23,519 (1971)

(21) M Pollak and T H Geballe Phys Rev 122.1742(1961)

(22) H Scher and M Lax Phys Rev B7,4491(1973) and ibid p4502

(23) R P Sharma,A K Shukla,A K Kapoor,R Shrivastava and P C Mathur J Appl Phys 57,2026(1985)

(24) R Stumpe Phys Stat Sol(a) 88.315(1985)

(25) Proceedings of the 7th international conference on amorphous and liquid semiconductors W E Spear (Ed),Centre for industrial and liason.University of Edinburgh,Edinburgh 1977

Table 6.1 A brief summary of hopping conduction models

Author(s)	Ref	Approach	material to which theory applied	general formula
Butcher and Summerfield[1]	2	Modified the Abrahams-Miller theory for the ac hopping case	n-Si Ge	for the pair approximation an analytical formula is $\pi\sigma(\infty)\omega\tau_o/48\{\ln^{-4}(\omega\tau_o)\}+(2i/5)\{\ln^5(\omega\tau_o)^{-1}\}$
Dissado and Hill[2]	5	2nd order interaction between the hopping entity and the medium it is in	"various"	$\sim \omega^s$
Dyre[3]	6	Modified CTRW method	n-Si,SO, a-Si,a-Ge and others	$\sigma_{dc}\cdot\tan^{-1}(\omega\tau)/(\ln^2(1+(\omega\tau)^2)^{1/2}+\tan^{-1}(\omega\tau)^2$
Elliot[4]	7	bipolaron hopping OVER a potential barrier	Chalcogenide glasses	Real part: $(\pi N^2 k/24\epsilon_o)[8e^2/(kW_m)]^6\omega^s$
Mott plus collaborators[5]	17	phonon assisted quantum tunnelling of electrons at the Fermi level	mainly amorphous semiconductors	$A(e^2/\alpha^5)\{[n(E_F]^2 kT \ln^4(\nu_{ph}/\omega)$
Odagaki and Lax[6]	18	CTRW + coherent medium approximation	Data of Pollak and Geballe	$(n^2e^2/kT)A\omega^s$
Pike[7]	19	Correlated barrier hopping	ScO_2	$\frac{3\epsilon(4a/R_s)^3(4a/R_p)^3\omega^{1-\beta}(1-(8a/R_s)^3(\omega^2\tau_1^{\beta/2}(4\cos^2(\beta\pi/2)-3))^{-1})}{\cosh^2(\Delta/2kT)\quad\tau_1^{\beta}\cos(\beta\pi/2)}$
Pollak[8] and Geballe	20	Original pair approximation	n Si (9)	$(4\pi/12)N_AN_D(e^2/kT)[14.8-0.5\ln\omega]^4(a^5)/2)\times$ $\omega(\pi/2-\text{atan}[5.5\times10^{-3}[14.8-0.5\ln\omega]^{3/2}\tanh(\Delta E/2kT)])$
Scher and Lax[9]	22	Stochastic nature of hopping continuous time random walk	data of Pollak and Geballe	$\sim\omega^s$
Stumpe[10]	24	Sample has regions characterised by different activation energies; decompose sample to R and C network	amorphous	none

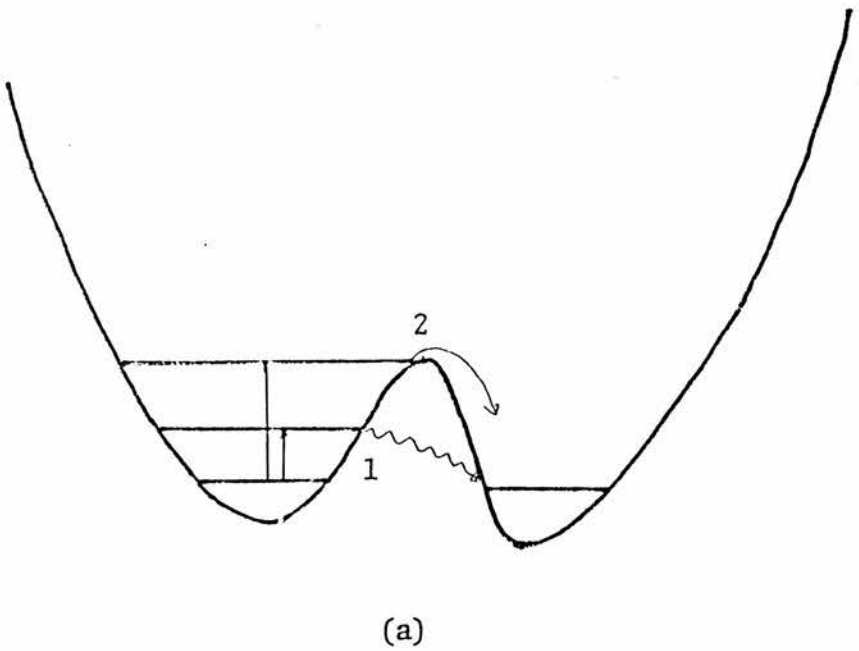

(a)

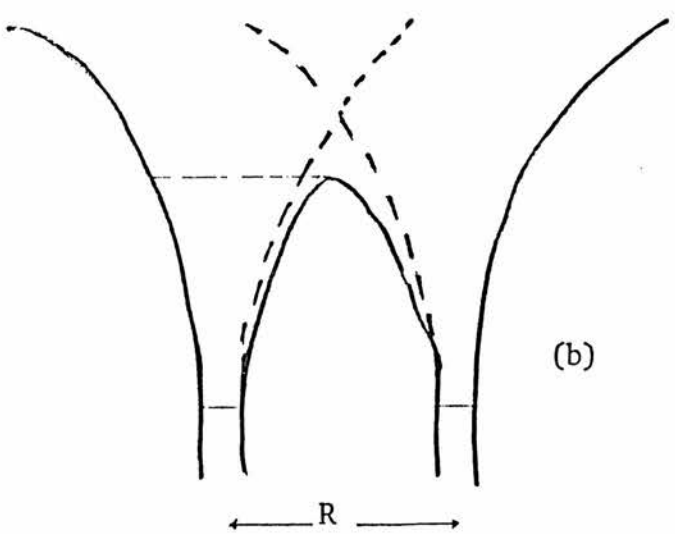

(b)

Fig. 6.1 (a)Schematic diagram of a double potential well (DPW).Shown on the figure are hopping due to phonon assisted quantum mechanical tunnelling (1) and that due to a transition surmounting the barrier (2),(b) a physical DPW produced by two impurity centres that have a Coulombic type of potential.

Fig. 6.2 The temperature dependence of s for three different systems.Shown in the inset is the data for Si on an enlarged scale.

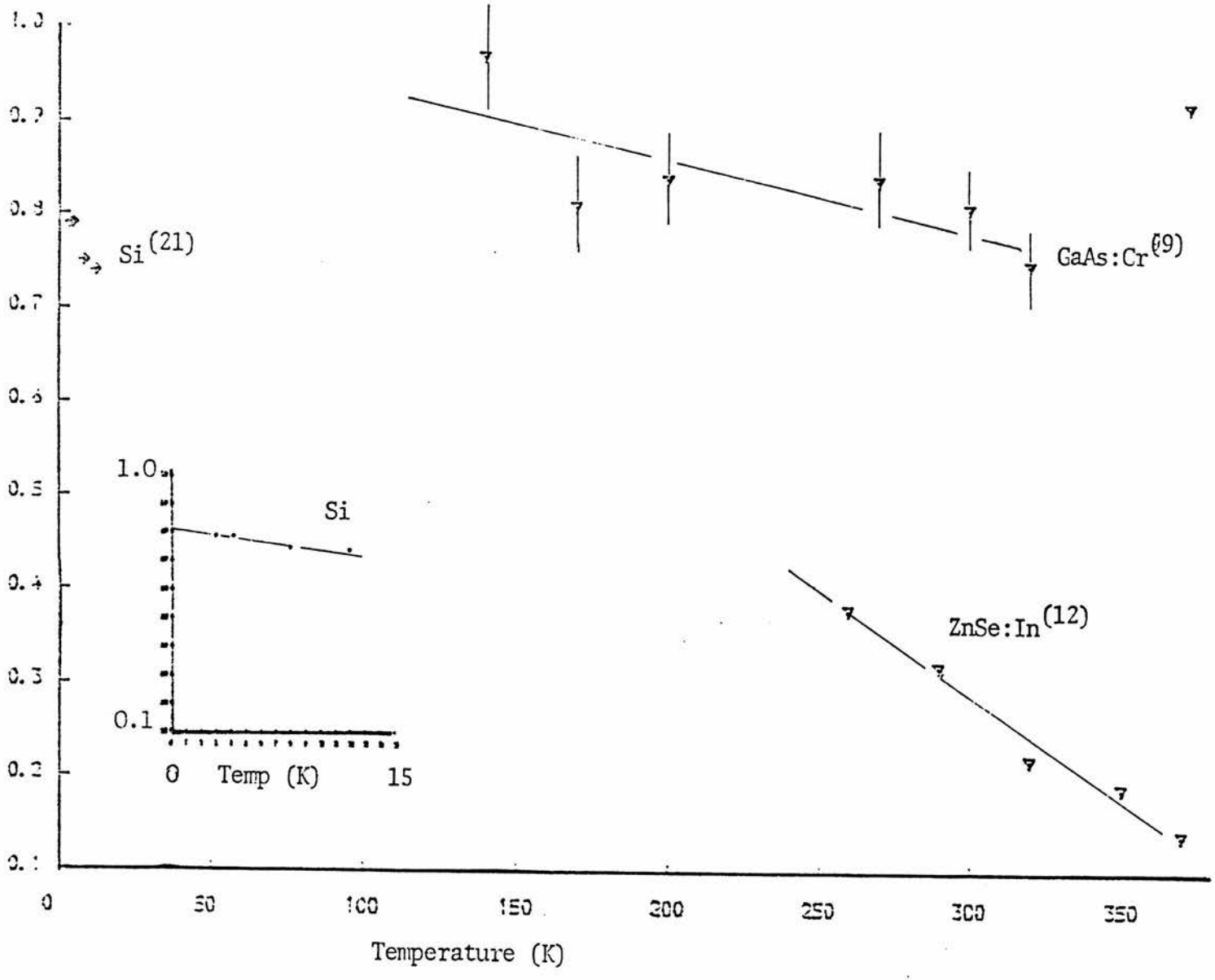

7 Conclusions

The work presented in chapters two through to six was the characterization of impurities in wide band gap semiconductors used in the optoelectronic industry and their influence on the ac electrical properties. Two experimental methods, photoconductivity (PCON) and photocapacitance (PCAP), were used to characterize the impurities. PCAP was used to characterise the Ni(d^9) impurity in GaP, while PCON was used to characterize the possible copper related complex in dc thin film electroluminescent devices (TFED) and the M centre in semi-insulating ZnSe. The Ni(d^9) centre in GaP was studied by the double light source steady-state (DLSS) photocapacitance technique. For this method, an appropriately filtered light is first shone on the diode to establish the initial electron occupancy of the nickel centre. Monochromatic light is then shone on the diode to study, for example, the optical cross section for electrons. The DLSS technique was found to be convenient as the steady-state change in the photocapacitance was shown to to be directly proportional to the optical cross section for electrons. Substitutional and isolated Ni(d^9) has two energy levels, $^2T_2$ and ^2E which are separated by a zero phonon energy of 0.664eV (Kaufmann et al (1979)). The band seen in the DLSS spectrum was shown to be consistent with the Ni in the d^9 configuration. A large onset in the band occurred at 0.7eV, with additional structure at 0.72eV and 0.76 eV. All three features are associated with a 31meV phonon in that the structure represents phonon replicas. The structure in the band has not been seen previously in photocapacitance experiments. Measuring the optical cross section for electrons over a large photon energy range revealed a photoionisation

process and a previously unseen dip at 1.24eV.The dip was shown to be consistent with the transition d^8 -> d^9 +h involving a photothermal process.The photoionisation process,which corresponds to the transition d^9 ->d^8 + e^- ,had a threshold of(0.88 $\pm$ 0.01)eV below the conduction band at 0^oC.A controversy in the literature reported by Szawelska et al(1982) that there was no correlation between the absorption spectrum of GaP:Ni and the photocapacitance spectrum of GaP:Ni was resolved by proposing that there are two centres:one that dominates the photocapacitance experiments (the isolated nickel centre) and a nickel related centre that dominates the absorption experiments.

The capacitance bridge used to characterise the nickel centre in GaP was also used to characterise deep centres in ZnS:Mn TFEDs.A sample connected to the the bridge is represented as an equivalent circuit consisting of a series combination of a capacitor and a resistor.For the GaP:Ni Schottky diode studied this equivalent circuit is correct.An equivalent circuit of the TFED consisting of a parallel combination of a capacitor and a resistor was found to be more reasonable.Hence the capacitance measured by the bridge contains terms from the true resistance of the device.The observed change in capacitance when light was shone on the device reflects a resistance change of the TFED rather than a photocapacitance change.We further note that the measured resistivity of the TFED was much greater than 10^6 Ωcm and thus we do not expect a depletion region to exist in the ZnS:Mn adjacent to the metal electrode.Two devices were studied:the hydrogenated TFED and the non-hydrogenated TFED (HTFED and NHTFED respectively).The active ZnS:Mn in both the non-hydrogenated and the hydrogenated devices was shown to have the same deep centre (possibly

a copper related complex) . The centre had a photoionisation threshold of (2.49 $\pm$0.25)eV below the conduction band. A slight difference was observed in the spectrum of the steady-state photoconductivity divided by the incident photon flux ($\Delta V/\phi$) for the NHTFED and the HTFED;the HTFED showed a quenching in the spectrum of ($\Delta V/\phi$) for photon energies larger than 3.1eV.The quenching is associated with another deep centre in the band gap that has a concentration smaller than the main copper related complex centre.It is rather surprising that the effect of hydrogenation has been to introduce extra levels in the band gap. One would have hoped,in analogy with a-Si:H,that the effect of hydrogenation would have resulted in the reduction of such impurity levels in the band gap.

A material that is similar to ZnS is ZnSe.Photoconductivity was used to characterise two samples (1 and 2) cut from an ingot of ZnSe. The rise of photoconductivity (PCON) following shining light on the samples was complicated.For sample 1,PCON went through a minimum before increasing to a steady-state value.Sample 2 showed three features in the rise of PCON.A shoulder in the initial rise,followed by a rise to reach a maximum and then decreasing to a steady-state value after going through a small minimum.The main features of the rise of PCON for both samples could be understood in terms of a model where the semiconductor has at least two centres that produce a deep level and at least two shallow levels.The rise of the experimental PCON,within the framework of the model,was understood as follows.Electrons excited optically from the deep centre into the conduction band will be captured by the shallow centre(s) and thermally emitted at a rate that depends,amongst other factors, on the location of the shallow levels below the conduction band.If the rate

of thermal emission of electrons from the shallow centres is less than the optical rate then the resulting (modelled) PCON showed strong similarity to the experimental PCON.Modelling of the rise of PCON indicated that the shallow centres producing the shallow levels were relatively deeper in sample 2 than in sample 1.

The spectrum of the steady-state PCON divided by the incident photon flux ($\Delta V/\phi$) was similar for samples 1 and 2 with a small difference that sample 2 showed a quenching of PCON for incident photon energies approaching the band gap of ZnSe.Comparison of the spectrum of ($\Delta V/\phi$) for sample 1 with the optical cross section of electrons (σ_n^o) for the M centre as reported by Grimmeiss et al (1976) showed that the M centre was present in both samples.However,PCON experiments carried out by us showed that the optical cross section for electrons could be obtained from the inverse rise time constant of post-minimum PCON for sample 1 and from the square of the steady-state PCON for sample 2. For sample 2,the relationship that the square of the steady-state photoconductivity was proportional to the optical cross section for electrons was obtained from the above mentioned model.It was shown that if the shallow centres are of sufficiently small concentration,then the capture of the photoexcited electrons leads to the a situation whereby the shallow centres are completly occupied by electrons.The resulting photoconductivity is then governed by the rate of thermal emission of electrons from the shallow centres.Photoconductivity experiments presented in chapter 5 gave a spectrum of σ_n^o over a larger photon energy range than that reported by Grimmeiss et al. The photoionisation threshold for the centre observed in PCON experiments was approximately 2.01eV below the conduction band which agrees well with the location of the M centre in

the band gap as found by Grimmeiss et al.One surprising result found from the PCON experiments was that when monochromatic light had been blocked off,the photocurrent decayed approximately as a power law once the dark current had been subtracted.A qualitative understanding of this behaviour was that of photoexcited electrons captured and thermally emitted into the conduction band by progressively deeper shallow centres until the photoexcited electron recombines with a deep centre.No detailed calculations were done to test this explanation as the form of the energy distribution of the shallow levels below the conduction band was not known.

ZnS:Mn in the NHTFED and the ZnSe:Mn samples were further studied to determine the nature of the ac conduction.To do this a capacitance bridge and a frequency response analyser were used.The capacitance bridge and the frequency response analyser represent the material to be studied as an equivalent circuit consisting of a series combination of a capacitor (C_s) and a resistor (R_s) whose values are measured over a large frequency range.The dispersion observed in R_s and C_s can then be decomposed into the true equivalent circuit of the material.For both ZnS:Mn and ZnSe:Mn,it was found that when they were in the dark the dispersion in R_s and C_s could be understood in terms of an impedance network.A physical equivalent circuit of the NHTFED,when placed in the dark,was one which represented the ZnS:Mn as a leaky dielectric with the effect of contacts to the TFED taken into account.Thus the equivalent circuit of the NHTFED was that of a parallel combination of a capacitor (C) and a resistor (R_p) in series with a resistor representing the resistance of the contacts to the NHTFED.For ZnSe:Mn no resistive part of the equivalent series circuit of the samples could be measured by a capacitance bridge because the

dissipation factor was too small.However,when the samples were in the dark,no dispersion in the equivalent series capacitance was found.A simple experiment showed that the measured capacitance of ZnSe samples was a bulk effect as the value of the static dielectric permittivity was within 10% of the accepted value.An impedance picture of the ZnSe samples in the dark seems most likely.

When the NHTFED was exposed to white light dispersion in R_p and C was observed.The form of this dispersion was $R_p \propto f^{-p}$ and $C - C(\infty)\ f^{-q}$.Here $C(\infty)$,the value of the capacitance at high frequencies, was taken to be the dark capacitance and p and q are positive and less than one.Both R_p and $C - C(\infty)$ varied with frequency as power laws with three values of the exponents in the frequency range from 1Hz to 100kHz.For frequencies less than 10Hz both R_p and $C - C(\infty)$ varied with frequency as $f^{-0.26}$.Similarly for frequencies larger than 3kHz they varied with frequency as $f^{-0.80}$ within experimental errors.The fact that both R_p and $C - C(\infty)$ should vary with frequency in a similar way was a rather unexpected result.Between 10Hz and 3kHZ $R_p \propto f^{-0.63}$ and $C - C(\infty) \propto f^{-0.36}$. The two exponents are apparently related through the Kramers-Kronig relationship.We use the word "apparent" because it was shown in appendix 6A that the Kramers-Kronig relationship is not valid for functions which (increase) with frequency as fractional powers. The reason is that such functions fail to be analytical throughout the entire frequency range.The dispersion observed in R_p and C when the NHTFED had light shining on it was extended to the ZnSe samples.When light was shone on the the ZnSe samples it was found that C_s decreased with increasing frequency as f^{-n} where n was less than unity.Investigations revealed that n was temperature,photon energy and photon flux dependent. The

temperature dependence of n could be described by an empirical relation of the form n =aT - b.Here a and b are constants (different for samples 1 and 2) and T is the absolute temperature.A plot of n with photon energy showed that n decreased from a value of 0.52 when light of photon energy 2.1eV was shone on sample 2 to a value 0.33 for incident photon energies tending towards the band gap of ZnSe.

The dispersion observed in R_p and $C - C(\infty)$ for ZnS:Mn and in C_s for the ZnSe samples is ultimately connected with the photoconductive process of capture and thermal release of carriers from a set of traps (assumed to be donors for this discussion).A photoexcited electron captured by a trap will spend time at the trap before it either tunnels to another trap site with or without phonon assistance or it is thermally excited into the conduction band.The end result of such a process is that the electron willexecute a random walk amongst the trap sites.Electrons tunnelling between the shallow trap sites is highly probable since the overlap integral will be large.Scher and Lax (1973) showed in their paper on continuous time random walk (CTRW) applied to hopping conduction that a carrier executing a random walk in a lattice could reproduce the frequency dependence of the ac conductivity which is associated with hopping. That is it successfully showed that $\sigma_{ac} \propto f^s$ where s was positive and less than unity.The CTRW model is applicable to explain the dispersion observed in R_p, $C - C(\infty)$ and C_s.Thus the power law behaviour of these quantities is understood in general terms.However a close inspection of the CTRW model revealed that s is independent of temperature. The CTRW model cannot be applied to the dispersion observed in C_s as n was shown to be temperature dependent.(This statement will also be true for the ZnS material as it is very similar to ZnSe.)The dependence of n upon

photon energy can be understood in qualitative terms.We hypothosize that n is controlled by thermal emission of electrons from the shallow centres.For photon energies near the photoionisation threshold the number of electrons excited into the conduction band is small and they are expected to occupy the deeper lying shallow centres.In terms of the hypothesis this implies that the value of n is large.As the number of electrons excited into the conduction band increases,then they will occupy centres that produce shallow levels close to the band edge.The value of n tends to a constant value for photon energies approaching the band gap presumably because the shallowest level lies more than a few kT away from the band edge.The variation of n with temperature is to be regarded as an empirical relationship at present.

Hopping conduction of the type described above for ZnS and ZnSe,is not expected to be observable with the nickel impurity in GaP:Ni.The ground level of Ni(d^9) is 0.88eV below the conduction band and thus the thermal escape time of electrons from the ground state of Ni(d^9) at room temperatures is expected to be the order of 10^8s.Hence the frequency at which the effects of hopping become observable will the order of 10^{-8}Hz. This frequency lies outside conventional capacitance bridges and also frequency response analysers.

A survey of the literature connected with hopping conduction showed that there are many models that use the pair approximation.In particular we showed that the model of a hopping entity jumping over a potential barrier adequately describes the hopping observed in heavily doped ZnSe. Furthermore it was shown that for non-heavily doped semiconductors the dispersion parameter s decreased linearily with increasing temperature with the value at 0 K dependent on the

material.For the chalcogenide glasses,the linear decrease of s has been shown by Elliot (1977) with the value of s at 0 K equal to 1.The fact that a linear decrease of s with temperature was also observed in non-heavily doped semiconductors was unexpected.In such lightly doped semiconductors the pair approximation (in particular the model of Elliot) may not be valid.The temperature dependence of s is often omitted in theories,especially those that attempt to describe the hopping conduction in semiconductors.We have suggested that the temperature dependence of s is a useful tool to determine the nature of the process giving rise to the dispersion observed in hopping conduction.We further showed in the same literature survey that the analytical assumption which is used to derive the Kramers-Kronig relationship is violated at zero frequency for functions which increase with frequency as f^s wher s is positive and less than unity.Consequently,the so-called universal law connected with hopping conduction,namely that $[(\chi' - \chi'(\infty)]/\chi'' = \tan(s\pi/2)$ is not a consequence of the Kramers-Kronig relationship but has to be regarded as an experimental fact that is sometimes observed in experiments.

Hopping conduction has been seen in semiconductors at low temperatures.For example Pollak and Geballe (1961) had to cool their n-type Si down to liquid helium temperatures to observe hopping conduction.The reason for this is that the free electrons have to be frozen onto the donors and thus reduce the free electron current which masks the current due to hopping conduction. Hopping conduction then observed is similar to that described above except that no electrons have to be photoexcited to occupy the donor states. The temperature where the electrons are frozen onto the donors will be related to the location of the energy level of the shallow centres below the

conduction band.The above work has shown that hopping conduction can be observed at room temperatures if the shallowest impurity level is more than a few kT away from the band edge.However to observe the form of hopping conduction described above,electrons (or holes) will have to be photoexcited so that they occupy the shallow impurity states.An added advantage to observe this form of hopping conduction is that the relative number of electron or holes photoexcited can be easily varied by changing the spectral content of the light or by the change of photon flux.

The work presented above has shown that it is possible to observe a form of hopping conduction at room temperatures.However,this form of hopping conduction should be observable from liquid helium temperatures to room temperatures and above.Work is in progress to observe the above form of hopping conduction in other materials.Preliminary measurements on InP:Fe have shown that the above form of hopping conduction becomes observable at liquid nitrogen temperatures (Chernyaev (1985) - private communication).The work on InP:Fe will be presented elsewhere.

References

S R Elliot Phil Mag 36,121(177)

H G Grimmeiss,C O Ovren and J W Allen J Appl Phys 47,1103(1976)

U Kaufmann,W H Kochel and J Schneider Phys Rev B19,3343(1979)

M Pollak and T H Geballe Phys Rev 122,1742(1961)

H Scher and M Lax Phys Rev B7,4491(1973)